State of California
The Natural Resources Agency
DEPARTMENT OF WATER RESOURCES
Bay-Delta Office

Methodology for Flow and Salinity Estimates in the Sacramento-San Joaquin Delta and Suisun Marsh

32nd Annual Progress Report to the
State Water Resources Control Board in
Accordance with Water Right Decisions 1485 and 1641

August 2011

Edmund G. Brown Jr.	**John Laird**	**Mark W. Cowin**
Governor	Secretary for Natural Resources	Director
State of California	The Natural Resources Agency	Department of Water Resources

If you need this report in alternate format, call the Equal Opportunity and Management Investigations Office at (916) 653-6952 or TDD (916) 653-6934.

Foreword

This is the 32nd annual progress report of the California Department of Water Resources' San Francisco Bay-Delta Evaluation Program, which is carried out by the Delta Modeling Section. This report is submitted annually by the section to the California State Water Resources Control Board pursuant to its Water Right Decision 1485, Term 9, which is still active pursuant to its Water Right Decision 1641, Term 8.

This report documents progress in the development and enhancement of the Bay-Delta Office's Delta Modeling Section's computer models and reports the latest findings of studies conducted as part of the program. This report was compiled under the direction of Tara Smith, program manager for the Bay-Delta Evaluation Program.

Online versions of previous annual progress reports are available at:
http://baydeltaoffice.water.ca.gov/modeling/deltamodeling/annualreports.cfm.

For more information contact:

Tara Smith

tara@water.ca.gov

(916) 653-9885

State of California
Edmund G. Brown Jr., Governor

The Natural Resources Agency
John Laird, Secretary for Natural Resources

Department of Water Resources
Mark W. Cowin, Director

Susan Sims
Chief Deputy Director

Kasey Schimke
Asst. Director Legislative Affairs

Sandy Cooney
Asst. Director Public Affairs

Cathy Crothers
Chief Counsel

Kamyar Guivetchi
Acting Deputy Director
Integrated Water Management

Dale Hoffman-Floerke
Deputy Director
Delta/Statewide Water Management

Kathie Kishaba
Deputy Director
Business Operations

John Pacheco
Acting Deputy Director
California Energy Resources Scheduling

Ralph Torres
Deputy Director
State Water Project

Bay-Delta Office
Katherine Kelly, Chief

Modeling Support Branch
Francis Chung, Principal Engineer

Prepared under the supervision of
Tara Smith, program manager for the Bay-Delta Evaluation Program

Prepared by

Jamie Anderson	Senior Engineer	Bay-Delta Office
Eli Ateljevich	Engineer	Bay-Delta Office
Fabián Bombardelli	Asst. Professor	University of California, Davis
Joe Christen	Environmental Scientist	Office of Water Quality
Ralph Finch	Senior Engineer	Bay-Delta Office
En-Ching Hsu	Engineer	Bay-Delta Office
Lan Liang	Engineer	Bay Delta Office
Siqing Liu	Engineer	Bay Delta Office
Lianwu Liu	Engineer	Bay-Delta Office
Prabhjot Sandhu	Senior Engineer	Bay-Delta Office
Marcia Scavone-Tansey	Environmental Scientist	Office of Water Quality
Qiang Shu	Engineer	Bay-Delta Office
Robert Suits	Senior Engineer	Bay Delta Office
Kaveh Zamani	Graduate Student	University of California, Davis

Editorial review, graphics, and report production by Technical Publications & Communication Media

Gretchen Goettl, Supervisor of Technical Publications

Marilee Talley, Research Writer

Report Contents

Preface. ..... **xv**

Acronyms and Abbreviations ..... **xvii**

Metric Conversion Table ..... **xviii**

1 Improvements to DSM2-Qual Part 1 ..... **1-1**

1.1 Summary 1-1

1.2 Advection and Parcel Recombination 1-1

1.3 Dispersion Changes 1-3

1.3.1 Discretization Issue *1-3*

1.3.2 Proposed Scheme *1-5*

1.3.3 Estimating the Dispersion Coefficient (DC) *1-6*

1.4 Tests Using DSM2 Historical Setup 1-7

1.5 Conclusions 1-7

1.6 References 1-8

Figures

Figure 1-1 New parcel formed by inflow over a single time step 1-1

Figure 1-2 Parcel recombination strategy example 1-2

Figure 1-3 Explanation of mixing between parcels 1-2

Figure 1-4 Previous model result at Collinsville 1-9

Figure 1-5 Previous model result at Jersey Point 1-9

Figure 1-6 Previous model advection only result at Collinsville 1-10

Figure 1-7 Previous model advection only result at Collinsville (zoom in) 1-10

Figure 1-8 New model, advection-only at Collinsville, convergence at 15, 5, 3, 1 min time steps 1-11

Figure 1-9 New model, advection-only at Collinsville, convergence at 5, 3, 1 min time steps 1-11

Figure 1-10 New model, advection-only at Jersey Pt., convergence at 15, 5, 3, 1 min time steps 1-12

Figure 1-11 New model, advection-only at Jersey Pt., convergence of 5, 3, 1 minute time steps 1-12

Figure 1-12 New model, advection-only at Collinsville (parcel size sensitivity test, dt=5 min) 1-13

Figure 1-13 Result with previous dispersion model after advection fix at Collinsville 1-13

Figure 1-14 New model, result at Collinsville (time step sensitivity test, parcel size 500 ft) 1-14

Figure 1-15 New model, result at Jersey Point (time step sensitivity test, parcel size 500 ft) 1-14

Figure 1-16 New model, result at Bacon Island (time step sensitivity test, parcel size 500 ft) 1-15

Figure 1-17 New model, result at Clifton Court (time step sensitivity test, parcel size 500 ft) 1-15

Figure 1-18 New model, result at Collinsville (parcel size sensitivity test, time step=5min) 1-16

Figure 1-19 New model, result at Jersey Point (parcel size sensitivity test, time step=5min) 1-16

Figure 1-20 New model, result at Bacon Island (parcel size sensitivity test, time step=5min) 1-17

Figure 1-21 New model, result at Clifton Court (parcel size sensitivity test, time step=5min) 1-17

Figure 1-22 Comparison of previous (red line) and new (green) model results with field data (blue dots) at Collinsville 1-18

Figure 1-23 Comparison of previous (red line) and new (green) model results with field data (blue dots) at Jersey Point 1-18

2 Improvements to DSM2-Qual: Part 2 2-1

2.1 Introduction 2-1

2.2 Testing Scenarios and Result Analysis 2-1

2.2.1 Test 1: Compare With the Old Solver 2-1

2.2.2 Test 2: Test Minimum Dispersion Velocity (0.01 ft/s) 2-1

2.2.3 Test 3: Test Cold Start 2-2

2.3 Conclusions 2-2

2.4 References 2-2

Appendix 2-A 2-3

Appendix 2-B 2-4

Appendix 2-C 2-9

Figures

Figure 2-1 Delta Cross Channel (instantaneous, MDV=0 and 0.01) 2-5

Figure 2-2 Delta Cross Channel (monthly average, MDV=0 and 0.01) 2-5

Figure 2-3 Montezuma Slough (instantaneous, MDV=0 and 0.01) 2-6

Figure 2-4 Montezuma Slough (monthly average, MDV=0 and 0.01) 2-6

Figure 2-5 Montezuma Slough (monthly average, MDV=0 and 0.1) 2-7

Figure 2-6 Montezuma Slough (monthly average, MDV=0 and 0.001) 2-7

Figure 2-7 Old River at Tracy Road (instantaneous, ammonia) 2-8

Figure 2-8 Old River at Tracy Road (monthly average, ammonia) 2-8

Figure 2-9 Mallard Island cold vs. warm start, algae 2-9

Figure 2-10 Mallard Island cold vs. warm start, phosphate 2-10

Figure 2-11 Clifton Court cold vs. warm start, algae 2-10

Table

Table 2-1 Summary of maximum monthly percent difference 2-3

3 DSM2 Dissolved Organic Carbon Boundary Condition Improvement 3-1

3.1 Summary 3-1

3.2 Methods 3-1

3.2.1 Sites 3-1

3.2.2 Sample Collection and Analysis 3-2

3.2.3 Comparisons 3-2

3.3 Results 3-4

3.4 Discussion 3-9

3.5 Conclusions 3-10

3.6 References 3-10

Figures

Figure 3-1 Sampled Delta boundary stations 3-2
Figure 3-2 Shag Slough DOC, Sacramento River DOC, Yolo Bypass flow, and rainfall 3-5
Figure 3-3 DOC in the Sacramento River at Hood and Shag Slough, December 2008—March 2010..... 3-5
Figure 3-4 Mokelumne River DOC, Cosumnes River flow, and rainfall..... 3-6
Figure 3-5 Mokelumne River DOC > 4 mg/L and high flow boundary conditions..... 3-7
Figure 3-6 Mokelumne River DOC < 4 mg/L and low flow boundary conditions..... 3-7
Figure 3-7 Calaveras River DOC, Mormon Slough flow, and rainfall..... 3-8

Tables

Table 3-1 Water Data Library station numbers and the corresponding DSM2 geometry by location 3-2
Table 3-2 Statistics for DOC concentrations (mg/L) at boundary locations, Dec 2008—Mar 2010..... 3-4

4 South Delta Temporary Barriers Hydrodynamic Modeling 4-1

4.1 Summary 4-1
4.2 2008 Delta Boundary conditions 4-1
4.3 2008 Delta consumptive use..... 4-2
4.4 South Delta Structures 4-2
4.5 Delta Downstream Stage at Martinez..... 4-3
4.6 Delta Cross Channel Operation..... 4-3
4.7 Validation of DSM2 Simulation of Historical 2008 Delta Hydrodynamics 4-3
4.8 Effect of Temporary Barriers Installation and Operation on South Delta Hydrodynamics 4-16
4.9 Discussion 4-17

Figures

Figure 4-1 Daily average historical inflow from the Sacramento River, 2008 4-1
Figure 4-2 Daily average historical inflow from the Yolo Bypass, 2008 4-1
Figure 4-3 Daily average historical inflow from the San Joaquin River, 2008..... 4-2
Figure 4-4 Daily average historical pumping at Banks and Jones pumping plants, 2008 4-2
Figure 4-5 Locations where DSM2-simulated and measured stages and flows are presented, 2008..... 4-4
Figure 4-6 Comparison of DSM2-simulated and observed daily stage, 2008..... 4-5
Figure 4-7 Comparison of DSM2-simulated and measured daily flow, 2008..... 4-11
Figure 4-8 Locations where simulated Delta stages and flows for analysis of 2008 conditions are presented 4-17
Figure 4-9 Distribution of DSM2-simulated stages for historical 2008 with and without temporary barriers installed 4-19
Figure 4-10 Distribution of DSM2-simulated flows for historical 2008 conditions with and without temporary barriers installed 4-23
Figure 4-11 Simulated period-average flow and minimum stage for 2008 conditions with historical barrier configuration and no-barriers condition 4-27

Tables

Table 4-1 Historical South Delta Temporary Barriers installation and removal, 2008 4-3
Table 4-2 Characteristics of time intervals for presentation of simulation results, 2008 4-16

5 Adaptive Mesh, Embedded Boundary Model for Flood Modeling 5-1
5.1 Summary 5-1
5.2 Introduction 5-1
5.3 Governing Equations 5-1
5.4 Solution Algorithm 5-3
5.4.1 Adaptive Mesh Refinement 5-4
5.4.2 Embedded boundaries 5-5
5.4.3 Godunov algorithm 5-5
5.5 Wet/Dry Front Capture 5-6
5.6 Model Verification 5-7
5.6.1 Dam Break on a Dry Bottom 5-8
5.6.2 Dam Break on a Wet Bottom 5-9
5.6.3 Dam Break on a Dry Bottom with Friction 5-10
5.7 Applications and Challenges 5-10
5.8 Acknowledgements 5-11
5.9 References 5-11

Figures

Figure 5-1 A multiblock adaptive mesh hierarchy with a refinement factor of 2 between levels 5-4
Figure 5-2 Decomposition of a patch of cells into regular, irregular, and covered cells 5-5
Figure 5-3 Two depictions of flooding 5-6
Figure 5-4 AMR resolving a flood along a reach of the Sacramento River 5-7
Figure 5-5 Water depth (left) and velocity (right) after dam break at time 50.78 seconds 5-8
Figure 5-6 Water depth (left) and velocity (right) after dam break at time 50.52 seconds 5-9
Figure 5-7 Water depth (left) and velocity (right) after dam break at time 50.88 seconds 5-10

6 Using Software Quality and Algorithm Testing to Verify a One-Dimensional Transport Model 6-1
6.1 Introduction 6-1
6.2 1-D Transport Model 6-1
6.3 Testing Requirements 6-2
6.4 Testing Principles 6-2
6.4.1 Software Testing Principles 6-3
6.4.2 Numerical verification and algorithmic testing 6-4
6.5 Algorithm Test Suite Description 6-6
6.6 Architecture and Implementation 6-7

6.7 Challenges and Issues with Tests 6-8
6.8 Conclusions 6-9
6.9 Acknowledgments 6-10
6.10 References 6-10

Figures

Figure 6-1 Relationship between software testing components and algorithmic testing. 6-3
Figure 6-2 Transport algorithm testing with incremental complexity 6-7

7 Turbidity Modeling with DSM2 7-1

7.1 Introduction 7-1
7.2 Turbidity Modeling with DSM2 7-1
7.3 Boundary Conditions 7-2
7.4 2010 Wet Season Calibration 7-2
7.5 Discussion of Model limitations 7-3
7.6 Summary 7-5
7.7 Acknowledgments 7-5
7.8 References 7-5

Figures

Figure 7-1 CDEC turbidity stations 7-6
Figure 7-2 Calibrated settling rate values 7-7
Figure 7-3 Turbidity comparison, Sacramento River at Rio Vista (15 minute interval) 7-8
Figure 7-4 Daily-averaged turbidity comparison, Sacramento River at Rio Vista 7-8
Figure 7-5 Regression analysis of daily averaged values, Sacramento River at Rio Vista 7-9
Figure 7-6 Turbidity comparison, Sacramento River at Decker Island (15 minute interval) 7-9
Figure 7-7 Daily-averaged turbidity comparison, Sacramento River at Decker Island 7-10
Figure 7-8 Regression analysis of modeled result and field data, Sacramento River at Decker Island 7-10
Figure 7-9 Turbidity comparison at Jersey Point 7-11
Figure 7-10 Daily-averaged turbidity comparison at Jersey Point 7-11
Figure 7-11 Regression analysis of modeled result and field data at Jersey Point 7-12
Figure 7-12 Turbidity comparison at Old River Bacon Island 7-12
Figure 7-13 Daily-averaged turbidity comparison at Old River Bacon Island 7-13
Figure 7-14 Regression analysis of modeled result and field data at Old River Bacon Island 7-13
Figure 7-15 Turbidity comparison, Sacramento River at Prisoners Point 7-14
Figure 7-16 Daily-averaged turbidity comparison, Sacramento River at Prisoners Point 7-14
Figure 7-17 Regression analysis of modeled result and field data at Prisoners Point 7-15
Figure 7-18 Turbidity comparison, Sacramento River at Holland Cut 7-15
Figure 7-19 Daily-averaged turbidity comparison at Holland Cut 7-16
Figure 7-20 Turbidity comparison at Victoria Canal 7-16
Figure 7-21 Daily-averaged turbidity comparison at Victoria Canal 7-17
Figure 7-22 Compare turbidity spikes at Jersey Point with rainfall and wind data 7-17

Figure 7-23 Compare turbidity spikes at Bacon Island with rainfall and wind data 7-18
Figure 7-24 Compare turbidity spikes at Holland Cut with rainfall and wind data 7-18
Figure 7-25 Turbidity comparison at San Joaquin River Garwood 7-19
Figure 7-26 Daily-averaged turbidity comparison at San Joaquin River Garwood 7-19
Figure 7-27 Turbidity comparison at Grant Line Canal 7-20
Figure 7-28 Daily-averaged turbidity comparison at Grant Line Canal 7-20
Figure 7-29 Flow at San Joaquin River Mossdale (RSAN087) and Brandt Bridge (RSAN072) 7-21
Figure 7-30 Velocity at San Joaquin River Mossdale and Brandt Bridge 7-21
Figure 7-31 Settling rate sensitivity test result at Decker Island 7-22
Figure 7-32 Settling rate sensitivity test result at Prisoners Point 7-22
Figure 7-33 Settling rate sensitivity test result at Holland Cut 7-23
Figure 7-34 Settling rate sensitivity test result at False River 7-23
Figure 7-35 Settling rate sensitivity test result at Victoria Canal 7-24
Figure 7-36 Settling rate sensitivity test result at Rough and Ready Island 7-24
Figure 7-37 Settling rate sensitivity test result at Grant Line Canal 7-25
Figure 7-38 Daily-averaged turbidity comparison at Mallard 7-25
Figure 7-39 Adjusted turbidity comparison at Mallard 7-26
Figure 7-40 Daily-averaged turbidity comparison at Antioch 7-26
Figure 7-41 Adjusted turbidity comparison at Antioch 7-27
Figure 7-42 Adjusted turbidity comparison at Prisoners Point 7-27
Figure 7-43 Adjusted turbidity comparison at Holland Cut 7-28
Figure 7-44 Adjusted turbidity comparison at Victoria Canal 7-28

Table

Table 7-1 Turbidity sources 7-4

8 DSM2 Grid Map Tool 8-1
8.1 Introduction 8-1
8.2 Geographical Information 8-1
8.3 Design 8-2
8.4 Implementation Details 8-2
8.5 Storage Format 8-3
8.6 User Interface Overview 8-4
8.6.1 Login 8-4
8.6.2 Upload 8-5
8.6.3 Viewing the Grid 8-5
8.6.4 Viewing Channel Information 8-8
8.6.5 GIS Tools 8-9
8.6.6 Managing Studies 8-9
8.6.7 Editing Mode 8-10
8.6.8 Editing Nodes 8-10

8.6.9 Editing Channels *8-10*
8.6.10 Editing Reservoirs *8-14*
8.6.11 Editing Gates *8-14*
8.7 Conclusion 8-14
8.8 References 8-15

Figures

Figure 8-1 Data flow for DSM2 grid map 8-2
Figure 8-2 Sample grid 8-4
Figure 8-3 Example log in page 8-4
Figure 8-4 Example study upload 8-5
Figure 8-5 Example grid elements: reservoirs 8-6
Figure 8-6 Example grid elements: gates 8-6
Figure 8-7 Example base maps 8-7
Figure 8-8 Example channel display 8-8
Figure 8-9 GIS tools 8-9
Figure 8-10 Example study inputs 8-9
Figure 8-11 Node editing 8-10
Figure 8-12 Flow line editing 8-11
Figure 8-13 Edit Channel Cross section 8-11
Figure 8-14 Edit Channel Cross section (detail) 8-12
Figure 8-15 Edit Channel Cross section (profile points) 8-12
Figure 8-16 Edit Channel Cross section (elevation profile) 8-13
Figure 8-17 Edit Channel Cross section (generate or clear) 8-13
Figure 8-18 Editing reservoirs 8-14

Table

Table 8-1 GIS data format 8-3

9 DOC Validation with DSM2 9-1
9.1 Summary 9-1
9.2 Background 9-1
9.3 Study Methodology 9-1
9.4 Study Results 9-8
9.5 Conclusions 9-8
9.6 References 9-9

Figures

Figure 9-1 Assumed DOC for Delta inflows for simulation of historical conditions 9-3
Figure 9-2 DOC assumed for agricultural drainage by Delta region 9-5
Figure 9-3 Example of daily range and daily average DOC in DSM2-simulated conditions 9-6
Figure 9-4 Locations DSM2-simulated daily DOC compared to measured DOC 9-7

Figure 9-5 DSM2-simulated daily DOC and measured DOC, July 1990–1994 9-10
Figure 9-6 DSM2-simulated daily DOC and measured DOC, 1995–1998 9-18
Figure 9-7 DSM2-simulated daily DOC and measured DOC, 1999–2002 9-20
Figure 9-8 DSM2-simulated daily DOC and measured DOC, 2003–2006 9-22
Figure 9-9 DSM2-simulated daily DOC and measured DOC, 2007–2010 9-24
Figure 9-10 DSM2-simulated daily DOC fingerprint and measured DOC, 1991–1994 9-26

10 DSM2 Comparison Report Tool 10-1
10.1 Introduction 10-1
10.2 Development Framework 10-1
10.3 Tool Demonstration: Input Comparison Tool 10-2
10.4 Tool Demonstration: DSS Comparison Tool 10-4
10.4.1 Configuration File Preparation 10-5
10.4.2 DSM2 Planning Study 10-9
10.4.3 DSM2 Model Calibration 10-11
10.5 Conclusions 10-13
10.6 References 10-13

Figures

Figure 10-1 Working diagrams for input comparison report tool and output comparison report tool 10-2
Figure 10-2 Input comparison report tool GUI 10-2
Figure 10-3 Input comparison report 10-3
Figure 10-4 Highlighted differences from reservoir in example input comparison report 10-3
Figure 10-5 Extended reservoir table in example input comparison report 10-4
Figure 10-6 Input comparison example for non-unique lookup names 10-4
Figure 10-7 Example to execute output comparison tool 10-4
Figure 10-8 Sample configuration file for output comparison tool 10-7
Figure 10-9 Time series plot example for 5 comparison modes 10-8
Figure 10-10 DSM2 output comparison report for planning studies 10-10
Figure 10-11 A demonstration for displaying percentage root mean square differences on Google Map 10-10
Figure 10-12 Time series plot (1) daily average time series (2) monthly average time series (3) difference for daily time series (4) overlaid water year type on daily average time series 10-11
Figure 10-13 Percentage root mean square error for turbidity comparison (COMPARE_MODE 5) 10-12
Figure 10-14 Time series plot example for turbidity comparison (COMPARE_MODE 5) 10-12

Table

Table 10-1 Files required for each comparison mode 10-8

Preface

The California Department of Water Resources uses the Delta Simulation Model II (DSM2) to simulate conditions on the Sacramento-San Joaquin Delta (the Delta). The DSM2-Hydro model simulates flow and stage throughout the Delta, and the DSM2-Qual model simulates water quality (multiple conservative and non-conservative constituents).

The following are brief summaries of modeling work conducted during 2010.

Chapter 1 — Improvements to DSM2-Qual: Part 1

An important property of numerical models is that the simulation gets better as time and spatial steps are refined, with the model eventually "converging" to a solution determined by the underlying physics and equations. In qualitative testing, Delta Simulation Model II-Water Quality Model (DSM2-Qual) was found to converge slowly and to exhibit erratic behavior with very small (1 minute) steps. The poor qualitative convergence results from 2 ad hoc features of the code: parcel recombination in the Lagrangian advection scheme and a spatially dependent mixing scheme for dispersion. Corrections are proposed here to minimize both problems. Tests show that with these changes, DSM2-Qual's qualitative convergence is much improved.

Chapter 2 — Improvements to DSM2-Qual: Part 2

This chapter documents tests of DSM2 Version 8.0.5. The Bogacki-Shampine algorithm was implemented in the non-conservative constituent model to avoid negative value problems in the old solver. Also in Version 8.0.5, the user can set the minimum dispersion velocity to avoid zero-dispersion problems at dead-end channels/closed gates.

Chapter 3 — DSM2 Dissolved Organic Carbon Boundary Condition Improvement

In this chapter, the dissolved organic carbon data collected from the East Side Streams and Yolo Bypass are summarized, and comparisons are made between the collected data and the assumed boundary conditions of the DSM2. Based on these comparisons, the assumed boundary conditions for DOC concentrations may underestimate concentrations during high flows.

Chapter 4 — South Delta Temporary Barriers Hydrodynamic Modeling

This chapter presents an abbreviated sample of the simulation of historical 2008 Delta hydrodynamic conditions and the effect of the installation and operation of the south Delta temporary barriers. For this analysis, historical Delta inflows, consumptive use, and exports were simulated under 2 barrier conditions: (1) historical 2008 installation and operation of the temporary barriers, and (2) no installation of south Delta temporary barriers. DSM2-Hydro was used to simulate the Delta hydrodynamics.

Chapter 5 — Adaptive Mesh, Embedded Boundary Model for Flood Modeling

This chapter describes a 2-dimensional shallow water model designed to simulate water quality and flooding. The model uses a finite-volume discretization of the shallow water equations on an adaptive Cartesian mesh, using embedded boundaries to represent complex topography. The model is tested using analytical solutions of flood propagation on wet and dry channels and of a dam-break problem. Applications to flooding in arbitrary bathymetry are discussed.

Chapter 6 — Using Software Quality and Algorithm Testing to Verify a One-Dimensional Transport Model

In this chapter, we describe our approach and experiences developing a software verification framework for a one dimensional (1-D) transport model of advection, dispersion, and reactions or sources (ADR). The testing framework described was developed as part of a project to create a new transport module for the DSM2, a 1-D hydrodynamic and transport model for flow and water quality in the Delta. Our target problems include river and estuary advection, and 1-D approximations of common mixing mechanisms and source terms associated with conservative and non-conservative water quality kinetics including sediment transport.

Chapter 7 — Turbidity Modeling with DSM2

This chapter documents turbidity modeling with DSM2 Version 8.0.6. Turbidity has been deemed to be an important factor affecting delta smelt migration and entrainment. DSM2 is a promising tool in turbidity analysis and forecasting because of its speed as a 1-D model and its extensive applications in the Delta. A large number of stations with turbidity data became available in 2010, which makes a more detailed calibration possible for the 2010 wet season. The calibrated DSM2 model results generally match with the observed data. Further validation with another wet year will help improve its reliability.

Chapter 8 — DSM2 Grid Map Tool

DSM2 physical geometry is represented by channel lengths, channel cross sections, reservoir areas, and reservoir bottom elevations. These inputs are derived from geographical data, which are now available in computer systems and referred to as Geographical Information Systems (GIS).

Since 1998, DSM2 geometry has been handled with the Cross-Section Development Program. The project described in this chapter offers all the capabilities of CSDP and several more, and may serve to replace CSDP for DSM2 bathymetry and channel development. The application is built on the Google Maps API and is designed to be used within a modern web browser. The data is hosted online for ease of accessibility for a wide audience of users and to support the large datasets required to provide the elevation functionality.

Chapter 9 — DOC Validation with DSM2

Using DSM2, historical Delta DOC was simulated over the period 1990 through 2010 and compared to available measured data. DOC fingerprints were generated at several locations to evaluate how contributions of various sources of DOC in the Delta vary by location. This chapter summarizes the methods and results from an expanded DSM2 simulation of historical Delta DOC.

Chapter 10 — DSM2 Comparison Report Tool

While running DSM2 for different scenarios, knowing the changes that have been made to input files and subsequent changes to DSM2 outputs is essential for model investigation. Analyzing DSM2 model input and output changes with existing tools involves manual steps that are cumbersome and inefficient. The objective for the tool development described in this chapter is to automate the comparison process. The goal is to reduce duplicate effort and human errors, and provide a systematic way for study comparison.

Acronyms and Abbreviations

ADR	advection, dispersion, and reactions
AMR	adaptive mesh refinement
BLTM	Branched Lagrangian Transport Model
BOD	Biochemical Oxygen Demand
CADAM	Concerted Action on Dam Break Modeling
cfs	cubic feet per second
CSDP	Cross-Section Development Program
CTU	corner transport upwind
DCC	Delta Cross Channel
DEM	Digital Elevation Model
DICU	Delta Island Consumptive Use
DO	dissolved oxygen
DOC	dissolved organic carbon
DSM2	Delta Simulation Model II
DWR	California Department of Water Resources
EB	embedded boundaries
EC	electrical conductivity
FRUIT	FORTRAN Unit Testing Framework
ft	feet
ft/s	feet per second
FVM	finite-volume method
GIS	Geographical Information Systems
HEC-DSS	US Army Corps of Engineers' Hydrologic Engineering Center Data Storage System
HYDRO	hydrodynamic module (DSM2)
LBNL	Lawrence Berkeley National Laboratory
m	meter
mg/L	milligrams per liter
MMS	Method of Manufactured Solutions
MWQI	Municipal Water Quality Investigations
NTU	nephelometric turbidity units
PDE	partial differential equation
QUAL	water quality module (DSM2)
REALM	River, Estuary, and Land Model
RPA	Reasonable and Prudent Alternative
SQE	software quality engineering
SSC	suspended sediment concentration
tcfs	thousand cubic feet per second
USFWS	US Fish and Wildlife Service
WDL	Water Data Library

Metric Conversion Table

Quantity	*To convert from metric unit*	*To customary unit*	*Multiply metric unit by*	*To convert to metric units, multiply customary unit*
Length	millimeters (mm)	inches (in)*	0.03937	25.4
	centimeters (cm) for snow depth	inches (in)	0.3937	2.54
	meters (m)	feet (ft)	3.2808	0.3048
	kilometers (km)	miles (mi)	0.62139	1.6093
Area	square millimeters (mm^2)	square inches (in^2)	0.00155	645.16
	square meters (m^2)	square feet (ft^2)	10.764	0.092903
	hectares (ha)	acres (ac)	2.4710	0.40469
	square kilometers (km^2)	square miles (mi^2)	0.3861	2.590
Volume	liters (L)	gallons (gal)	0.26417	3.7854
	megaliters	million gallons (10*)	0.26417	3.7854
	cubic meters (m^3)	cubic feet (ft^3)	35.315	0.028317
	cubic meters (m^3)	cubic yards (yd^3)	1.308	0.76455
	cubic dekameters (dam^3)	acre-feet (ac-ft)	0.8107	1.2335
Flow	cubic meters per second (m^3/s)	cubic feet per second (ft^3/s)	35.315	0.028317
	liters per minute (L/mn)	gallons per minute (gal/mn)	0.26417	3.7854
	liters per day (L/day)	gallons per day (gal/day)	0.26417	3.7854
	megaliters per day (ML/day)	million gallons per day (mgd)	0.26417	3.7854
	cubic dekameters per day (dam^3/day)	acre-feet per day (ac-ft/day)	0.8107	1.2335
Mass	kilograms (kg)	pounds (lbs)	2.2046	0.45359
	megagrams (Mg)	tons (short, 2,000 lb.)	1.1023	0.90718
Velocity	meters per second (m/s)	feet per second (ft/s)	3.2808	0.3048
Power	kilowatts (kW)	horsepower (hp)	1.3405	0.746
Pressure	kilopascals (kPa)	pounds per square inch (psi)	0.14505	6.8948
	kilopascals (kPa)	feet head of water	0.33456	2.989
Specific Capacity	liters per minute per meter drawdown	gallons per minute per foot drawdown	0.08052	12.419
Concentration	milligrams per liter (mg/L)	parts per million (ppm)	1.0	1.0
Electrical Conducti vity	microsiemens per centimeter (µS/cm)	micromhos per centimeter (µmhos/cm)	1.0	1.0
Temperature	degrees Celsius (°C)	degrees Fahrenheit (°F)	(9/5 x °C)+32	(°F - 32) x 5/9

* When using “dual units,” inches are normally converted to millimeters (rather than centimeters).

Methodology for Flow and Salinity Estimates in the Sacramento-San Joaquin Delta and Suisun Marsh

32nd Annual Progress Report
June 2011

Chapter 1
Improvements to the DSM2-Qual: Part 1

Authors: Lianwu Liu and Eli Ateljevich,
Delta Modeling Section,
Bay-Delta Office,
California Department of Water Resources

Contents

1 Improvements to DSM2-Qual: Part 1 1-1
1.1 Summary 1-1
1.2 Advection and Parcel Recombination 1-1
1.3 Dispersion Changes 1-3
1.3.1 Discretization Issue 1-3
1.3.2 Proposed Scheme 1-5
1.3.3 Estimating the Dispersion Coefficient (DC) 1-6
1.4 Tests Using DSM2 Historical Setup 1-7
1.5 Conclusions 1-7
1.6 References 1-8

Figures

Figure 1-1 New parcel formed by inflow over a single time step 1-1
Figure 1-2 Parcel recombination strategy example 1-2
Figure 1-3 Explanation of mixing between parcels 1-2
Figure 1-4 Previous model result at Collinsville 1-9
Figure 1-5 Previous model result at Jersey Point 1-9
Figure 1-6 Previous model advection only result at Collinsville 1-10
Figure 1-7 Previous model advection only result at Collinsville (zoom in) 1-10
Figure 1-8 New model, advection-only at Collinsville, convergence at 15, 5, 3, 1 min time steps 1-11
Figure 1-9 New model, advection-only at Collinsville, convergence at 5, 3, 1 min time steps 1-11
Figure 1-10 New model, advection-only at Jersey Pt., convergence at 15, 5, 3, 1 min time steps 1-12
Figure 1-11 New model, advection-only at Jersey Pt., convergence of 5, 3, 1 minute time steps 1-12
Figure 1-12 New model, advection-only at Collinsville (parcel size sensitivity test, *dt*=5 min) 1-13
Figure 1-13 Result with previous dispersion model after advection fix at Collinsville 1-13
Figure 1-14 New model, result at Collinsville (time step sensitivity test, parcel size 500 ft) 1-14
Figure 1-15 New model, result at Jersey Point (time step sensitivity test, parcel size 500 ft) 1-14
Figure 1-16 New model, result at Bacon Island (time step sensitivity test, parcel size 500 ft) 1-15
Figure 1-17 New model, result at Clifton Court (time step sensitivity test, parcel size 500 ft) 1-15
Figure 1-18 New model, result at Collinsville (parcel size sensitivity test, time step=5min) 1-16
Figure 1-19 New model, result at Jersey Point (parcel size sensitivity test, time step=5min) 1-16
Figure 1-20 New model, result at Bacon Island (parcel size sensitivity test, time step=5min) 1-17
Figure 1-21 New model, result at Clifton Court (parcel size sensitivity test, time step=5min) 1-17
Figure 1-22 Comparison of previous (red line) and new (green) model results with field data (blue dots) at Collinsville 1-18
Figure 1-23 Comparison of previous (red line) and new (green) model results with field data (blue dots) at Jersey Point 1-18

1 Improvements to DSM2-Qual: Part 1

1.1 Summary

An important property of numerical models is that the simulation gets better as time and spatial steps are refined, with the model eventually "converging" to a solution determined by the underlying physics and equations. In qualitative testing, Delta Simulation Model II-Water Quality Model (DSM2-Qual) was found to converge slowly and to exhibit erratic behavior with very small (1 minute) steps. The poor qualitative convergence results from 2 ad hoc features of the code: parcel recombination in the Lagrangian advection scheme, and a spatially dependent mixing scheme for dispersion. Corrections are proposed here to minimize both problems. Tests show that with these changes, DSM2-Qual's qualitative convergence is much improved.

1.2 Advection and Parcel Recombination

DSM2 uses an adapted version of the Branched Lagrangian Transport Model (BLTM) (Schoellhammer and Jobson 1986).

The original BLTM and DSM2-Qual models rely on a Lagrangian scheme for advection. Every time step, they introduce a new "parcel" of water into each channel reach; then the models track the parcels as they move over time. The process of parcel creation is shown in Figure 1-1. The size of the parcel at creation time is the length of channel occupied by all the water coming in over one step Δt. This relationship binds the spatial discretization (parcel size) to the temporal discretization (time step).

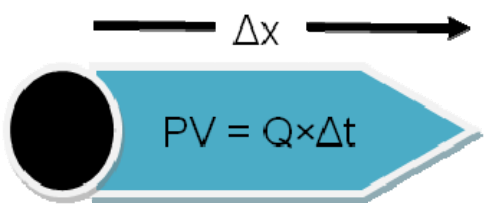

Figure 1-1 New parcel formed by inflow over a single time step

The parcel size Δx depicted in Figure 1-1 is the local parcel size at formation time. The parcel will deform over time as the parcel moves and occupies part of the channel with different cross-sectional area. DSM2-Qual does not track parcel length. The model is written in terms of parcel volume (*PV*), which does not change if not recombined. To estimate Δx, we need information about *PV* and cross sectional area occupied by the parcel $\bar{A}$ (Eq. 1-1):

$$\Delta x = \frac{PV}{\bar{A}} \qquad \textbf{Eq. 1-1}$$

In practice, PV is tracked exactly, but average area must be estimated from channel-averaged areas. Accuracy of Δx is limited by this approximation.

Due to memory considerations, the original code enforced a maximum number of parcels per channel. Once the number of parcels in a channel exceeded the maximum number (22 was used for DSM2-Qual), the smallest parcel in a channel would be combined with a parcel next to it.

Several problems existed with the original method of parcel recombination. The global maximum parcel number approach does not distinguish longer channels and shorter channels. In very long channels, the maximum might not be adequate to resolve the concentration field. The concept of a maximum number of parcels also introduces step-dependent behavior because of tidal influence. For instance, 22 parcels at a time step of 15 minutes samples 6 hours of flow; once you sample a half tide period, the average parcel size tends to vary less. With a 15 minute step, the maximum parcel number rule is seldom invoked because the parcels are big and travel a long way per time step. In contrast, 22 parcels at a time step of 1 minute are created in 22 minutes. In the absence of recombination, this spacing would tend to make the parcels locally uniform. However, in practice the maximum is always exceeded and recombination leaves small uniform parcels next to monolithic combined parcels.

In version 8.1, the parcel combination approach is altered. At every time step, the new parcel entering a reach is checked. If the new parcel is smaller than a user defined minimum size and the parcel on the interior side is also smaller, the parcels will be combined (Figure 1-2 and Figure 1-3). This has the effect of holding the parcel adjacent to the beginning of the reach until it has met a minimum size criterion. As far as time stepping, the scheme acts somewhat like an adaptive time step at the point of parcel creation: time steps are combined (made longer) when flow is gentle and parcels are small.

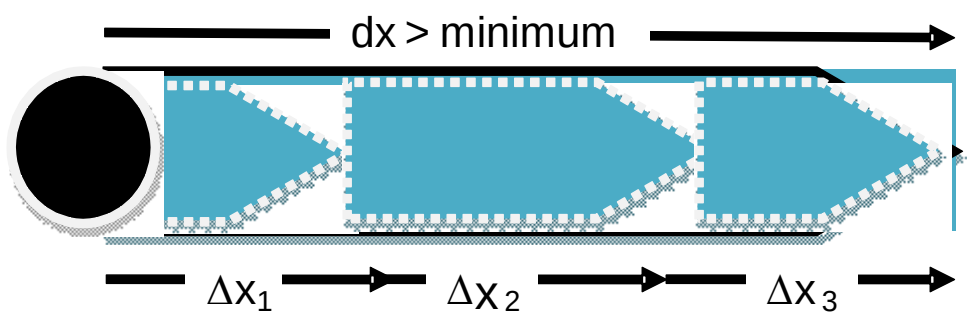

Figure note: The estimated parcel lengths of 3 existing parcels are bigger than the minimum. Next time step the parcels will advect freely and a new parcel will start forming behind it.

Figure 1-2 Parcel recombination strategy example

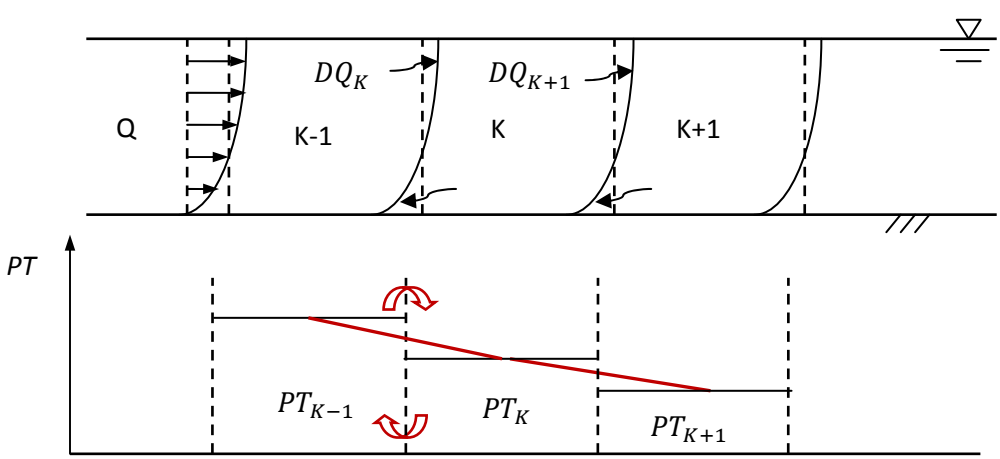

Figure 1-3 Explanation of mixing between parcels

The goal of the new parcel recombination scheme is to keep neighboring parcels similar in size and close to the defined minimum. The scheme is actively used: the minimum parcel size is set large enough compared to typical new parcels that the recombination scheme controls parcel size and number. The maximum parcel number (the one that used to be 22) is set to a large value (e.g. 100), and is almost never reached. In the rare case where the maximum parcel number is reached, the model reverts to the original method and the smallest parcel will be combined with a parcel next to it.

This modification appears to work well, comparing the old model results (Figure 1-4 through Figure 1-7) in the new model advection-only test results (Figure 1-8 to Figure 1-11[1]). Results at Collinsville and Jersey Point show the model converges well at 5-, 3-, and 1-minute time steps (Figure 1-8 and Figure 1-9, and Figure 1-10Figure 1-11). Figure 1-12 shows sensitivity test of minimum parcel sizes. The difference between 1,000 ft and others are obvious, while 600, 500, and 400 ft results are very close. We believe that numerical diffusion in advection previously attributed to mixing at nodes was actually due to parcel recombination.

Figure 1-13 shows the full scheme after advection fix, including advection and dispersion. The odd behavior with a time step of 1 minute is fixed and the model is qualitatively much more convergent. Some of the remaining issues are addressed in the next section.

1.3 Dispersion Changes

1.3.1 Discretization Issue

The BLTM dispersion equation was derived from an "exchange flow" mixing concept. The exchange flow rate between parcels (volume of exchange per time) was defined as a fraction of the river discharge (illustrated in **Error! Reference source not found.**) (Eq. 1-2):

$$DQ = DQQ * Q \qquad \textbf{Eq. 1-2}$$

in which *DQ* is the exchange flow rate, *DQQ* is the ratio of exchange flow to river discharge, and *Q* is the river discharge. DQQ is defined by user in the input file for every reach. The mixing equation for parcel K is thus (Eq. 1-3):

$$\Delta PT = DT * (DQ_K PT_{K-1} - DQ_K PT_K + DQ_{K+1} PT_{K+1} - DQ_{K+1} PT_K)/PV_K \qquad \textbf{Eq. 1-3}$$

where Δ*PT* is the change in parcel concentration and *DT* is the simulation time step. In the original BLTM programmer's manual (Schoellhammer and Jobson 1986), it was indicated (Eq. 1-4):

$$DQQ = \frac{D_x}{U\Delta x} \qquad \textbf{Eq. 1-4}$$

in which D_x is the classic longitudinal dispersion coefficient, *U* is the mean cross-sectional velocity. This shows *DQQ* is a function of the size of a parcel Δx.

[1] Figures 1-4 through 1-23 are presented at the back of this chapter.

This involvement of Δx in the physics of mixing is problematic. Changing the time/spatial step doesn't just change the accuracy of the solution; it changes the physical description of the problem. Moreover, in DSM2-Qual, the parcel size varies from parcel to parcel and changes with time step; how big a parcel depends on the time step and velocity at the time the parcel entered the channel.

In terms of standard diffusion analogs models of mixing, the DSM2-Qual scheme appears to discretize something akin to the following (Eq. 1-5):

$$\frac{\partial C}{\partial t} = \frac{1}{A}\frac{\partial}{\partial x}\left(\Delta x DQ \frac{\partial C}{\partial x}\right) \qquad \textbf{Eq. 1-5}$$

in which *C* is concentration, *t* is the time coordinate, *x* is the longitudinal axis, *A* is the cross sectional area, Δx is grid size in a finite difference scheme or parcel size in DSM2-Qual—usually people use ξ to represent the Lagrangian longitudinal axis, but the equations are similar and we feel this notation is more familiar for discussion.

The relationship of the parcel mixing scheme to Eq. 1-5 is easy to demonstrate when the spatial grid is uniform (which in the original DSM2-Qual usually implies steady uniform flow). Ignoring the mix of discrete and continuous quantities, Eq. 1-5 can be discretized using central finite differences (Eq. 1-6 through Eq. 1-8):

$$\frac{\Delta C}{\Delta T} = \frac{\Delta x}{A_K} \cdot \frac{\left(DQ\frac{\partial C}{\partial x}\right)^{+} - \left(DQ\frac{\partial C}{\partial x}\right)^{-}}{\Delta x} \qquad \textbf{Eq. 1-6}$$

$$\frac{\Delta C}{\Delta T} = \frac{1}{A_K}\left[DQ_{K+1}\frac{C_{K+1} - C_K}{\Delta x} - DQ_K\frac{C_K - C_{K-1}}{\Delta x}\right] \qquad \textbf{Eq. 1-7}$$

$$\Delta C = \frac{\Delta T}{PV_K}\left[DQ_{K+1}(C_{K+1} - C_K) - DQ_K(C_K - C_{K-1})\right] \qquad \textbf{Eq. 1-8}$$

Eq. 1-8 is identical to Eq. 1-3. The factor of Δx in Eq. 1-5 is not explicitly included in the discretization, but rather arises due to omission—from failing to divide by Δx in the original DSM2-Qual dispersion scheme. This represents the involvement of a discretization artifact in what should be a physical equation. Possible reasons for this in the original formulation are either (1) accurate estimates of Δx are not available or (2) a sentiment that sub-grid mixing processes are greater with larger parcels. The practical consequence for any particular grid is that an "effective average" $\widehat{\Delta x}$ gets built into the estimation of the dispersion factor *DQQ*. This makes the calibrated coefficient less meaningful, a problem that was compounded by the numerical dispersion from advection.

1.3.2 Proposed Scheme

The dispersion flux (rate of mass exchange) in the original scheme was (Eq. 1-9):

$$F = DQ_K(PT_{K-1} - PT_K) \qquad \textbf{Eq. 1-9}$$

The problem is that it is not normalized by parcel size. A new scheme is proposed to fix the problem. The dispersion flux (rate of mass exchange) at each side of the parcel is defined as (Eq. 1-10):

$$F = f\left(Q, \frac{\partial C}{\partial x}\right) = -DC \cdot |Q| \cdot \frac{\partial C}{\partial x} \qquad \textbf{Eq. 1-10}$$

in which *DC* is a coefficient with a length unit. The mixing equation for parcel K can be written as following (Eq. 1-11):

$$\Delta PT = DT * (DC_K|Q_K|\frac{PT_{K-1} - PT_K}{(\Delta x_K + \Delta x_{K-1})/2} + DC_{K+1}|Q_{K+1}|\frac{PT_{K+1} - PT_K}{(\Delta x_K + \Delta x_{K+1})/2})/PV_K \qquad \textbf{Eq. 1-11}$$

where Δx_K is the parcel length estimated based on parcel volume and channel-wide average cross-sectional area (Eq. 1-1).

The parcel exchange in Eq. 1-11 roughly discretizes the following partial differential equation with a simple explicit finite difference scheme (Eq. 1-12):

$$\frac{\partial C}{\partial t} = \frac{1}{A}\frac{\partial}{\partial x}\left(DC \cdot |Q| \cdot \frac{\partial C}{\partial x}\right) \qquad \textbf{Eq. 1-12}$$

The generally accepted form of 1-D river Lagrangian dispersion equation can be written as (Rutherford 1994) (the advection term is not shown here, only the dispersion term for discussion) (Eq. 1-13):

$$\frac{\partial C}{\partial t} = \frac{1}{A}\frac{\partial}{\partial x}\left(A \cdot K_x \frac{\partial C}{\partial x}\right) \qquad \textbf{Eq. 1-13}$$

in which *C* is concentration, *t* is the time coordinate, K_x is the classic longitudinal dispersion coefficient (same as D_x in the original BLTM manual).

Comparing equations Eq. 1-12 and Eq. 1-13, we get (Eq. 1-14 and Eq. 1-15):

$$DC \cdot |Q| = A \cdot K_x \qquad \textbf{Eq. 1-14}$$

$$DC = \frac{A}{|Q|} \cdot K_x = \frac{K_x}{|\bar{u}|} \qquad \textbf{Eq. 1-15}$$

in which $\bar{u}$ is the mean cross-sectional velocity. The coefficient *DC* is used as the input variable for "Dispersion Coefficient" in new versions of DSM2. *DC* can be estimated using Eq. 1-15 and calibrated for

each reach. Comparing this formula to Eq. 1-4, it can be seen that the scaling by Δx is not involved anymore[2].

1.3.3 Estimating the Dispersion Coefficient (DC)

A formula for K_x in natural streams by (Fischer, et al. 1979) may be used to estimate DC as a starting value (Eq. 1-16).

$$K_x = 0.011\frac{\bar{u}^2 W^2}{du^*} \qquad \textbf{Eq. 1-16}$$

in which $\bar{u}$ is the mean cross-sectional velocity, *W* is river width, *d* is flow depth, and u^* is shear velocity. For a steady uniform flow in a prismatic channel (Eq. 1-17),

$$u^* = \sqrt{\bar{\tau}_0/\rho} = \sqrt{gRS} \qquad \textbf{Eq. 1-17}$$

in which $\bar{\tau}_0 = \gamma RS$ is the average shear stress; γ=specific weight of the fluid; ρ = density; *g* = gravitational acceleration; *R* = hydraulic radius; *S* = friction slope or energy slope, which can be estimated using Manning's equation (Eq. 1-18):

$$Q = \frac{1.486}{n} A R^{\frac{2}{3}} S^{\frac{1}{2}} \qquad \textbf{Eq. 1-18}$$

Combining the 4 equations (equations Eq. 1-15 through Eq. 1-18), we get (Eq. 1-19):

$$DC = 0.011\frac{1.486}{n}\frac{W^2 R^{\frac{1}{6}}}{d\sqrt{g}} \qquad \textbf{Eq. 1-19}$$

Which shows *DC* is not directly a function of discharge or velocity, although width and depth do change with discharge, but the change is secondary to discharge/velocity change. Eq. 1-19 shows the wider the channel, the larger the coefficient.

Eq. 1-16 has been found to agree with observations within a factor of 4 or so in real streams (Fischer, et al. 1979). The book also listed experimental measurement data for Sacramento River as 15 m^2/s (161 ft^2/s) with depth 4 m, mean velocity 0.53 m/s. *DC* can be calculated as 93 ft. The exact location is not known.

Most part of the Delta is influenced by tidal flow. The tidal flow effects have to be considered. Equations for dispersion coefficient in estuaries (Fischer, et al. 1979) may be used to consider tidal effects. Values of the longitudinal dispersion coefficient in estuaries are approximately in the range of 100-300 m^2/s (1000-3000 ft^2/s) (Fischer, et al. 1979). The book also listed the value for San Francisco Bay as 200 m^2/s.

Dispersion is a complicated process, and is influenced by river irregularity, curvature, and tidal effects, etc. We have not so far been successful using empirical formulas to predict the coefficients. From the

[2] In our prototype code, the user input values for *DC* are scaled down by 1500, i.e., a user input value of 2.0 corresponds to DC=2.0*1500 = 3000. Users might feel more comfortable to calibrate a coefficient between 0 to 2 than 0 to 3000, although they are actually the same. The coefficient is strongly related to river geometry, with bigger value for the wider reaches near downstream. We are still actively discussing the most user-friendly form input for our official release of v8.1.

literature and initial trial runs, the range for *DC* in Delta is most likely between 100 in small channels to about 2000 in the large channels near Martinez, with a strong correlation to channel width. Calibration based on field data should be performed to find the appropriate value for each reach.

1.4 Tests Using DSM2 Historical Setup

The DSM2 historical run setup was used to test the models. The runs are from July 1, 1996 to July 1, 1998. Figure 1-14 to Figure 1-17 show that the new model converges well with various time steps. Figure 1-18 to Figure 1-21 show the new model converges well with different parcel sizes.

A natural question is: what is the bottom line? How much will this change results? The new model needs a fresh calibration to find proper dispersion coefficients for each channel. A trial run by merely rescaling all the original dispersion coefficients by 1500 produced similar results as previously calibrated. Figure 1-22 and Figure 1-23 show historical results for using DSM2-Qual v8.0.5 with a 15 minute time step (red line) compared to DSM2-Qual v8.1 (green line) and field data (blue dots).

We hope to see numerous benefits from the modifications in version 8.1, including a greater tendency to get answers for the "right reason"—apportioning advection and dispersion correctly, eliminating numerical diffusion in the advection scheme, and making the interpretation of calibrated parameters less arbitrary.

With a 5 minute time step, the model runs 9 minutes for the 2 year historical run with 3.2 GHz PC, which means 72 minutes for 16 year planning run. The new model is slower compared to the original model (about 48 minutes for 16 year run with 5 minute time step). Slowness may be due to a greater number of parcels and more subcycles in dispersion calculations.

1.5 Conclusions

- The new model with corrections to advection and dispersion formulation shows good convergence with respect to time step and parcel size.
- Recommended time step is 5 minute, and minimum parcel size 500 feet.
- The new model is expected to do a better job of partitioning transport into advection and dispersion and may be easier to calibrate.
- The prediction of dispersion coefficient using empirical formulas is not recommended. Calibration seems the only feasible way to determine the coefficients.
- The new model is slower compared to the original model (72 minutes for 16 year planning run with 3.2 GHz PC), but still fast enough for planning studies.
- The new model needs to be calibrated before we can compare new results with previous model results thoroughly. However, early indication is that model results can be coerced to be very similar.

1.6 References

Fischer, H. B., E. J. List, R. C.Y. Koh, J. Imberger, and N. H. Brooks. *Mixing in Inland and Coastal Waters.* Academic Press, 1979.

Rutherford, J. C. *River Mixing.* John Wiley & Sons, 1994.

Schoellhammer, D. H., and H. E. Jobson. *Programmers Manual for a One-dimensional Lagrangian Transport Model.* Manual, U.S. Geological Survey, 1986.

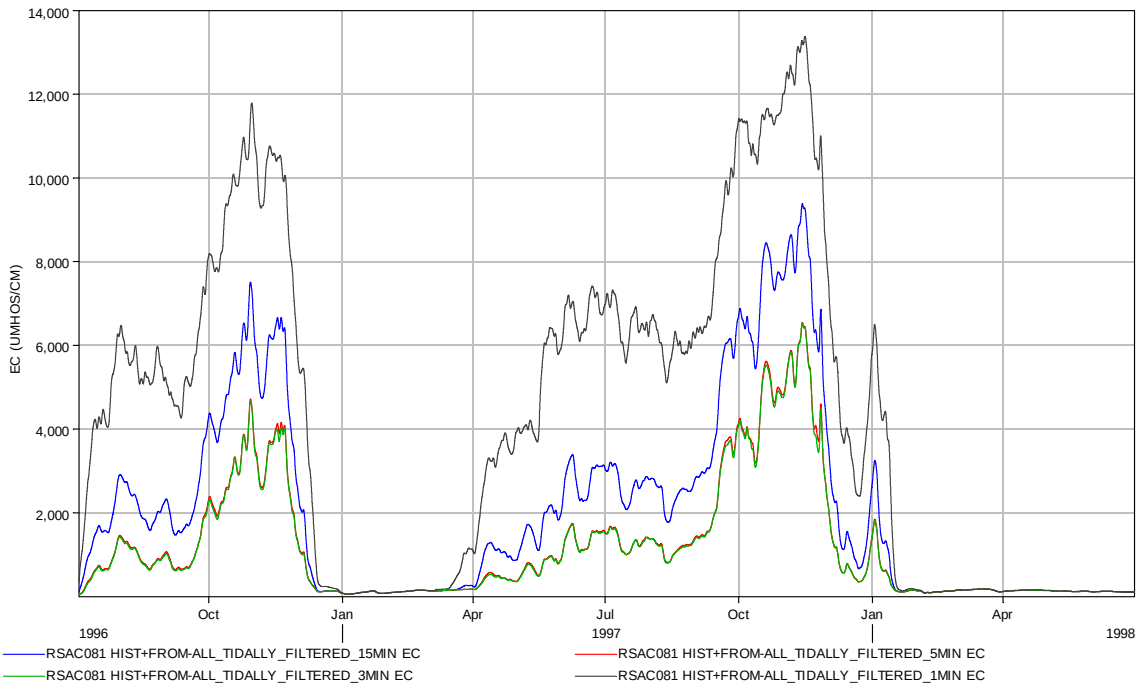

Figure 1-4 Previous model result at Collinsville

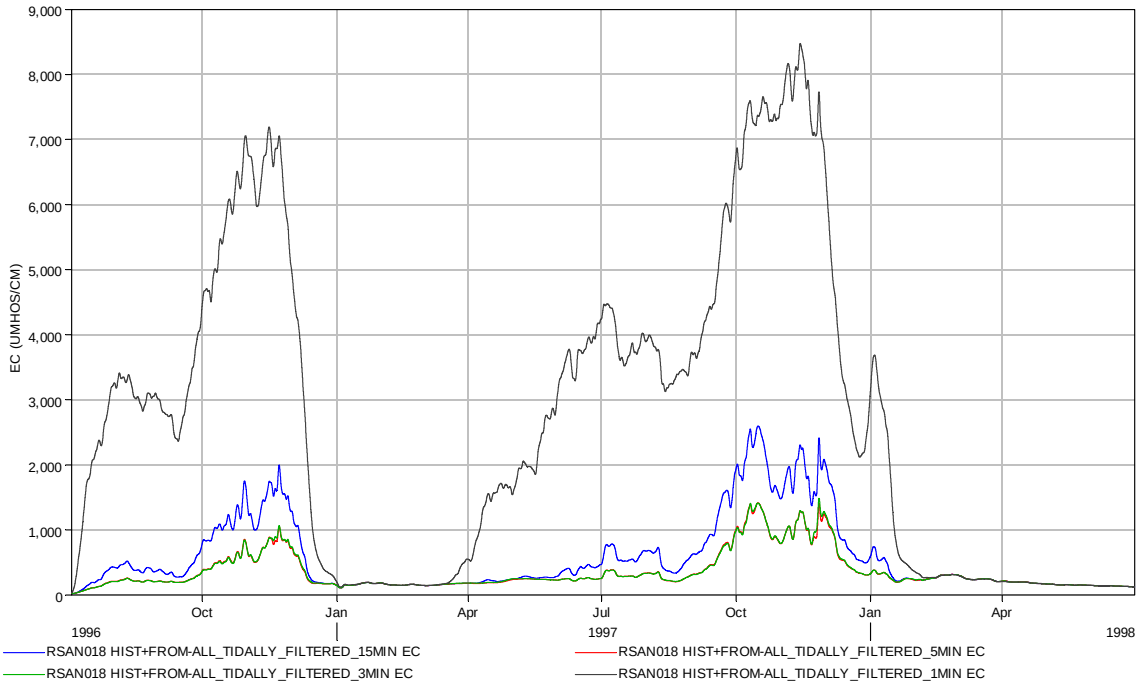

Figure 1-5 Previous model result at Jersey Point

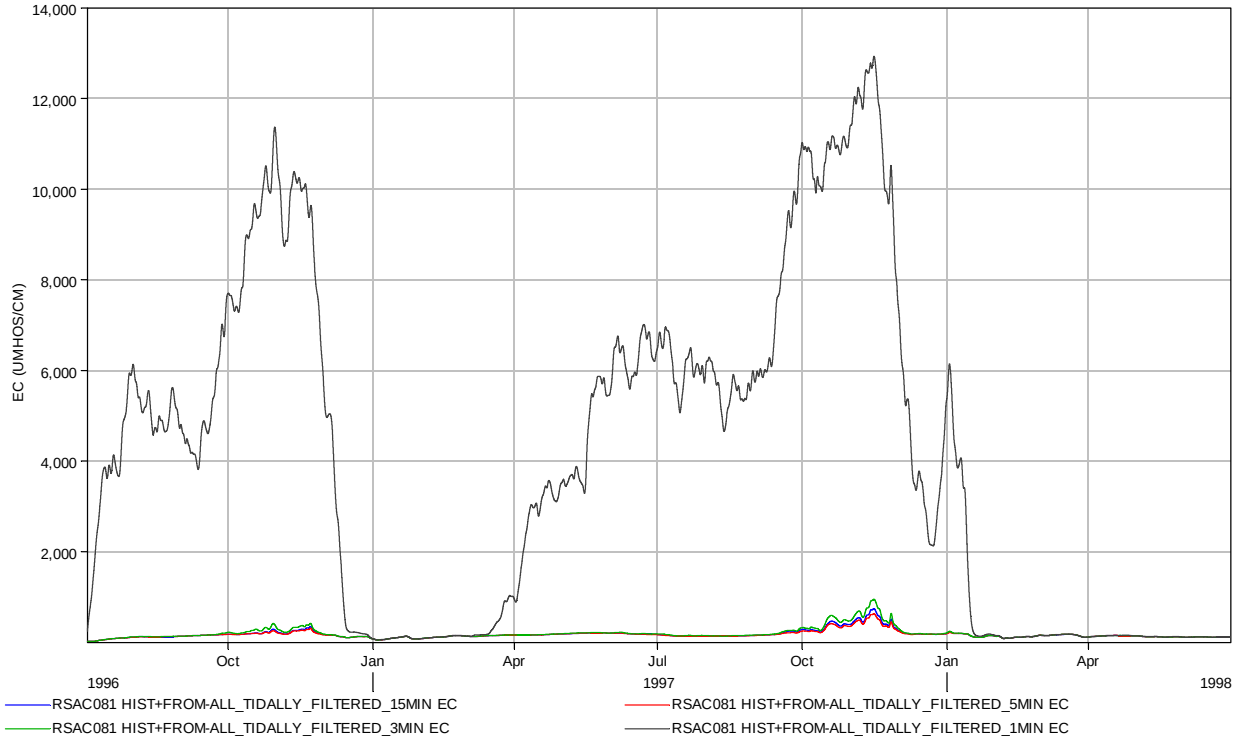

Figure 1-6 Previous model advection only result at Collinsville

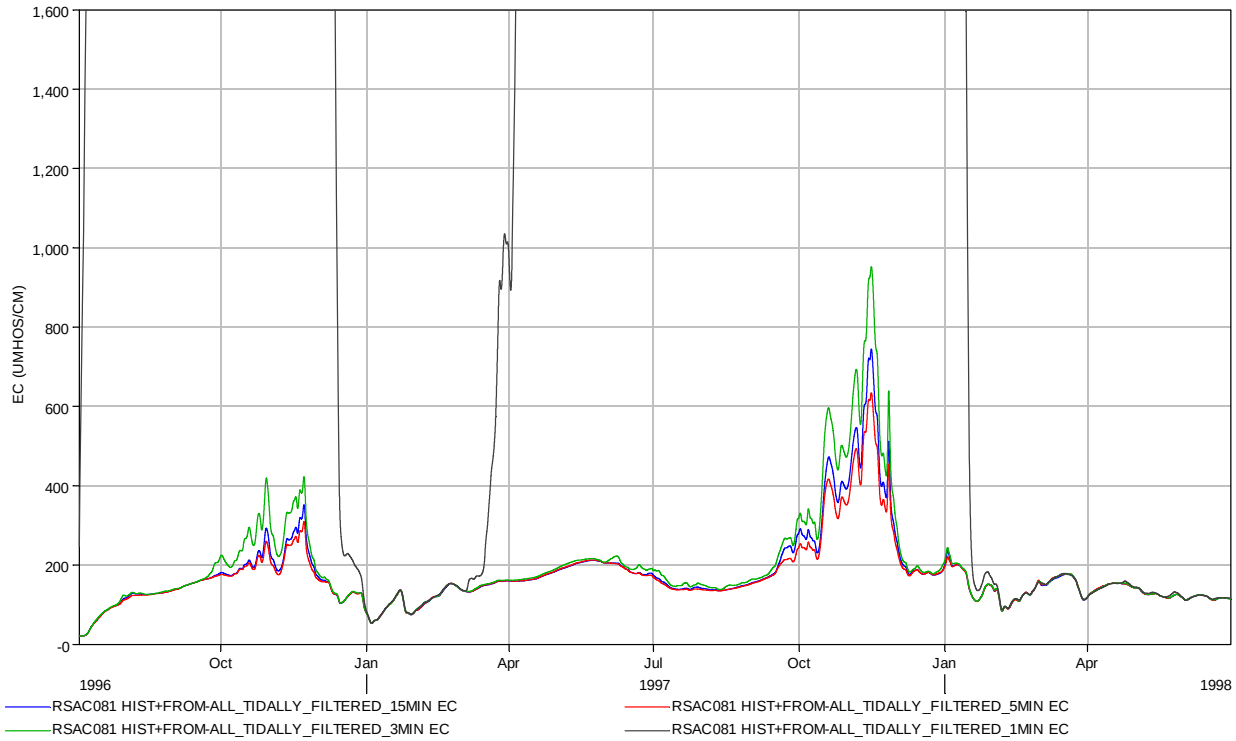

Figure 1-7 Previous model advection only result at Collinsville (zoom in)

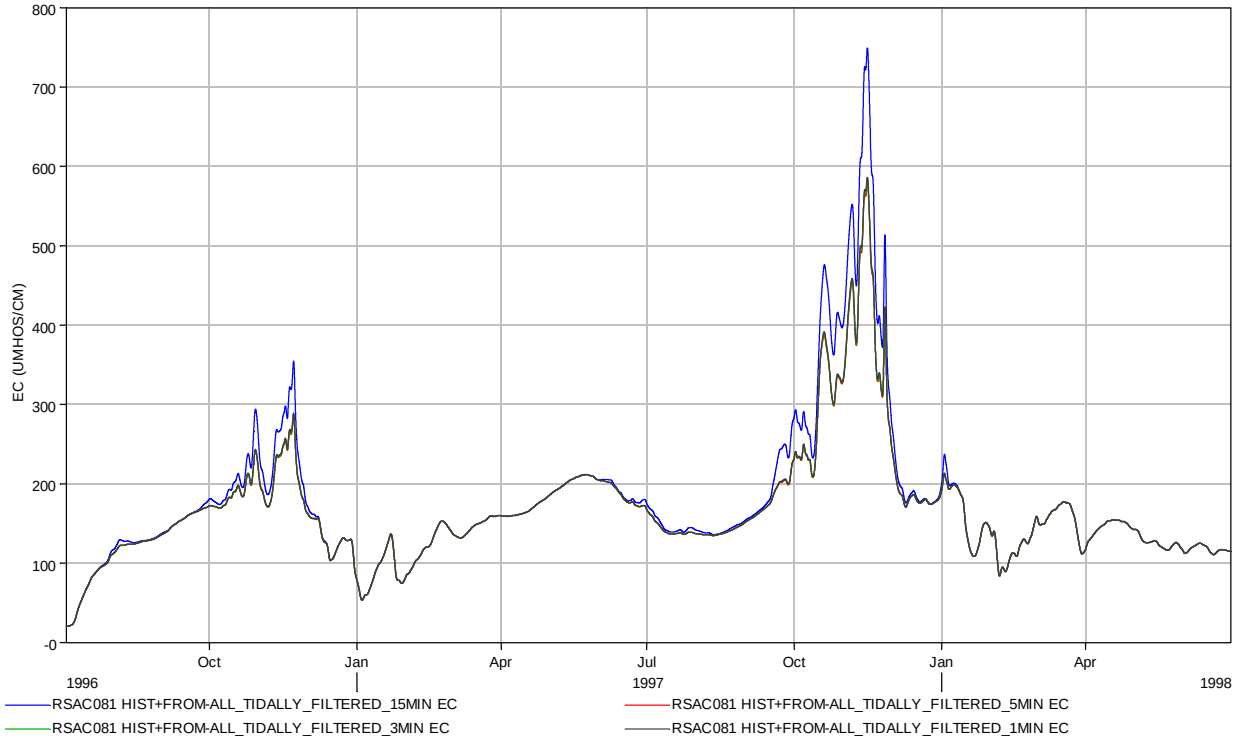

Figure 1-8 New model, advection-only at Collinsville, convergence at 15, 5, 3, 1 min time steps

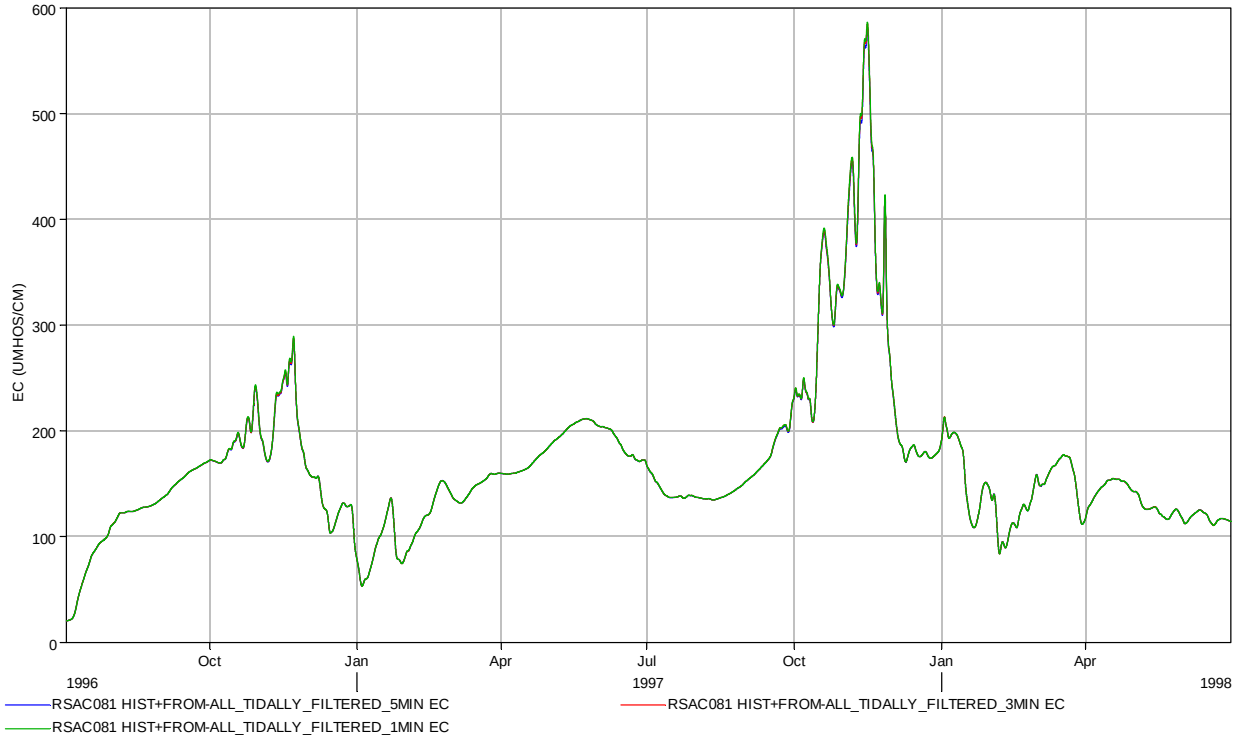

Figure 1-9 New model, advection-only at Collinsville, convergence at 5, 3, 1 min time steps

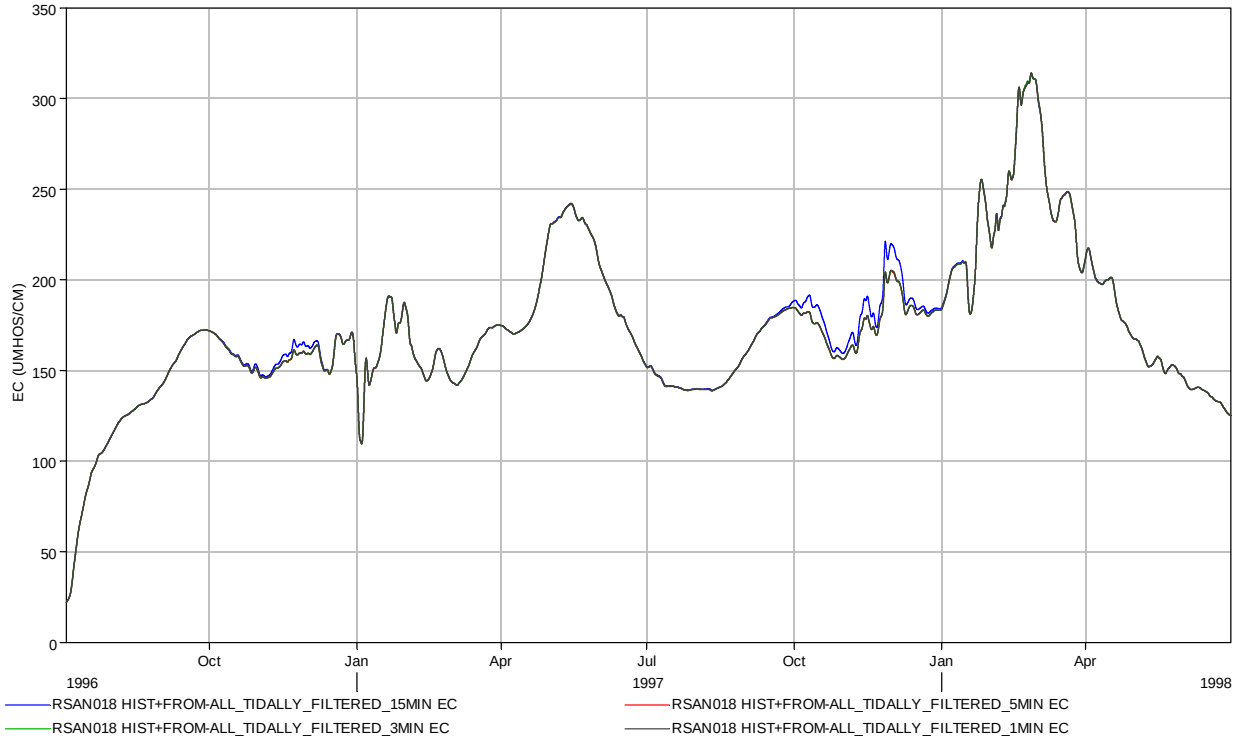

Figure 1-10 New model, advection-only at Jersey Pt., convergence at 15, 5, 3, 1 min time steps

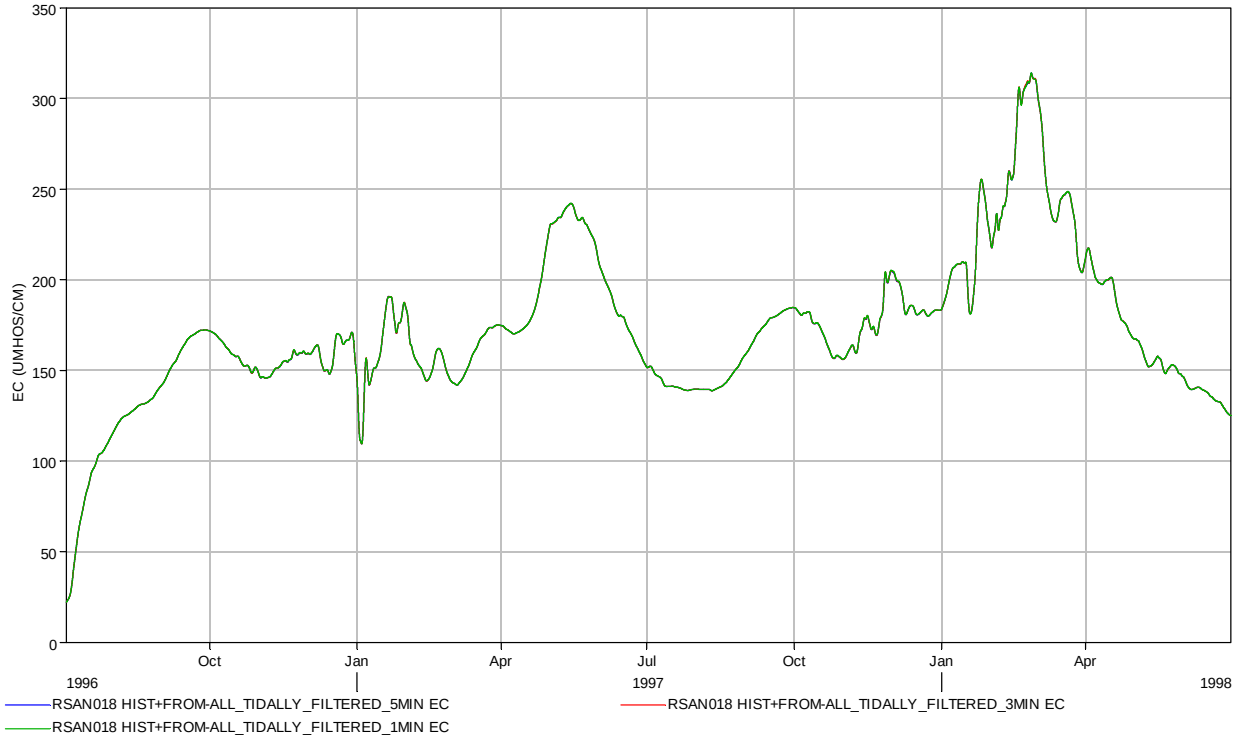

Figure 1-11 New model, advection-only at Jersey Pt., convergence of 5, 3, 1 minute time steps

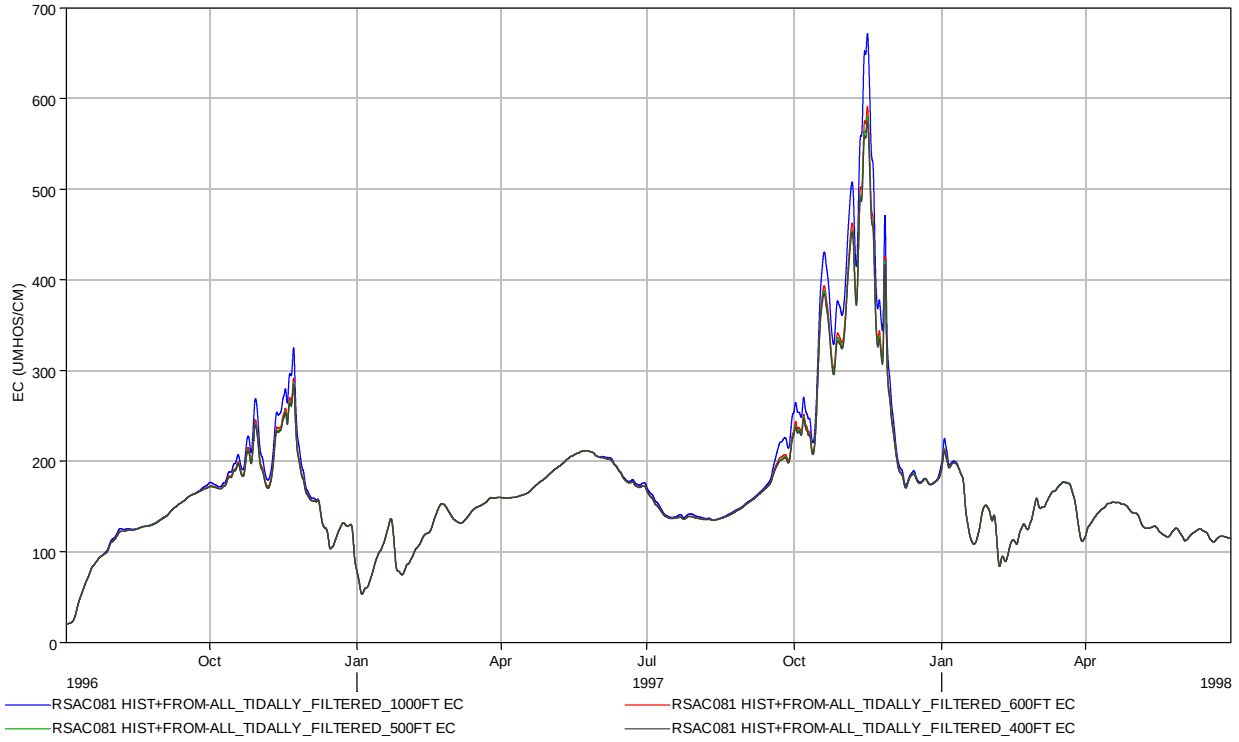

Figure 1-12 New model, advection-only at Collinsville (parcel size sensitivity test, *dt*=5 min)

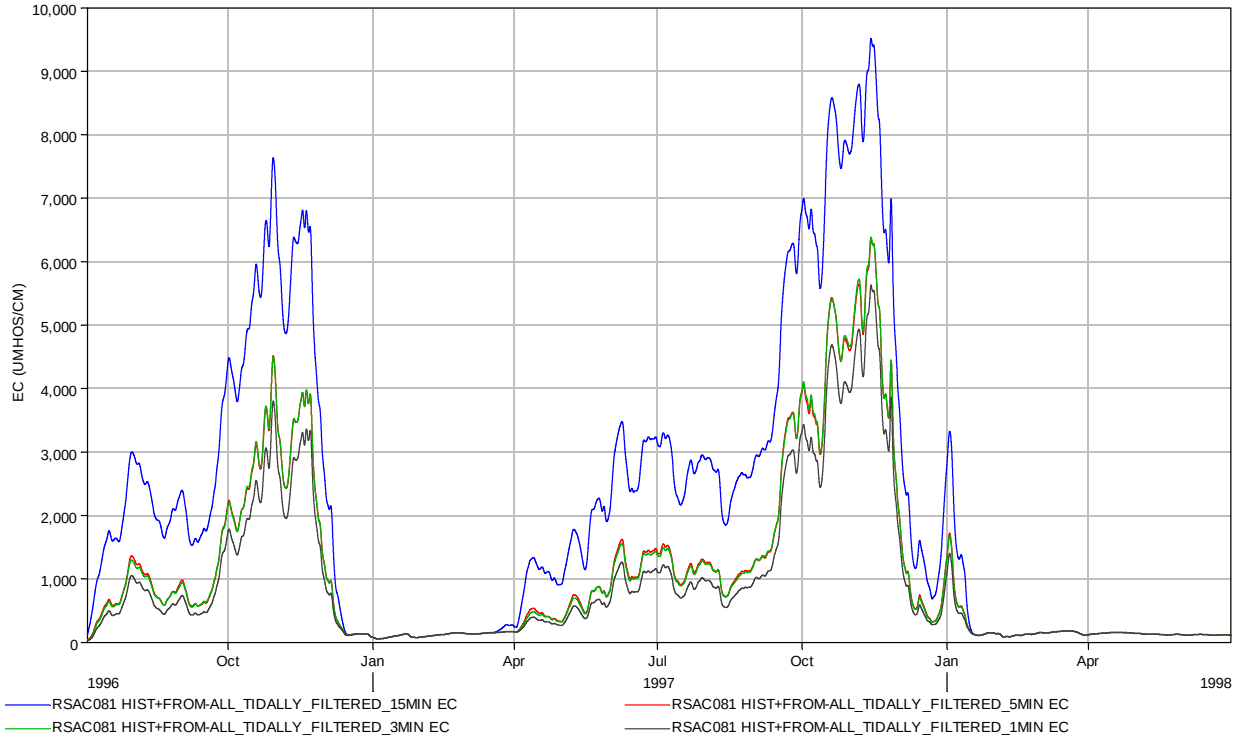

Figure 1-13 Result with previous dispersion model after advection fix at Collinsville

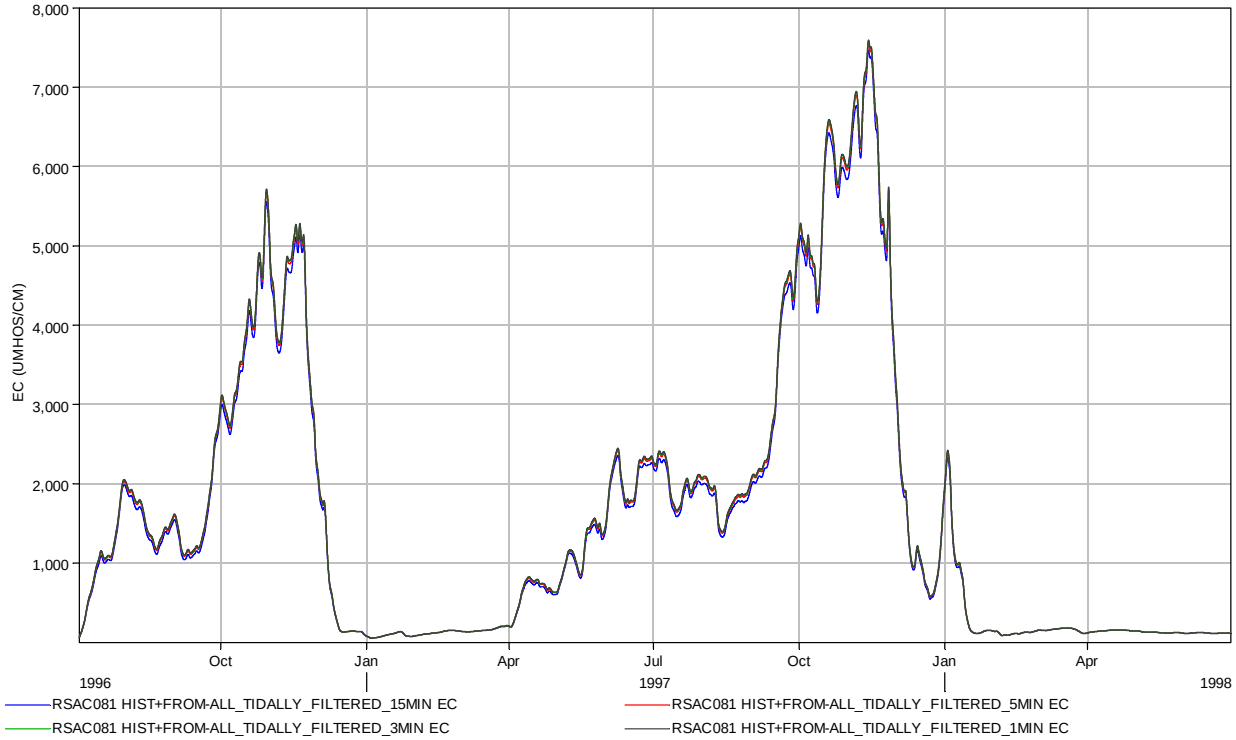

Figure 1-14 New model, result at Collinsville (time step sensitivity test, parcel size 500 ft)

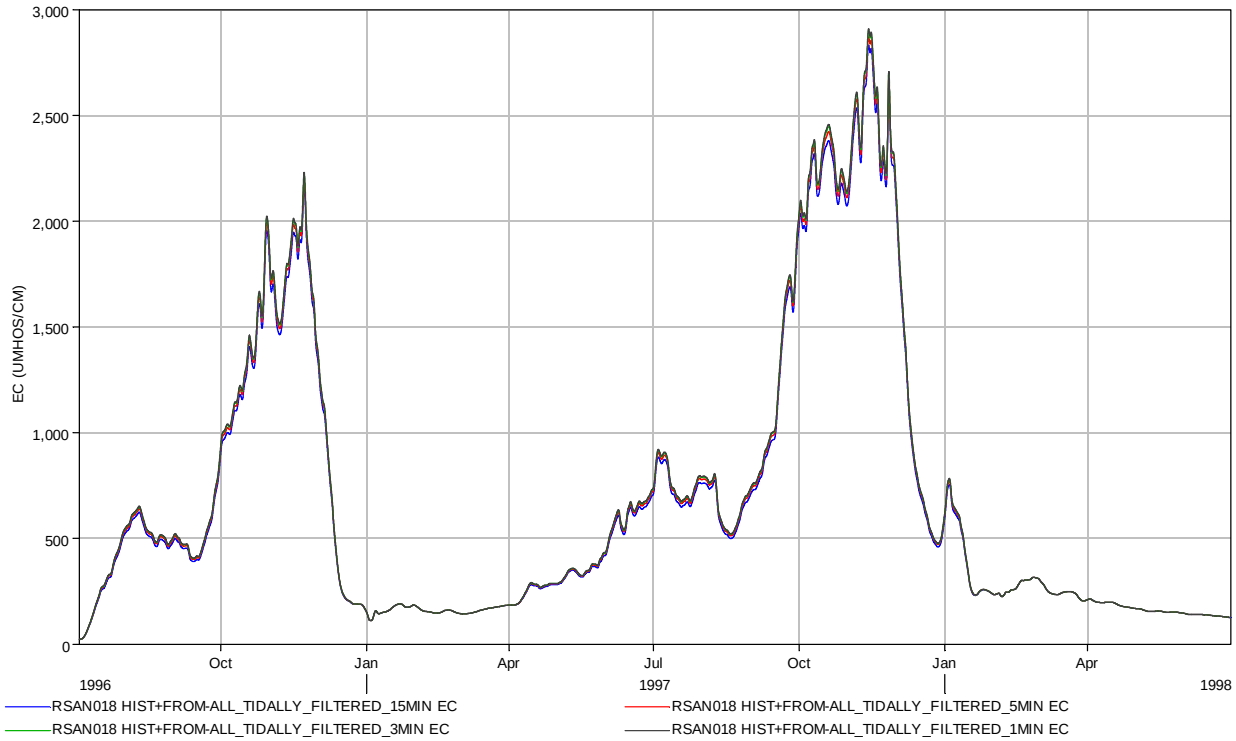

Figure 1-15 New model, result at Jersey Point (time step sensitivity test, parcel size 500 ft)

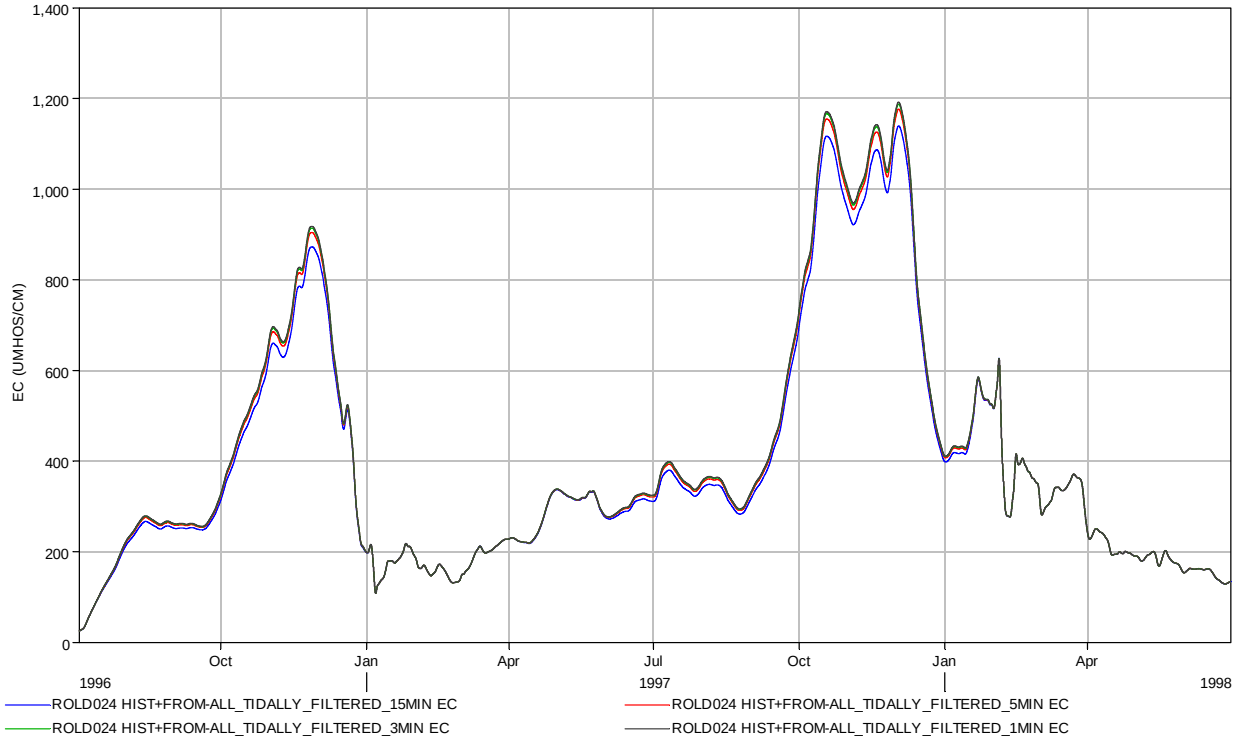

Figure 1-16 New model, result at Bacon Island (time step sensitivity test, parcel size 500 ft)

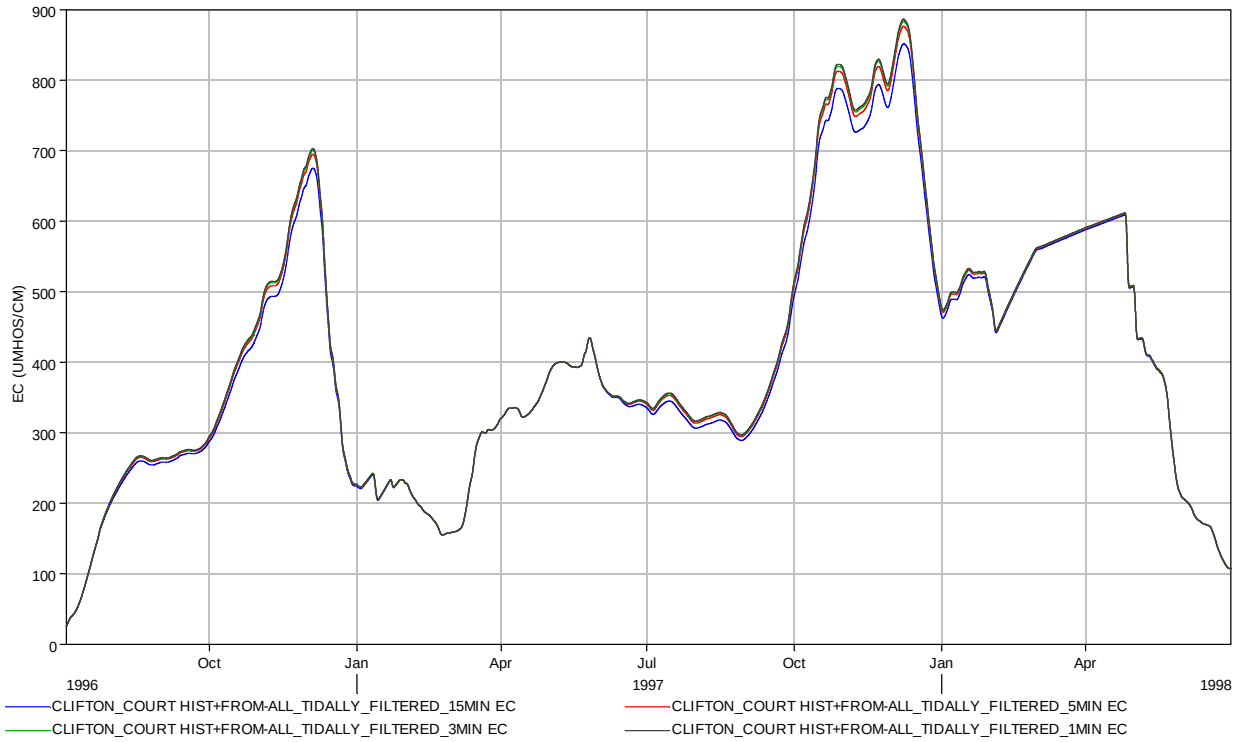

Figure 1-17 New model, result at Clifton Court (time step sensitivity test, parcel size 500 ft)

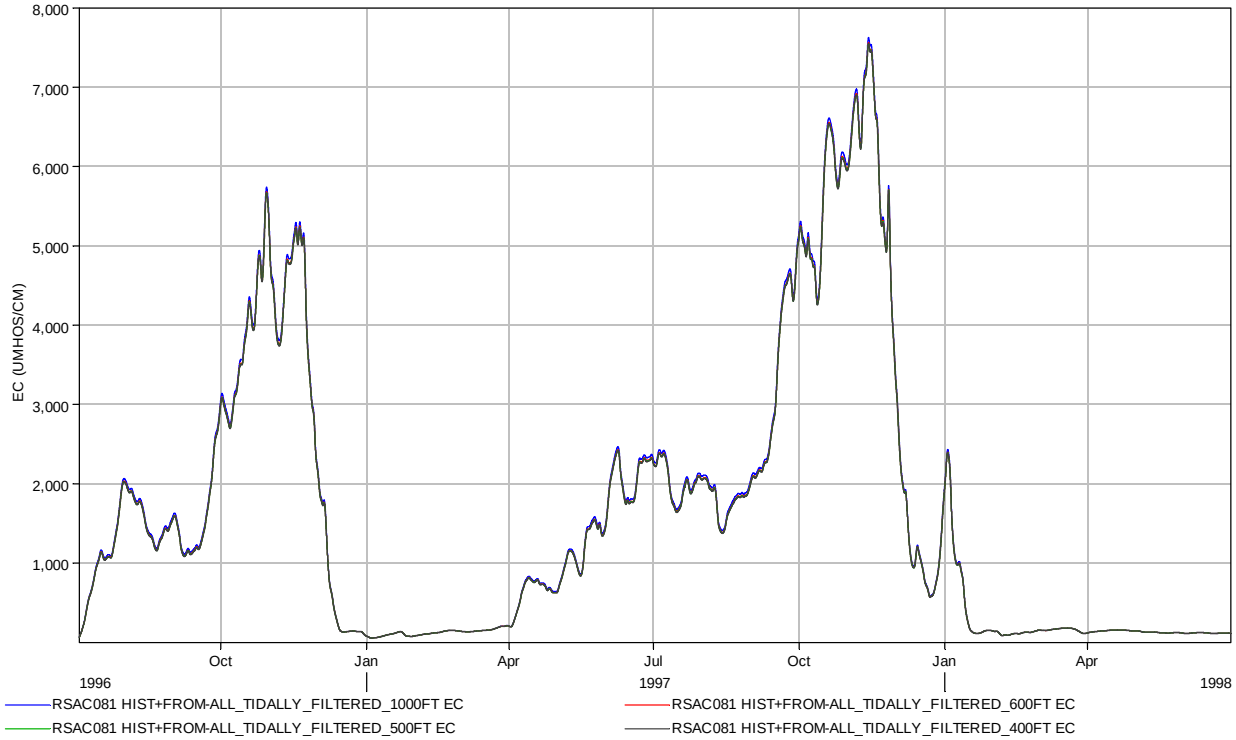

Figure 1-18 New model, result at Collinsville (parcel size sensitivity test, time step=5min)

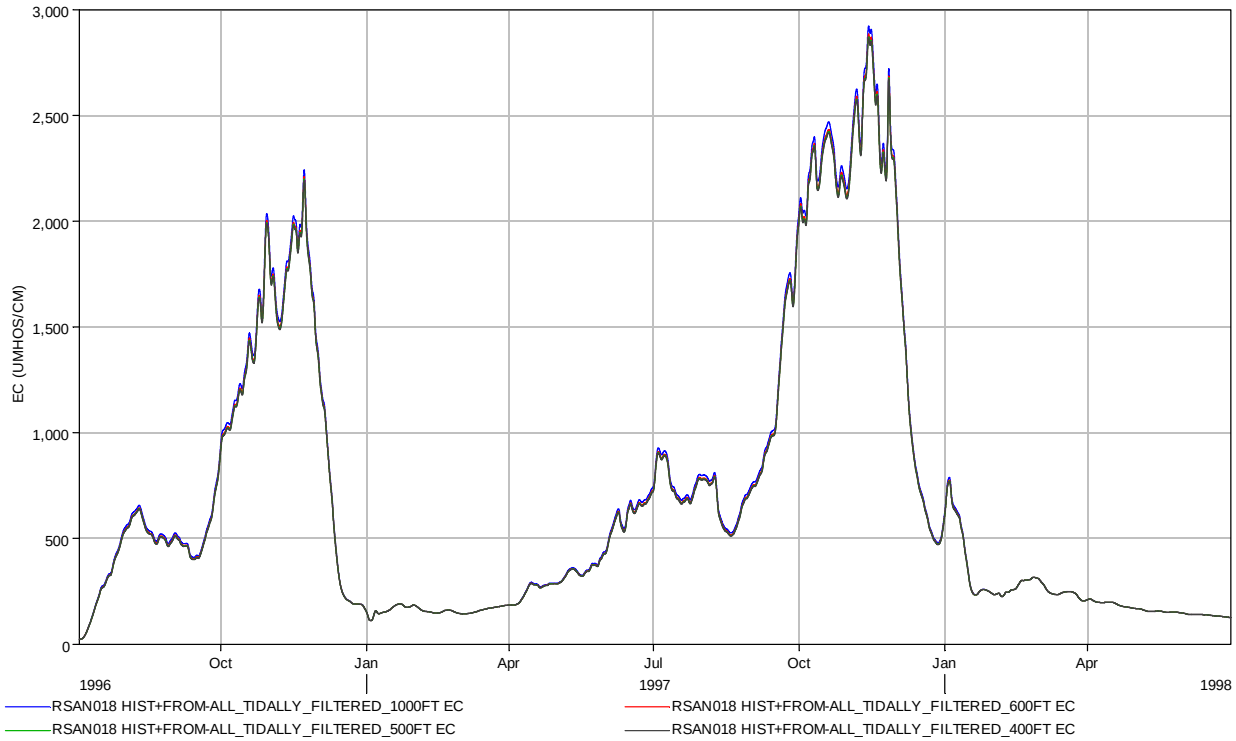

Figure 1-19 New model, result at Jersey Point (parcel size sensitivity test, time step=5min)

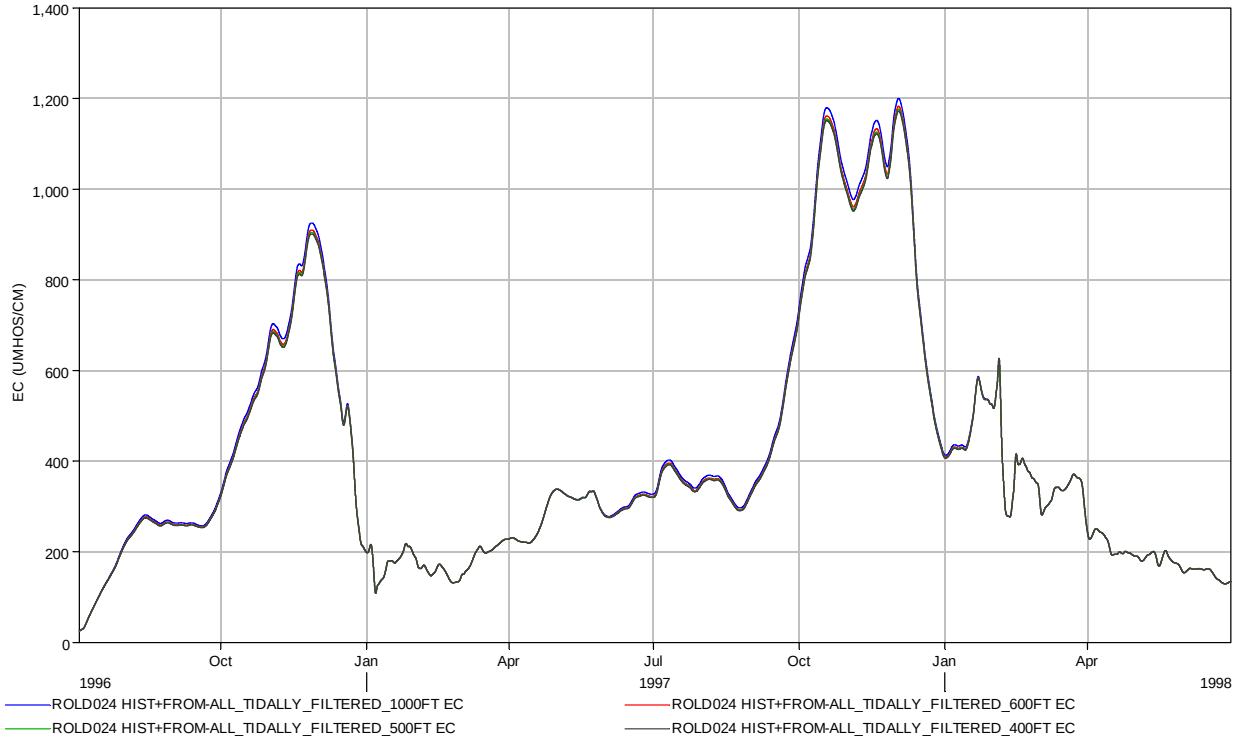

Figure 1-20 New model, result at Bacon Island (parcel size sensitivity test, time step=5min)

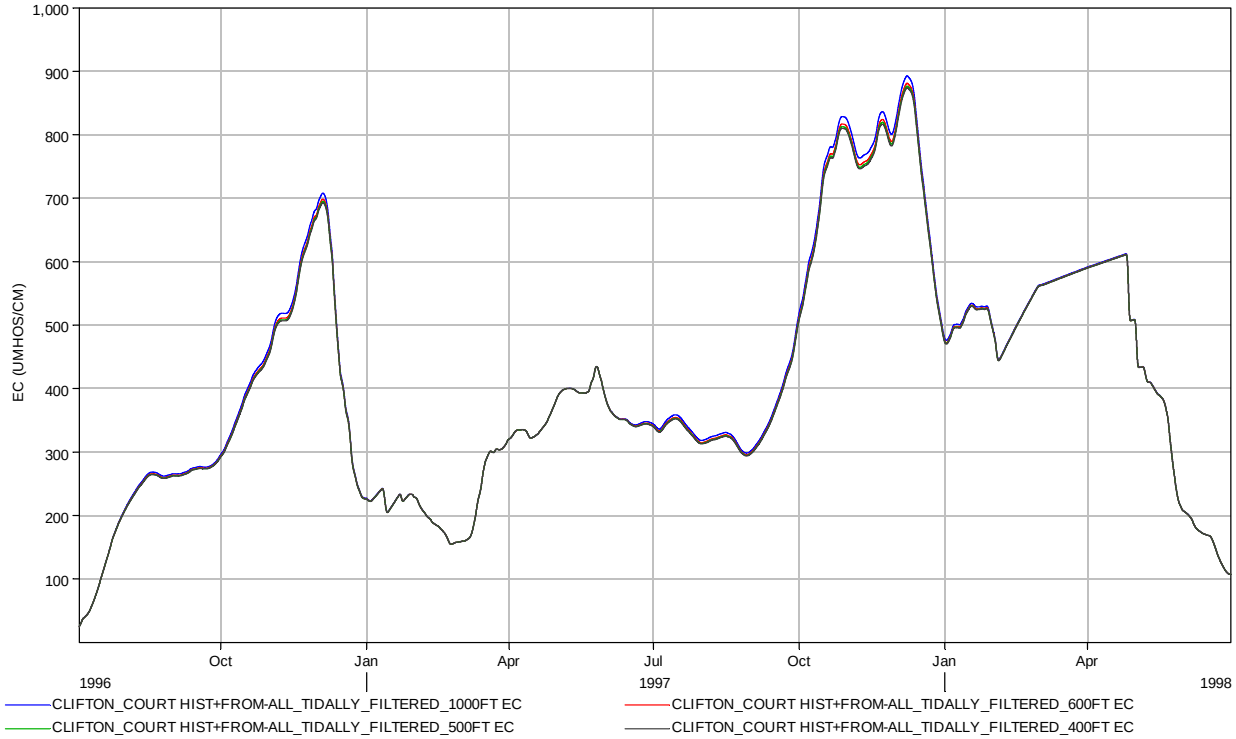

Figure 1-21 New model, result at Clifton Court (parcel size sensitivity test, time step=5min)

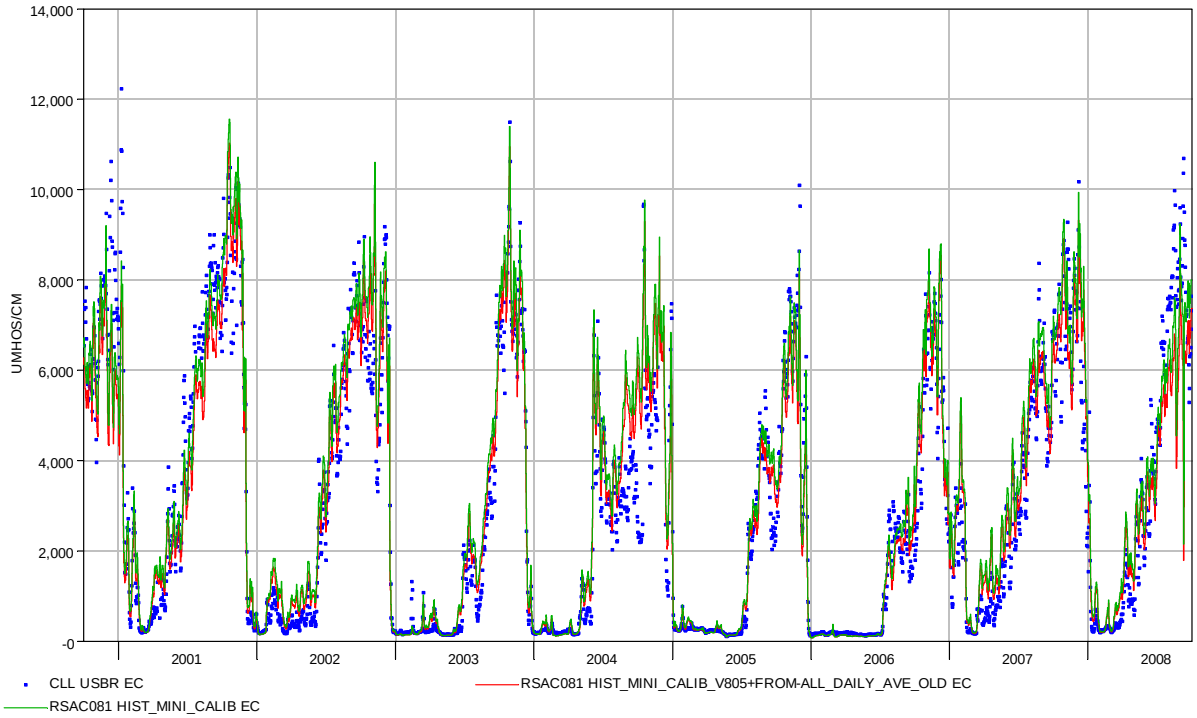

Figure 1-22 Comparison of previous (red line) and new (green) model results with field data (blue dots) at Collinsville

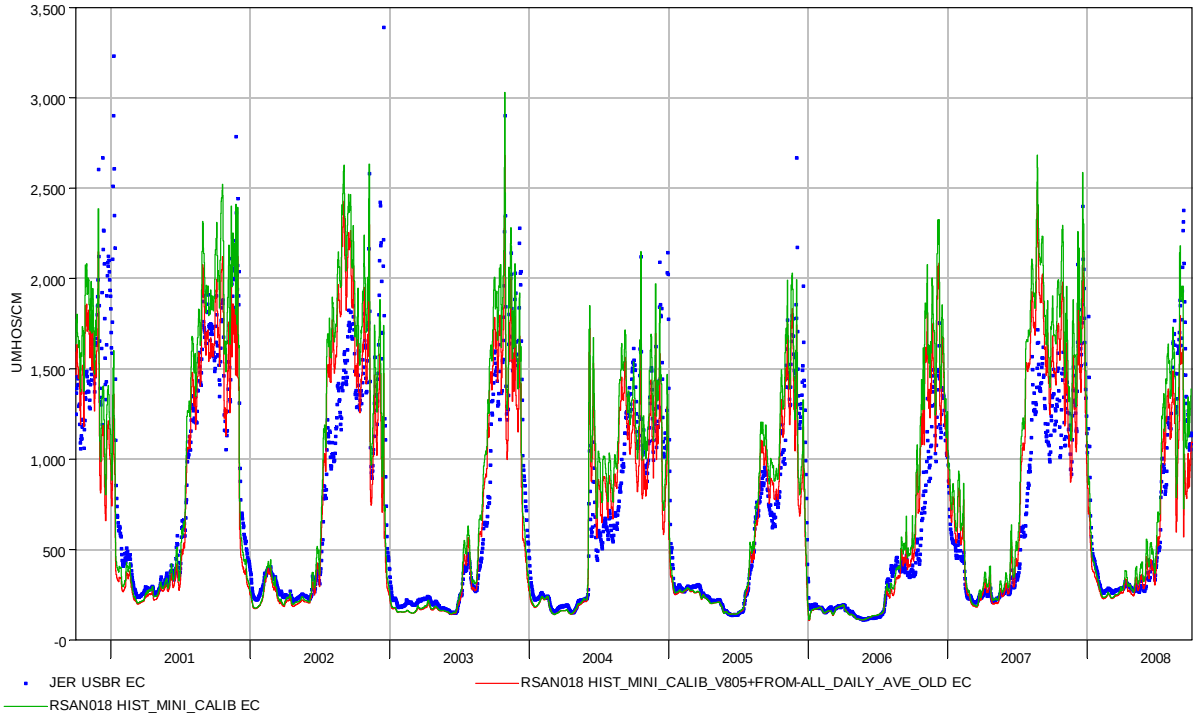

Figure 1-23 Comparison of previous (red line) and new (green) model results with field data (blue dots) at Jersey Point

Methodology for Flow and Salinity Estimates in the Sacramento-San Joaquin Delta and Suisun Marsh

32nd Annual Progress Report
June 2011

Chapter 2
Improvements to DSM2-Qual: Part 2

Authors: Lianwu Liu and Prabhjot Sandhu
Delta Modeling Section,
Bay Delta Office,
California Department of Water Resources

Contents

2 Improvements to DSM2-Qual: Part 2 2-1
2.1 Introduction 2-1
2.2 Testing Scenarios and Result Analysis 2-1
2.2.1 Test 1: Compare With the Old Solver 2-1
2.2.2 Test 2: Test Minimum Dispersion Velocity (0.01 ft/s) 2-1
2.2.3 Test 3: Test Cold Start 2-2
2.3 Conclusions 2-2
2.4 References 2-2
Appendix 2-A 2-3
Appendix 2-B 2-4
Appendix 2-C 2-9

Figures

Figure 2-1 Delta Cross Channel (instantaneous, MDV=0 and 0.01) 2-5
Figure 2-2 Delta Cross Channel (monthly average, MDV=0 and 0.01) 2-5
Figure 2-3 Montezuma Slough (instantaneous, MDV=0 and 0.01) 2-6
Figure 2-4 Montezuma Slough (monthly average, MDV=0 and 0.01) 2-6
Figure 2-5 Montezuma Slough (monthly average, MDV=0 and 0.1) 2-7
Figure 2-6 Montezuma Slough (monthly average, MDV=0 and 0.001) 2-7
Figure 2-7 Old River at Tracy Road (instantaneous, ammonia) 2-8
Figure 2-8 Old River at Tracy Road (monthly average, ammonia) 2-8
Figure 2-9 Mallard Island cold vs. warm start, algae 2-9
Figure 2-10 Mallard Island cold vs. warm start, phosphate 2-10
Figure 2-11 Clifton Court cold vs. warm start, algae 2-10

Table

Table 2-1 Summary of maximum monthly percent difference 2-3

2 Improvements to DSM2-Qual: Part 2

2.1 Introduction

This chapter documents tests of Delta Simulation Model II (DSM2) Version 8.0.5 (release 8.0.6). The Bogacki-Shampine algorithm (Bogacki–Shampine method 2009) was implemented in the nutrient model to avoid negative value problems in the old solver. Also in Version 8.0.5, the user can set the minimum dispersion velocity (defined as `min_disperse_vel` in DSM2 input file) to avoid zero-dispersion problems at dead-end channels/closed gates.

2.2 Testing Scenarios and Result Analysis

The simulations used the historical run setup from July 1, 1996, to December 31, 2000.

2.2.1 Test 1: Compare With the Old Solver

In test 1, compare with the old non-conservative constituent solver, the minimum dispersion velocity was set to 0 to be consistent with the old model run. A restart file was used as the initial condition. The results are plotted and summarized in Appendix 2-A. Electrical conductivity (EC) results are identical and not plotted. The maximum monthly averaged difference of temperature is 0.06%. The maximum monthly averaged difference of dissolved oxygen (DO) is 1.3% at RSAC075. The differences are small enough to believe that both models are working properly in this historical run setup.

2.2.2 Test 2: Test Minimum Dispersion Velocity (0.01 ft/s)

In test 2, test minimum dispersion velocity, two historical runs were made with minimum dispersion velocities set to 0 and 0.01 feet per second. The results are plotted and summarized in Appendix 2-B.

Conservative Constituent (EC) Comparison

The maximum monthly averaged EC difference for Emmaton, Jersey Point, Rock Slough, Collinsville, and Clifton Court Forebay is less than 0.2%. This shows that a minimum dispersion velocity of 0.01 ft/s will not change the general results in main channels in Delta.

The minimum dispersion velocity helps mixing at dead-end channels or channels with gates; see plots for Delta Cross Channel in Appendix 2-B (Figure 2-1 and Figure 2-2).

The difference of EC in Montezuma Slough near the salinity control structure at SLMZU025 is larger as a percentage; maximum difference in this case is 5.6%.

A test with minimum dispersion velocity set to 0.1 ft/s showed bigger differences in the Delta (e.g., 0.7% at ROLD024, 0.6% at Clifton Court Forebay). Another test with minimum dispersion velocity set to 0.001 ft/s showed much smaller differences. The maximum difference becomes 1.5% at SLMZU025, but it may not give enough dispersion near dead ends.

Non-conservative Constituents

Comparisons are plotted at stations RSAC075, ROLD059, RSAN058, and Clifton Court. The instantaneous percent differences can be large at times (e.g., ammonia [NH3] at ROLD059, a maximum of 8%), but maximum monthly averaged differences of all constituents are less than 1.0% at all these locations. Maximum difference at Clifton Court is less than 0.2%.

In conclusion, the differences using 0.01 ft/s are not significant, minimum dispersion velocity can be used to improve mixing at dead-end channels/gates.

2.2.3 Test 3: Test Cold Start

In test 3, test cold start, all constituents' initial value was 20, `min_disperse_vel`= 0.01 ft/s). The results were compared with a run made with proper initial condition (using restart file) and are summarized in Appendix 2-C. The results are compared at stations RSAC075, ROLD059, RSAN058, and Clifton Court. At RSAC059 and RSAN058, the constituents converge within 1 year. It takes longer to converge at RSAC075. After 2 years, the difference for algae is still 5%; phosphate (PO4) is 10%. It takes 2 years at Clifton Court to converge. A proper initial condition should be used.

2.3 Conclusions

Version 8.0.5 tested as being successful:

- The new non-conservative constituent solver (Bogacki-Shampine method) is working properly.
- Minimum dispersion velocity can be used to avoid zero dispersion problems at dead-end channels and gates. Suggest using a very small value, such as 0.01 ft/s.
- A proper initial condition (using restart file) is recommended. Cold start can take more than 2 years to converge.

2.4 References

Bogacki–Shampine method. 2009 Aug 31.
http://en.wikipedia.org/wiki/Bogacki%E2%80%93Shampine_method (accessed February 2011).

Appendix 2-A

Test 1: Compare with the old non-conservative constituent solver

The historical setup from July 1, 1996, to December 31, 2000, was run with the old solver for non-conservative constituents and Version 8.0.5 (new solver). In these runs, a restart file was used as the initial condition. The non-conservative constituent results were compared at stations RSAC075, ROLD059, RSAN058, and Clifton Court. The maximum monthly percent differences are summarized in Table 2-1. The maximum difference of any parameter and any location is DO: 1.3% at RSAC075. The differences are small and show that both solution methods are working correctly in this historical run setup.

Table 2-1 Summary of maximum monthly percent difference

Maximum % difference	RSAC075	ROLD059	RSAN058	Clifton Court
TEMP	0.06	0.06	0.05	0.06
DO	1.30	0.16	0.28	0.11
ALGAE	0.60	0.40	0.30	0.60
BOD	0.70	0.20	0.18	*
NH3	0.25	0.17	0.11	*
NO2	0.20	0.14	0.08	*
NO3	0.25	0.17	0.15	*
ORGANIC_N	0.40	0.14	0.11	*
ORGANIC_P	0.40	0.20	0.13	*
PO4	0.15	0.32	0.25	*

*did not output

Appendix 2-B

Test 2: Test of minimum dispersion velocity

Historical runs from July 1, 1996, to December 31, 2000, were made with the minimum dispersion velocity (defined as `min_disperse_vel` in the input file) set to 0.00, 0.01, 0.1, and 0.001 ft/s.

Conservative Constituent (EC)

The maximum monthly averaged EC difference between the 0.00 and 0.01 runs for Emmaton, Jersey Point, Rock Slough, Collinsville, and Clifton Court Forebay was less than 0.2%. This shows the minimum dispersion velocity of 0.01 ft/s will not change the general results in main channels within the Delta. This result makes sense because main channels seldom have flow velocities near zero, and then only briefly during a tidal change.

The minimum dispersion velocity helps mixing at dead-end channels and channels with closed gates. For instance, the maximum instantaneous or monthly average difference of EC in the Delta Cross Channel during gate closures is greater than 100% (Figure 2-1 and Figure 2-2). In Montezuma Slough north of the salinity control structure (SLMZU025), a maximum instantaneous difference of 14.1% and maximum monthly average difference of 5.6% is noted (Figure 2-3 and Figure 2-4).

A test with minimum dispersion velocity set to 0.1 ft/s showed bigger differences in the Delta (e.g., 0.7% at ROLD024, 0.6% at Clifton Court Forebay) and in Montezuma Slough (Figure 2-5). Another test with minimum dispersion velocity set to 0.001 ft/s showed much smaller differences. The maximum difference in the latter case is 1.5% at SLMZU025 (Figure 2-6), but such a low value may not give enough dispersion near channel dead ends.

Non-conservative Constituents

Comparisons were done at stations RSAC075, ROLD059, RSAN058, and Clifton Court with 15 minute intervals. The instantaneous percent differences can be large at times (e.g., NH3 at ROLD059, maximum 8%, Figure 2-7), but maximum monthly averaged differences of all constituents were less than 1.0 % at all these locations (e.g., NH3 at ROLD059, Figure 2-8). Maximum differences at Clifton Court were less than 0.2%.

In conclusion, the differences are not significant and minimum dispersion velocity can be used to improve mixing at dead-end channels/gates.

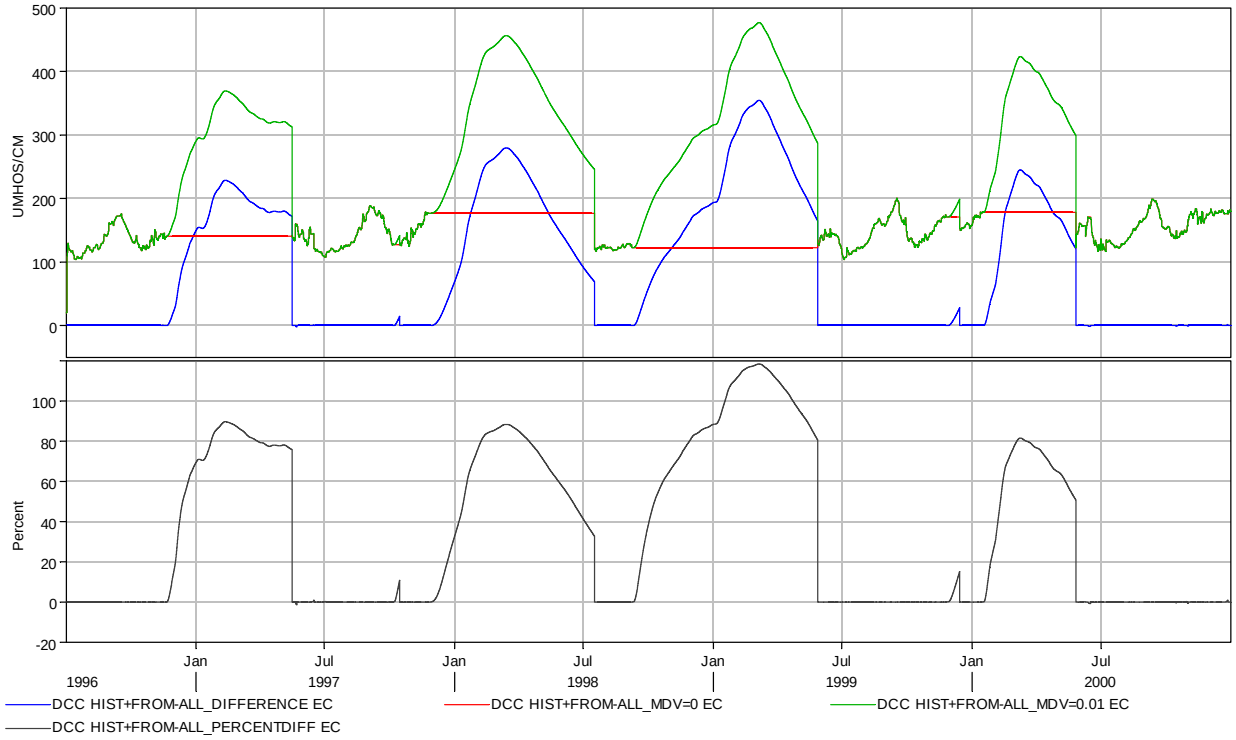

Figure 2-1 Delta Cross Channel (instantaneous, MDV=0 and 0.01)

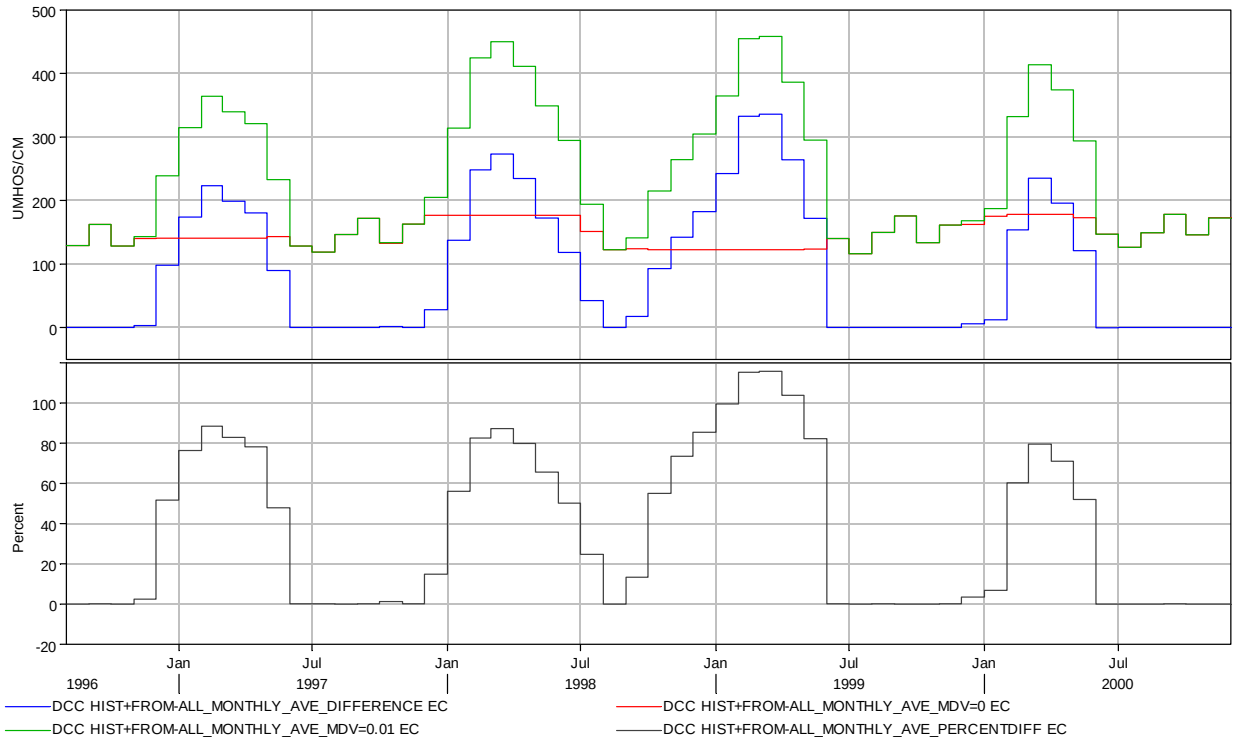

Figure 2-2 Delta Cross Channel (monthly average, MDV=0 and 0.01)

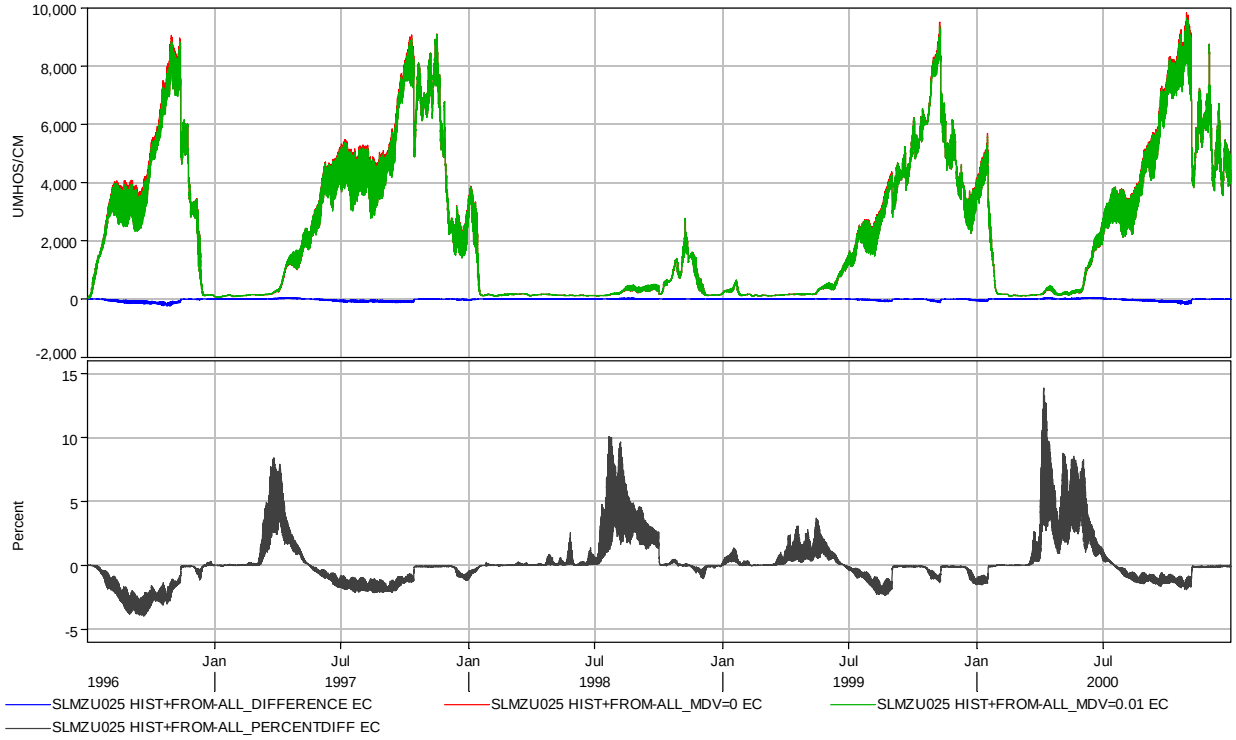

Figure 2-3 Montezuma Slough (instantaneous, MDV=0 and 0.01)

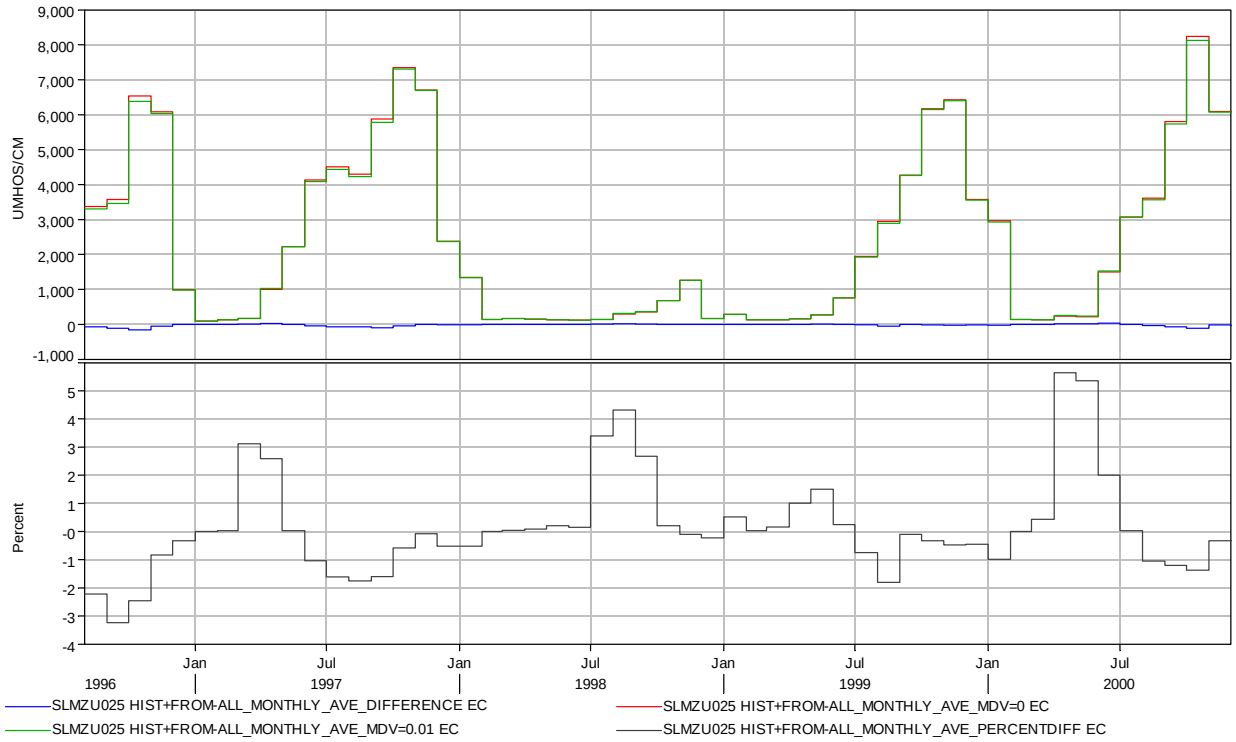

Figure 2-4 Montezuma Slough (monthly average, MDV=0 and 0.01)

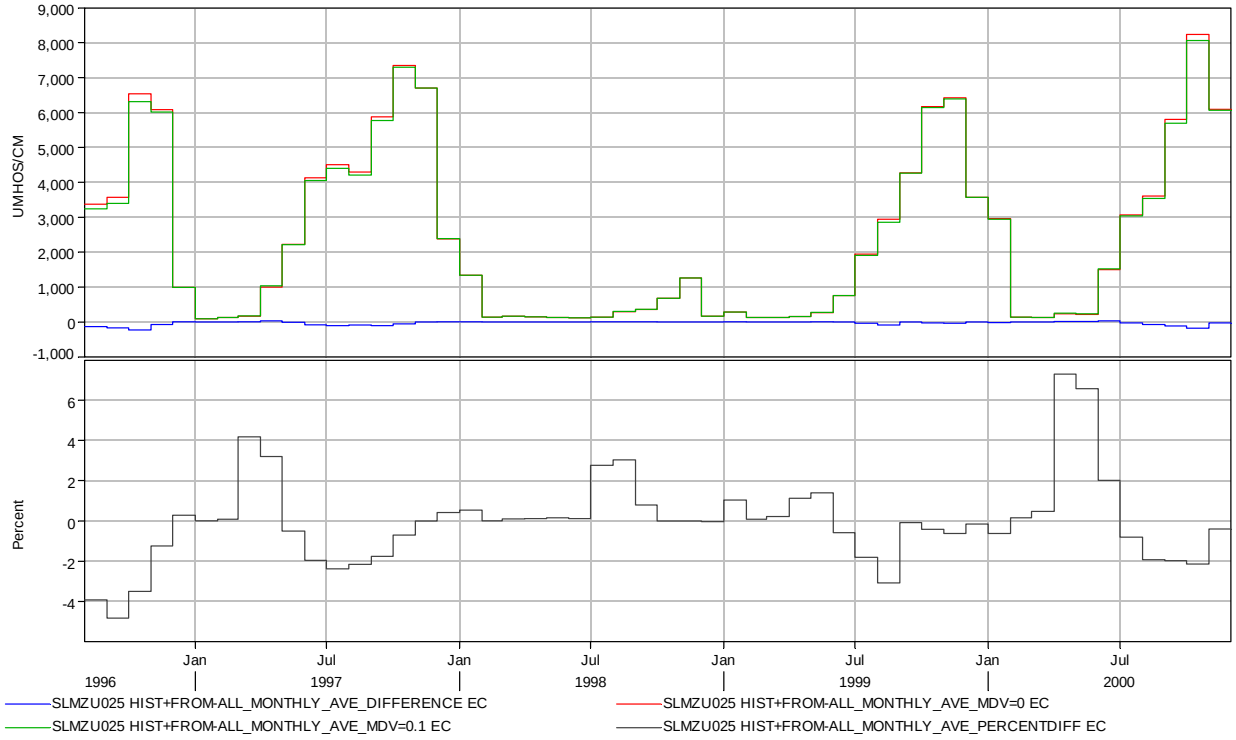

Figure 2-5 Montezuma Slough (monthly average, MDV=0 and 0.1)

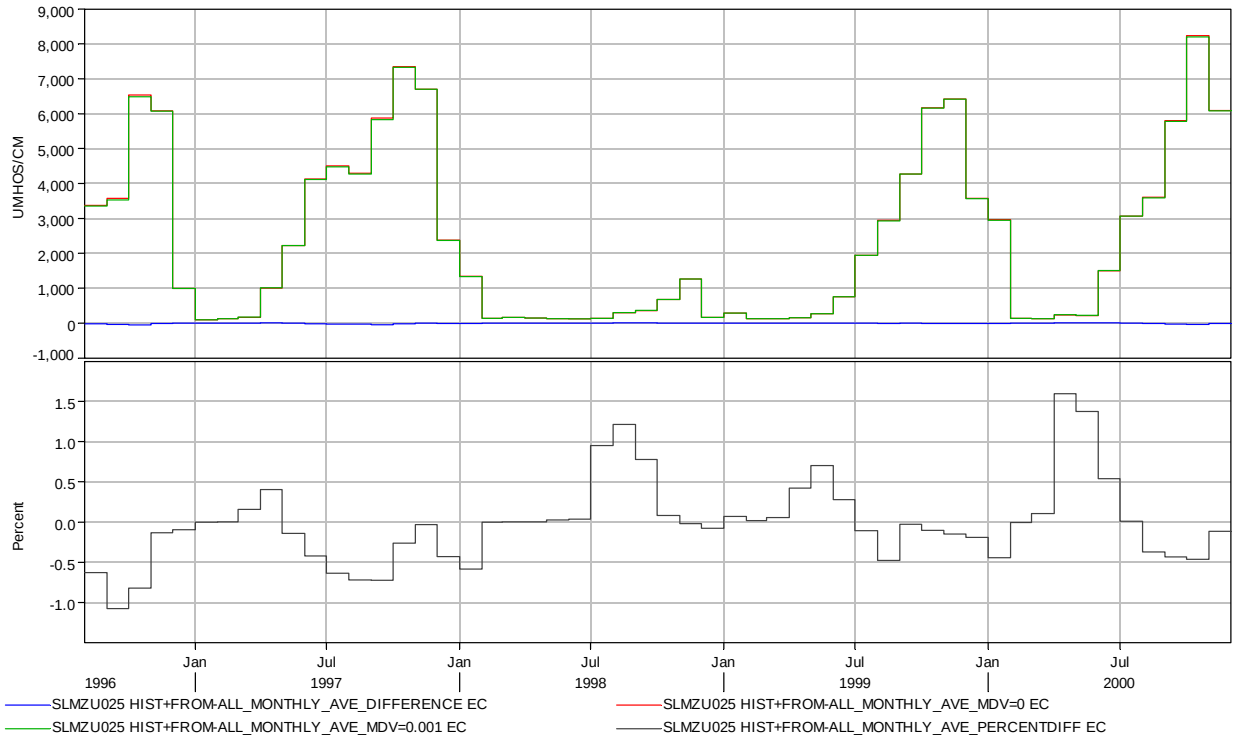

Figure 2-6 Montezuma Slough (monthly average, MDV=0 and 0.001)

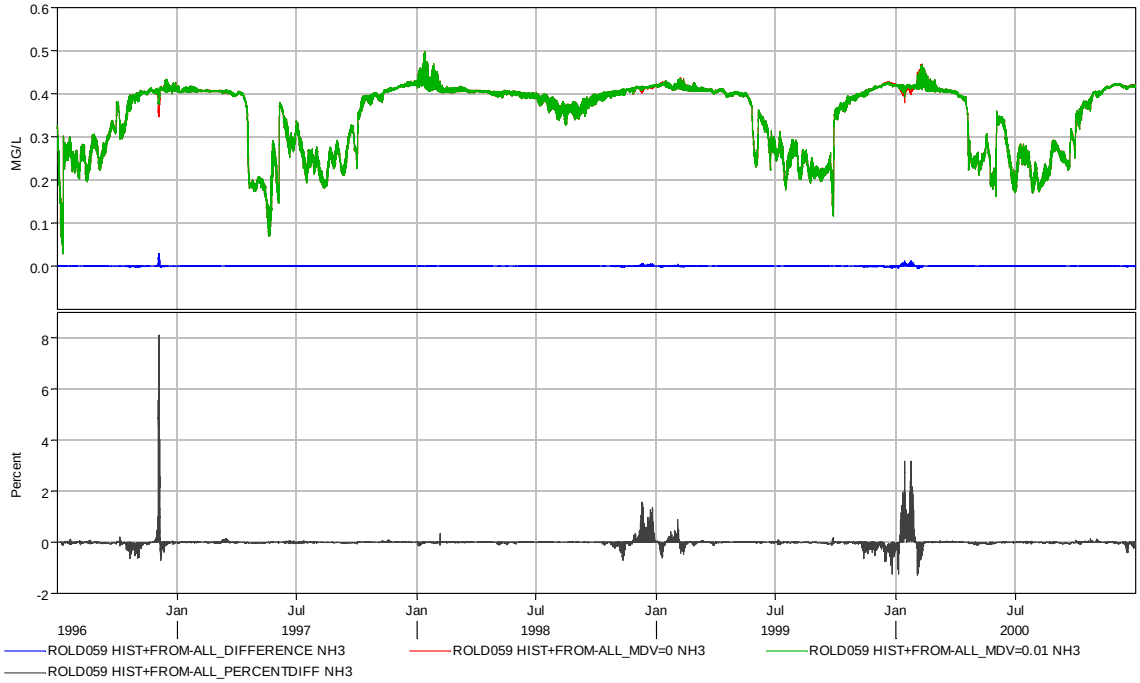

Figure 2-7 Old River at Tracy Road (instantaneous, ammonia)

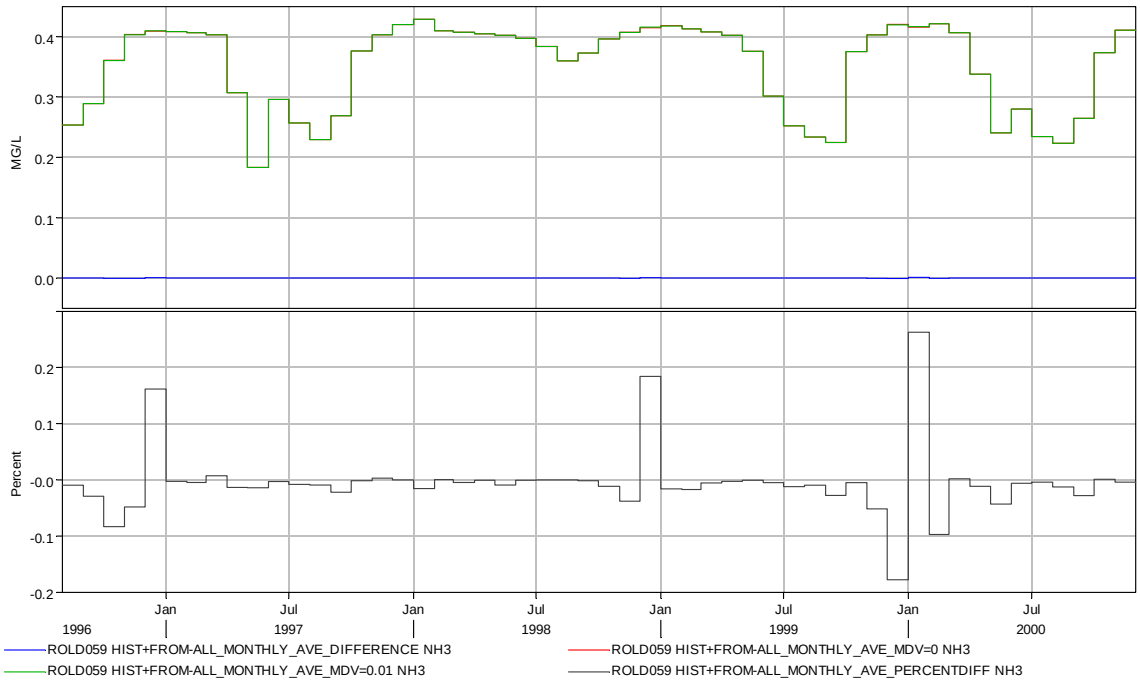

Figure 2-8 Old River at Tracy Road (monthly average, ammonia)

Appendix 2-C

Test 3: Cold Start

In test 3, a cold-start run (all constituents with initial value of 20) was made, starting with the date October 1, 1996, and continuing for several simulated years. The results were compared with a run made with proper initial condition using a restart file. The non-conservative constituent results were compared at stations RSAC075, ROLD059, RSAN058, and Clifton Court. At RSAC059 and RSAN058, all constituents converge within 1 year. It takes longer to converge at RSAC075. After a little more than 2 years (October–December 1998), the difference for algae was still 5% (Figure 2-9) and for PO4, 10% (Figure 2-10). It takes up to 2 years at Clifton Court to converge (Figure 2-11).

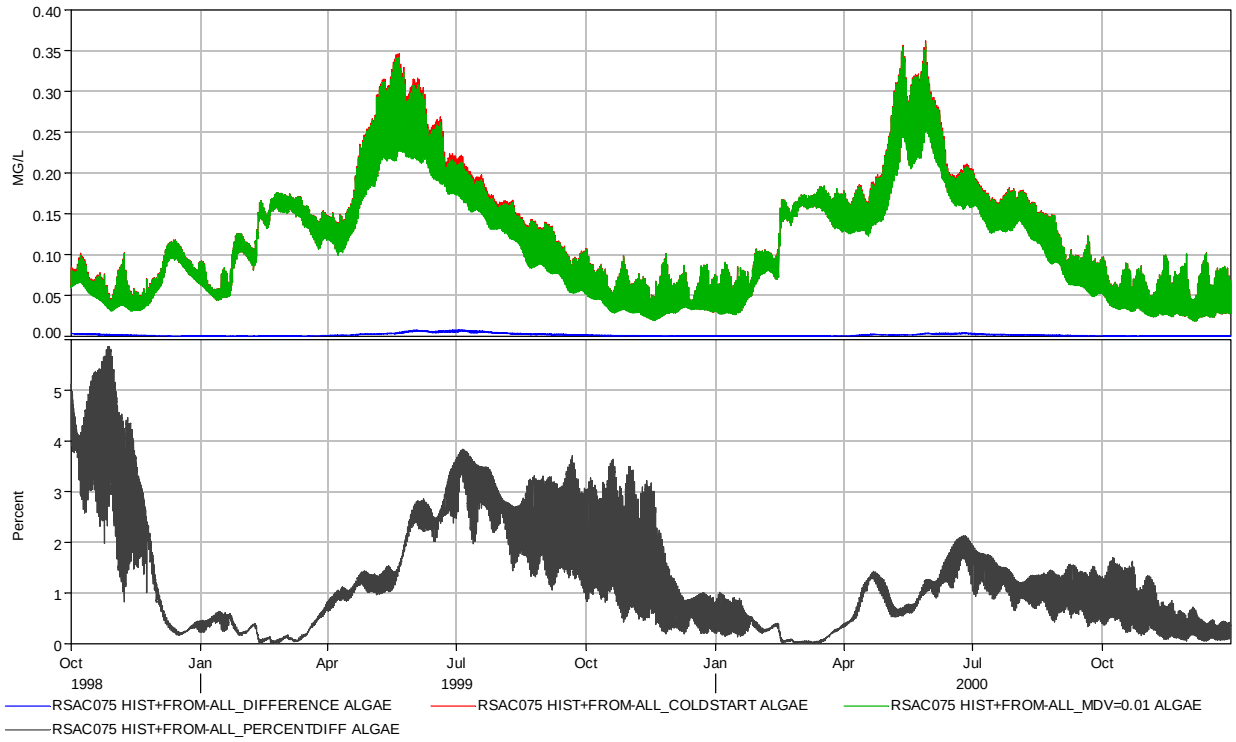

Figure 2-9 Mallard Island cold vs. warm start, algae

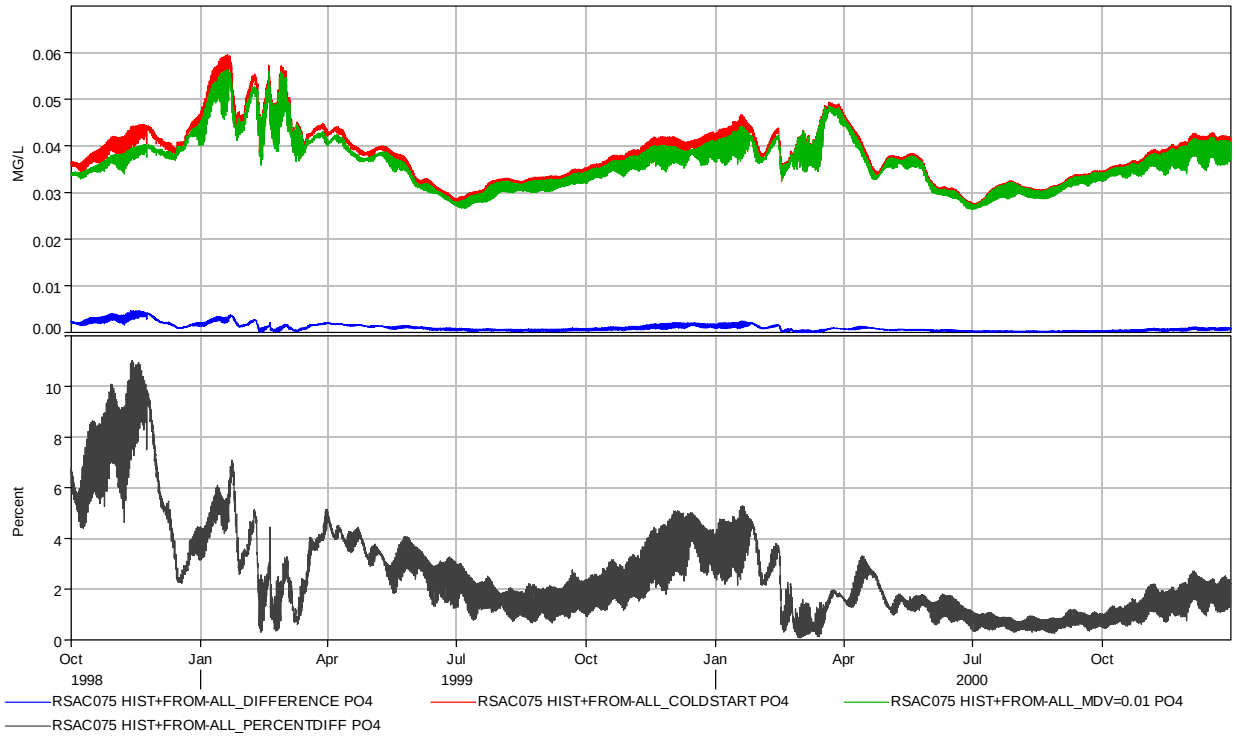

Figure 2-10 Mallard Island cold vs. warm start, phosphate

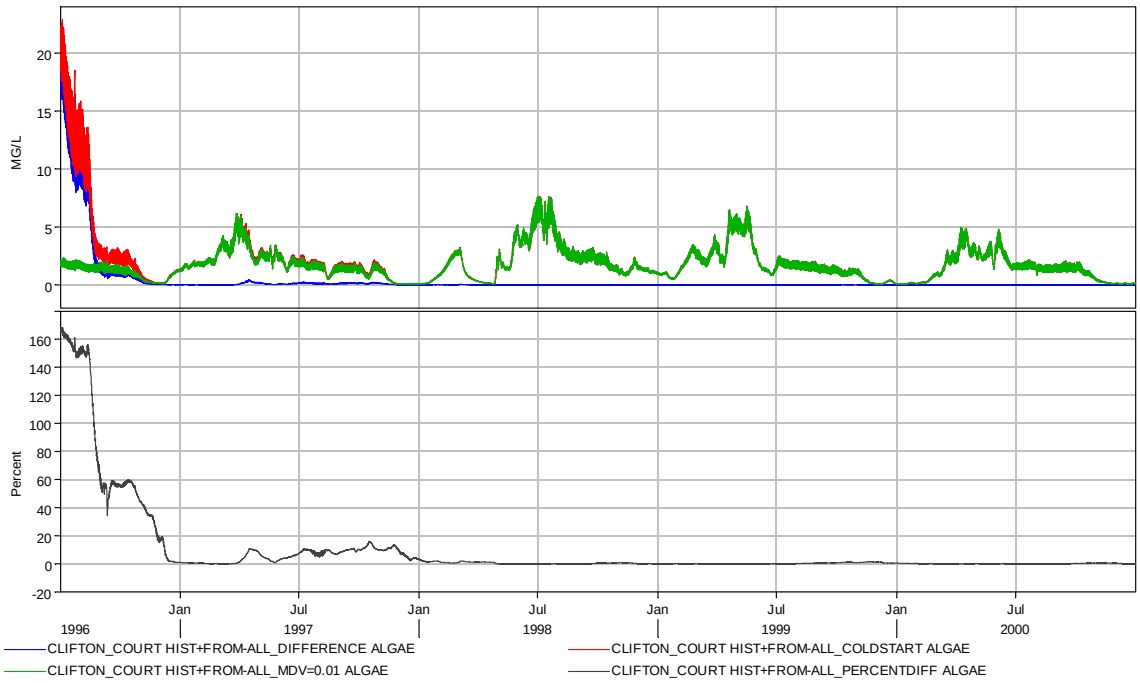

Figure 2-11 Clifton Court cold vs. warm start, algae

Methodology for Flow and Salinity Estimates in the Sacramento-San Joaquin Delta and Suisun Marsh

32nd Annual Progress Report
June 2011

Chapter 3
DSM2 Dissolved Organic Carbon Boundary Condition Improvement

Author: Joe Christen,
Municipal Water Quality Investigations,
Office of Water Quality,
Division of Environmental Services,
California Department of Water Resources

Contents

3 DSM2 Dissolved Organic Carbon Boundary Condition Improvement 3-1
3.1 Summary 3-1
3.2 Methods 3-1
3.2.1 Sites 3-1
3.2.2 Sample Collection and Analysis 3-2
3.2.3 Comparisons 3-2
3.3 Results 3-4
3.4 Discussion 3-9
3.5 Conclusions 3-10
3.6 References 3-10

Figures

Figure 3-1 Sampled Delta boundary stations 3-2
Figure 3-2 Shag Slough DOC, Sacramento River DOC, Yolo Bypass flow, and rainfall 3-5
Figure 3-3 DOC in the Sacramento River at Hood and Shag Slough, December 2008—March 2010 3-5
Figure 3-4 Mokelumne River DOC, Cosumnes River flow, and rainfall 3-6
Figure 3-5 Mokelumne River DOC > 4 mg/L and high flow boundary conditions 3-7
Figure 3-6 Mokelumne River DOC < 4 mg/L and low flow boundary conditions 3-7
Figure 3-7 Calaveras River DOC, Mormon Slough flow, and rainfall 3-8

Tables

Table 3-1 Water Data Library station numbers and the corresponding DSM2 geometry by location 3-2
Table 3-2 Statistics for DOC concentrations (mg/L) at boundary locations, Dec 2008—Mar 2010 3-4

3 DSM2 Dissolved Organic Carbon Boundary Condition Improvement

3.1 Summary

The Municipal Water Quality Investigations (MWQI) group conducted a 15 month, biweekly sampling program to acquire representative dissolved organic carbon (DOC) data for the Yolo Bypass and the East Side Streams (Mokelumne, Cosumnes, and Calaveras Rivers).

Previously, little data for organic carbon concentrations was available for the East Side Streams and the Yolo Bypass near the Delta boundary. Historical Delta Simulation Model II (DSM2) simulations of DOC concentrations in the Delta relied on assumed boundary conditions based on surrogate data. The current sources of the surrogate data used for generating the East Side Streams and Yolo Bypass boundary conditions for DOC are the Sacramento and American Rivers, and the Delta Island Consumptive Use (DICU) model.

In this chapter, the DOC data collected from the East Side Streams and Yolo Bypass are summarized and comparisons are made between the collected data and the assumed boundary conditions of the DSM2. Based on these comparisons, the assumed boundary conditions for DOC concentrations may underestimate concentrations during high flows.

3.2 Methods

3.2.1 Sites

Samples were collected at (1) Shag Slough at the Liberty Island Bridge to represent the Yolo Bypass, (2) the Mokelumne River at Wimpy's Marina in Walnut Grove to represent both the Cosumnes and Mokelumne Rivers, and (3) the Calaveras River in Stockton (Figure 3-1). The corresponding DSM2 segment or node is listed by station in Table 3-1 as is the Water Data Library (WDL) station number.

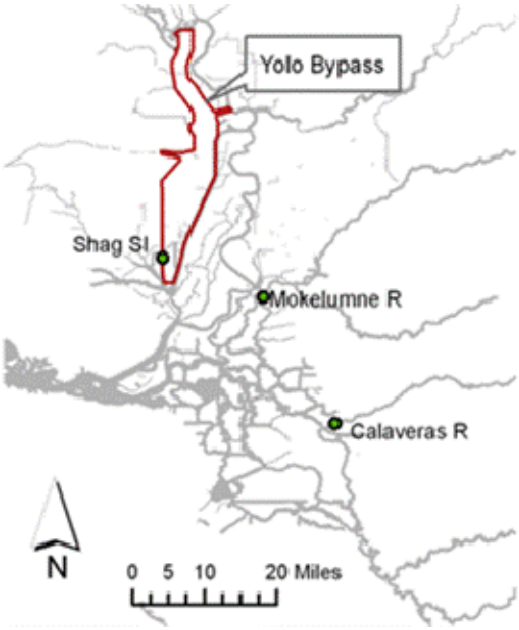

Figure 3-1 Sampled Delta boundary stations

Table 3-1 Water Data Library station numbers and the corresponding DSM2 geometry by location

Location	WDL station number	DSM2 geometry
Shag Slough (Yolo Bypass)	B9S81841416	Segment 401
Mokelumne River	B9D81371295	Segment 336
Calaveras River	B9D75851208	RCAL009

3.2.2 Sample Collection and Analysis

Grab samples were collected biweekly from December 2008 through March 2010. In the 2010 water year, additional samples were taken during significant storm flows to better capture the elevated DOC concentrations that typically coincide with storm flows. Storm flow event samples were collected after an estimated peak in storm flow. Bryte Laboratory conducted analyses for organic carbon concentrations using standard method 5310D, chemical oxidation, on an OIC 1010 analyzer. The dissolved fraction was the filtrate that passed through a 0.45 µm filter prior to analysis.

3.2.3 Comparisons

DOC concentrations from this study were compared to their respective assumed boundary condition for DOC concentrations used in DSM2 simulations. The DOC boundary conditions are outlined in the Department of Water Resources' Bay-Delta Office annual progress reports on DSM2 methodology (Suits 2002) (Pandey 2001).

Yolo Bypass

When flows in the Yolo Bypass are greater than 50 cfs, DSM2 assumes that Yolo Bypass DOC concentrations are equivalent to those of the Sacramento River. All samples collected from December 2008 through September 2009 occurred when Yolo Bypass flows were greater than 50 cfs. Dayflow data were not available for the Yolo Bypass for the October 2009 through March 2010 period when this report was authored; for this period, it was assumed that flows were greater than 50 cfs. Data collected from the Sacramento River at Hood (Hood) during the study interval were used to represent an assumed high-flow (> 50 cfs) boundary condition for DOC in the Yolo Bypass.

Mokelumne and Cosumnes Rivers

Based on visual examination, DOC concentrations from the Mokelumne River were divided into a high observed DOC group (> 4 mg/L) and a low observed DOC group (< 4 mg/L). All DOC concentrations greater than 4 mg/L were associated with high flows. The high observed DOC group was compared to the early winter high flow DOC boundary condition assumption of 3.95 mg/L. The low observed DOC group was compared to the assumed base flow boundary conditions of 1.74 mg/L for the wet season (November through May) and 1.66 mg/L for the dry season (June through October). Flow data for the Cosumnes River at Michigan Bar were used to represent flow in the Mokelumne River at Wimpy's Marina.

Calaveras River

The existing documentation on DSM2 methodology does not explicitly state the assumed boundary conditions for the Calaveras River; therefore, data for the Calaveras River were not compared to an assumed boundary condition. The collected DOC data are presented as a time series along with flow and precipitation data. Flow data used to represent Calaveras River were from the head of Mormon Slough. Outflow data for the New Hogan Reservoir were considered inappropriate because they did not capture the storm flow dynamics of the lower Calaveras River.

Hydrological Data

All rainfall data and flow data for the Cosumnes and Calaveras Rivers were obtained online from the California Data Exchange Center (http://cdec.water.ca.gov/). Flow data for the Yolo Bypass were obtained from Dayflow (http://www.water.ca.gov/dayflow/). Flow data are presented graphically as daily averages in thousand cfs. Rainfall data are presented as daily totals in inches.

3.3 Results

Descriptive statistics for DOC concentrations from the study locations are summarized in Table 3-2.

Table 3-2 Statistics for DOC concentrations (mg/L) at boundary locations, Dec 2008—Mar 2010

Location	mg/L				n
	Min	Max	Mean	Median	
Shag Slough (Yolo Bypass)	3.3	9.7	5.6	4.9	35
Mokelumne River	1.3	9.4	3.0	2.2	38
Calaveras River	3.3	18.7	6.5	5.0	35

Yolo Bypass

Storm flow responses in DOC concentrations were evident in a time series plot with flow and rainfall (Figure 3-2). Throughout the study period, DOC concentrations at Shag Slough were consistently greater than at Hood. The difference in mean concentrations between the 2 stations was relatively large, 3.3 mg/L (Figure 3-3). The relative percent difference in means was 83%. Daily average Yolo Bypass flow was greater than 50 cfs on 97% of the days between December 11, 2008, and September 30, 2009.

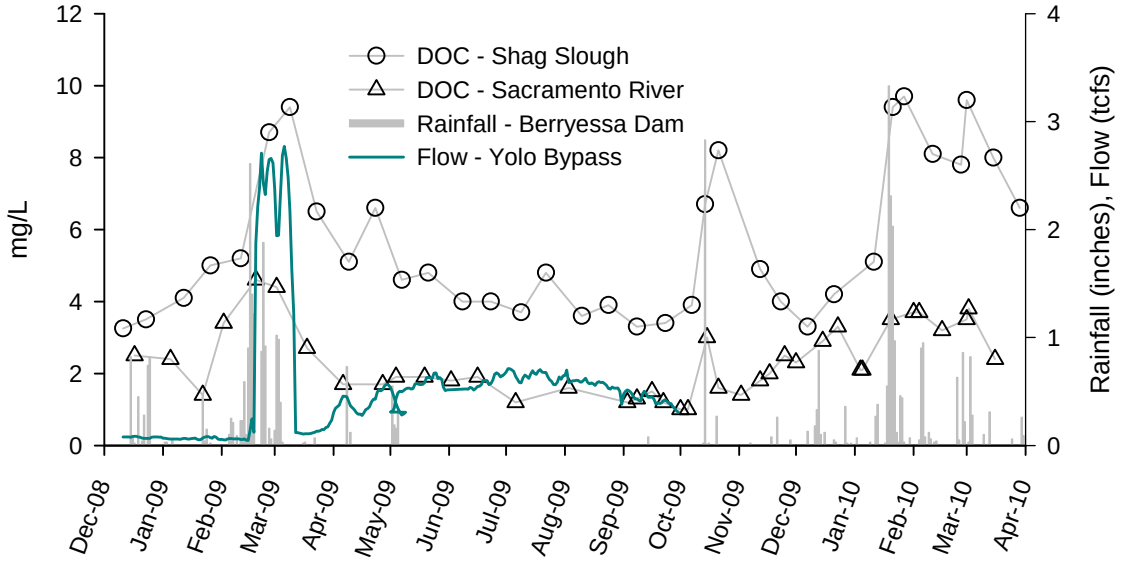

Figure 3-2 Shag Slough DOC, Sacramento River DOC, Yolo Bypass flow, and rainfall

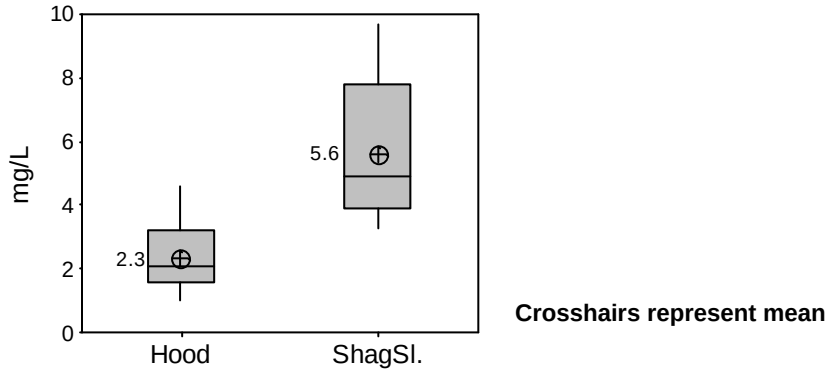

Figure 3-3 DOC in the Sacramento River at Hood and Shag Slough, December 2008—March 2010

Mokelumne River

The Mokelumne River DOC concentrations showed increases during storm flows that appeared to vary in the strength of the response (Figure 3-4). All DOC data over 4 mg/L were associated with increased flow and were grouped together as a high observed DOC group. All other values were grouped together to represent a low observed DOC group which includes concentrations that occurred during base flows and during low storm water flows. The mean of the high observed DOC group (6.07 mg/L) was 2.12 mg/L greater than the assumed early winter high flow boundary condition of 3.95 mg/L (Figure 3-5), a relative difference of 43%. The mean of the low observed DOC group (1.98 mg/L) was 0.32 mg/L and 0.24 mg/L greater than the assumed low flow boundary conditions for the dry season and wet season, respectively (Figure 3-6). These low flow differences were less than the 0.5 mg/L reporting limit of the analytical method for determining DOC concentrations (Calif. Dept. of Water Resources 2006).The relative percent difference between the assumed low flow DOC conditions and the mean of the observed low DOC group were less than 19%.

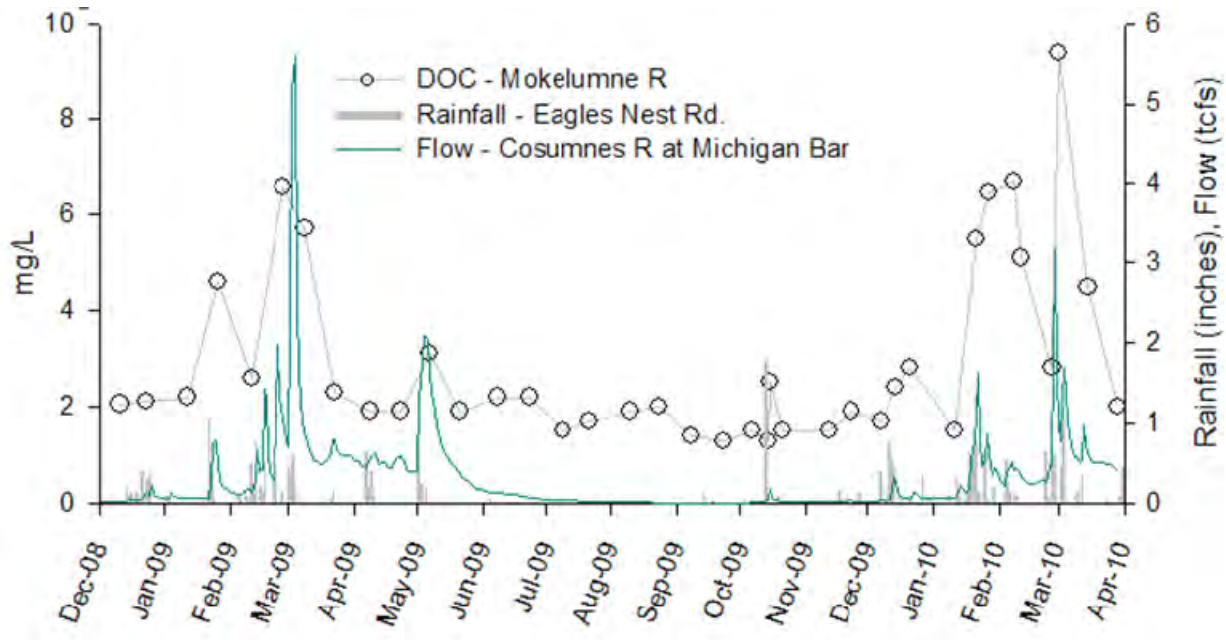

Figure 3-4 Mokelumne River DOC, Cosumnes River flow, and rainfall

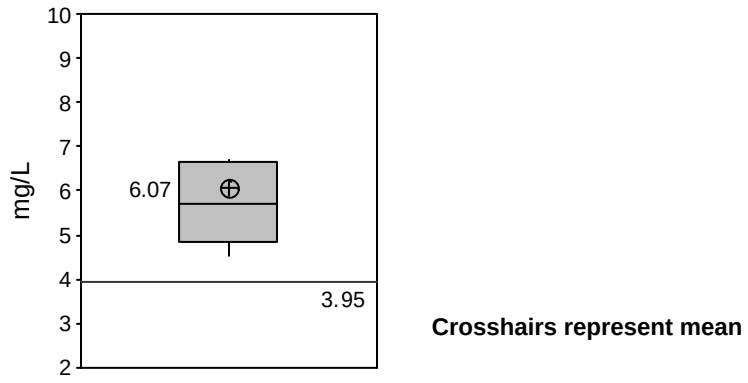

Figure 3-5 Mokelumne River DOC > 4 mg/L and high flow boundary conditions

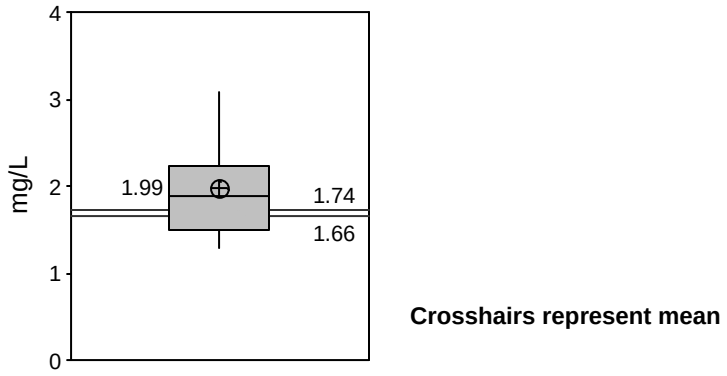

Figure 3-6 Mokelumne River DOC < 4 mg/L and low flow boundary conditions

Calaveras River

Figure 3-7 demonstrates the seasonality and the flow response behavior of DOC concentrations in the Calaveras River at Stockton.

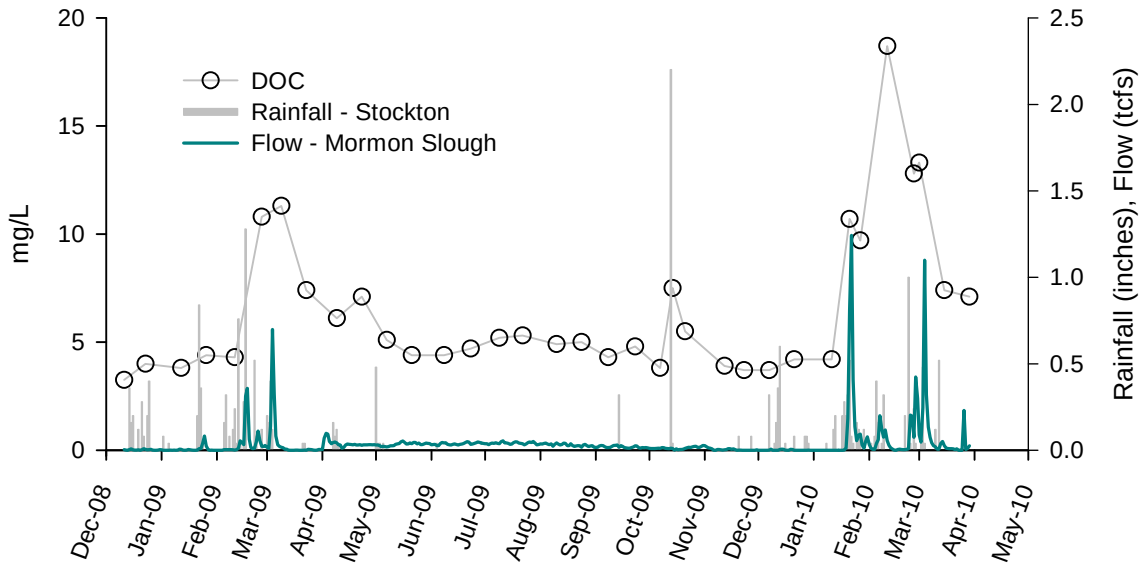

Figure 3-7 Calaveras River DOC, Mormon Slough flow, and rainfall

3.4 Discussion

Land Use Influence

The consistent difference in concentrations between the Hood and Shag Slough stations and the large relative difference (83%) in the means of the data are evidence that DOC data from Hood are not an adequate surrogate for DOC in the Yolo Bypass. The high DOC values of Shag Slough are likely due to the large areas of agricultural land in the watershed of the bypass, agriculture drainage into Shag Slough, and the wetlands of Liberty Island. Limited data suggest that storm flow from the waterways draining agriculture lands to the west of the Yolo Bypass have DOC concentration greater than 9 mg/L. A study in the predominately agricultural watershed of Willow Slough, a tributary of the Yolo Bypass, obtained a peak DOC concentration of 9.82 mg/L during storm water flow in February 2008 (Saraceno, et al. 2009). The DOC concentrations measured prior to the storm were between 2.3 mg/L and 2.7 mg/L (Saraceno, et al. 2009). Additionally, a sample of storm water from another predominately agricultural watershed tributary of the Yolo Bypass (Putah Creek at Mace Boulevard) had a DOC concentration of 9.5 mg/L on January 21, 2010. The elevated storm water DOC values from the agricultural watersheds of the tributary streams to the Yolo Bypass were close to those of the measured storm water values in Shag Slough (8.7 mg/L to 9.7 mg/L). Runoff from agriculture lands was likely the dominant factor for determining DOC concentrations in Shag Slough during storm water flows. Agricultural areas also appeared to have a strong influence during storm water flows in the Calaveras River. The Calaveras watershed downstream of the New Hogan Reservoir is predominately agricultural by area. Increased flows following rain events in Mormon Slough were not reflected in the outflow data for New Hogan Reservoir (data not shown) which demonstrates that runoff during this period was predominately from the watershed downstream of the New Hogan Dam or from tidal San Joaquin River water. Values for DOC in the Calaveras River during storm flows were greater than 7 mg/L.

Differences between the watersheds of the Mokelumne River and the American River were likely responsible for the large difference between the assumed DOC concentration for early winter high flow condition and the observed high DOC data. The boundary condition assumptions for the East Side Streams were developed from DOC data collected in the American River at the American River Treatment Plant Intake (Pandey 2001). The watershed upstream of the American River is predominately forested land and has very little influence from the lowland agriculture or wetlands. The upstream watershed of the Mokelumne River at Wimpy's Marina by contrast has a strong presence of agriculture and wetlands in the lower reaches. It is this difference between the watersheds of the surrogate data and the actual Mokelumne River that is likely responsible for the underestimation of DOC concentrations during high flow conditions. The division of the observed data by visual examination likely entered some bias into the comparisons; however, it is unlikely that introduced bias accounted for the majority of the difference between groups. The differences between the mean of the low observed DOC group and the DOC boundary conditions for low flow were less than the reporting limit (0.5 mg/L) of the analytical method for determining DOC concentration. Simulations of DOC in the Mokelumne using the current boundary condition methodology would more often than not underestimate DOC during low flow conditions, yet the difference between actual and modeled concentrations is not likely to be of practical significance.

3.5 Conclusions

The results of this study demonstrate that current DSM2 assumptions for DOC concentrations at the Delta boundaries of the Mokelumne River and Yolo Bypass underestimate actual DOC concentrations during high flow conditions. The differences between the low flow DOC assumptions in the Mokelumne River and the mean of the values measured under low flow conditions are less than the reporting limit for laboratory analysis for DOC concentration.

3.6 References

Calif. Dept. of Water Resources. *Bryte Chemical Laboratory Quality Assurance Manual.* 2006. http://www.wq.water.ca.gov/docs/bryte_pubs/Bryte_QA_Manual_2006.pdf.

Pandey, G. "Chapter 3 : Simulation of Historical DOC and UVA Conditions in the Delta." *Methodology for Flow and Salinity Estimates in the Sacramento-San Joaquin Delta and Suisun Marsh. 22nd Annual Progress Report to the State Water Resources Control Board*, 2001.

Saraceno, J. F., B. A. Pellerin, B. Downing, E. Boss, P.A.M. Bach, and B. Bergamaschi. "High-frequency In Situ Optical Measurements During a Storm Event: Assesing Relationships Between Dissolved Organic Matter, Sediment Concentrations, and Hydrologic Processes." *Journal of Geophysical Research* 114, no. G00F09 (2009).

Suits, B. "Chapter 7 : Generating Monthly Dissolved Organic Carbon and UVA at DSM2 Boundaries." *Methodology for Flow and Salinity Estimates in the Sacramento-San Joaquin Delta and Suisun Marsh. 23rd Annual Progress Report to the State Water Resources Control Board*, 2002.

Methodology for Flow and Salinity Estimates in the Sacramento-San Joaquin Delta and Suisun Marsh

32nd Annual Progress Report
June 2011

Chapter 4
South Delta Temporary Barriers Hydrodynamic Modeling

Authors: Lan Liang, Siqing Liu, Robert Suits,
Delta Modeling Section,
Bay-Delta Office,
California Department of Water Resources

Contents

4 South Delta Temporary Barriers Hydrodynamic Modeling 4-1
4.1 Summary 4-1
4.2 2008 Delta Boundary conditions 4-1
4.3 2008 Delta consumptive use 4-2
4.4 South Delta Structures 4-2
4.5 Delta Downstream Stage at Martinez 4-3
4.6 Delta Cross Channel Operation 4-3
4.7 Validation of DSM2 Simulation of Historical 2008 Delta Hydrodynamics 4-3
4.8 Effect of Temporary Barriers Installation and Operation on South Delta Hydrodynamics 4-16
4.9 Discussion 4-17

Figures

Figure 4-1 Daily average historical inflow from the Sacramento River, 2008 4-1
Figure 4-2 Daily average historical inflow from the Yolo Bypass, 2008 4-1
Figure 4-3 Daily average historical inflow from the San Joaquin River, 2008 4-2
Figure 4-4 Daily average historical pumping at Banks and Jones pumping plants, 2008 4-2
Figure 4-5 Locations where DSM2-simulated and measured stages and flows are presented, 2008 4-4
Figure 4-6 Comparison of DSM2-simulated and observed daily stage, 2008 4-5
Figure 4-7 Comparison of DSM2-simulated and measured daily flow, 2008 4-11
Figure 4-8 Locations where simulated Delta stages and flows for analysis of 2008 conditions are presented 4-17
Figure 4-9 Distribution of DSM2-simulated stages for historical 2008 with and without temporary barriers installed 4-19
Figure 4-10 Distribution of DSM2-simulated flows for historical 2008 conditions with and without temporary barriers installed 4-23
Figure 4-11 Simulated period-average flow and minimum stage for 2008 conditions with historical barrier configuration and no-barriers condition 4-27

Tables

Table 4-1 Historical South Delta Temporary Barriers installation and removal, 2008 4-3
Table 4-2 Characteristics of time intervals for presentation of simulation results, 2008 4-16

4 South Delta Temporary Barriers Hydrodynamic Modeling

4.1 Summary

This chapter presents an abbreviated sample of the simulation of historical 2008 Delta hydrodynamic conditions and the effect of the installation and operation of the south Delta temporary barriers. For this analysis, historical Delta inflows, consumptive use, and exports were simulated under 2 barrier conditions: (1) historical 2008 installation and operation of the temporary barriers, and (2) no installation of south Delta temporary barriers. Delta Simulation Model II hydrodynamic module (DSM2-Hydro) was used to simulate the Delta hydrodynamics.

4.2 2008 Delta Boundary conditions

Flow and stage information required at model boundaries were downloaded from the California Data Exchange Center web site (cdec.water.ca.gov). Input data was visually examined before any simulation. Any gaps or errors in data were of short duration and values were estimated via simple interpolation. The resulting boundary conditions for the 2008 simulation are shown in Figure 4-1 through Figure 4-4.

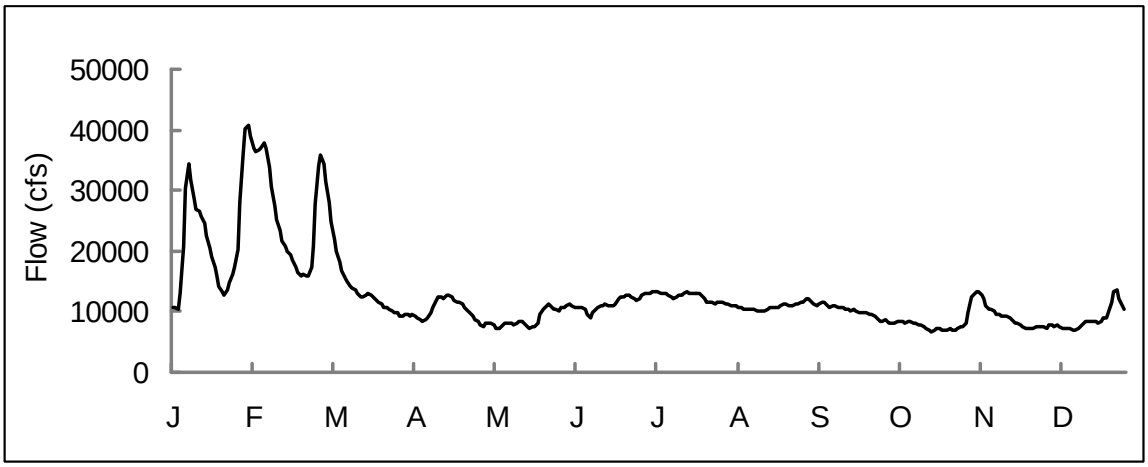

Figure 4-1 Daily average historical inflow from the Sacramento River, 2008

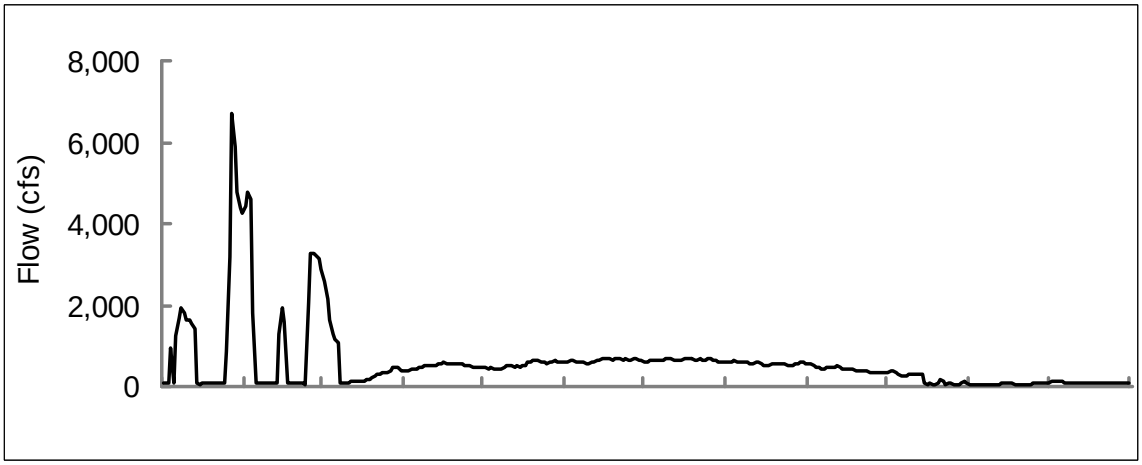

Figure 4-2 Daily average historical inflow from the Yolo Bypass, 2008

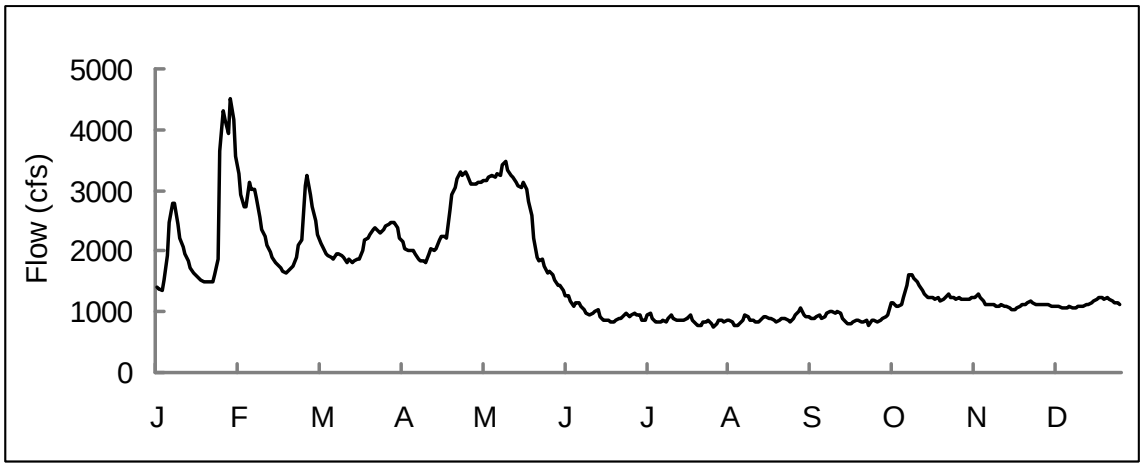

Figure 4-3 Daily average historical inflow from the San Joaquin River, 2008

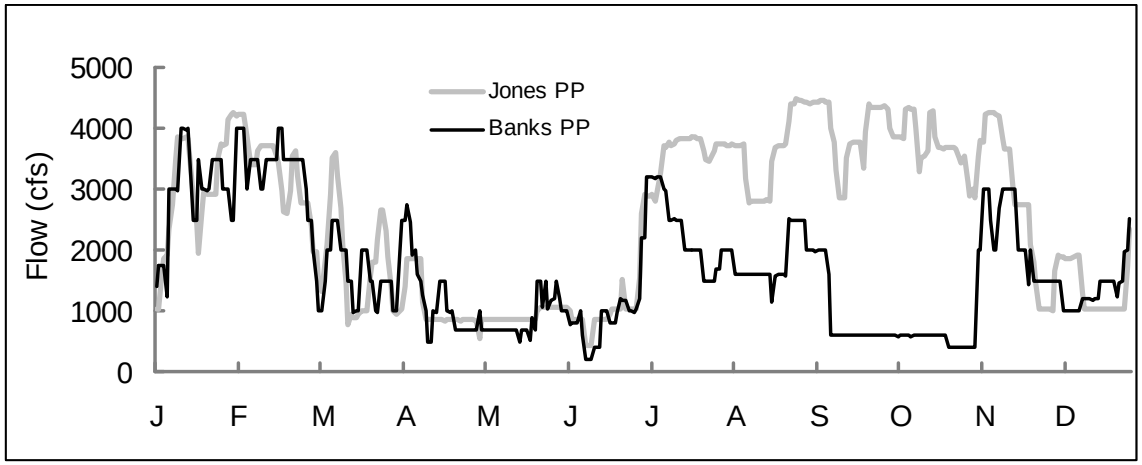

Figure 4-4 Daily average historical pumping at Banks and Jones pumping plants, 2008

4.3 2008 Delta consumptive use

The Delta Island Consumptive Use (DICU) model provided an estimate of the amount of water diverted from and returned to Delta channels due to agricultural activities. Input to the DICU model includes precipitation, pan evaporation data, and water year type. The water year type determines which of 2 possible cropping patterns in the Delta is assumed. Delta land use in turn contributes to the estimation of agricultural water needs.

4.4 South Delta Structures

All 3 temporary agricultural barriers were installed in 2008. The head of Old River barrier was only installed in the fall. The DSM2 simulation timed the installation and removal of the barriers to the changes in actual observed stages which indicated effective closure or opening of the channel. Table 4-1 lists the historical installation and removal of the South Delta Barriers. The Grant Line Canal barrier is typically installed in 2 stages. The first stage installs the boat ramp but leaves the center of the channel open. The second stage closes the channel. The date and time shown in Table 4-1 for Grant Line Canal refers to the second phase installation because this is the time significant changes in stage upstream due to this barrier are first evident. Flap gates in the barrier culverts were at times tied open or allowed to

tidally operate. This level of detail of operation, while incorporated in the historical simulation, is not shown in Table 4-1.

Table 4-1 Historical South Delta Temporary Barriers installation and removal, 2008

	Installation			Removal		
Barrier	**Started[1]**	**Ended[1]**	**DSM2 simulation**	**Started[1]**	**Ended[1]**	**DSM2 simulation**
Middle River	5/21/08	5/21/08	5/25/08 1700 hrs	11/11/08	11/11/08	11/05/08 1600 hrs
Old River nr Delta Mendota Canal	6/04/08	6/04/08	6/04/08 1500 hrs	11/4/08	11/4/08	11/03/08 1200 hrs
Grant Line Canal	6/26/08	6/26/08	6/26/08 0800 hrs	11/11/08	11/11/08	11/10/08 1100 hrs
Old River @ Head (spring)	---	---	---	---	---	---
Old River @ Head (fall)	10/16/08	10/16/08	10/16/08 0800 hrs	11/03/08	11/03/08	11/03/08

[1] As reported by Temporary Barriers Program, DWR

4.5 Delta Downstream Stage at Martinez

The downstream boundary of DSM2 is Martinez where a time series of observed historical 15-minute data from 2008 were used for the simulation.

4.6 Delta Cross Channel Operation

The Delta Cross Channel gates were operated in 2008 and modeled in the historical DSM2 simulation from historical operation data.

4.7 Validation of DSM2 Simulation of Historical 2008 Delta Hydrodynamics

Delta hydrodynamics were simulated according to the conditions presented above. Stage and flow results of the DSM2 simulation of historical Delta hydrodynamics were compared to available observed data in Figure 4-5. Figure 4-6 presents observed and simulated daily minimum and maximum stage, and Figure 4-7 presents observed and simulated daily minimum, maximum, and average flow.

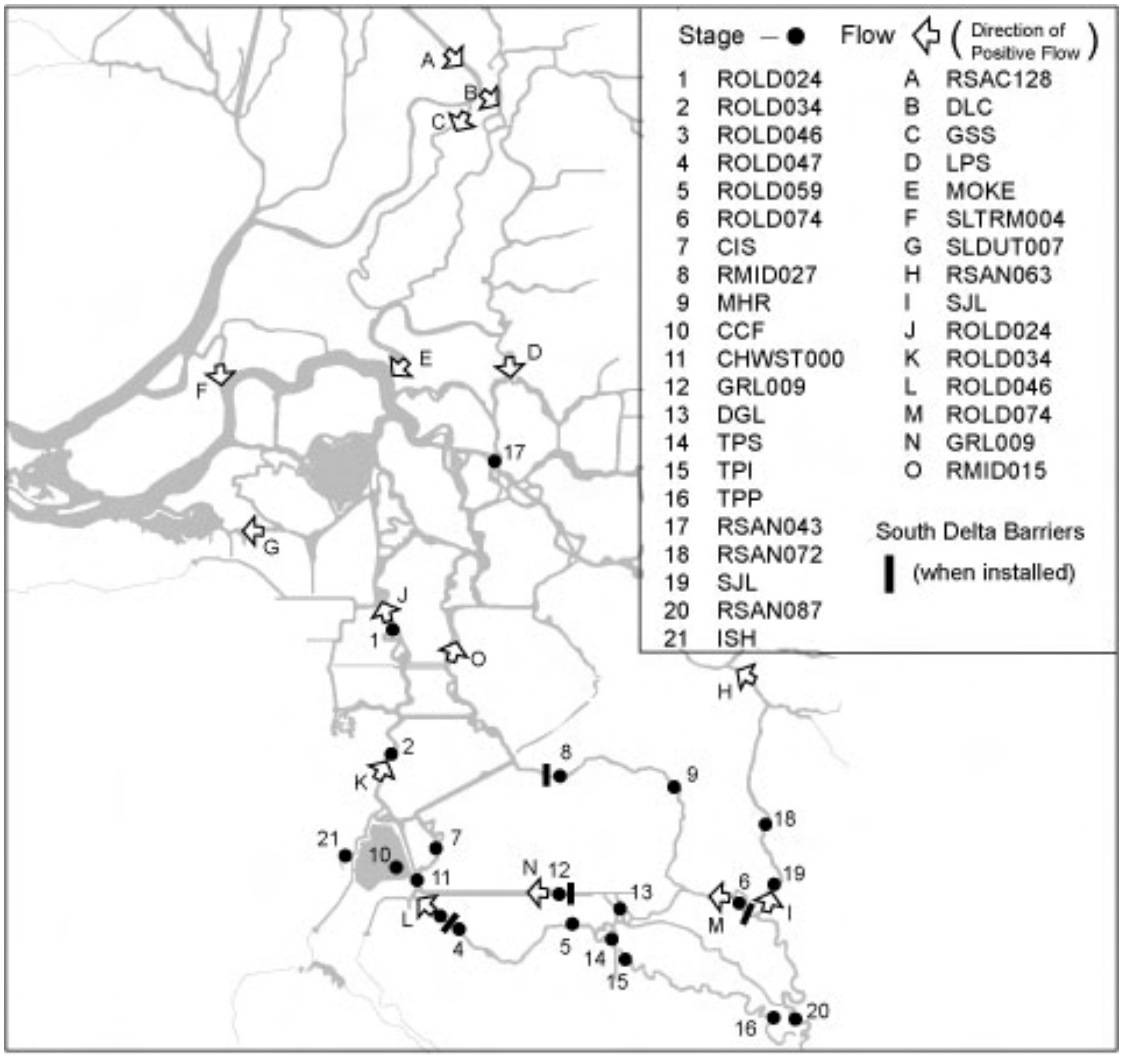

Figure 4-5 Locations where DSM2-simulated and measured stages and flows are presented, 2008

Figure 4-6 indicates that the DSM2 simulation reproduces the observed effect the temporary agriculture barriers have on upstream minimum (see stations RMID027, MHR, DGL, ROLD047, ROLD059, and TPS). Simulated daily levels generally match observed values well, with the exceptions of stages in Clifton Court Forebay and Tom Paine Slough. Model errors at these locations have been noted before and appear to occur for most all DSM2 historical simulations.

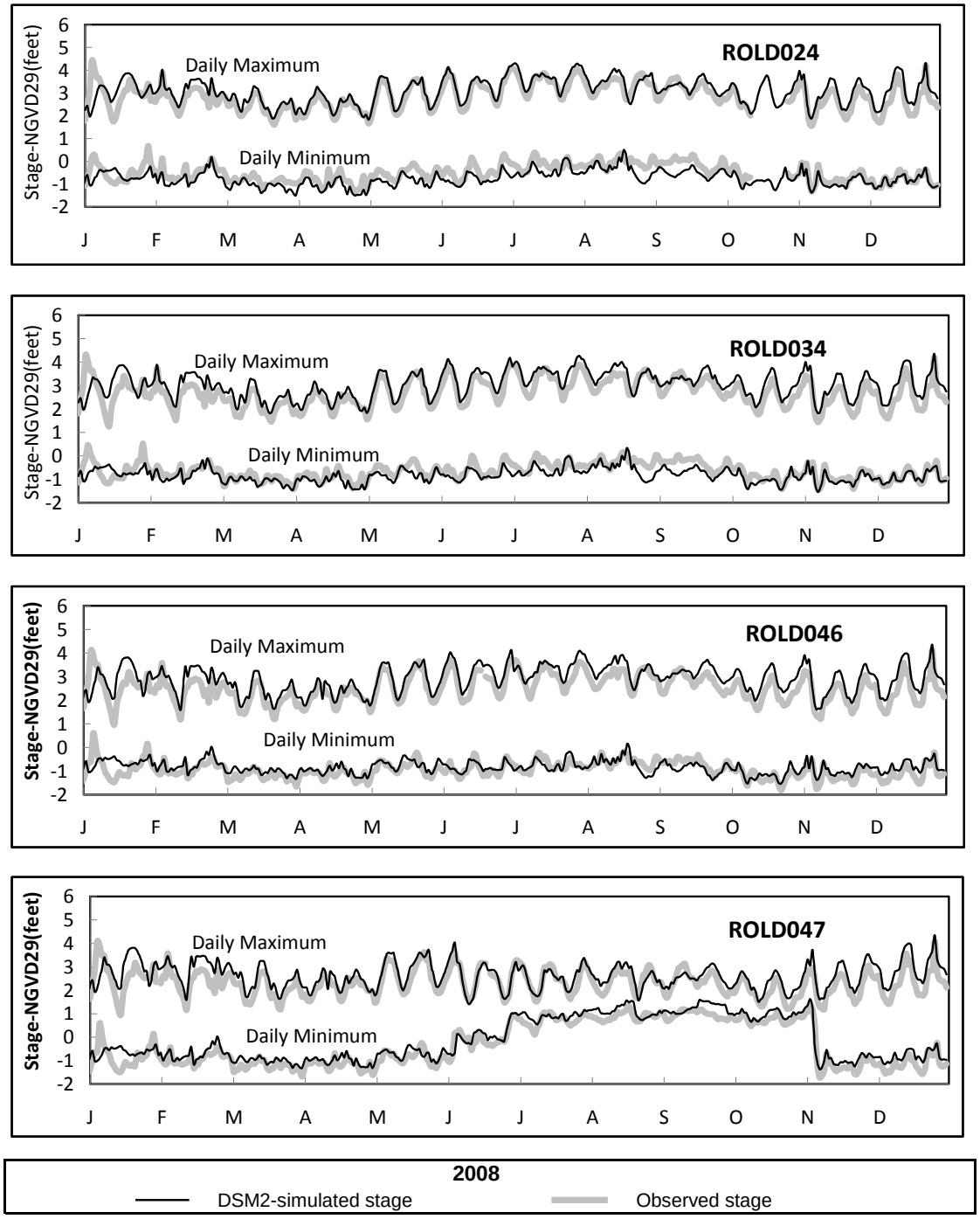

Figure 4-6 Comparison of DSM2-simulated and observed daily stage, 2008

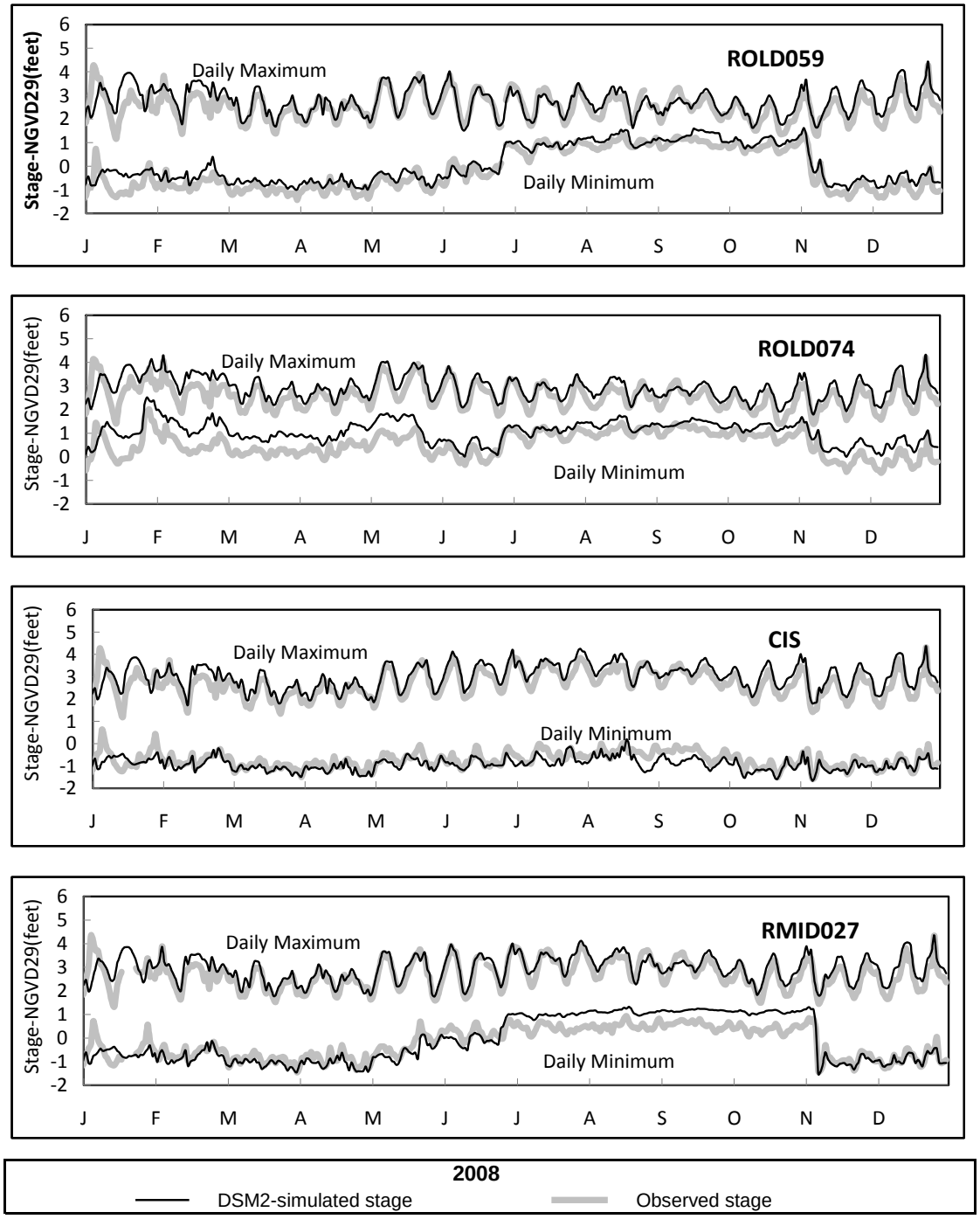

Figure 4-6 (cont.) Comparison of DSM2-simulated and observed daily stage, 2008

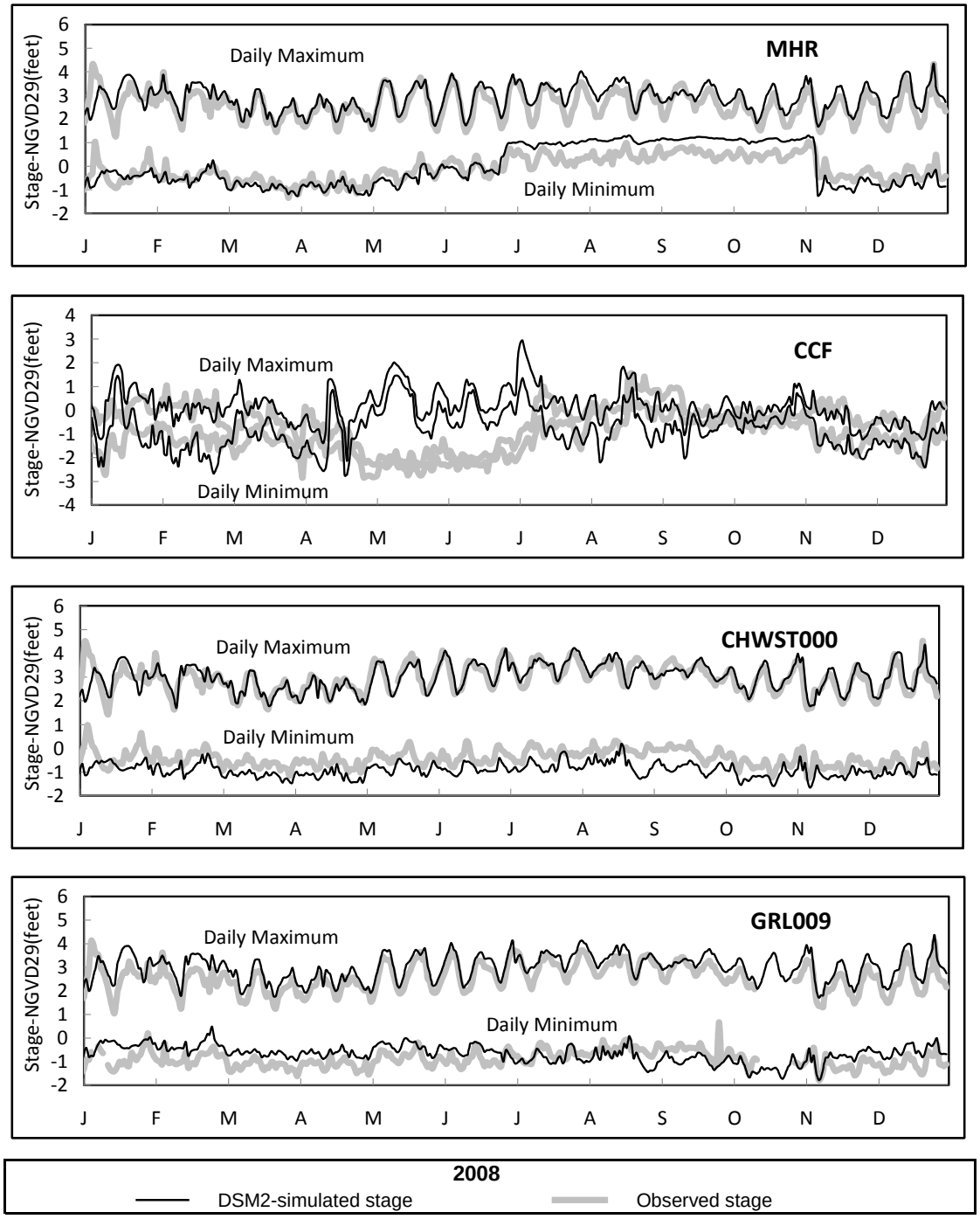

Figure 4-6 (cont.) Comparison of DSM2-simulated and observed daily stage, 2008

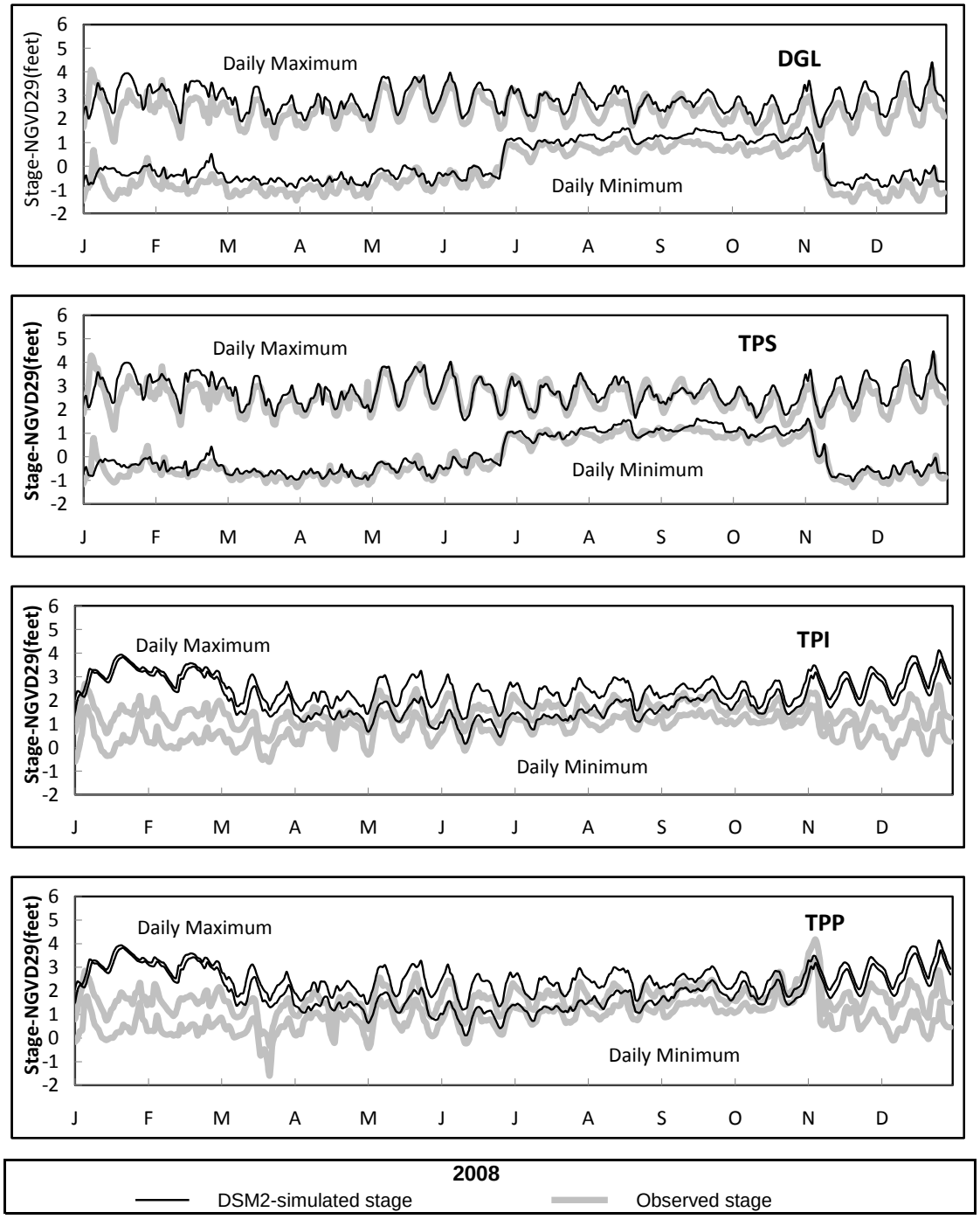

Figure 4-6 (cont.) Comparison of DSM2-simulated and observed daily stage, 2008

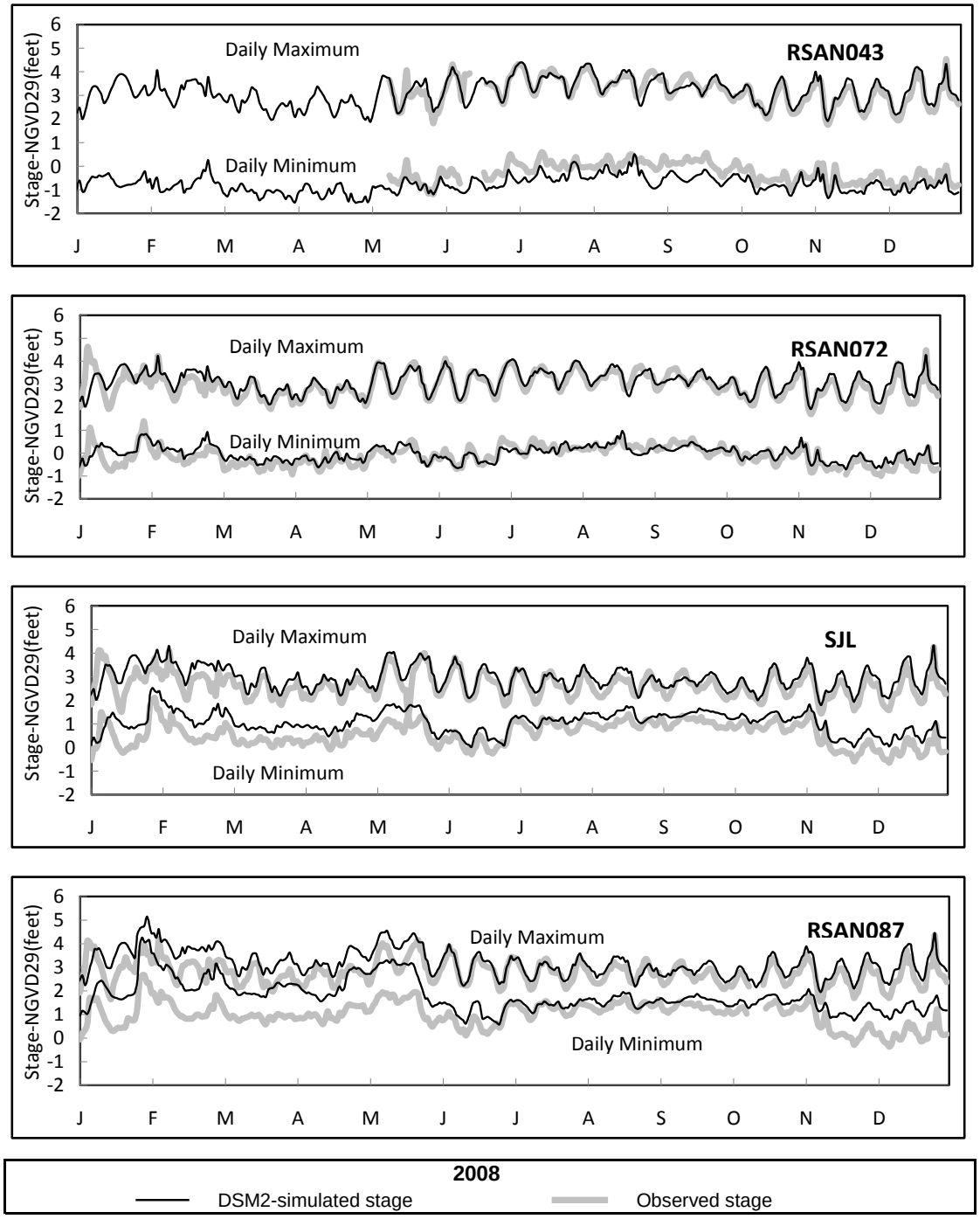

Figure 4-6 (cont.) Comparison of DSM2-simulated and observed daily stage, 2008

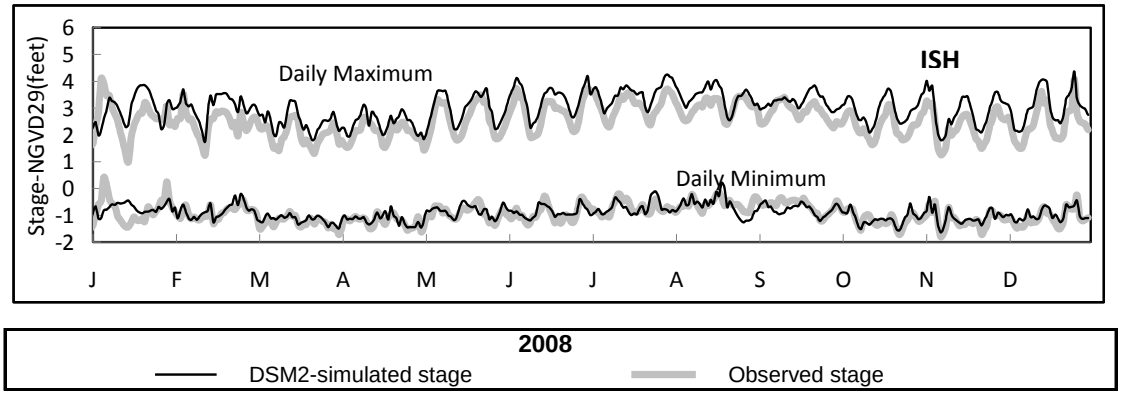

Figure 4-6 (cont.) Comparison of DSM2-simulated and observed daily stage, 2008

Figure 4-7 shows DSM2-simulated and observed daily maximum, average, and minimum flow wherever measured flow data are available in the Delta for 2008. The DSM2 simulation matched observed peak and average flows well at almost all locations in the Delta outside of the area affected by the temporary barriers in the south Delta. Locations where flow was measured and are within the influence of the barriers are Old River downstream of barrier near Delta Mendota Canal (DMC) intake (ROLD046), Old River at Head (ROLD074), and Grant Line Canal downstream of barrier site (GRL009). All 3 of these locations are actually downstream of the temporary barrier site, but flow at OLD074 can be assumed influenced by the installation of the temporary barriers in Old River near DMC intake and Grant Line Canal.

At ROLD046, ROLD074, and GRL009, the simulated daily average flow matches the observed daily average flow well. At ROLD046, observed peak upstream flows were near zero while DSM2 simulated peak upstream flows of approximately 1,000 cfs. Peak downstream flows matched better once the Grant Line Canal was installed; otherwise, the DSM2 simulation showed peak downstream flows that were less than those observed. At ROLD074, simulated peak upstream and downstream flows matched observed flows well. Changes in tidal flow here in response to temporary barrier installation in Old River and Grant Line Canal are evident in both observed and simulated flows. At GRL009, although the observed and simulated daily average flows match well, the observed daily peak upstream and downstream flows can significantly exceed simulated flows. This pattern has been noted in other years and may reflect the currently assumed Grant Line Canal bathymetry used in DSM2.

Taken together, Figure 4-6 and Figure 4-7 indicate that the DSM2 simulations of historical 2008 Delta conditions with and without barrier installation should provide meaningful results with which to evaluate how the barriers affected water levels and circulation in the south Delta.

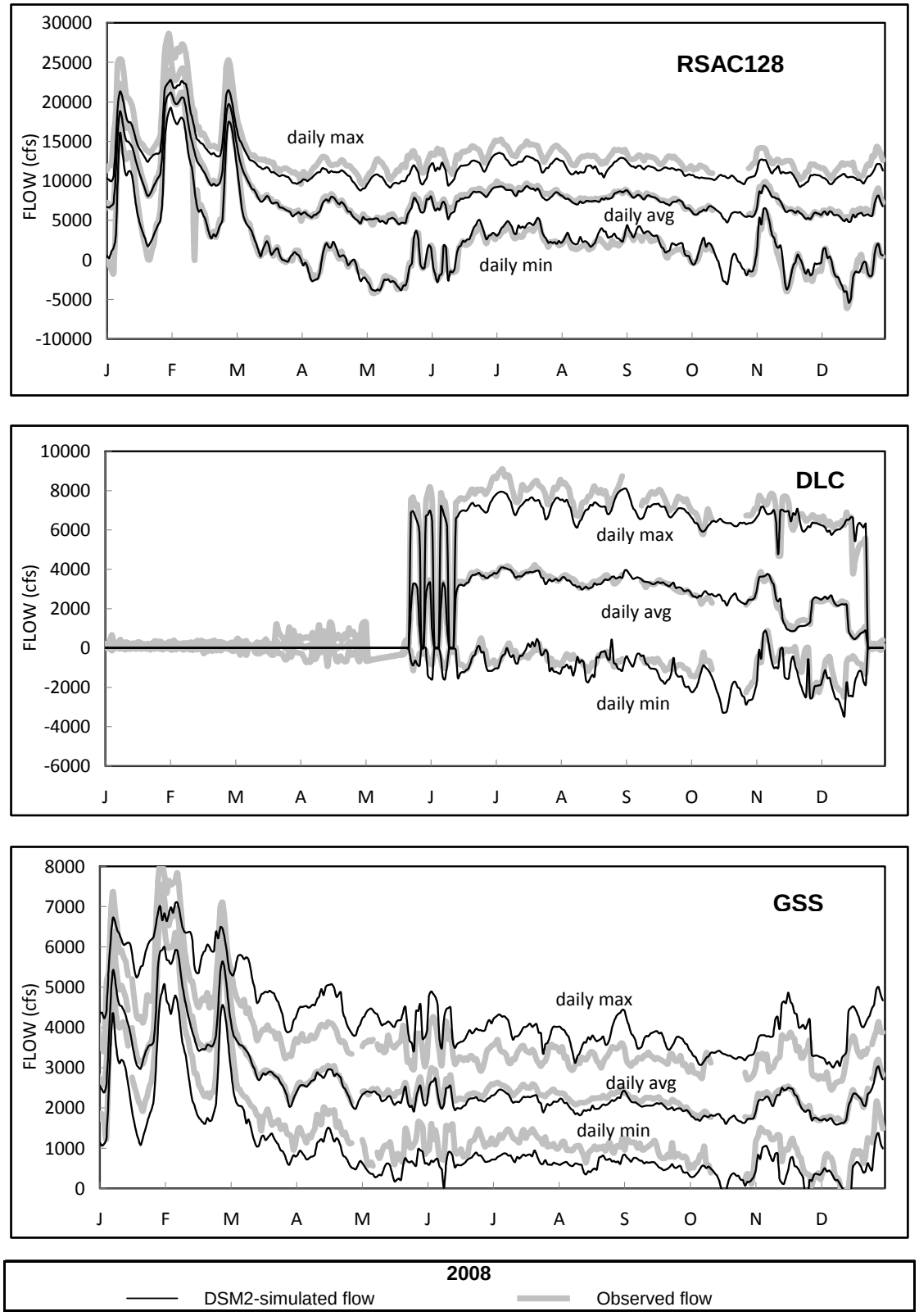

Figure 4-7 Comparison of DSM2-simulated and measured daily flow, 2008

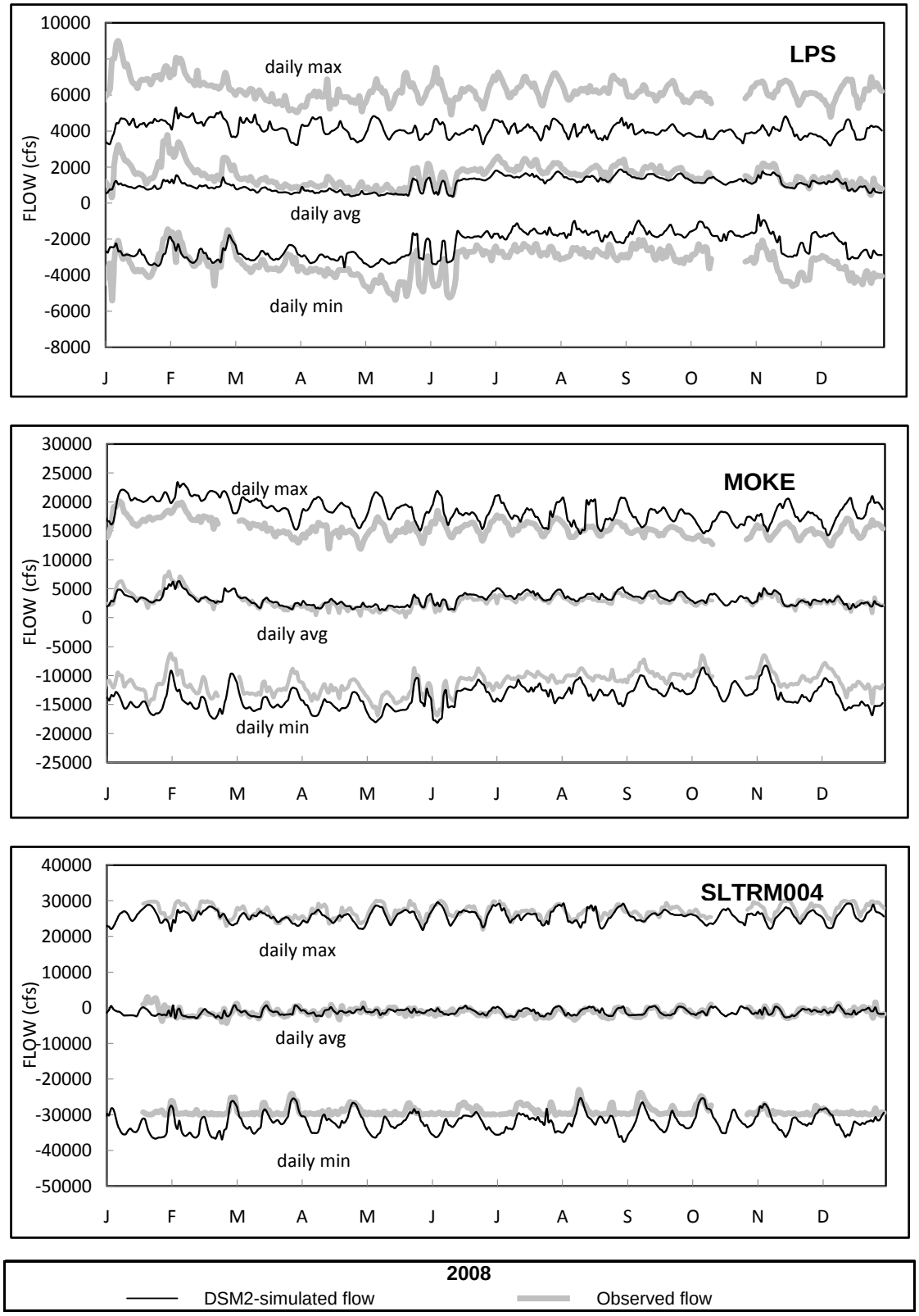

Figure 4-7 (cont.) Comparison of DSM2-simulated and measured daily flow, 2008

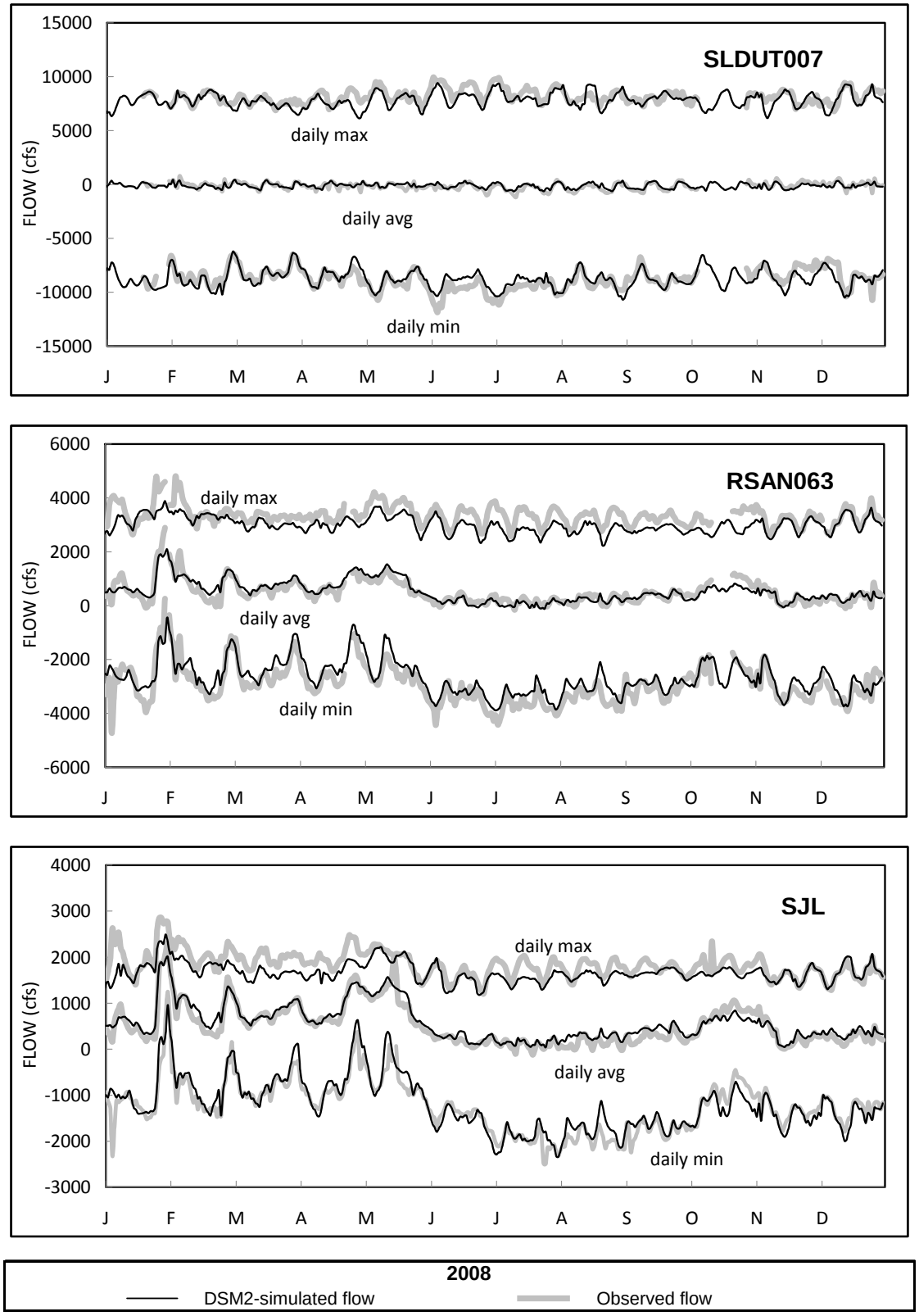

Figure 4-7 (cont.) Comparison of DSM2-simulated and measured daily flow, 2008

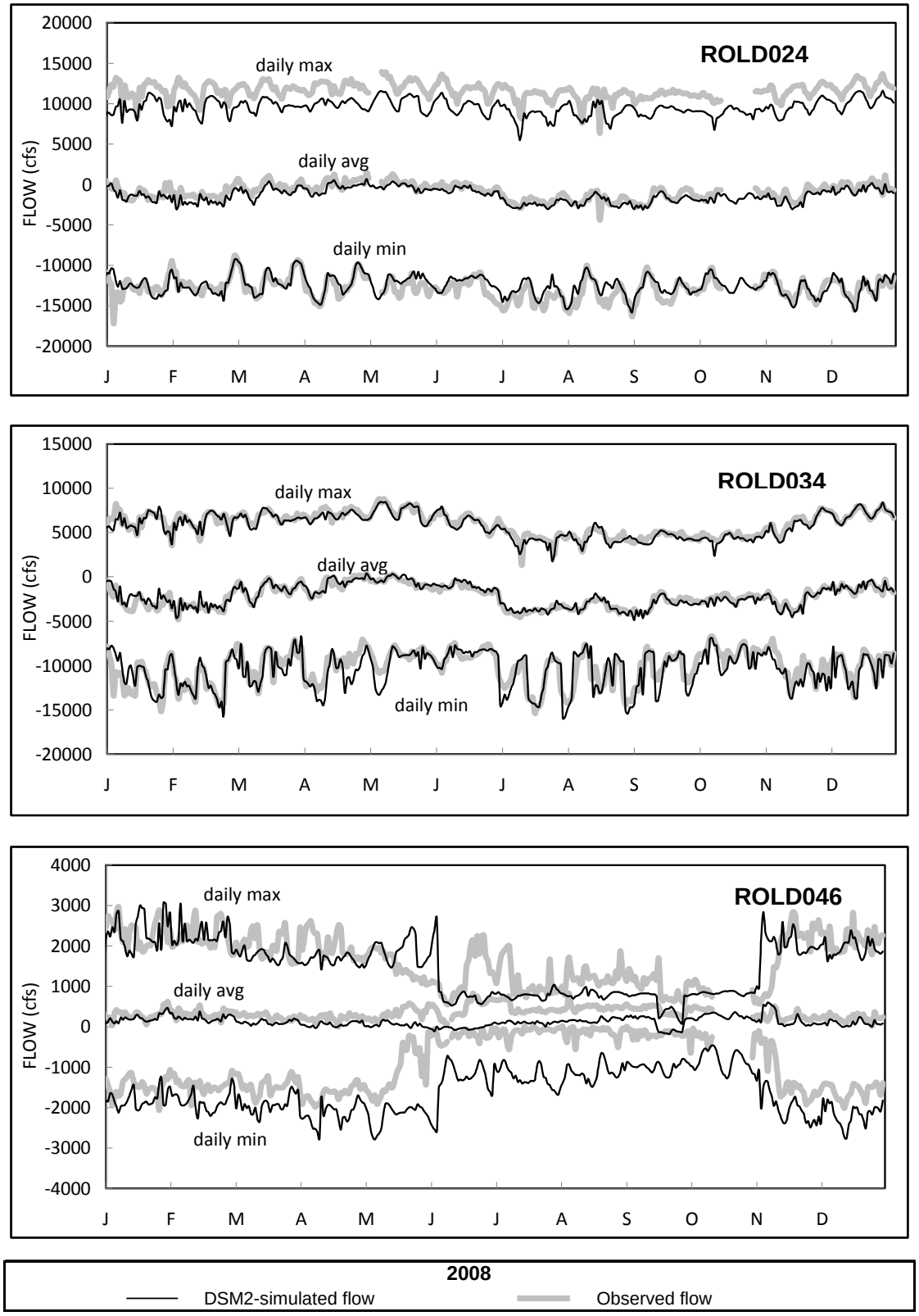

Figure 4-7 (cont.) Comparison of DSM2-simulated and measured daily flow, 2008

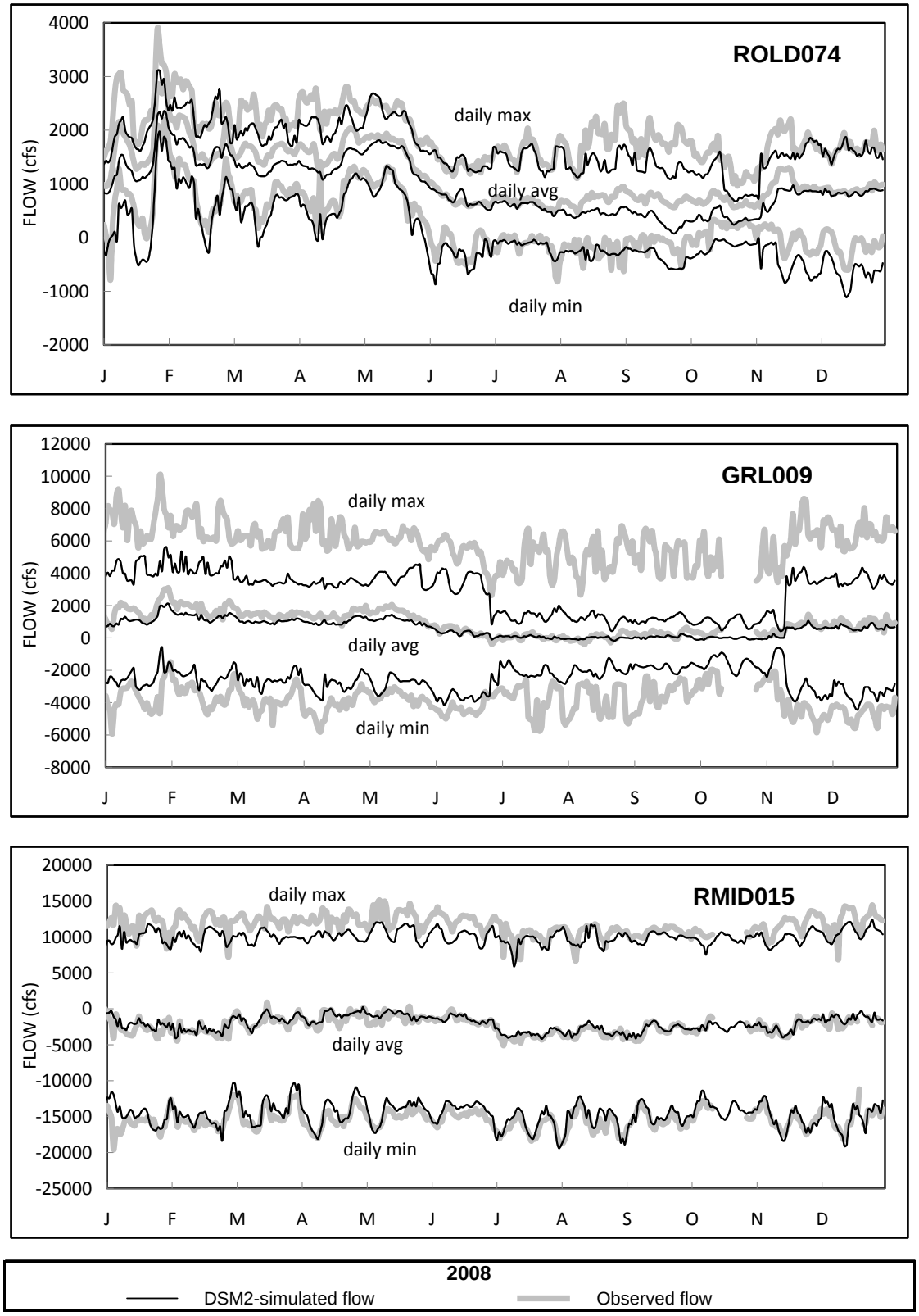

Figure 4-7 (cont.) Comparison of DSM2-simulated and measured daily flow, 2008

4.8 Effect of Temporary Barriers Installation and Operation on South Delta Hydrodynamics

In order to better process the 2008 Delta hydrodynamics, DSM2 simulation results were separated into 19 periods for which significant Delta inflows and exports were fairly constant and basic south Delta barrier configurations were unchanging. The 19 periods and their characteristics are shown in Table 4-2 below. The Delta hydrodynamics, as modeled by DSM2, are presented for each of the periods, excluding these periods when barriers were in the process of installation or removal: June 1-4, June 27-30, October 16, and November 1-11. Operational changes to the temporary barriers of having flap gates tied open or operated tidally were not factored into the processing of the simulation results. The Grant Line Canal barrier was not considered installed until the middle of the channel was closed. Therefore, the period of June 5 to 26 is presented as only Old River and Middle River barriers being installed.

Table 4-2 Characteristics of time intervals for presentation of simulation results, 2008

Period in 2008		Period Average Flows				Period Barrier Status			
		Sac R. + Yolo Bypass (cfs)	SJR (cfs)	DMC Pumping (cfs)	SWP Pumping (cfs)	MR	OR	GLC	ORH
JAN	1 - 5	11,159	1,351	1,302	1,441	--	--	--	--
	6 - 21	23,556	1,772	2,835	2,190	--	--	--	--
	22 - 31	25,604	3,138	3,235	2,906	--	--	--	--
FEB	1 - 4	47,854	3,176	4,174	3,971	--	--	--	--
	5 - 13	31,263	2,773	3,575	3,325	--	--	--	--
	14 - 29	22,263	2,274	2,827	3,448	--	--	--	--
MAR	1 - 31	14,710	2,179	1,813	1,594	--	--	--	--
APR	1 - 30	10,733	2,356	1,080	1,237	--	--	--	--
MAY	1 - 20	8,688	3,167	825	632	--	--	--	--
	21 - 31	11,088	2,023	999	1,073	IN	--	--	--
JUN	5 - 26	11812	984	884	756	IN	IN	--	--
JUL	1 - 31	13,216	903	3,406	2,127	IN	IN	IN	--
AUG	1 - 31	11,457	860	3,428	1,733	IN	IN	IN	--
SEP	1 - 30	10,976	812	3,942	1,052	IN	IN	IN	--
OCT	1 - 15	8,445	935	3,950	571	IN	IN	IN	--
	17 - 31	7,442	1,034	3,686	485	IN	IN	IN	IN
NOV	12 - 19	9,917	1,037	3,572	2,805	--	--	--	--
	20 - 30	8,028	1,173	1,992	1,777	--	--	--	--
DEC	1 - 31	8,785	1,193	1,314	1,315	--	--	--	--

Hourly simulated stage and flow data for each period were used to generate data for box plots, which graphically show period minimum, maximum, 25% quartile, 75% quartile, and median values. By the usual sign convention, negative flow values correspond to upstream flow. The locations where box plots of stage and flow are presented are shown in Figure 4-8 with arrows indicating assumed positive flow direction.

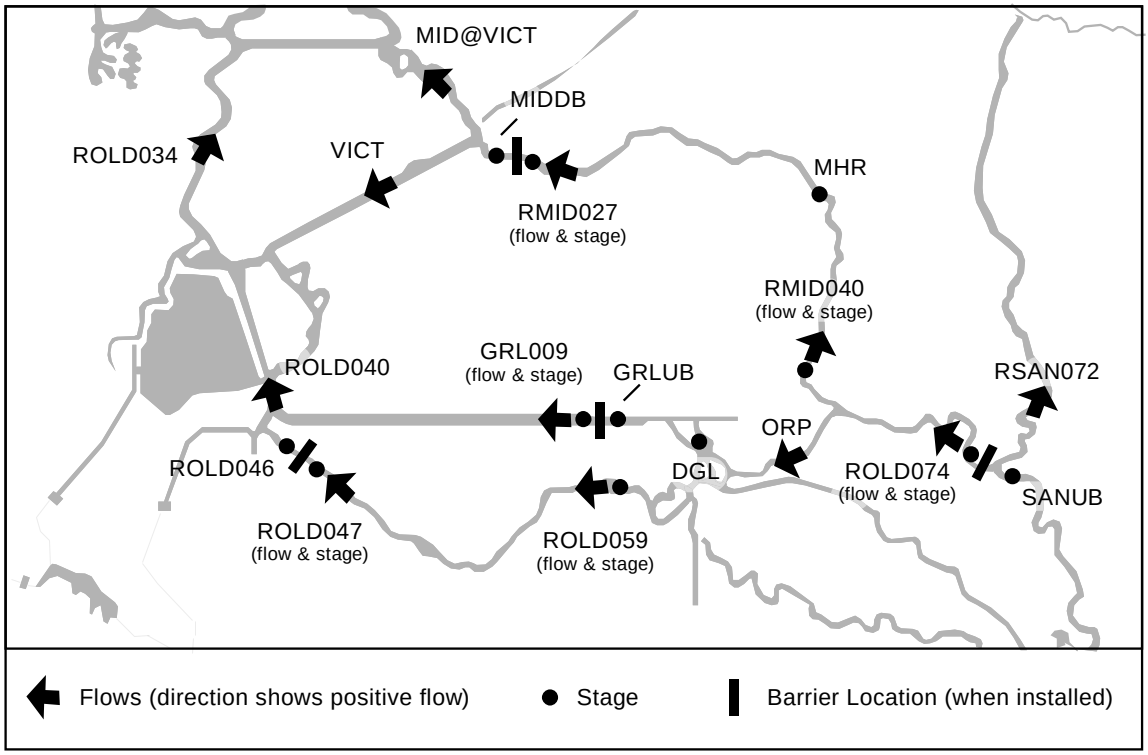

Figure 4-8 Locations where simulated Delta stages and flows for analysis of 2008 conditions are presented

Shown in Figures 4-9 and 4-10 are the box plots of simulated stages and flow for time periods when at least one barrier was historically installed. Stages are presented upstream and downstream of each barrier location, and flows are presented throughout the south Delta in order to convey the general circulation patterns. Distributions of flow and stage from both the historical simulation and the condition of no barriers assumed installed are provided to help analyze the effect of the installation of the barriers.

Figure 4-11 graphically presents the effects of the temporary barriers in 2008 on flow circulation and minimum water levels in the south Delta under the same time periods presented in Figures 4-9 and 4-10.

4.9 Discussion

The installation of the temporary barriers in 2008 significantly altered stages and flows in the south Delta. When the barrier in Middle River was installed in May, minimum water levels immediately upstream of the barrier were raised approximately a half-foot. This improvement decreased moving upstream until it essentially was eliminated at the junction of Old River. Thus, the effects on water levels due to the installation of the Middle River barrier alone were essentially limited to Middle River. The installation of the Old River barrier at the beginning of June in 2008 raised minimum water levels immediately upstream of the barrier approximately a half-foot, an effect which decreased farther upstream. The Old River barrier had little effect on water levels in Middle River or Grant Line Canal. For the period of June 5 to June 26, 2008, only the barriers at Middle River and Old River were fully installed. During this time, these barriers' primary impact was significantly raising water levels immediately upstream, an effect which diminished farther upstream until becoming negligible in Grant Line Canal. The overall circulation pattern in the south Delta during this period was only modestly altered by the

2 barriers since the flow split from the San Joaquin River down the head of Old River and the subsequent flow down Grant Line Canal weren't strongly affected.

The complete installation of the Grant Line Canal barrier in the beginning of July raised the minimum water level in Grant Line Canal upstream of the barrier approximately 1-½ feet and levels in Middle River and Old River an additional 1 foot and a half-foot, respectively. Also, circulation patterns were altered as shown by a reduced portion of San Joaquin River flow down the head of Old River and less of a portion of this water then passing down Grant Line Canal and more going down Old River. Thus, the full impact on minimum water levels and changed flow patterns was not realized until the Grant Line Canal barrier was completely installed.

In general, the installation of the temporary barriers also resulted in reduced tidal variation in flows near the barriers, a trend once again made more pronounced in Old and Middle Rivers with the installation of the barrier in Grant Line Canal. Each of the barriers still allowed some downstream flow, while both upstream and downstream flow was suppressed in the channels upstream of each barrier site.

The installation of the notched barrier at the head of Old River in October significantly further reduced the amount of San Joaquin River flowing down Old River and Grant Line Canal.

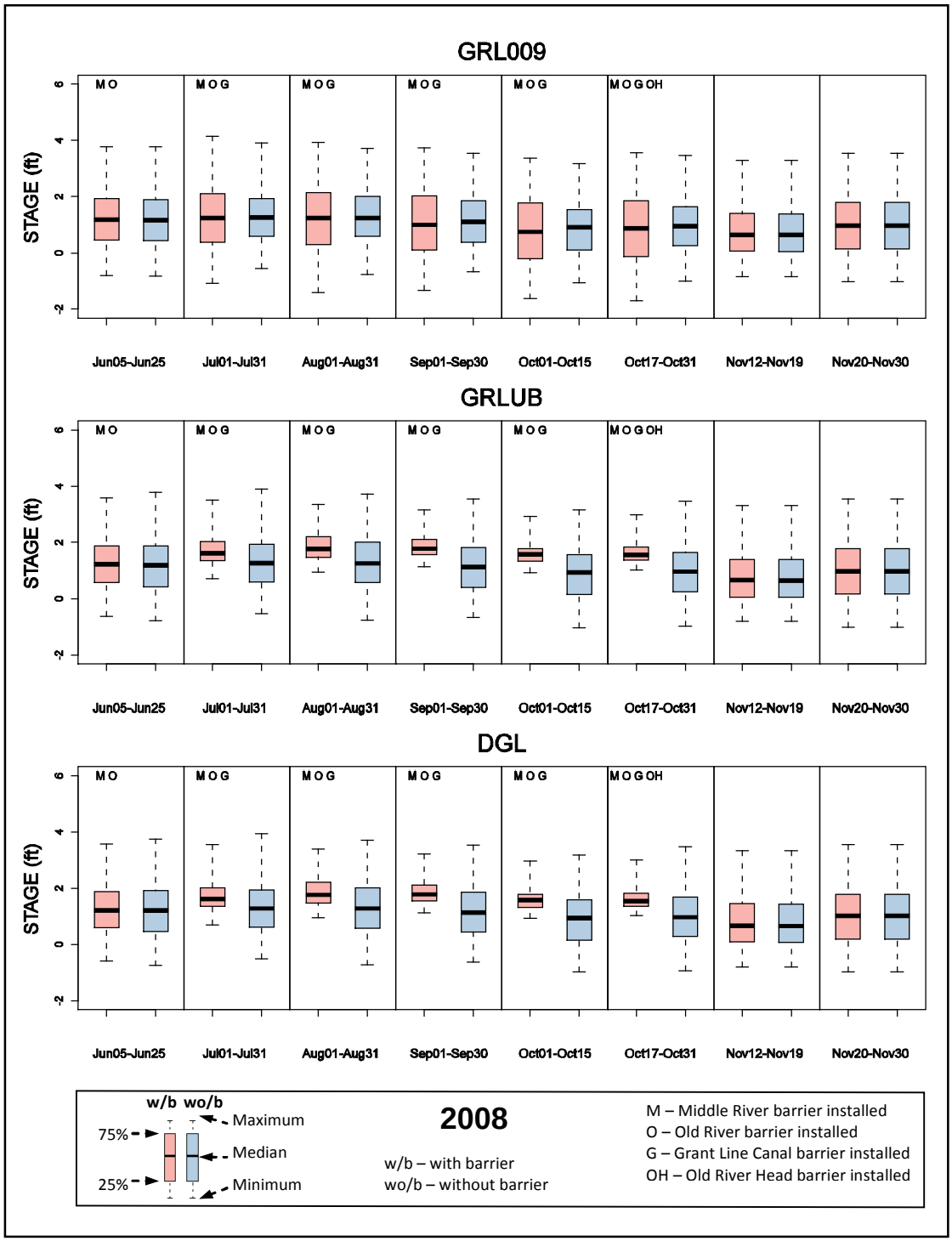

Figure 4-9 Distribution of DSM2-simulated stages for historical 2008 with and without temporary barriers installed

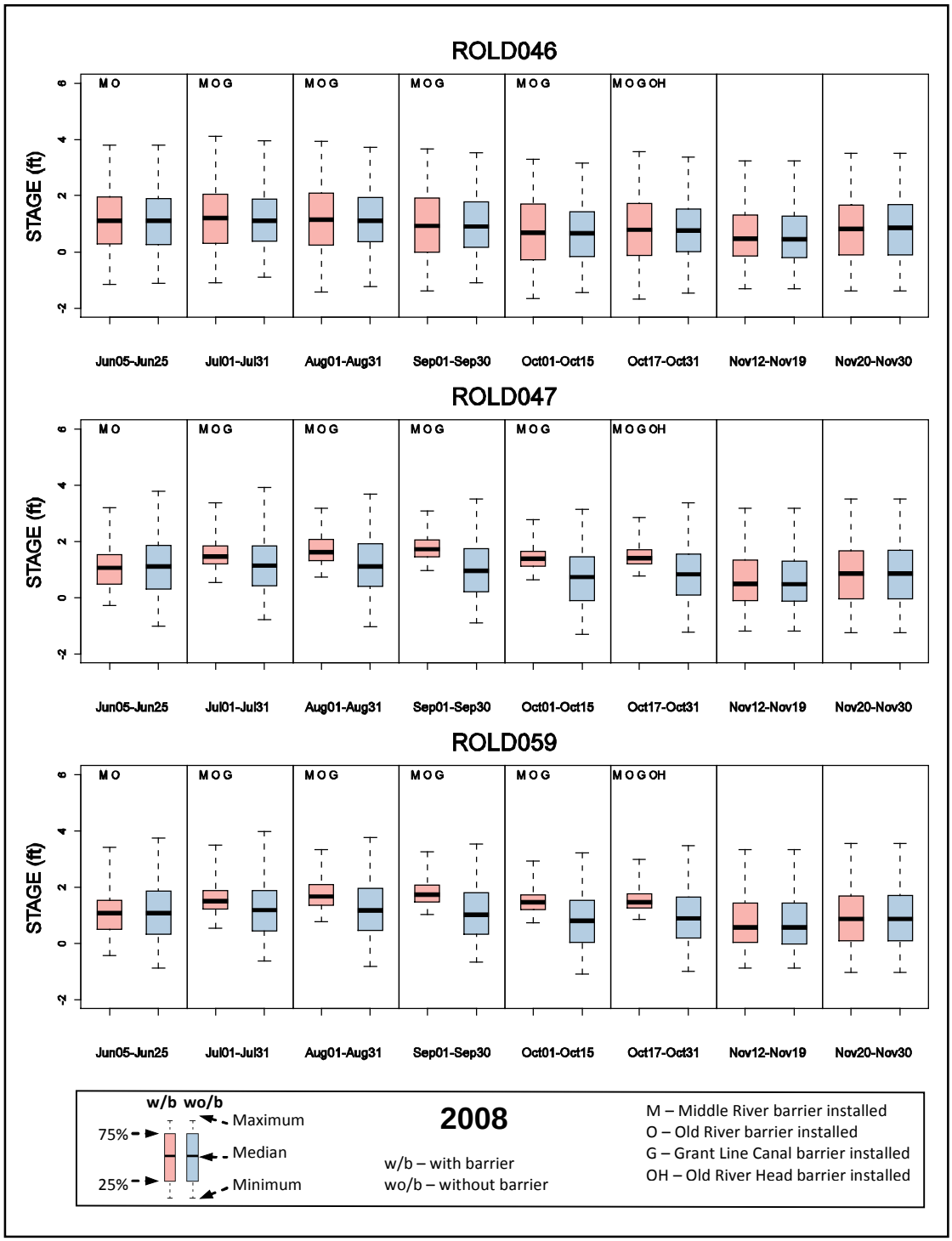

Figure 4-9 (cont.) Distribution of DSM2-simulated stages for historical 2008 conditions with and without temporary barriers installed

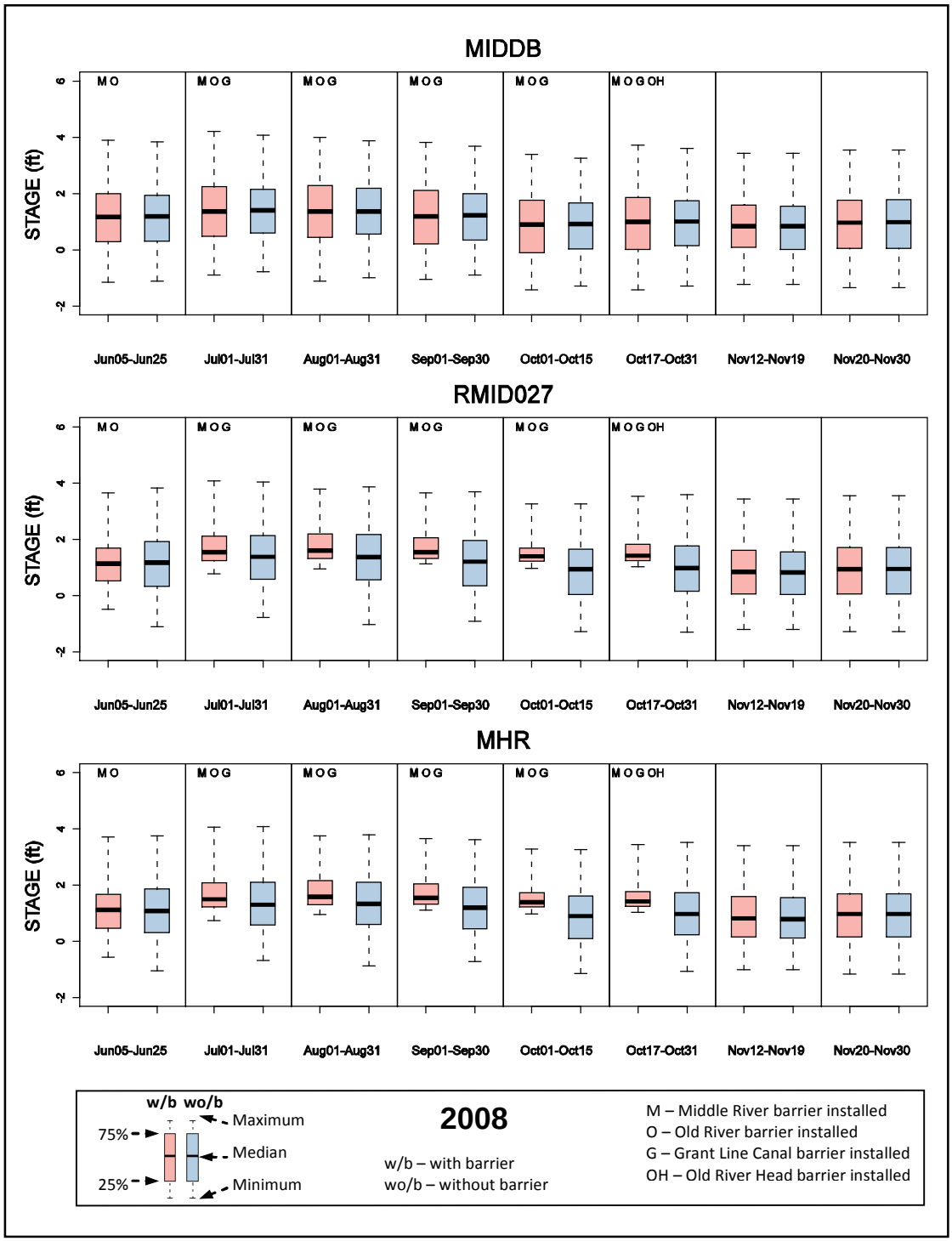

Figure 4-9 (cont.) Distribution of DSM2-simulated stages for historical 2008 conditions with and without temporary barriers installed

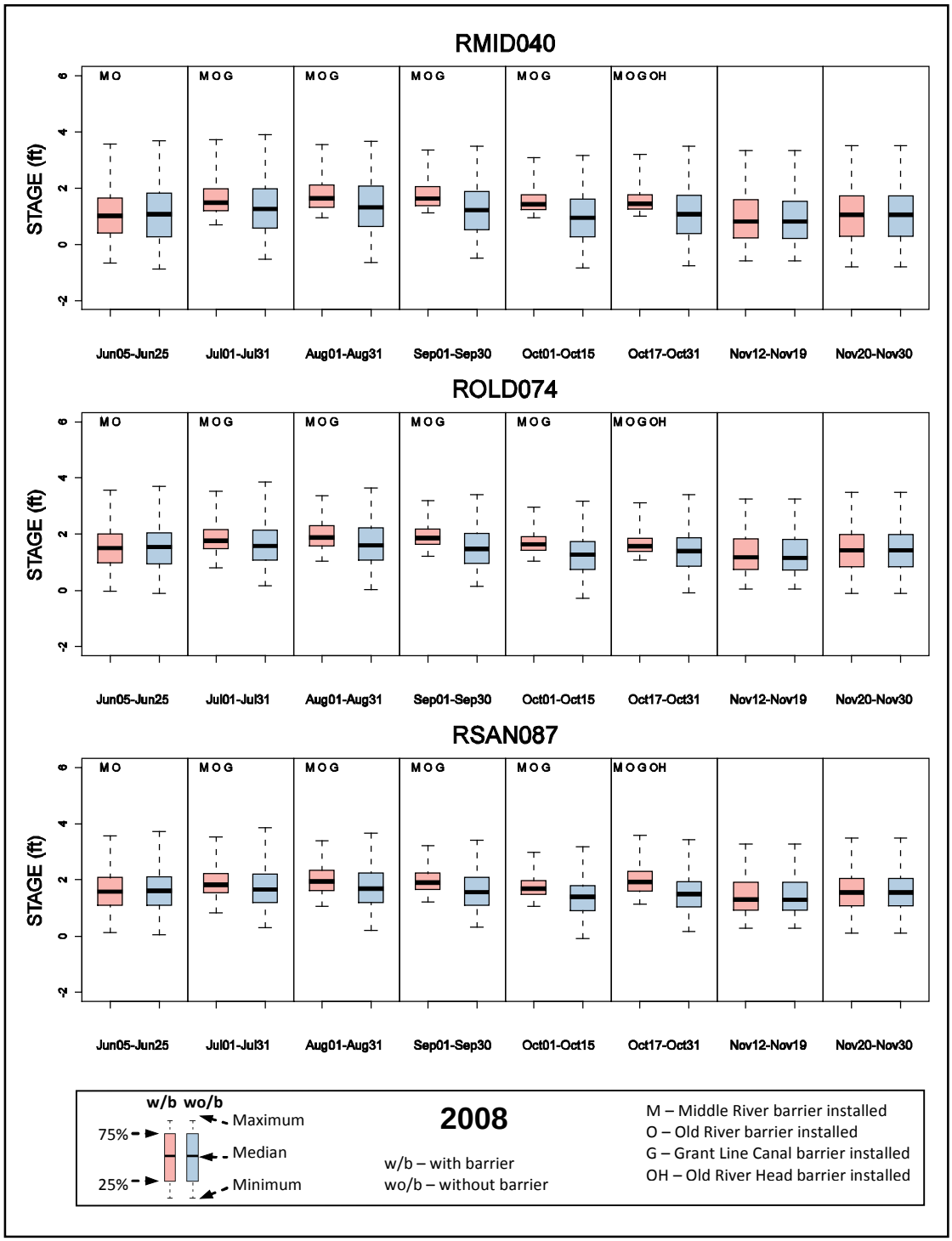

Figure 4-9 (cont.) Distribution of DSM2-simulated stages for historical 2008 conditions with and without temporary barriers installed

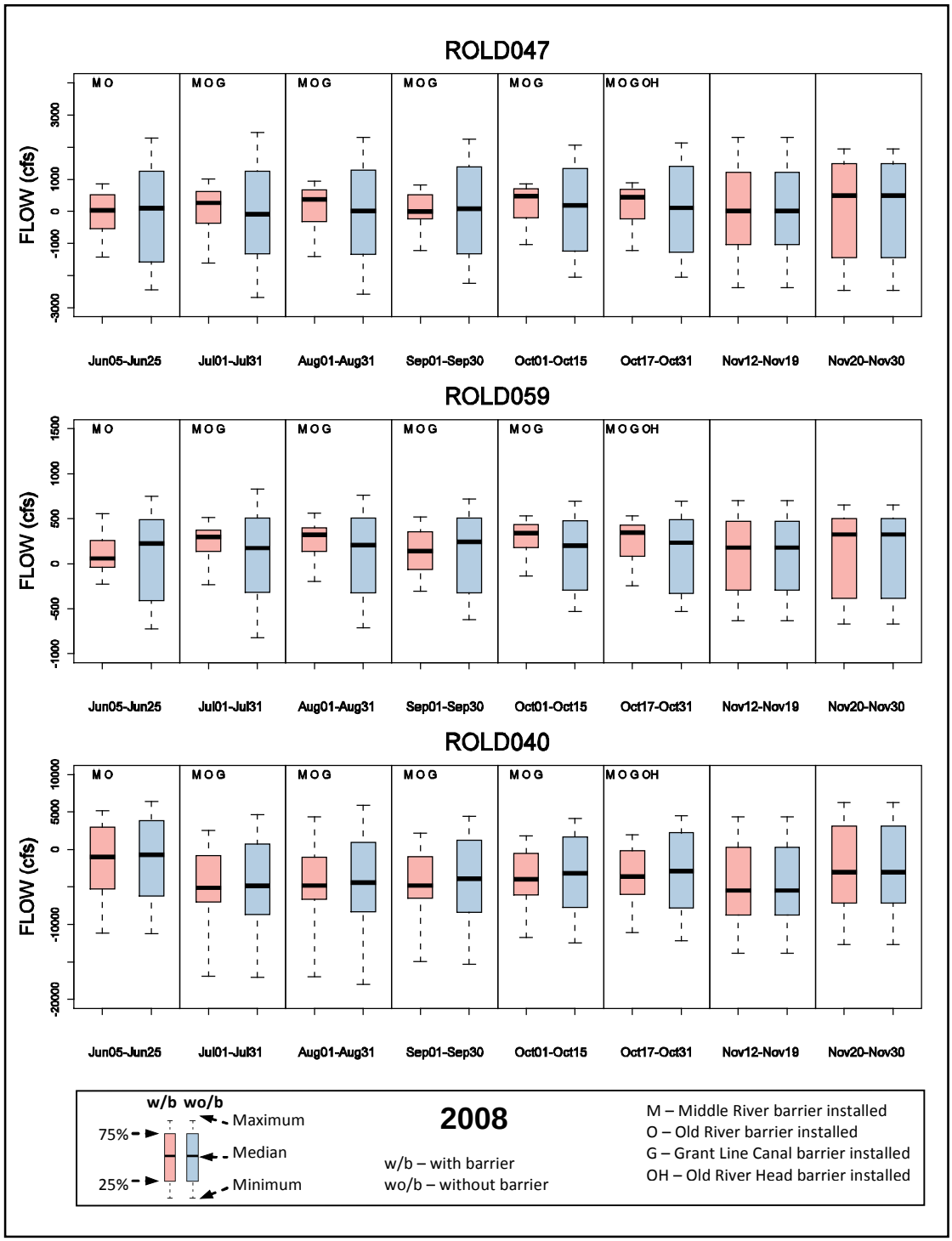

Figure 4-10 Distribution of DSM2-simulated flows for historical 2008 conditions with and without temporary barriers installed

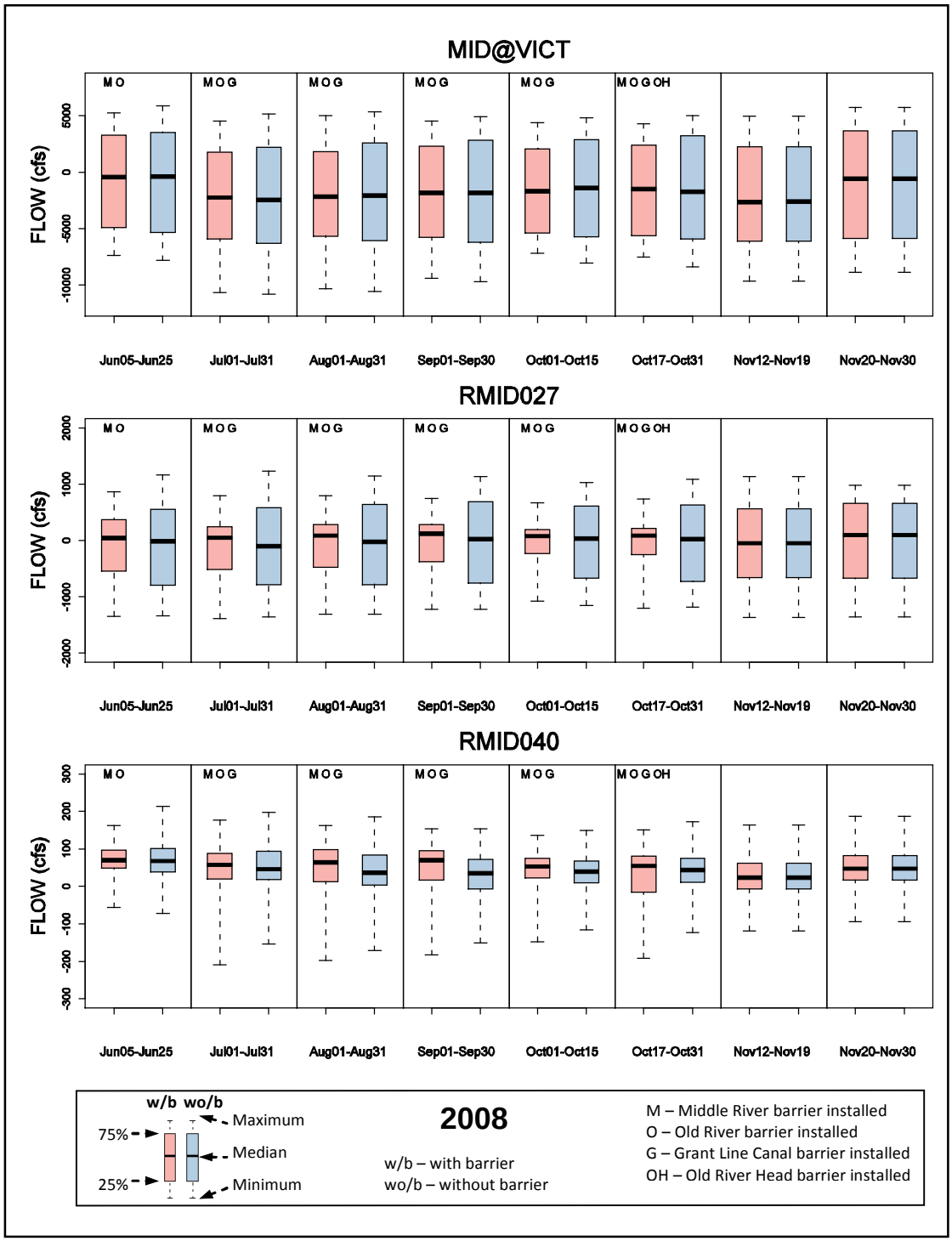

Figure 4-10 (cont.) Distribution of DSM2-simulated flows for historical 2008 conditions with and without temporary barriers installed

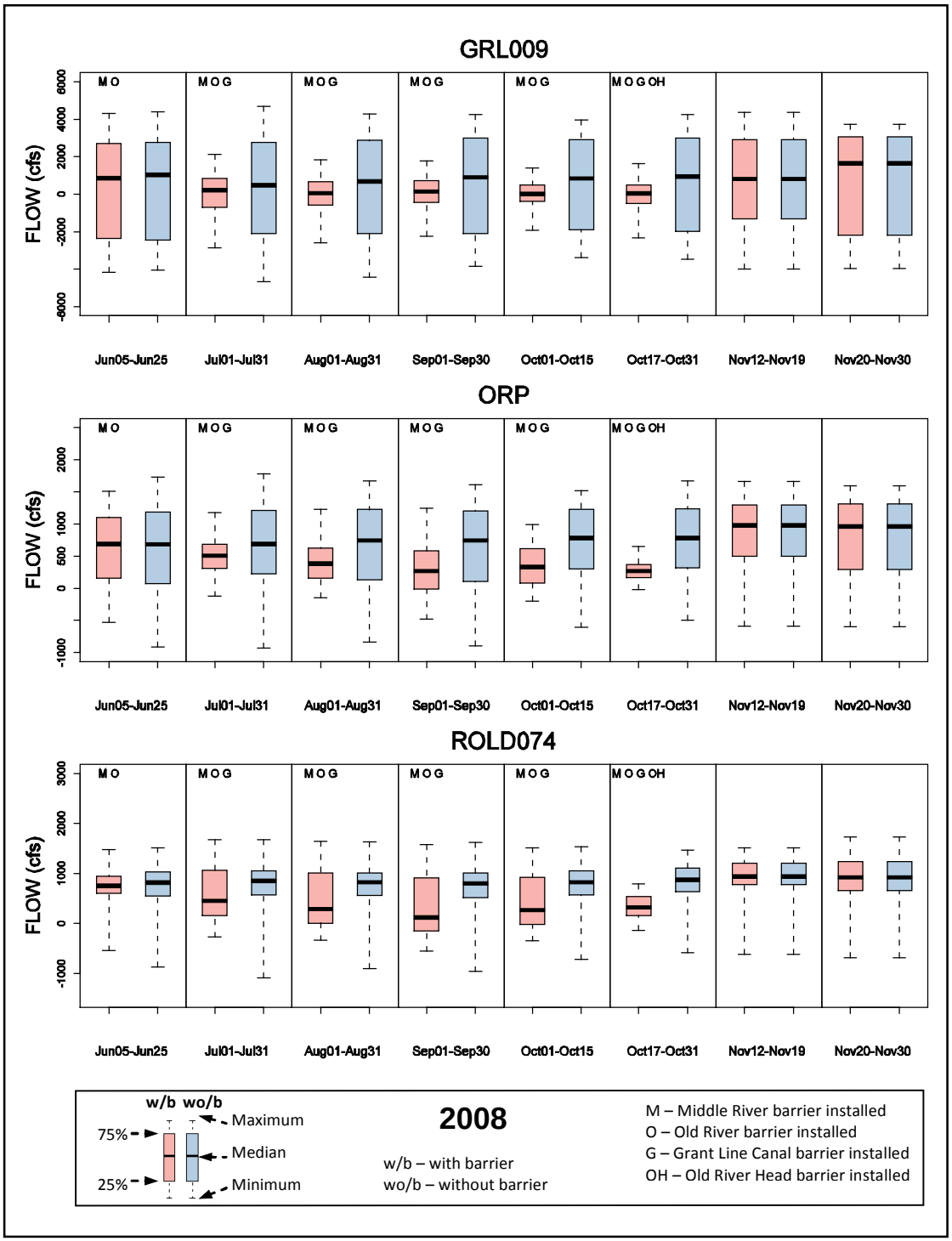

Figure 4-10 (cont.) Distribution of DSM2-simulated flows for historical 2008 conditions with and without temporary barriers installed

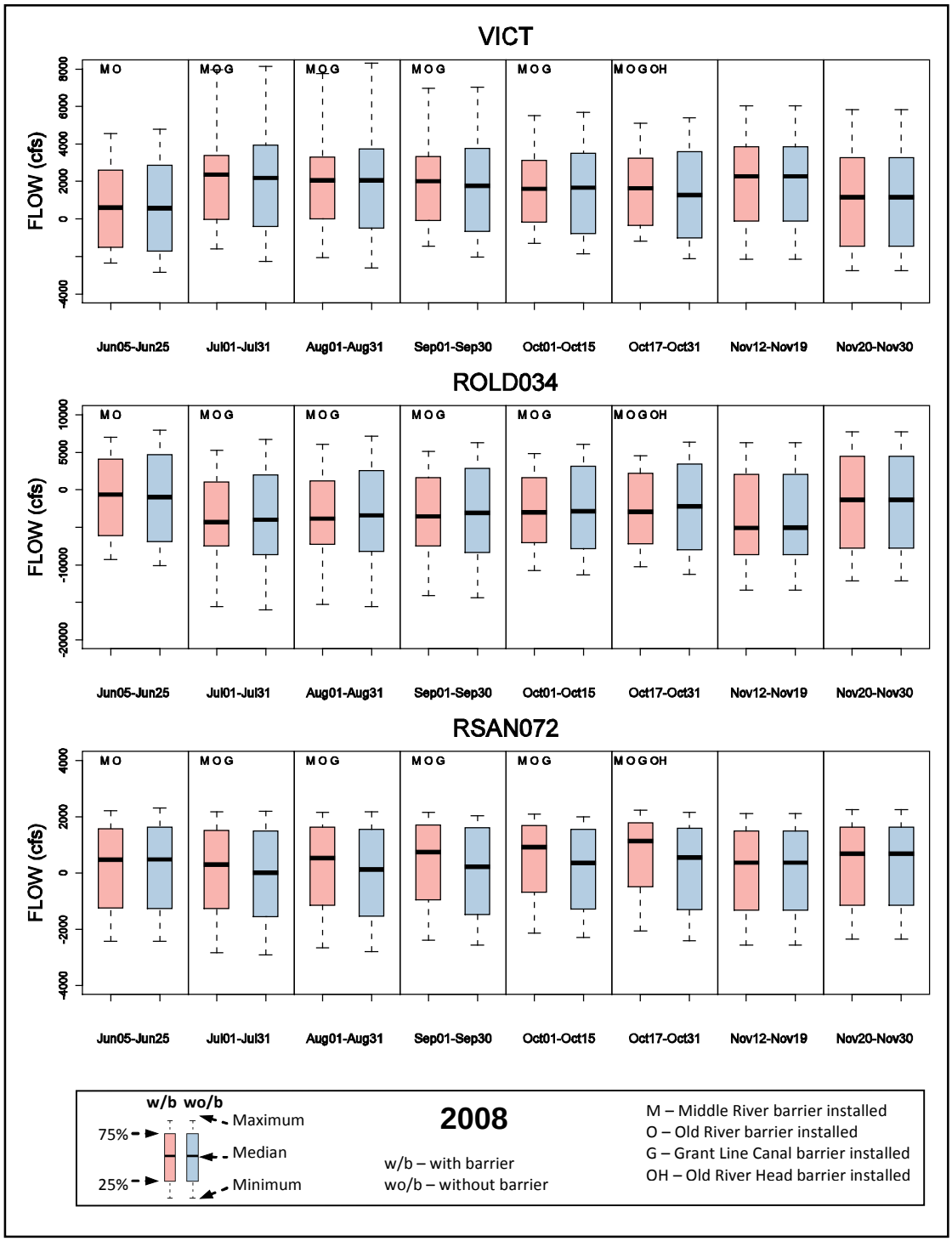

Figure 4-10 (cont.) Distribution of DSM2-simulated flows for historical 2008 conditions with and without temporary barriers installed

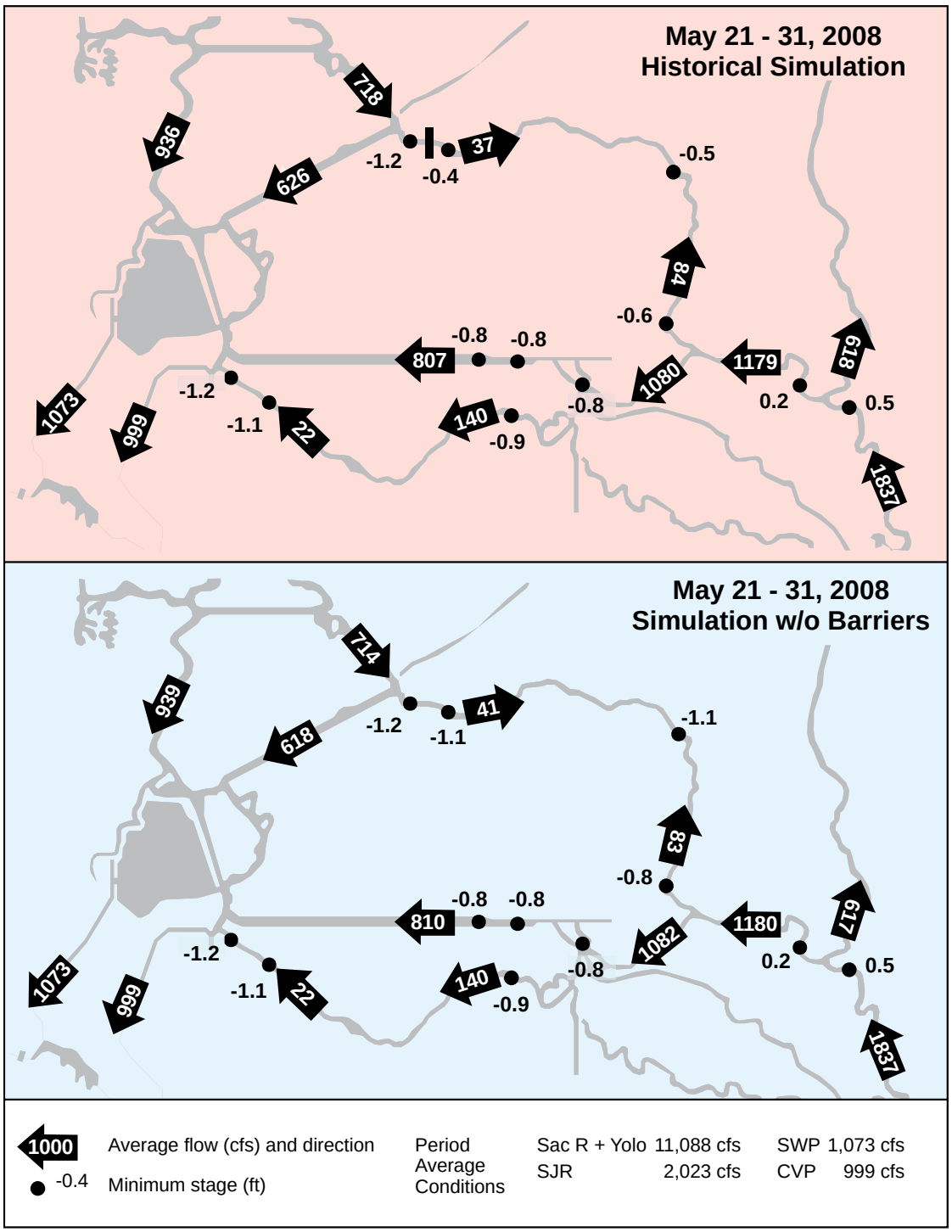

Figure 4-11 Simulated period-average flow and minimum stage for 2008 conditions with historical barrier configuration and no-barriers condition

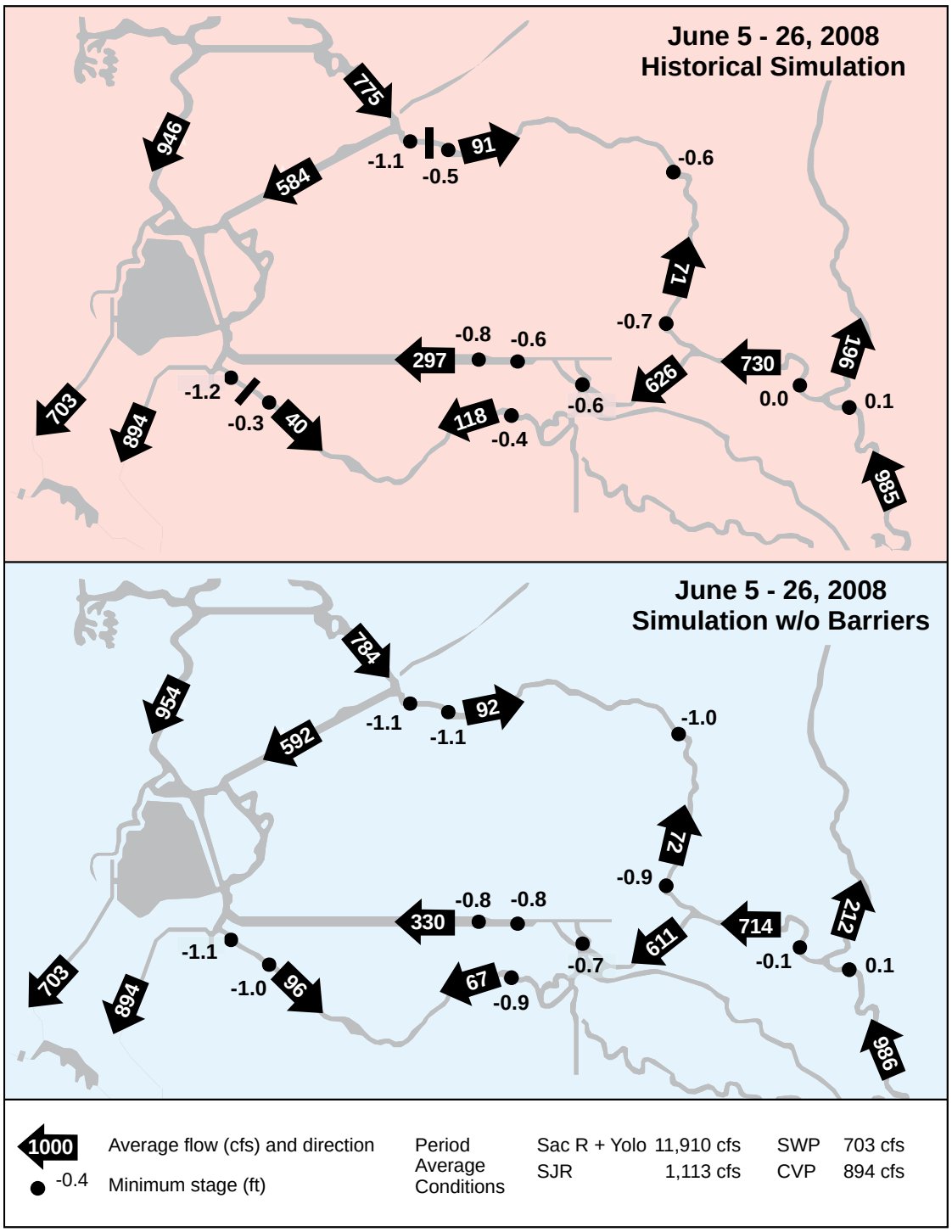

Figure 4-11 (cont.) Simulated period-average flow and minimum stage for 2008 conditions with historical barrier configuration and no-barriers condition

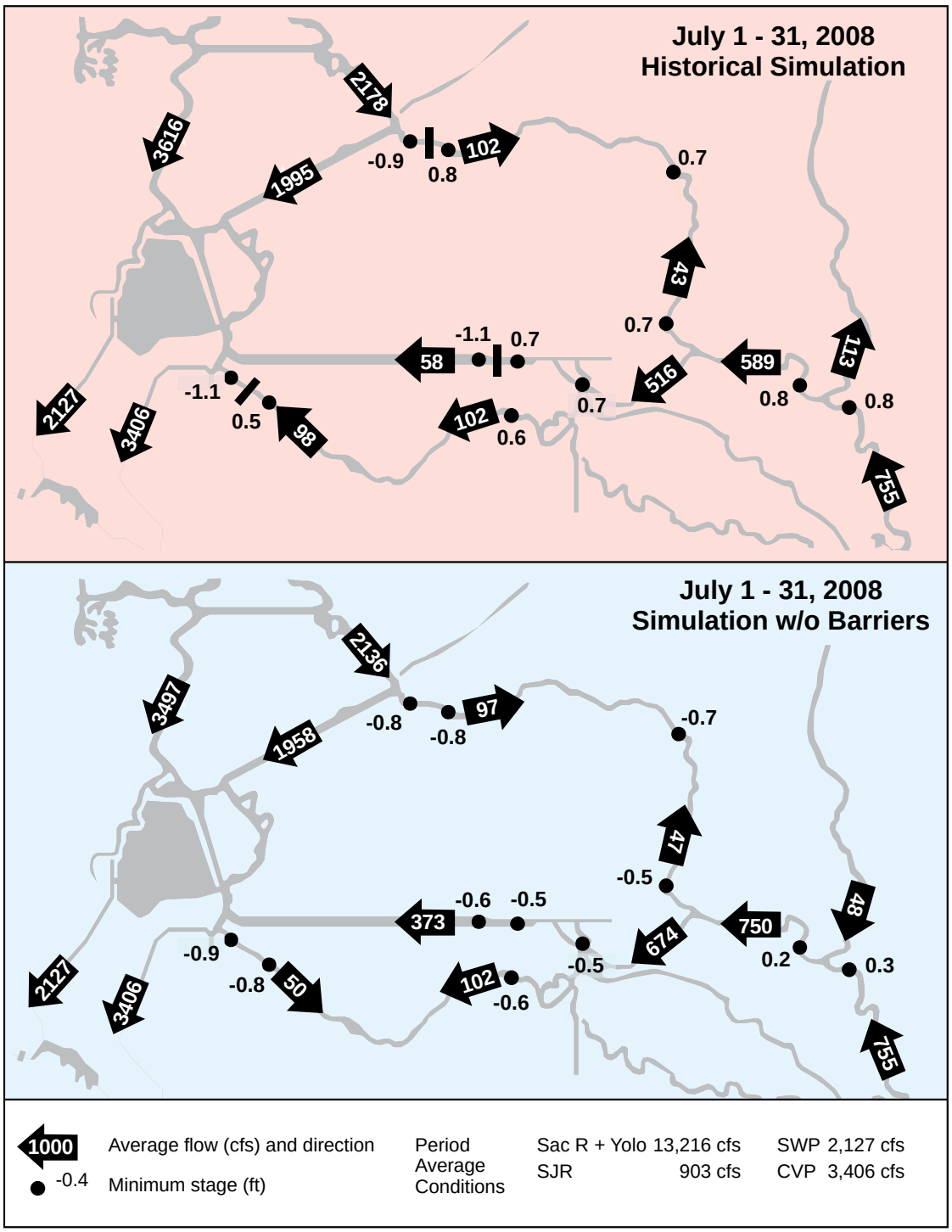

Figure 4-11 (cont.) Simulated period-average flow and minimum stage for 2008 conditions with historical barrier configuration and no-barriers condition

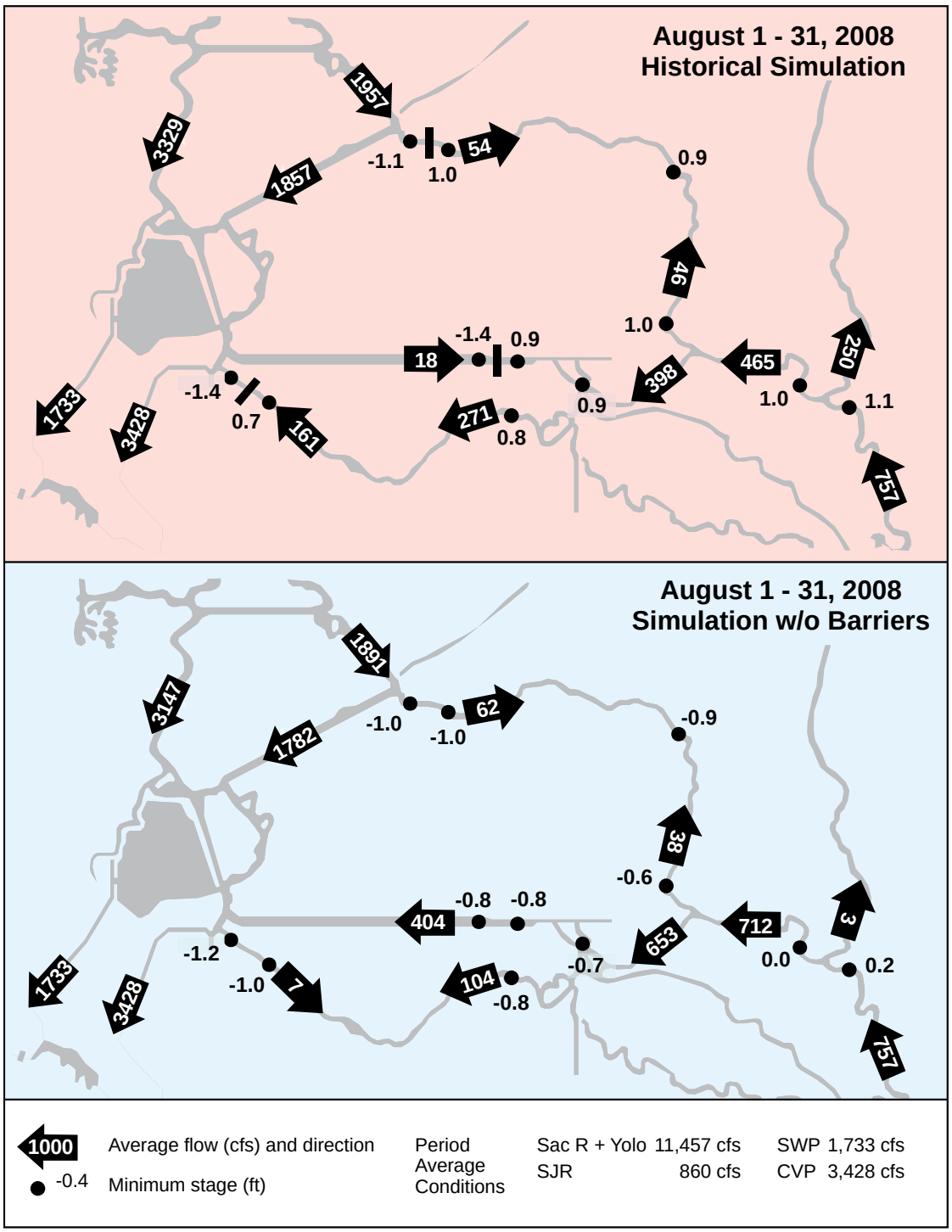

Figure 4-11 (cont.) Simulated period-average flow and minimum stage for 2008 conditions with historical barrier configuration and no-barriers condition

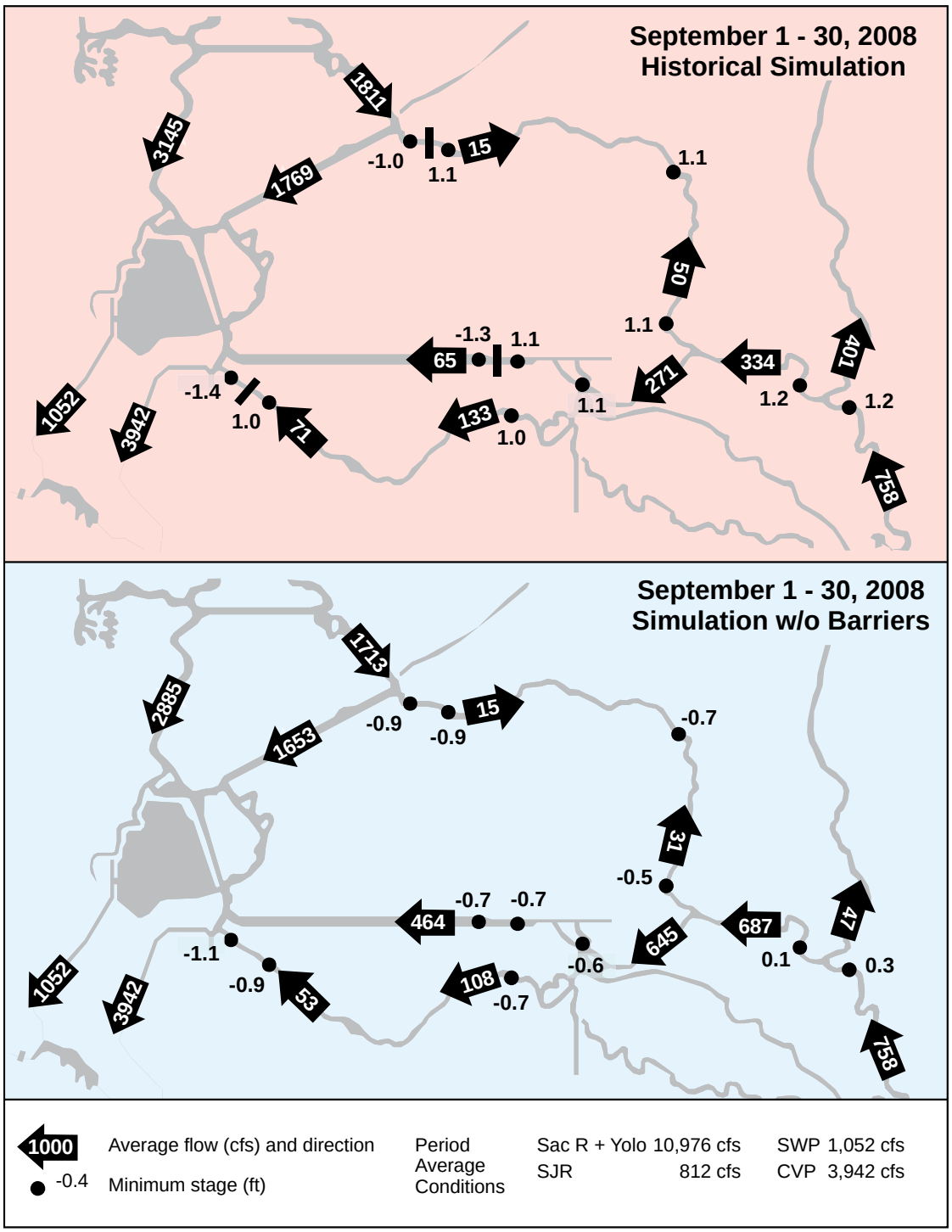

Figure 4-11 (cont.) Simulated period-average flow and minimum stage for 2008 conditions with historical barrier configuration and no-barriers condition

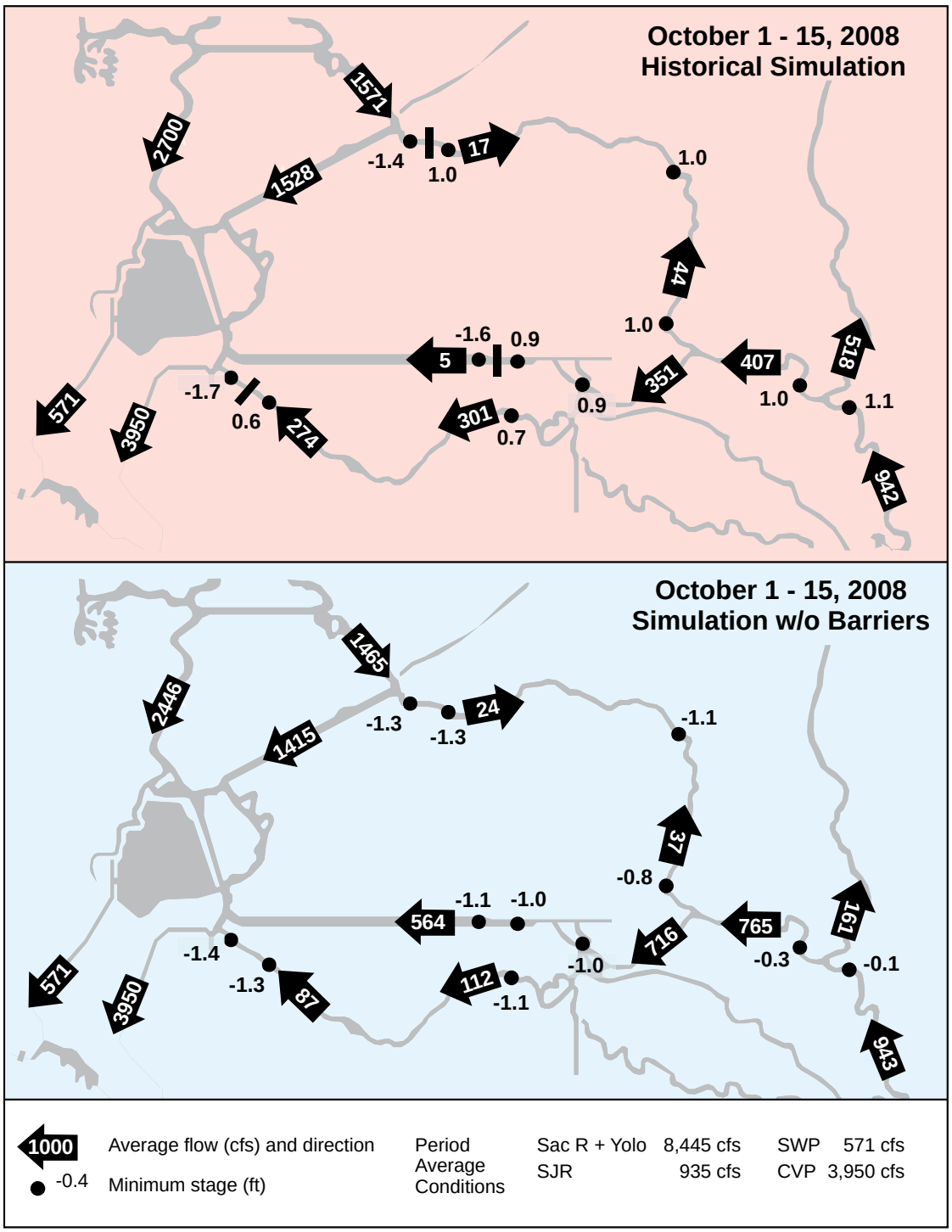

Figure 4-11 (cont.) Simulated period-average flow and minimum stage for 2008 conditions with historical barrier configuration and no-barriers condition

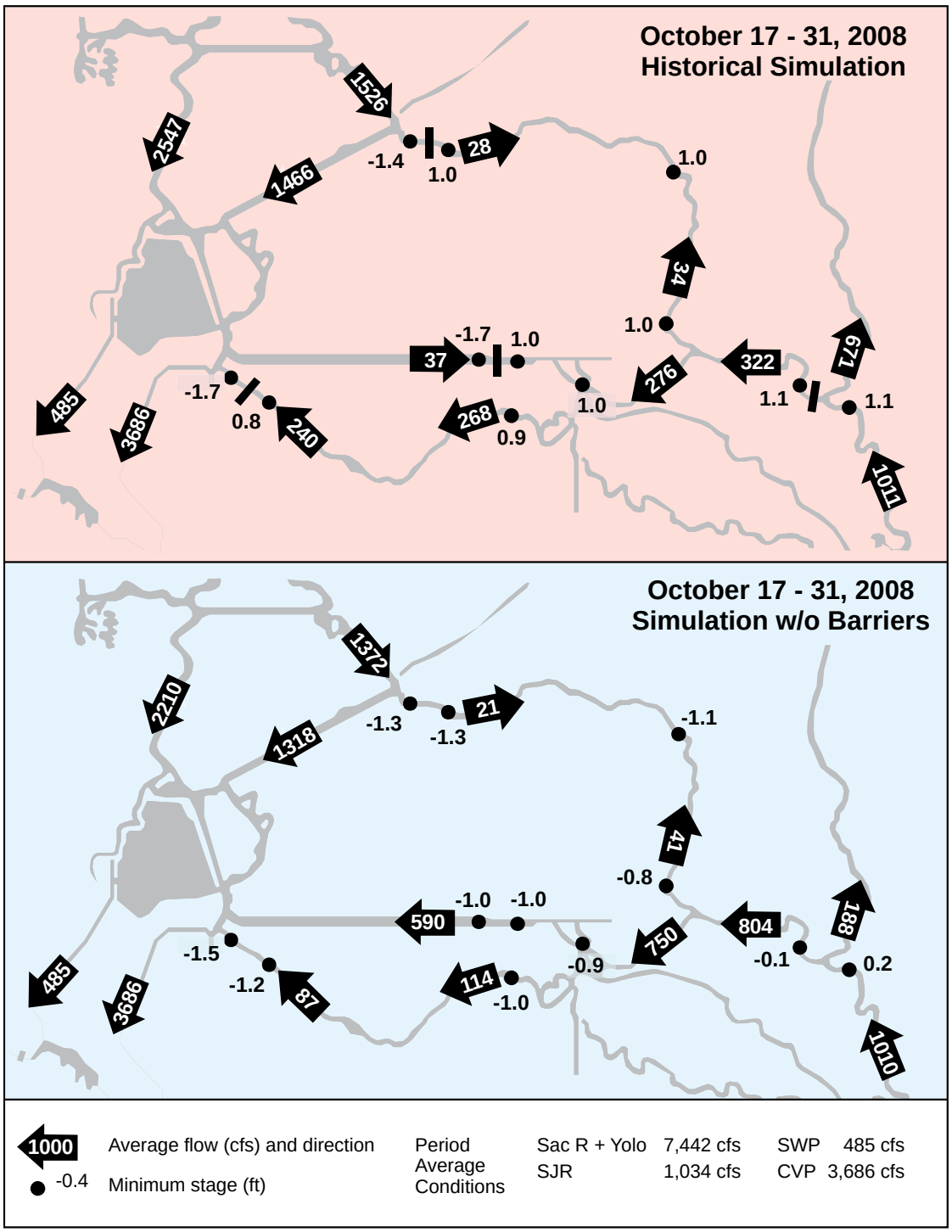

Figure 4-11 (cont.) Simulated period-average flow and minimum stage for 2008 conditions with historical barrier configuration and no-barriers condition

Methodology for Flow and Salinity Estimates in the Sacramento-San Joaquin Delta and Suisun Marsh

32nd Annual Progress Report
June 2011

Chapter 5
Adaptive Mesh, Embedded Boundary Model for Flood Modeling

Authors: Qiang Shu and Eli Ateljevich,
Delta Modeling Section,
Bay-Delta Office,
California Department of Water Resources

Contents

5 Adaptive Mesh, Embedded Boundary Model for Flood Modeling 5-1
5.1 Summary 5-1
5.2 Introduction 5-1
5.3 Governing Equations 5-1
5.4 Solution Algorithm 5-3
5.4.1 Adaptive Mesh Refinement 5-4
5.4.2 Embedded boundaries 5-5
5.4.3 Godunov algorithm 5-5
5.5 Wet/Dry Front Capture 5-6
5.6 Model Verification 5-7
5.6.1 Dam Break on a Dry Bottom 5-8
5.6.2 Dam Break on a Wet Bottom 5-9
5.6.3 Dam Break on a Dry Bottom with Friction 5-10
5.7 Applications and Challenges 5-10
5.8 Acknowledgements 5-11
5.9 References 5-11

Figures

Figure 5-1 A multiblock adaptive mesh hierarchy with a refinement factor of 2 between levels 5-4
Figure 5-2 Decomposition of a patch of cells into regular, irregular, and covered cells 5-5
Figure 5-3 Two depictions of flooding 5-6
Figure 5-4 AMR resolving a flood along a reach of the Sacramento River 5-7
Figure 5-5 Water depth (left) and velocity (right) after dam break at time 50.78 seconds 5-8
Figure 5-6 Water depth (left) and velocity (right) after dam break at time 50.52 seconds 5-9
Figure 5-7 Water depth (left) and velocity (right) after dam break at time 50.88 seconds 5-10

5 Adaptive Mesh, Embedded Boundary Model for Flood Modeling

5.1 Summary

We describe a 2-dimensional shallow water model designed to simulate water quality and flooding. The model uses a finite-volume discretization of the shallow water equations on an adaptive Cartesian mesh, using embedded boundaries to represent complex topography. For flooding applications, we use adaptive mesh refinement (AMR) to evolve Cartesian sub-grids near a flood front, which leads to a resolved local result. Fluxes on the front itself are described using wet-dry Riemann solutions. The algorithms are implemented in parallel and highly scalable. The model is tested using analytical solutions of flood propagation on wet and dry channels and of a dam-break problem. Applications to flooding in arbitrary bathymetry are discussed.

5.2 Introduction

The California Department of Water Resources (DWR) and Lawrence Berkeley National Laboratory (LBNL) are collaboratively developing a multi-dimensional computer model to solve the shallow-water equations. The motivation of the project is to provide a high performance, accurate, and open-source tool for decision making support in the San Francisco Bay and Sacramento-San Joaquin Delta. The Bay-Delta system is a nexus of water policy debate and scientific scrutiny, with constantly shifting concerns including salt intrusion, fish and pollutant transport, water supply reliability, and flooding of Delta islands. In particular, the property and infrastructure risk posed by flood events underscores the need for models in flood risk assessment and planning.

Our shallow water model REALM (River, Estuary, and Land Model) includes a shock-capturing algorithm and 2 technologies relevant to flood modeling: adaptive mesh refinement and embedded boundaries. We employ adaptive mesh refinement (AMR) [(Berger and Oliger 1984) (Berger and Colella 1989)] to refine fronts, maintain resolution at local length scales and concentrate computational resources on predefined areas of interest. We use a Cartesian mesh with embedded boundaries (EB) to represent the natural shoreline. Although adaptive mesh refinement has been used before in flood modeling [e.g. (George 2006); (Begnudelli, Sanders and Bradford 2008)], we believe that the use of AMR and EB together is novel, particularly in context of a scalable, parallel computer architecture.

This chapter summarizes our algorithm, describes details relevant to flood modeling, and describes the verification of our model for transient flooding events using problems from the literature on wet and dry beds. We discuss wet bed applications in a natural setting with arbitrary topography, as well as some of the challenges and ambiguities of the EB-AMR approach on 2 different types of wetting and drying problems.

5.3 Governing Equations

Our shallow water model REALM is based on the 2D depth-integrated Navier-Stokes equations, with a hydrostatic treatment of pressure, Boussinesq assumption concerning salt-induced horizontal (baroclinic) density variation and friction. The shallow water equations are commonly and efficiently used as models of flood propagation and inundation, a practice that is noted and critiqued in (Alcrudo 2002).

In terms of the height of the water column h, local velocities u and v and salt concentration s, the shallow water equations in conservation form are

$$\frac{\partial U}{\partial t} + \frac{\partial (F^x)}{\partial x} + \frac{\partial (F^y)}{\partial y} = S \qquad \text{Eq. 5-1}$$

where the conserved variable vector $U = (h, hu, hv, hs)^T$ and the flux across cell faces in x and y directions are

$$F^x = \begin{pmatrix} hu \\ hu^2 + \dfrac{g\rho h^2}{2\rho_0} \\ huv \\ hus \end{pmatrix} \qquad \text{Eq. 5-2}$$

$$F^y = \begin{pmatrix} hv \\ huv \\ hv^2 + \dfrac{g\rho h^2}{2\rho_0} \\ hvs \end{pmatrix} \qquad \text{Eq. 5-3}$$

In these equations, g denotes the gravitational constant, ρ_0 denotes the density of fresh water, and $\rho = \rho(s)$ is an equation of state. To focus on flooding and the hyperbolic component of our solver, viscous terms, including horizontal eddy diffusivity and salt dispersion are not discussed here.

The sources and sinks include pressure forces from the bed, friction stress, and other local sources of mass or momentum such as wind or Coriolis acceleration. Here we consider only bottom pressure and friction:

$$S = \left[0, -\frac{g\rho}{\rho_0} hb_x - \tau_x, -\frac{g\rho}{\rho_0} hb_y - \tau_y, 0 \right]^T \qquad \text{Eq. 5-4}$$

where b_x and b_y are the slope of the bed in x and y direction and τ_x is a bottom stress given by the Chezy formula (Molls, Zhao and Molls 1998):

$$\tau_x = \frac{\rho}{\rho_0 C^2} u\sqrt{u^2 + v^2} \qquad \text{Eq. 5-5}$$

$$\tau_y = \frac{\rho}{\rho_0 C^2} v\sqrt{u^2 + v^2} \qquad \text{Eq. 5-6}$$

where C is the Chezy coefficient.

5.4 Solution Algorithm

We use a finite volume discretization of the shallow water equations, based on a Cartesian grid with embedded boundaries representing shorelines. Data are collocated at cell centers. Our algorithm is best articulated in 3 tiers:

AMR: Adaptive mesh refinement orchestrates integration over the multiple levels of grids refined in space and time.

EB: We use a special treatment on the cell containing shoreline.

Godunov: Single grid computations are handled by a second order Godunov scheme with corner transport upwind (CTU) treatment of fluxes at cell faces.

5.4.1 Adaptive Mesh Refinement

In the organization of our algorithm, adaptive mesh refinement plays the role of an outer controller, sequentially advancing the time step at different levels of refinement. The AMR component of our algorithm follows Berger and Colella (1989) as modified by Colella, Graves, et al. (2006) and Pember, et al. (1995) for embedded boundaries. The cycle of information is depicted in Figure 5-1. Levels of the AMR hierarchy are integrated from coarse to fine. Between levels, results in coarse cells abutting fine-coarse interfaces (dots) are used to help estimate boundary conditions for the next finer level. Upon completion of the time step, fine cell states and fine cell fluxes are averaged and used to replace data in underlying coarse cells. When regridding occurs, further interpolation is required to fill new levels. The result is a conservative, consistent estimate over the hierarchy. Our AMR approach allows flexible criteria for refining cells, including user-prescribed refinement, refinement based on (Richardson extrapolation) error estimates, presence of a wet-dry interface, or sharp gradients.

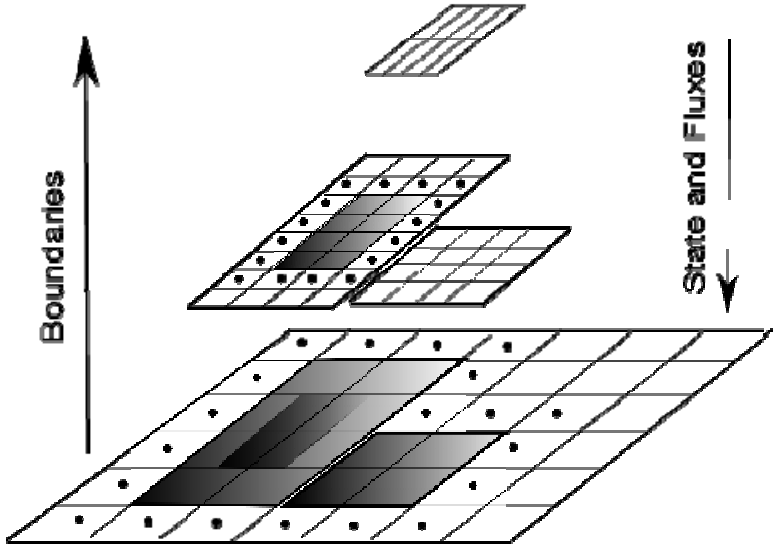

Note: Coarse cells adjacent to fine cells (dots) are used to provide boundary conditions for the fine mesh

Figure 5-1 A multiblock adaptive mesh hierarchy with a refinement factor of 2 between levels

5.4.2 Embedded boundaries

We use Cartesian cut cells (Colella, Graves, et al. 2006) to represent natural boundaries with high fidelity without a steep time step penalty in partial cells due to the use of an explicit integration method. Figure 5-2 shows a grid intersecting the boundary at a shoreline. The grid is decomposed into regular, irregular, and covered cells (covered cells are implied by elimination).

Regular cells are integrated using methods for a square Cartesian mesh. Irregular volumes of fluid are treated using a hybrid update that combines a conservative small cell estimate with a non-conservative full cell estimate, using weights proportional to the fraction of the irregular cell that is wet. The non-conservative divergence contributes stability; the conservative divergence preserves mass and momentum, induces the boundary condition, and is accurate. The combination induces a mass and momentum discrepancy, and the mismatch is mitigated by redistribution of the discrepancy to nearby cells. Further details are discussed in Colella, Graves, et al. (2006).

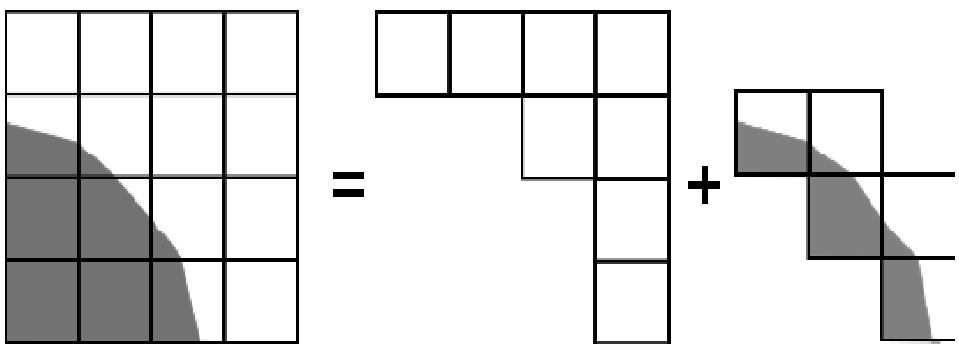

Note: Gray regions are outside the domain. Covered cells have been removed from the illustration on the right side.

Figure 5-2 Decomposition of a patch of cells into regular, irregular, and covered cells

5.4.3 Godunov algorithm

Within one multiblock grid, we employ the solution algorithm in Colella, Graves, et al. (2006), which is a finite volume predictor-corrector method: We construct accurate, upwinded estimates of the fluxes on cell faces and then update cell average values. The technique has the following attributes:

1. Calculation of spatial gradients using limiters to avoid oscillations near discontinuities.
2. Extrapolation in one space dimension and time of variables from cell centers to edge centers at the half time.
3. Solution of a Riemann problems for upwinding, which convert the dual estimates of extrapolated variables on each side of a face into upwinded fluxes. We use a primitive solver based on the linearized problem as described in Toro (2006). The solution is modified to include salinity-induced density variation.
4. Modification of the dual, one dimension estimate with fluxes in the transverse direction, as in the Corner Transport Upwind method of Colella (1990).

The algorithm produce upwinded fluxes and primitive variable estimates that are shock-capturing, second order accurate in smooth flow, and robust to flow oblique to the coordinate faces. In cells that

intersect the shore, the upwinded primitive variables are further interpolated and combined into a conservative divergence as described in the previous section.

Source terms are integrated using Heun's method. A well known difficulty with explicit finite volume representations is maintaining quiescent flow. The pressure component of the flux must be discretized in such a way to balance the bed pressure source in quiescent flow. Otherwise, the discretization can excite flow from a fluid at rest. Our characterization of bed pressure is based on this balance using a source discetization with face contributions analogous to the face contributions to the flux divergence under the conditions that the water surface is level (at the cell center level) and velocity is zero. Because the flux divergence is a hybrid, the bed source is too. The approximation is consistent with the source terms $-\frac{g\rho}{\rho_0}hb_x$ and $-\frac{g\rho}{\rho_0}hb_y$ in the original partial differential equation (PDE) and preserves quiescent flow well.

5.5 Wet/Dry Front Capture

In flood modeling, one of 2 treatments of an evolving flood front is usually adopted. The first, which is common for modeling tsunamis and intertidal mudflats, is to treat front propagation as a side effect of rising or falling water on bathymetry (Figure 5-3a). The second propagates the flood as a discontinuity (Figure 5-3b) and requires the ability to track or capture the evolving front.

The results we present here are for evolution over a flood plain. We use our hyperbolic algorithm, wet-dry Riemann solvers, and AMR to capture flood waves (Figure 5-3b). We use embedded boundaries to model shores that do not move. The capability to model the interaction between water levels and bathymetry (Figure 5-3a) is a work in progress.

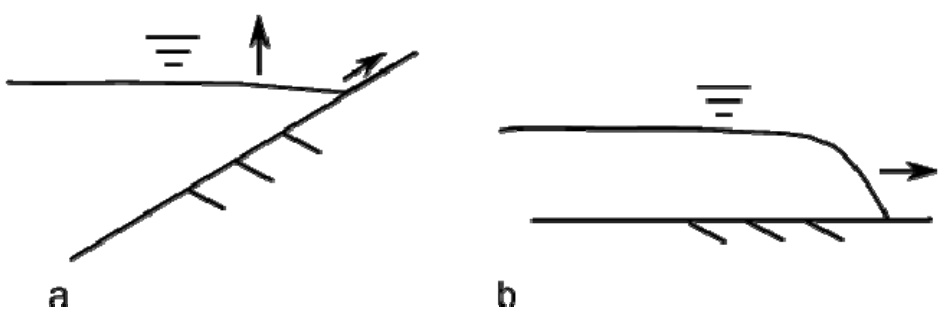

Figure 5-3 Two depictions of flooding

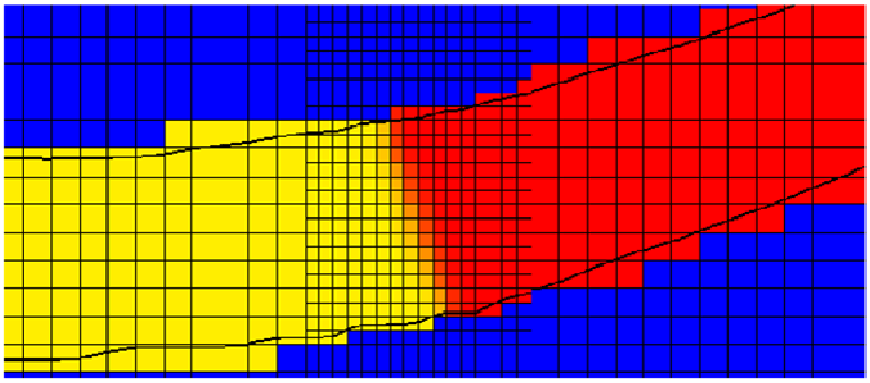

Figure 5-4 AMR resolving a flood along a reach of the Sacramento River

Adaptive mesh refinement is used to help resolve the flood wave front. Figure 5-4 shows subgrids spawned around a flood wave front on a reach of the Sacramento River based on the gradient of the solution. We also use dry-wet interfaces as a criterion for re-gridding. Embedded boundaries represent the (in this case, static) levee boundaries.

Due to the Godunov finite volume discretization, upwinding, and use of gradient limiters, our algorithm is inherently able to capture discontinuities such as flood waves and wet-dry fronts. In the Godunov algorithm, we estimate the state on the faces and switch between an exact wet/dry Riemann solution and approximate state wet/wet Riemann solution based on whether the faces are wet or dry. On faces with both sides dry, depth and velocity are of course always set to zero.

As will be seen in the next section, the model is capable of resolving and reproducing the shallow water physics of an advancing flood on both wet and dry beds.

5.6 Model Verification

We have applied our code to several flood and dam-break test cases proposed by CADAM (Concerted Action on Dam Break Modeling) to verify the stability and accuracy flood algorithms. A detailed description of the test suite is available in Goutal and Maurel (1997). Here we present results for CADAM tests 3, 4 and 5.

5.6.1 Dam Break on a Dry Bottom

This test problem has data containing a dry bed to the right of dam in a rectangular channel with a flat bottom. An instantaneous dam break is assumed, and unsteady flow velocity and water depth are computed by the model. An analytical solution (Ritter Solution) exists for the test and is given in Goutal and Maurel (1997). The objective of this test is to test the stability of the code in simulating the propagation of a wave over the dry zone.

The spatial domain is represented by a 2048x16 m rectangular cross section channel, which is discretized using 1 m square cells. The channel bottom is assumed frictionless and initial condition is set to:

$$\begin{cases} h = 6m, \quad u = 0 \quad \text{if} \quad x < 0 \\ h = 0m, \quad u = 0 \quad \text{if} \quad x > 0 \end{cases}$$

The dam break occurs at x=0. The time step is adapted to maintain a Courant number of 0.9. Results for this test are shown at time=50.78 s in Figure 5-5.

The simulated dry/wet surface matches the analytical solution well. In Figure 5-5 REALM correctly simulates the jump of velocity at the front without obvious oscillation.

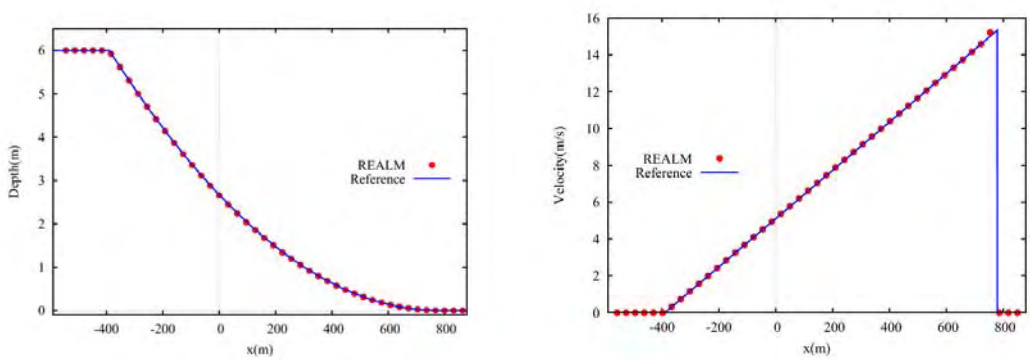

Figure 5-5 Water depth (left) and velocity (right) after dam break at time 50.78 seconds

5.6.2 Dam Break on a Wet Bottom

This test problem has data containing a wet bed to the right of dam in a rectangular channel with a flat bottom. An instantaneous dam break is assumed, and unsteady flow velocity and water depth are computed by the model. An analytical solution (Goutal and Maurel 1997) exists for the test. The objective of this test is to observe the ability of the code to resolve (a) the speed of wave propagation, (b) the strength of the jump on the shock front, (c) the width of the shock layer and (d) stability in the vicinity of the shock.

The spatial domain is again represented by a 2048x16 m rectangular cross section channel discretized using 1 m size square cells. The channel bottom is assumed frictionless and initial condition is set to:

$$\begin{cases} h = 6m, \quad u = 0 \quad \text{if} \quad x < 0 \\ h = 2m, \quad u = 0 \quad \text{if} \quad x > 0 \end{cases}$$

The dam is at x=0. The time step is adaptive to maintain a Courant number of 0.9.

Results for this test are shown at time 50.52 seconds in Figure 5-6.

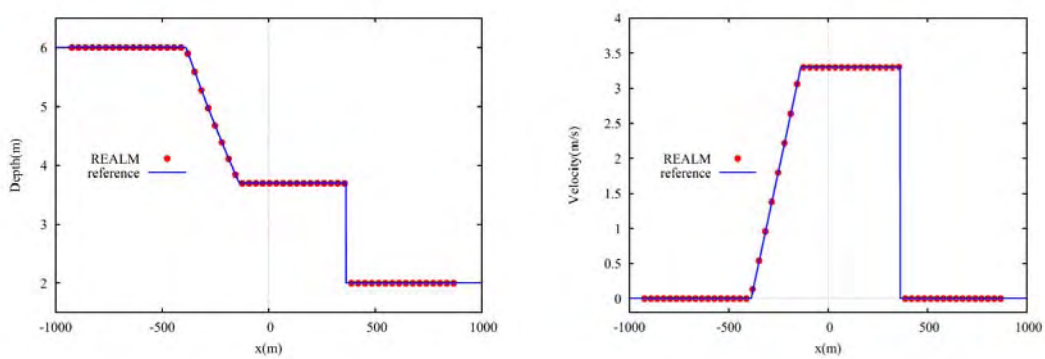

Figure 5-6 Water depth (left) and velocity (right) after dam break at time 50.52 seconds

Again REALM performs well with respect to the objectives of this test. The simulated left transonic rarefaction wave and right shock wave match their analytical counterparts as shown in Figure 5-6. The downstream wave moves faster than upstream wave, a feature of the analytical solution. In the left rarefaction wave, simulated water depth and velocity are smooth without any distinct break point. In the middle shock layer zone, both the computed water depth and velocity match the analytical solution well. There are no oscillations in the vicinity of the computed shock.

5.6.3 Dam Break on a Dry Bottom with Friction

In this test, REALM is applied to the unsteady flow resulting from an instantaneous dam breaking in a rectangular channel with constant width and with friction. Only the approximate Dressler solution (Dressler 1952) is available, the validity of which is limited to a region comprising less than one-third the distance to the point where the solution gives a zero value of flow. The objectives of this test are to validate the ability of the code to propagate a wave front over a dry bed with friction.

The spatial domain is again represented by a 2048x16 m rectangular cross section channel discretized using 1 m size square cells. The Chezy coefficient is set to 40 and the initial condition is set to:

$$\begin{cases} h = 6m, \quad u = 0 \quad \text{if} \quad x < 0 \\ h = 0m, \quad u = 0 \quad \text{if} \quad x > 0 \end{cases}$$

The dam is at x=0. The time step is adaptive to maintain a Courant number of 0.9.

Results for this test are shown at time 50.88 seconds in Figure 5-7.

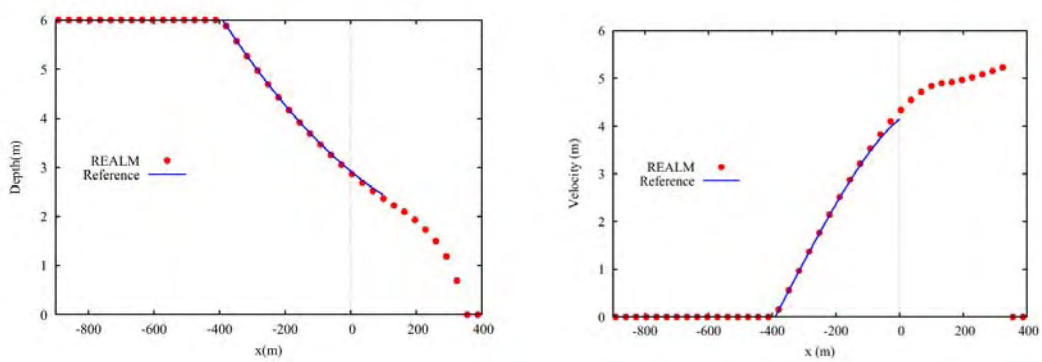

Figure 5-7 Water depth (left) and velocity (right) after dam break at time 50.88 seconds

The simulated result shows an apparent slowing down of the wave front. This effect is caused by the friction term. Upstream of the dam, REALM correctly computes water depth and velocity. The behavior of REALM is stable in the vicinity of the wave front.

5.7 Applications and Challenges

REALM appears to do well on a class of flood evolution problems involving flat bathymetry regardless of whether the bed is wet or dry. Anecdotally, we have observed that the model also handles practical flooding problems in fully wetted channels robustly. We point out, however, that the benchmarks presented in this paper focus on flat beds. This class of problem poses some of the greatest numerical challenges for flooding, but application of REALM on wetting and drying problems dominated by topography is still under development.

One problem during drying is caused by inaccurate reconstruction of volumes, depths, and face apertures in partially wet cells from the water surface. As a cell dries, its 2D area shrinks. The relationship between average depth and surface becomes more difficult to estimate. The cell can dry out early, and inconsistencies can develop between whether the cell is considered wet and whether a face is considered wet.

Begnudelli, Sanders, and Bradford (2008) noted similar problems and reconstruct the depth of partially dry faces by extrapolating a surface from the wet neighbors. Casulli (1990) proposes the use of a subgrid bathymetry model comprised of piecewise flat elements.

We are working to address the problem by updating the embedded boundary depiction of the domain along with fluctuations in the surface. On a domain with a steep bed, the treatment amounts to a subgrid bathymetry model. On a domain with a shallow bed slope, the flood front can move across the cell easily as a wave and be captured by the numerics, as was the case in the results presented here.

Another issue we have experienced is that high fluxes tend to overdraw the adjacent cells of mass and momentum. Sleigh et al. (1998) used a limited flux to solve this issue, in which momentum flux is set to zero and only mass flux is considered. Another solution in keeping with the mechanics of our algorithm is to include the overdraft as part of mass and momentum redistribution in the EB component algorithm, donating it to neighboring cells in proportion to the mass already contained in the cells. We also continue to hone our Riemann solutions for this application, as our approximate state Riemann solver is sometimes the source of unrealistic fluxes in extremely shallow flows.

5.8 Acknowledgements

Phillip Colella and Peter O. Schwartz of Lawrence Berkeley National Laboratory assisted with this investigation.

5.9 References

Alcrudo, F. "A state of the art review on mathematical modelling of flood propagation." *1st IMPACT Project Workshop.* 2002.

Begnudelli, L., B. F. Sanders, and S. F. Bradford. "Adaptive godunov based model for flood simulation." *J. Hydraul. Eng.* 34(6) (2008): 714–725.

Berger, M., and J. Oliger. "Adaptive mesh refinement for hyperbolic partial differential equations." *J. Comput. Phys.* 53 (1984): 484–512.

Berger, M., and P. Colella. "Local adaptive mesh refinement for shock hydrodynamics." *J. Comput. Phys.* 82(1) (1989): 64-68.

Casulli, V. "A high-resolution wetting and drying algorithm for free-surface hydrodynamics." *Int. J. Numer. Meth. Fluids* 60 (1990): 391–408.

Colella, P. "Multidimensional upwind methods for hyperbolic conservation laws." *J. Comput. Phys.* 87 (1990): 171–200.

Colella, P., D. T. Graves, B. J. Keen, and D. Modiano. "A cartesian grid embedded boundary method for hyperbolic conservation laws." *J. Comput. Phys.*, 2006: 347–366.

Dressler, R. F. "Hydraulic resistance effect upon the dam-break functions." *J. Res. Natl. Bur. Stand.* 49(3) (1952): 217–225.

George, D. "Finite volume methods and adaptive refinement for tsunami propagation and inundation." PhD thesis, University of Washington, 2006.

Ghidaglia, J. M., and F. Pascal. "On boundary conditions for multidimensional hyperbolic systems of conservation laws in the finite volume framework." *CMLA, ENS de Cachan.* 2002.

Goutal, N., and F. Maurel. "Description of the test cases." *Proceedings of the 2nd Workshop on Dam-Break Wave Simulation.* 1997. 18–28.

Molls, T., G. Zhao, and F. Molls. "Friction slope in depth-averaged flow." *J. Hydraul. Eng.* 124(1) (1998): 81-85.

Pember, R. B., J. B. Bell, P. Colella, and W. Y. Crutchfield. "An adaptive Cartesian grid method for unsteady compressible flow in irregular regions." *J. Comput. Phys.* 120(2) (1995): 278–304.

Sleigh, P. A., M. Berzins, P. H. Gaskell, and N. G. Wright. "An unstructured finite-volume algorithm for predicting flow in rivers and estuaries." *Computers & Fluids* 27(4) (1998): 479–508.

Toro, E. F. *Shock-Capturing Methods for Free-Surface Shallow Flows.* Chichester: John Wiley and Sons, 2006.

Methodology for Flow and Salinity Estimates in the Sacramento-San Joaquin Delta and Suisun Marsh

32nd Annual Progress Report
June 2011

Chapter 6
Using Software Quality and Algorithm Testing to Verify a One-dimensional Transport Model

Authors: Eli Ateljevich and Jamie Anderson,
Delta Modeling Section,
Bay-Delta Office,
California Department of Water Resources

K. Zamani and F. A. Bombardelli,
Department of Civil and Environmental Engineering,
University of California, Davis

Contents

6 Using Software Quality and Algorithm Testing to Verify a One-Dimensional Transport Model.....6-1

6.1 Introduction.....6-1

6.2 1-D Transport Model.....6-1

6.3 Testing Requirements.....6-2

6.4 Testing Principles.....6-2

6.4.1 Software Testing Principles.....6-3

6.4.2 Numerical verification and algorithmic testing.....6-4

6.5 Algorithm Test Suite Description.....6-6

6.6 Architecture and Implementation.....6-7

6.7 Challenges and Issues with Tests.....6-8

6.8 Conclusions.....6-9

6.9 Acknowledgments.....6-10

6.10 References.....6-10

Figures

Figure 6-1 Relationship between software testing components and algorithmic testing..... 6-3

Figure 6-2 Transport algorithm testing with incremental complexity..... 6-7

6 Using Software Quality and Algorithm Testing to Verify a One-Dimensional Transport Model

6.1 Introduction

In this chapter, we describe our approach and experiences developing a software verification framework for a one dimensional (1-D) transport model of advection, dispersion, and reactions or sources (ADR). We begin by describing the motivation and requirements for testing. Our acceptance criteria are driven by the requirements for the model, but are crafted according to principles from both the software and numerical testing fields. We then describe the components and implementation of the test suite, emphasizing the incremental nature of the tests, quantitative criteria for testing, and the similarities and tension between the silent, automatic perspective of software testing and the verbose, graphical outputs required for public reporting of numerical verification results.

The testing framework described in this paper was developed as part of a project to create a new transport module for the Delta Simulation Model 2 (DSM2), a 1-D hydrodynamic and transport model for flow and water quality in the Sacramento-San Joaquin Delta. Our target problems include river and estuary advection, and 1-D approximations of common mixing mechanisms and source terms associated with conservative and non-conservative water quality kinetics including sediment transport. The transport code is described briefly below followed by the development of the testing framework. The 2 are tightly coupled—since the transport module was created from scratch, it provided an opportunity to structure the code to be rigorously tested.

6.2 1-D Transport Model

The model used to illustrate the testing framework is based on the 1-D transport equations in conservative form:

$$\underbrace{\frac{\partial\big(A(x,t)C(x,t)\big)}{\partial t}}_{\text{Time evolution}} + \underbrace{\frac{\partial\big(A(x,t)C(x,t)u(x,t)\big)}{\partial x}}_{\text{Advection}} = \underbrace{\frac{\partial}{\partial x}\left(A(x,t)K(x,t)\frac{\partial C(x,t)}{\partial x}\right)}_{\text{Dispersion}} + \underbrace{R\big(x,t,C(x,t)\big)}_{\text{Source/Reaction}} \qquad \text{Eq. 6-1}$$

where x is the distance, t is time, A is the wetted area, C is the scalar concentration, u is the flow velocity, K is the longitudinal dispersion coefficient, and R is the source term (deposition, erosion, lateral inflow, and other forms of sources and sinks). Eq. 6-1 describes the mass conservation of a pollutant in dissolved phase, or suspended sediment away from the streambed.

The problem domain includes estuarine river channels and even some small open water areas roughly approximated as channels. The main transport process is advection, and the mixing mechanisms we anticipate are turbulent diffusion, gravitational circulation, and shear dispersion (Fischer, et al. 1979) (Abbott and Price 1994). We anticipate the shear dispersion to dominate over the turbulent diffusion. We also expect the gravitational circulation to exert an important role in mixing. We additionally contemplate significant, non-linear source terms from sediment, chemical and biological processes, though none of the processes are so quickly varying as to constitute truly stiff reactions.

Our algorithms include an explicit scheme for advection based on a finite-volume method (FVM) discretization and the Lax 2-step method (Colella and Puckett 1998) with van Leer flux limiter (Saltzman 1994). It also includes an implicit, time-centered Crank-Nicolson scheme for dispersion (Fletcher 1991). The advection and reaction solver are coupled as a predictor corrector pair, and dispersion is implemented separately using operator splitting.

6.3 Testing Requirements

The tests described in this chapter are all designed around suitability of the solver for estuary transport problems. The required accuracy on target modeling applications and choice of algorithm influence the testing requirements and the components of our algorithm test suite.

The scales of estuary transport determine the range of relative strength over which we test advection, diffusion and reactions, which is mostly intermediate Peclet number flow. Our target accuracy is strict second order for individual operators and near second order for the algorithm as a whole. Second order allows a coarser discretization for a modest increase in work per volume of fluid, which is efficient. A second-order algorithm also gives us a buffer of accuracy as details like networks of channels and coarse boundary data are added. At the time of this writing, our splitting is first order Godunov splitting. Some authors, e.g. (Leveque 1986), have observed that near second-order accuracy can be achieved with first order splitting, and the design of the tests probes this point.

Two features of the algorithm feature into the design of our test. First, the scheme requires a flow field (flow discharges and flow areas) that preserves mass continuity. In some cases, tests from the literature were written in non-conservative or primitive form and had to be reworked in conservative form. Second, we employ operator splitting and wanted to exercise the equations with and without known vulnerabilities (such as time-varying boundaries and nonlinear source terms) of this class of algorithm.

6.4 Testing Principles

Flow and transport codes inherently comprise both numerical algorithms and pieces of software. Well-developed testing literature exists for both. Oberkampf and Trucano (2002) describe some elements of software quality engineering (SQE) in the context of numerical verification and note some cultural reasons why it is seldom implemented.

Figure 6-1 is adapted from this work and depicts the relationship between software testing components and algorithmic testing such as convergence tests. We regard numerical verification as our key responsibility and the numerical verification toolset as our greatest assets. Nonetheless, we also comment below on how these tools feature as tests and how, at times, they seem in tension with the principles of good software testing.

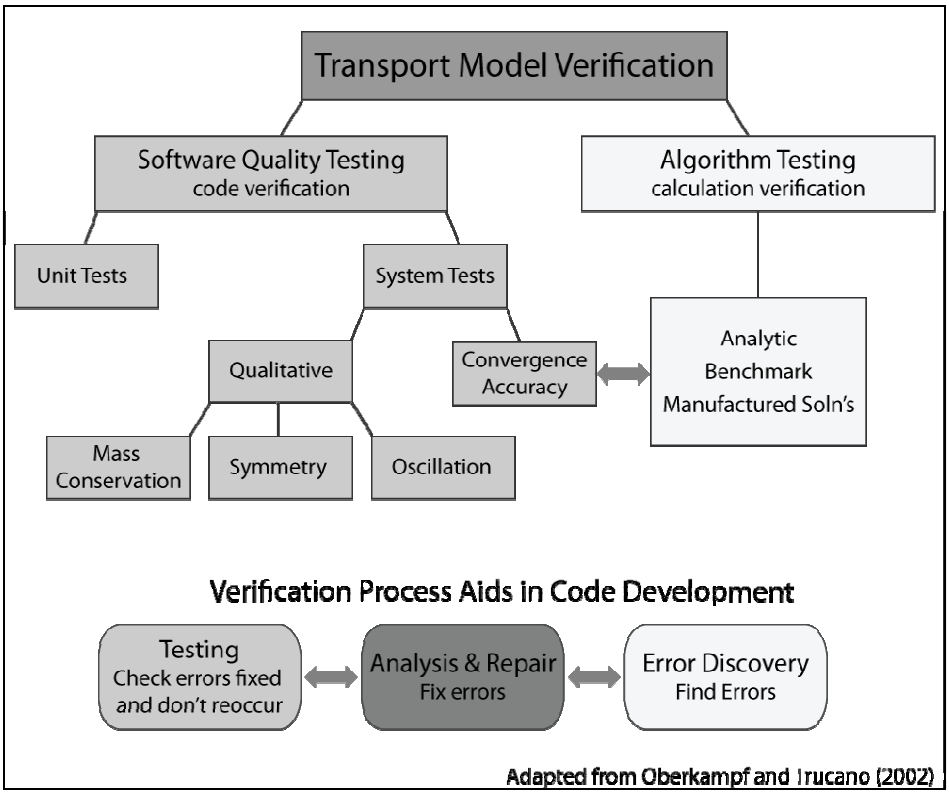

Figure 6-1 Relationship between software testing components and algorithmic testing

6.4.1 Software Testing Principles

The principles that we want to emphasize are:

1. Testing should be automatic and continuous.
2. The approach should foster exact specification of every unit of code.
3. Testing should provide assurance of whether a set of specifications is met.

One goal of tests is that they be a continuous assessment of the code. The entire testing system is a regression suite that establishes a gauntlet through which future code changes must be passed. A consequence of automation is that tests must be phrased in terms of binary assertions, true and false statements that can be tested without human intervention and that reveal whether the aspect of the code under consideration is correct. Convergence criteria are a rigorous basis for assertions, either by requiring strict convergence criteria ("the algorithm is second order accurate in time and space") or a regression criterion ("convergence will not get any worse than last time the code was tested").

The software testing literature further distinguishes between unit tests of atomic routines and system tests of larger subtasks. For example, the evaluation of a gradient might be a unit of code, and it would have a unit test. Convergence tests and other algorithm tests are examples of system tests.

The unit testing point of view is that code must be exercised over a range of inputs that covers every line. For instance, to test a gradient routine with a slope limiter, a developer would want to cover:

1. smooth cases in the middle of the mesh;
2. behavior near the edges of the mesh, where one-sided differences may be used instead of central differences;
3. cases that test the limiters with steep or zero gradients in both directions.

Any system test will certainly exercise the gradient code in the middle of the mesh, which in any event can seldom be wrong without being obvious. However, system-level tests might miss the more unusual cases. For example, a convergence test may miss a bug in the limiter for the case of steep decreasing slope for several reasons. First, convergence is often assessed with limiters turned off, as they are locally order reducing. Second, it is hard to fiddle with the problem in just the right way to make sure the left, right, and center cases of the gradient limiter are all triggered. This is particularly true when trying to exercise other units of code at the same time—parameter choices made to fully exercise gradient limiter may lessen the coverage of another unit.

Although the software and algorithm tests are separate, information discovered during one test can aid in the further development of another test. We began our coding with near-100% coverage by unit tests. These tests were part of the debugging and development processes. Later, discoveries made in the context of system tests were analyzed and pushed back into unit tests whenever possible. The unit test was expanded to verify that the newly discovered error from the algorithm test was fixed and does not reoccur. This flow of information is indicated in Figure 6-1.

One example of this accumulation of tests is our unit test for fluid mass conservation. The observation that our algorithm requires accurate mass conservation of the fluid came from the tidal test case. The flow field we used for this case was adapted for 1-D from Wang et al. (2009). The original solution was based on a linearization and is not mass conservative in 1-D, causing significant problems with transport convergence. Once this requirement was discovered, a unit test was introduced into the suite to check this property for any flow field. At the same time, we found we had to tailor some of the analytical results we were using for other tests.

A second example involved periodic flow. Our uniform flow convergence tests originally had a reversal of flow midway through the test. The out-and-back setup is convenient for advection because the initial condition and final concentration field are the same. We also believed we were exercising the code in 2 directions. In fact, an error accumulated in the positive direction was cancelled by the return pass in the negative direction. We passed the periodic test but failed analogous unidirectional tests. Originally, the discovery was fortuitous because the unidirectional test was “unofficial”; now we test directional dependence using a combination of periodic and unidirectional flow

6.4.2 Numerical verification and algorithmic testing

An important category of a system test includes the algorithm tests normally associated with verification of numerical codes. Algorithm tests serve multiple purposes. They are intended in part to discover bugs and in part to convince ourselves and others of the merit of the algorithm to solve the equations to which it is directed.

One of the well-recognized and standard verification methods of computational fluid dynamics codes is based on the notion of mesh convergence (Roache 2009). Mesh convergence for models that solve

partial differential equations is assessed by successively refining the spatial and temporal discretizations. As the mesh is refined, the error estimates (for us usually an L_1 norm, or sum absolute error) should decrease at a *convergence rate* that is algorithm dependent (Leveque 2002). A second order accurate algorithm, denoted O(2) or $O(\Delta t^2, \Delta x^2)$ should have its error go down proportional to the square of the step sizes. By checking convergence, we ensure that the model is consistent with an underlying formulation rather than numerical artifacts. Failure to converge usually represents either a bug in the implementation or a difficulty of the algorithm on a class of problem.

The verification toolkit is largely targeted at providing test problems and methods to estimate error in situations where an analytical solution is not available from the literature. When nonlinearity, spatially varying coefficients and other complexities are introduced, tricks must be introduced to obtain good test problems.

Depending on the context, error and convergence are usually estimated one of 2 ways:

- When successive refinements are assessed relative to an analytical solution, we have a direct estimate of error and the ratio allows us to estimate a *convergence rate.*

- When successive grids are compared to one another, we can invoke the concept of Richardson extrapolation and Grid Convergence Index (Roache 2009) to indirectly estimate error and convergence even when no solution is available.

In practice, we found the Method of Manufactured Solutions (MMS) (Roache 2009) was able to supply analytical verification problems for all the cases not covered directly in the literature.

At least in theory, convergence rates can be stipulated as a project requirement and software testing assertion. Convergence rates, not absolute error, are what numerical methods tend to promise, and they are very useful in the discovery of code defects. Still, the main goal in practice is a more accurate solver. Therefore, the superiority of methods should be assessed based on both convergence and accuracy (Roache 2009).

The convergence ratio in a very coarse grid oscillates around its main value; as the grid size is refined, convergence becomes monotonic until the mesh size reaches a point where the machine precision overtakes the truncation error of the numerical scheme. At this point, error norms do not change, and the convergence rate is zero. Convergence ratios should be checked for intermediate grid sizes, preferably at the scale of the real phenomenon and discretization used in practice. In the conclusions, we describe the challenge of dealing with tests that returned failed results when the convergence was just slightly below the target level.

As acceptance tests, algorithm tests should be conducted over a range of problems that exercise the major physical features that are to be modeled. The community may help with this by providing benchmarks, but we were unable to ascertain any widely accepted benchmarks for a 1-D transport code. As system tests we believe that the tests should be *glass box*, targeting known or discovered vulnerabilities of the algorithm. The ability to use remote and active boundaries in our convergence tests, for instance, is specifically motivated by known problems related to operator splitting.

Finally, distinction might be made between the reportable set of algorithm tests and other types of system tests aimed at defect discovery. Important examples of the latter are tests of symmetry, such as a whether a 1-D model gives the same result when the upstream and downstream boundaries are

swapped. Others are positivity preservation of constituents, mass conservation, and oscillation detection. In the case of positivity preservation and mass conservation, it is typical to abstract this code for use both in the test suite and in the driver as a user option.

Overall, we agree with the conclusions of Salari and Knupp (2000) that system tests—particularly convergence tests—expose bugs well, particularly when an attempt is made to test symmetrically and over special cases. We feel that the incremental approach we describe in the next section further helps to isolate problems. Nevertheless, a close reading of Salari and Knupp (2000) does reveal that the convergence tests sometimes initially failed to pick up bugs that are exactly the sorts unit tests might catch (e.g., gaffes in corner cells).

6.5 Algorithm Test Suite Description

The algorithm testing used an incremental building block approach that adds complexity on 2 major dimensions (Figure 6-2):

- Operators: The tests were developed for a 1-D transport code that will be applied to an estuary. Thus the key processes tested are the operators of advection, dispersion, and reaction (e.g., growth or decay). These are tested individually, then in combinations of growing complexity

- Flow field and physical setup: Our fixtures included the following cases

  - Uniform flow: This test involved uniform steady flow on a channel, sometimes with a reverse in direction halfway through the simulation. The mass transported is Gaussian. The suite includes advection, diffusion, and reaction alone and in the combinations indicated in Figure 6-2.

  - Tidal flow: This test used a tidal flow field from Wang et al. (2009), adapted to be 1-D and mass conserving, to test advection and reaction. The test itself has no analytical solution, but is periodic in a way that is not symmetric.

  - Spatial variation (Zoppou): This test is due to Zoppou and Knight (1997), and includes velocity proportional to distance and diffusion coefficients proportional to distance squared. This test had to be modified for a conservative fluid flow.

- Boundary complexity: For the uniform flow and Zoppou tests, we include cases where the boundary is far away from the transported mass and cases where the boundary is actively part of the problem. This allows us to determine the extent to which convergence rates are affected by boundaries.

- Nonlinearity: In our final case, which uses the Zoppou and Knight (1997) fixture adapted using the MMS, we include a non-linear source term.

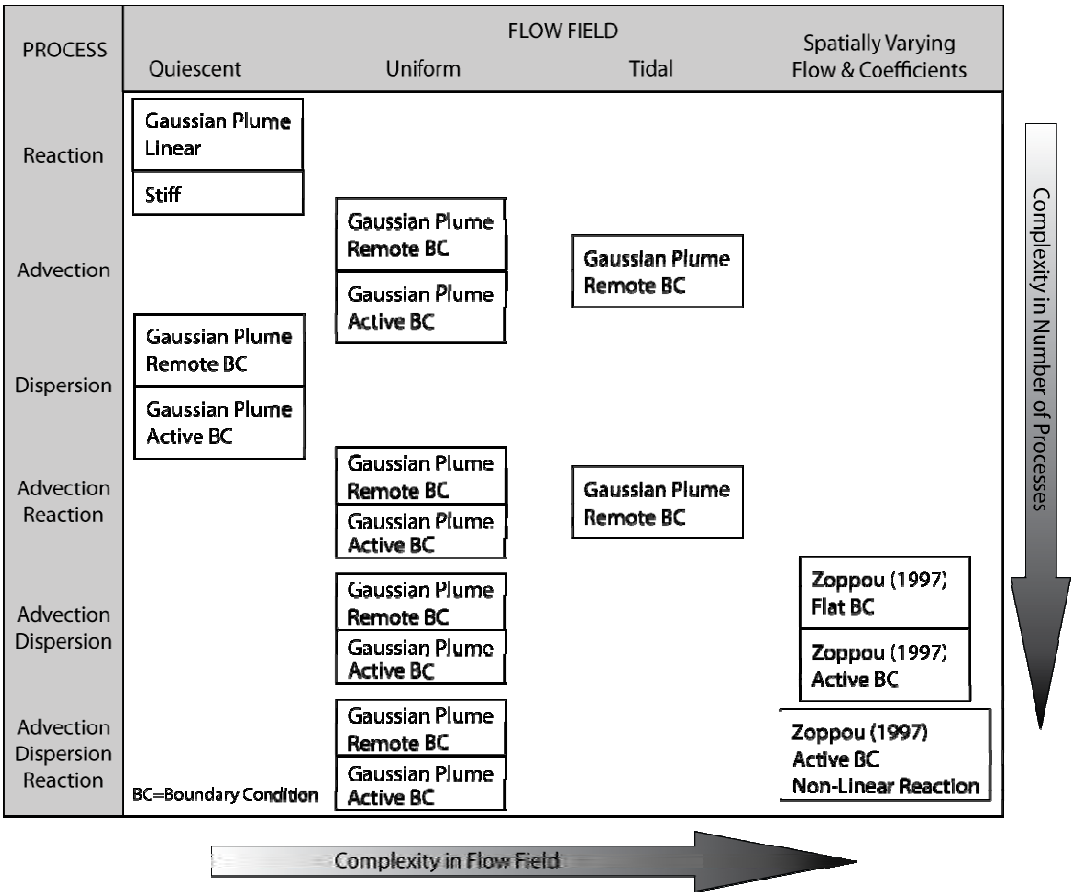

Figure 6-2 Transport algorithm testing with incremental complexity

These tests were conducted for a range of parameter values. Typically the Courant number (a measure of numerical stability of the algorithm), domain length, and dispersion and decay coefficients were fixed; and the grid spacing and time steps were adjusted to maintain the same Courant number. Detailed descriptions of the tests are beyond the scope of this paper and will appear in a planned journal article.

Our incremental suite can identify with good precision exactly which added layer of complexity causes a drop in order of accuracy. For instance, our example algorithm performs well when boundaries are remote, but drops to a convergence rate of *O(1.4)* or so in the presence of active boundaries.

6.6 Architecture and Implementation

The test architecture was implemented using the FORTRAN Unit Testing Framework (FRUIT) for logging assertions and counting pass rates. FRUIT is one of the few test frameworks available in this computer language. FRUIT does not appear to adhere to industry practices in the way it formats results (e.g., the JUnit format), but provides a variety of predefined assertions.

Both the system tests and the unit tests were developed with FRUIT, and the granularity for unit tests is one unit test module per solver module, one unit test routine per solver routine.

Our code was designed for testing. In particular, computational routines were crafted according to the following 3 architectural considerations:

- We isolated any computations that could be described with easy-to-understand names, with the caveat that we did not want to degrade performance or prevent vectorization. Our routines tend to be simple, homogenous calculations over arrays (such as calculating the gradient over the entire domain) rather than long sequences of instructions on individual cells.

- Data are passed to computational routines by argument list. This leads to longer argument lists, but makes the description of input and output much surer—tests are much harder to program when data required by the routine is passed in "behind the scenes" using imported modules.

- The design allows us to dynamically swap in new sources, flow fields, and boundary conditions without halting the tests or recompiling the code. This ability required function pointers and abstract interfaces, a relatively new FORTRAN feature.

6.7 Challenges and Issues with Tests

The key issues associated with unit tests were different than those associated with algorithm tests. The main challenge with unit tests seems to be culture: generating the will to write them and the skills to write them in a way that covers the unusual cases. Without the aid of special coverage tools, test coverage is up to the diligence and craftiness of the developers.

For algorithm tests, nominally we sought a second order convergence rate. A convergence criterion seemed in-keeping with the way numerical algorithm accuracy is expressed and is less arbitrary than a hard-wired, scale-dependent absolute standard. Early on, however, it was clear that the normal noise from observed convergence rates could spoil even a success when the rate is expressed as a hard assertion. It is challenging to deal with situations when a convergence test fails with a value close to the criterion, e.g., 1.97 instead of 2.0, which surely would pass a graphical acceptance test. This issue can be exacerbated by sensitivity to problem parameters.

When one of our tests did not cleanly converge at the specified level, we generally either fixed the code successfully or we searched for bugs until both of the following things happened:

- Convergence properties corresponded well to the expected strengths and limitations of our algorithm; and

- The solution was accurate: convergent above first order, excellent qualitative results when compared graphically to solutions and with relative errors of a hundredth of a percent.

We have done our best to support our claims when attributing any convergence deviations to specific algorithmic or problem quirks. Our incremental suite can identify with good precision exactly which added layer of complexity causes a drop in order of accuracy. Where we intend to relax convergence criteria, we are in the process of changing our assertion criteria to an absolute accuracy requirement coupled with a regression standard for convergence. In our numerical code, cases with multiple operators and very active boundaries are the only ones in which we currently expect such a compromise.

Finally, there is sometimes a tradeoff between the requirements for verification and best practices for error discovery. Part of the community verification process for transport codes is the presentation of results in graphical format. Accommodating this type of display requires output beyond mere reports of assertion failures. We added the required verbosity option, but graphical interpretation plays no part in our regular testing practices other than as a debugging tool.

6.8 Conclusions

Our test suite succeeds both in finding bugs and in elucidating the strengths and weaknesses of a 1-D transport algorithm. We feel that our test suite is parsimonious and reasonably complete for tidal applications. Applying the framework to our own code, we have been able to work towards second order convergence for many tests and to isolate problems in special cases.

We believe the essential ideas in our approach are:

- Codes must be written in a modular format with software testing in mind in order to apply the principals of software quality engineering. Each piece of code must have a clear purpose and criterion for success.

- Tests should be silent and automatic. Test criteria must be binary assertions. Assertions are written to provide more information than simply assessing graphs of expected vs. computed results; however, we include verbosity options to export data for graphs.

- There is a symbiotic relationship between software and algorithm tests; Code bugs detected with algorithm tests can lead to development of additional software regression tests to verify that a bug is fixed and to provide assurance that it does not reoccur.

- Convergence tests are the principal tool used in the algorithm verification literature. Our suite includes convergence tests on a combination of analytical problems from the literature and a manufactured solution using MMS.

- When convergence criteria are implemented as hard test assertions, account must be made of the small random noise typical of convergence results.

- Incremental addition of complexity helps to isolate the causes of problems and to establish that lower complexity solutions are correct.

- Symmetry and directionality tests help discover errors that may be hidden by the setup of the problem.

The software quality and algorithm testing framework described in this paper provides a useful starting point for researchers and practitioners wanting to verify transport codes. Having this rigorous test suite allows developers (1) to verify that each piece of code works properly both individually and as a combined system, (2) to ensure additions to the code do not adversely affect existing code, and (3) to find and fix code bugs that might otherwise be missed. Providing the end user with test results and the ability to rerun the tests themselves, assures the user that the code performs as expected and quantifies the code's strengths and weaknesses.

6.9 Acknowledgments

This work has been possible due to the support given by the California Dept. of Water Resources through a contract with UC Davis. We thank Tara Smith and Dr. Francis Chung from DWR for their support of this project.

6.10 References

Abbott, M. B. and W. A. Price. 1994. *Coastal, Estuarial, and Harbour Engineers' Reference Book.* Chapman & Hall.

California Department of Water Resources. *Delta Simulation Model 2 (DSM2). [Web page].* http://baydeltaoffice.water.ca.gov/modeling/deltamodeling/models/dsm2/dsm2.cfm (accessed 2011).

Colella, P. and E. G. Puckett. 1998. "Modern Numerical Methods for Fluid Flow.".

Fischer, B. H., J. E. List, R. C. Koh, J. Imberger, and N. H. Brooks. 1979. *Mixing in Inland and Coastal Waters.* Academic Press, Inc.

Fletcher, C. A. J. 1991. *Computational Techniques for Fluid Dynamics.* Springer.

Leveque, J. R. 2002. *Finite Volume Methods for Hyperbolic Problems.* Cambridge University Press.

Leveque, J. R. 1986. "Intermediate Boundary Conditions for Time-Split Methods Applied to Hyperbolic Partial Differential Equations." *Mathematics of Computation* 47: 37-54.

Oberkampf, W. L., Trucano T. G. 2002. *"Verification and Validation in Computational Fluid Dynamics .* SANDIA REPORT, No. SAND2002-0529.

Roache, P. J. 2009. *Fundamentals of Verification and Validation.* Hermosa Publishers.

Salari, K., Knupp, P. 2000. *Code Verification by the Method of Manufactured Solutions.* SANDIA REPORT, No. SAND2000-1444.

Saltzman, J. 1994. "An Unsplit 3D Upwind Method for Hyperbolic Conservation Laws." *J. of Computational Physics* 115: 153-168.

Wang, S. Y., P. J. Roache, R. A. Schmalz, Y. Jia, and P. E. Smith. 2009. "Verification and Validation of 3D Free-Surface Flow Models." *ASCE, EWRI.*

Zoppou, C., and J. H. Knight. 1997. "Analytical Solution for Advection and Advection-Diffusion Equation with Spatially Variable Coefficients." *J. Hydraulic Eng.* 123(2): 144-148.

Methodology for Flow and Salinity Estimates in the Sacramento-San Joaquin Delta and Suisun Marsh

32nd Annual Progress Report
June 2011

Chapter 7
Turbidity Modeling with DSM2

Authors: Lianwu Liu and Prabhjot Sandhu,
Delta Modeling Section,
Bay-Delta Office,
California Department of Water Resources

Contents

7 Turbidity Modeling with DSM2 7-1
7.1 Introduction 7-1
7.2 Turbidity Modeling with DSM2 7-1
7.3 Boundary Conditions 7-2
7.4 2010 Wet Season Calibration 7-2
7.5 Discussion of Model limitations 7-3
7.6 Summary 7-5
7.7 Acknowledgments 7-5
7.8 References 7-5

Figures

Figure 7-1 CDEC turbidity stations 7-6
Figure 7-2 Calibrated settling rate values 7-7
Figure 7-3 Turbidity comparison, Sacramento River at Rio Vista (15 minute interval) 7-8
Figure 7-4 Daily-averaged turbidity comparison, Sacramento River at Rio Vista 7-8
Figure 7-5 Regression analysis of daily averaged values, Sacramento River at Rio Vista 7-9
Figure 7-6 Turbidity comparison, Sacramento River at Decker Island (15 minute interval) 7-9
Figure 7-7 Daily-averaged turbidity comparison, Sacramento River at Decker Island 7-10
Figure 7-8 Regression analysis of modeled result and field data, Sacramento River at Decker Island 7-10
Figure 7-9 Turbidity comparison at Jersey Point 7-11
Figure 7-10 Daily-averaged turbidity comparison at Jersey Point 7-11
Figure 7-11 Regression analysis of modeled result and field data at Jersey Point 7-12
Figure 7-12 Turbidity comparison at Old River Bacon Island 7-12
Figure 7-13 Daily-averaged turbidity comparison at Old River Bacon Island 7-13
Figure 7-14 Regression analysis of modeled result and field data at Old River Bacon Island 7-13
Figure 7-15 Turbidity comparison, Sacramento River at Prisoners Point 7-14
Figure 7-16 Daily-averaged turbidity comparison, Sacramento River at Prisoners Point 7-14
Figure 7-17 Regression analysis of modeled result and field data at Prisoners Point 7-15
Figure 7-18 Turbidity comparison, Sacramento River at Holland Cut 7-15
Figure 7-19 Daily-averaged turbidity comparison at Holland Cut 7-16
Figure 7-20 Turbidity comparison at Victoria Canal 7-16
Figure 7-21 Daily-averaged turbidity comparison at Victoria Canal 7-17

Figure 7-22 Compare turbidity spikes at Jersey Point with rainfall and wind data 7-17
Figure 7-23 Compare turbidity spikes at Bacon Island with rainfall and wind data 7-18
Figure 7-24 Compare turbidity spikes at Holland Cut with rainfall and wind data..... 7-18
Figure 7-25 Turbidity comparison at San Joaquin River Garwood 7-19
Figure 7-26 Daily-averaged turbidity comparison at San Joaquin River Garwood 7-19
Figure 7-27 Turbidity comparison at Grant Line Canal..... 7-20
Figure 7-28 Daily-averaged turbidity comparison at Grant Line Canal 7-20
Figure 7-29 Flow at San Joaquin River Mossdale (RSAN087) and Brandt Bridge (RSAN072) 7-21
Figure 7-30 Velocity at San Joaquin River Mossdale and Brandt Bridge..... 7-21
Figure 7-31 Settling rate sensitivity test result at Decker Island..... 7-22
Figure 7-32 Settling rate sensitivity test result at Prisoners Point 7-22
Figure 7-33 Settling rate sensitivity test result at Holland Cut..... 7-23
Figure 7-34 Settling rate sensitivity test result at False River 7-23
Figure 7-35 Settling rate sensitivity test result at Victoria Canal 7-24
Figure 7-36 Settling rate sensitivity test result at Rough and Ready Island 7-24
Figure 7-37 Settling rate sensitivity test result at Grant Line Canal..... 7-25
Figure 7-38 Daily-averaged turbidity comparison at Mallard..... 7-25
Figure 7-39 Adjusted turbidity comparison at Mallard..... 7-26
Figure 7-40 Daily-averaged turbidity comparison at Antioch..... 7-26
Figure 7-41 Adjusted turbidity comparison at Antioch 7-27
Figure 7-42 Adjusted turbidity comparison at Prisoners Point..... 7-27
Figure 7-43 Adjusted turbidity comparison at Holland Cut 7-28
Figure 7-44 Adjusted turbidity comparison at Victoria Canal..... 7-28

Table

Table 7-1 Turbidity sources..... 7-4

7 Turbidity Modeling with DSM2

7.1 Introduction

This chapter documents turbidity modeling with Delta Simulation Model II (DSM2) Version 8.0.6. Turbidity has been deemed to be an important factor affecting delta smelt migration and entrainment. DSM2 is a promising tool in turbidity analysis and forecasting because of its speed as a 1-D model and its extensive applications in the Delta. A large number of stations with turbidity data became available in 2010, which makes a more detailed calibration possible for the 2010 wet season. The calibrated DSM2 model results generally match with the observed data. Further validation with another wet year will help improve its reliability.

7.2 Turbidity Modeling with DSM2

Turbidity measures the scattering effect that suspended solids have on light and is typically reported in nephelometric turbidity units (NTU): the higher the intensity of scattered light, the higher the turbidity. Material that causes water to be turbid includes (Swanson and Baldwin 2011):

- clay
- silt
- finely divided organic and inorganic matter
- soluble colored organic compounds
- plankton
- microscopic organisms

Although turbidity is not a material, it is directly related to suspended sediment concentration (SSC), and researchers found that turbidity and SSC are proportional throughout San Francisco Bay (Resource Management Associates, Inc. [RMA] 2010). It is reasonable to simulate turbidity directly with DSM2 as a constituent that is governed by advection-dispersion equation with decay/loss due to settling.

DSM2 does not have a sediment transport or turbidity component. The Carbonaceous Biochemical Oxygen Demand (BOD) function is adapted to simulate turbidity with the deoxygenation rate coefficient (K_1) set to zero, and settling rate K_3 calibrated to simulate the loss due to settling. The BOD function as expressed in the QUAL2E model document (Brown and Barnwell 1987) takes into account BOD removal due to sedimentation:

$$\frac{dL}{dt} = -K_1 L - K_3 L \qquad \text{Eq. 7-1}$$

where

L = the concentration of ultimate carbonaceous BOD, mg/L

K1 = deoxygenation rate coefficient, day^{-1}

K3 = the rate of loss of carbonaceous BOD due to settling, day^{-1}

The equation for turbidity function can be written as:

$$\frac{dT}{dt} = -K_3 T \qquad \text{Eq. 7-2}$$

where

T = turbidity, NTU

K3 = the rate of decrease of turbidity due to settling, day^{-1}

7.3 Boundary Conditions

The simulations used the latest Mini-Calibration historical run setup. Observed turbidity data at Hood, Vernalis, and Martinez were the main boundary conditions used (Figure 7-1)[1]. Observed turbidity data at Hood were shifted 12 hours to account for the travel time from upstream boundary and verified at Hood to match the observed timing (we use Hood data instead of Freeport because we had only Hood data for the 2008 winter season). The initial turbidity and agricultural drainage were set at 10 NTU. At other tributary inflows that didn't have observed turbidity data, RMA formulas (Resource Management Associates, Inc. [RMA] 2010) were used to calculate the turbidities based on flows, including the Yolo Bypass, Mokelumne River, Cosumnes River, and Calaveras River. The total contribution from these tributaries was verified to be very small compared to Sacramento River and San Joaquin River for the calibration period of 2010. Possible errors by using the formulas should not affect the calibration much. Observed data will be used when available.

7.4 2010 Wet Season Calibration

In this effort, DSM2 was calibrated on the 2010 wet season (December 2009 to April 2010). Previous studies (Chandra Chilmakuri, CH2M Hill 2010) (Resource Management Associates, Inc. [RMA] 2008 Oct) used uniform settling or decay coefficients for the entire Delta (RMA 2010 new model used 3 regions for the decay rate). In this calibration, we tried to match the observed turbidity at most of the locations by making more groups of channels by region and adjusting the settling rate in each group.

The calibration was started with a settling rate (K_3) of 0.05 day^{-1} everywhere (as recommended by previous studies by CH2M Hill and RMA). The simulated turbidities on stations along the Sacramento River side were satisfactory. We adjusted the settling rates on the San Joaquin, Old, and Middle Rivers to get the simulated turbidity close to the field data. Altogether, 10 groups (5 distinct values) were used as shown in the map of Figure 7-2.

The results were mainly compared by visual inspection. Due to the model limitations (discussed later), big differences occur in some locations and time periods due to local storm events and other factors. By visual comparison, it is easy to ignore differences due to local storm events and pay attention to the general trend and peak values.

A complete comparison report at all stations was generated using the newly developed DSM2 report tool (Hsu 2010). This tool was a tremendous help in calibration because numerous runs were made to

[1] All figures appear at the back of this chapter

test the sensitivity of result output to parameters. It made it feasible to plot the results after every run. Final results are plotted with HEC-DSSVUE and pasted here for discussion.

The simulated results compare well with field data along the Sacramento River, as seen at Rio Vista and Decker Island (Figure 7-3 to Figure 7-8). At central and south Delta, the general trends compare well as seen at Jersey Point, Prisoners Point, Holland Cut, Bacon Island, Victoria Canal (Figure 7-9 to Figure 7-21). Some turbidity spikes shown in field data but not seen in the modeling results are due to local storm events and can be verified to be co-related with rainfall and wind data, as shown in Figure 7-22 Figure 7-24. Figure 22 shows strong winds are associated with the turbidity spikes at Jersey Point.

Very large settling rates were used for San Joaquin River from Mossdale to Garwood (0.7 day^{-1}) and Old River upstream of Clifton Court Forebay and Grant Line Canal (0.5 day^{-1}) in order to bring down the turbidity to field observed levels (Figure 7-25 to Figure 7-28). One reason to justify the bigger values at these reaches is that the rivers just enter tidal influence zone. Flood tides cause flow to slow down to zero velocity and even reverse direction, and cause rapid sediment settling. As seen in Figure 7-29, the flow patterns at Mossdale (RSAN087) and Brandt Bridge (RSAN072) are quite different. The flow velocity at Mossdale is always positive, but at Brandt Bridge velocity goes to zero and negative during flood tides (Figure 7-30). Other reasons may include additional dilution due to missing tributary inflows as discussed in RMA report (2010).

Figure 7-31 to Figure 7-37 show sensitivity test results by increasing and decreasing the calibrated settling rates (K_3) 50%. Along the Sacramento River, the settling rate was very small and not very sensitive to the change, as seen at Decker Island (Figure 7-31). At central Delta stations, the results are very sensitive to the changes, as seen in plots of Prisoners Point, Holland Cut, False River, and Victoria Canal (Figure 7-32 to Figure 7-35). Figure 7-36 and Figure 7-37 show the sensitivity test at San Joaquin River at Rough and Ready Island and Grant Line Canal. It can be seen that lower settling rates would result in the simulated turbidity peaks being too high.

7.5 Discussion of Model limitations

The settling rate in DSM2 model is essentially the same as using first order decay rate as used by RMA (2010). RMA (2010) discussed limitations of the simple modeling approach. Similar to RMA modeling, there are several mechanisms affecting turbidity but not reflected in the DSM2 modeling:

- The model does not have the mechanism of sediment re-suspension. It will not calculate turbidity created by wave/current caused by wind and tide.
- The settling rate should be co-related to flow velocity and suspended sediment properties. Instead, it is calibrated only on locations.
- Discrepancies between the model results and field data can be contributed also to in-Delta precipitation, missing runoff/inflow, etc. It can be seen in the comparison plots that big discrepancies occur during local rainfall/storm events (Figure 7-22 to Figure 7-24)

The sources of turbidity can be categorized and summarized in Table 7-1.

Table 7-1 Turbidity sources

Source	Included in model	Comments
Turbidity from boundaries	Main boundaries: Sacramento, San Joaquin, Martinez; Tributaries: Yolo Bypass, Mokelumne River, Cosumnes River, Calaveras River.	Transport and settling are modeled. Results match the general trend and magnitude well.
Local storm contributions	No	Turbidity spikes can be seen in the field data due to local storms (runoff, wave/current re-suspension by strong storm wind). Big differences can be seen when comparing modeling results with field data. The monthly averaged DICU input cannot reflect the flows during storm events.
Re-suspension by normal wave/current	No	This is the main source of turbidity under normal conditions (when there are no storm events) besides turbidity transported from boundaries. An ad hoc procedure is proposed to compensate this effect in the model results.

The observed turbidity values at west Delta stations (Mallard, Antioch) are always much higher than in central Delta/south Delta under normal conditions (before any significant storm occurs in December or January). This may be contributed to re-suspension by stronger wind wave and tidal current effects in west Delta.

The model simulates turbidity using one settling rate at each location. The different types of sediment and materials are not considered separately. The model is calibrated during big events, the calibrated settling rate may reflect more coarse sediment, and may not reflect the finer or lighter materials under normal conditions well, i.e., the calibrated settling rates may tend to be high under normal conditions and cause more settling during the normal condition period.

Due to these limitations, the model does not simulate the turbidity well under normal conditions. The shortcomings are more obvious in west Delta than in south Delta. It can be seen in Figure 7-38 and Figure 7-40, the model could not match the observed turbidity at Mallard and Antioch in December and early January, as highlighted in the figures. At south Delta, the wind wave effect is smaller, and turbidities are usually less than 5 NTU.

The simulated turbidity may be adjusted for the missing re-suspension mechanism when comparing with field data, especially at west Delta stations. In Figure 7-39, the simulated turbidity at Mallard was adjusted by adding 11.0 NTU (the smallest difference between observed and simulated turbidity in late December and early January). This adjustment eliminates the differences under normal

conditions and may improve prediction. In Figure 7-41, the simulated turbidity at Antioch was adjusted by adding 8.0 NTU (the smallest difference between observed and simulated turbidity in late December and early January). Figure 7-42 to Figure 7-44 show the adjusted turbidity comparison at Prisoners Point (adjusted 3.0 NTU), Holland Cut (adjusted 1.5 NTU), and Victoria Canal (adjusted 1.0 NTU). These 3 stations were used in the US Fish and Wildlife Service (USFWS) Delta Smelt Biological Opinion (December 15, 2008) as a trigger in the Reasonable and Prudent Alternative action (3-day average is greater than or equal to 12 NTU at these stations). Although the differences adjusted are very small at these stations, the adjustment helps improve the comparison and accuracy of the modeled turbidity.

7.6 Summary

DSM2 can be adapted to simulate transport and settling of turbidity in the Delta. Factors, such as local storm runoff/inflow, wave/current re-suspension, were not modeled. Despite the limitations, the calibrated model generally simulated the main turbidity events well. The comparison of simulated turbidity and field data are convincing. A validation of another wet year will give more confidence in the model calibration.

Further improvements are desirable to incorporate re-suspension and local storm runoff/inflow effects, but these improvements may require much greater efforts and are beyond the scope of this study. A simple ad hoc adjustment is proposed to compensate wave/current re-suspension effect, and help improve model accuracy.

7.7 Acknowledgments

Marianne Guerin (of Resource Management Associates, Inc.) provided quality-checked 2010 turbidity data; Siqing Liu (of DWR) updated the historical run to 2010.

7.8 References

Brown, Linfield C., and Jr., Thomas O. Barnwell. "The Enhanced Stream Water Quality Models QUAL2E and QUAL2E-UNCAS: Documentation and User Manual." 1987.

Chandra Chilmakuri, CH2M Hill. *Turbidity Simulation in the Delta using DSM2.* Sacramento: DSM2UG Newsletter, DWR, 2010.

Hsu, En-Ching. "Chapter 10: DSM2 Comparison Report Tool." *Methodology for Flow and Salinity Estimates in the Sacramento-San Joaquin Delta and Suisun Marsh. 32nd Annual Progress Report from the California Department of Water Resources to the State Water Resources Control Board*, 2010.

Resource Management Associates, Inc. [RMA]. *Near-Real-time Turbidity and Adult Delta Smelt Forecasting with RMA 2-D Models (draft).* Fairfield, California: Prepared for the Metropolitan Water District of Southern California, 2010.

Resource Management Associates, Inc. [RMA]. *Sacramento-San Joaquin Delta Turbidity Modeling.* Appendix A Technical Memorandum, Fairfield, California: Prepared for the Metropolitan Water District of Southern California, 2008 Oct.

Swanson, H. A., and H. L. Baldwin. *Information on this page is from "A Primer on Water Quality", U.S. Geological Survey, 1965.* Feb 8, 2011. http://ga.water.usgs.gov/edu/characteristics.html.

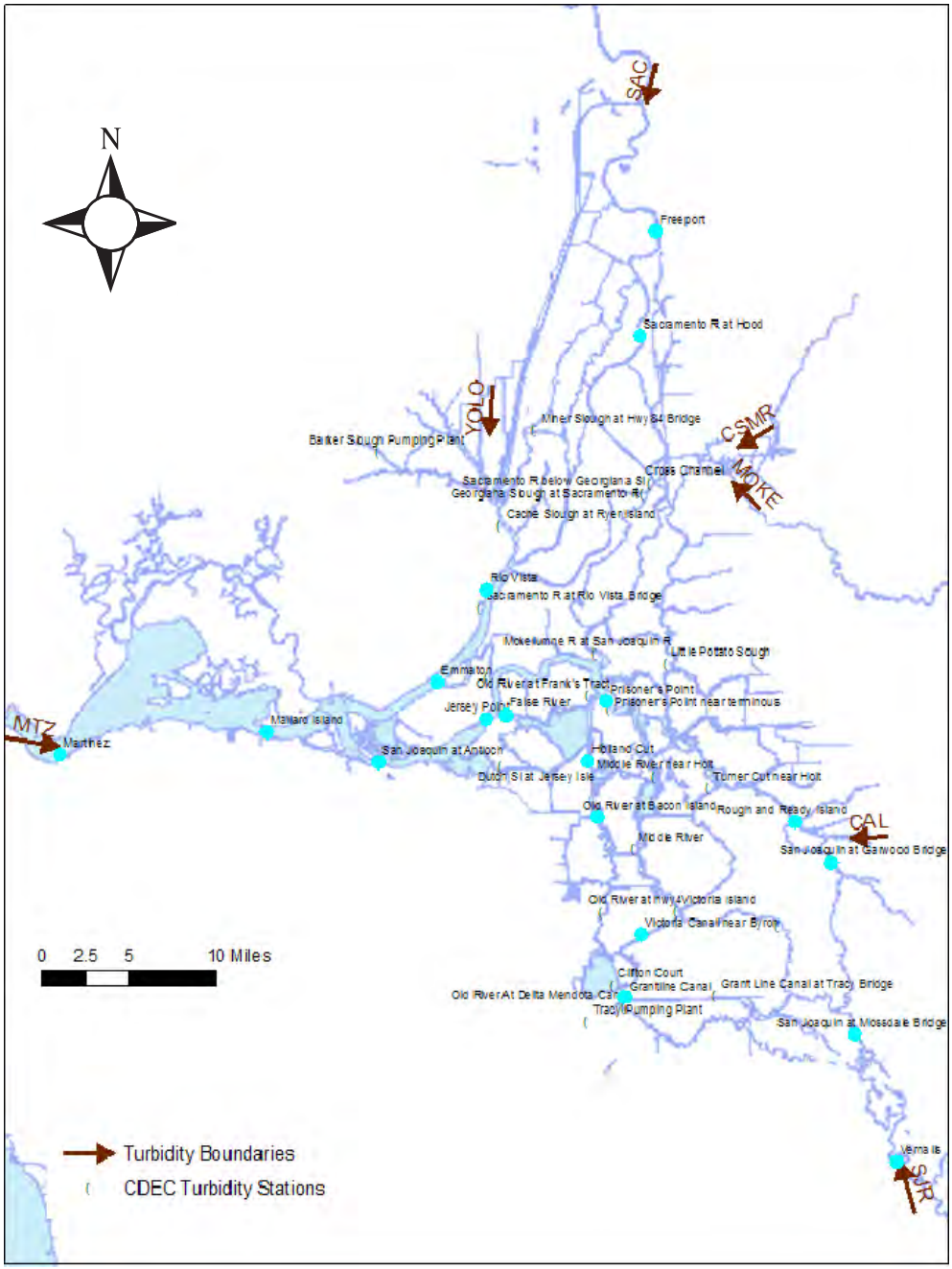

Note: Stations discussed in this chapter are highlighted

Figure 7-1 CDEC turbidity stations

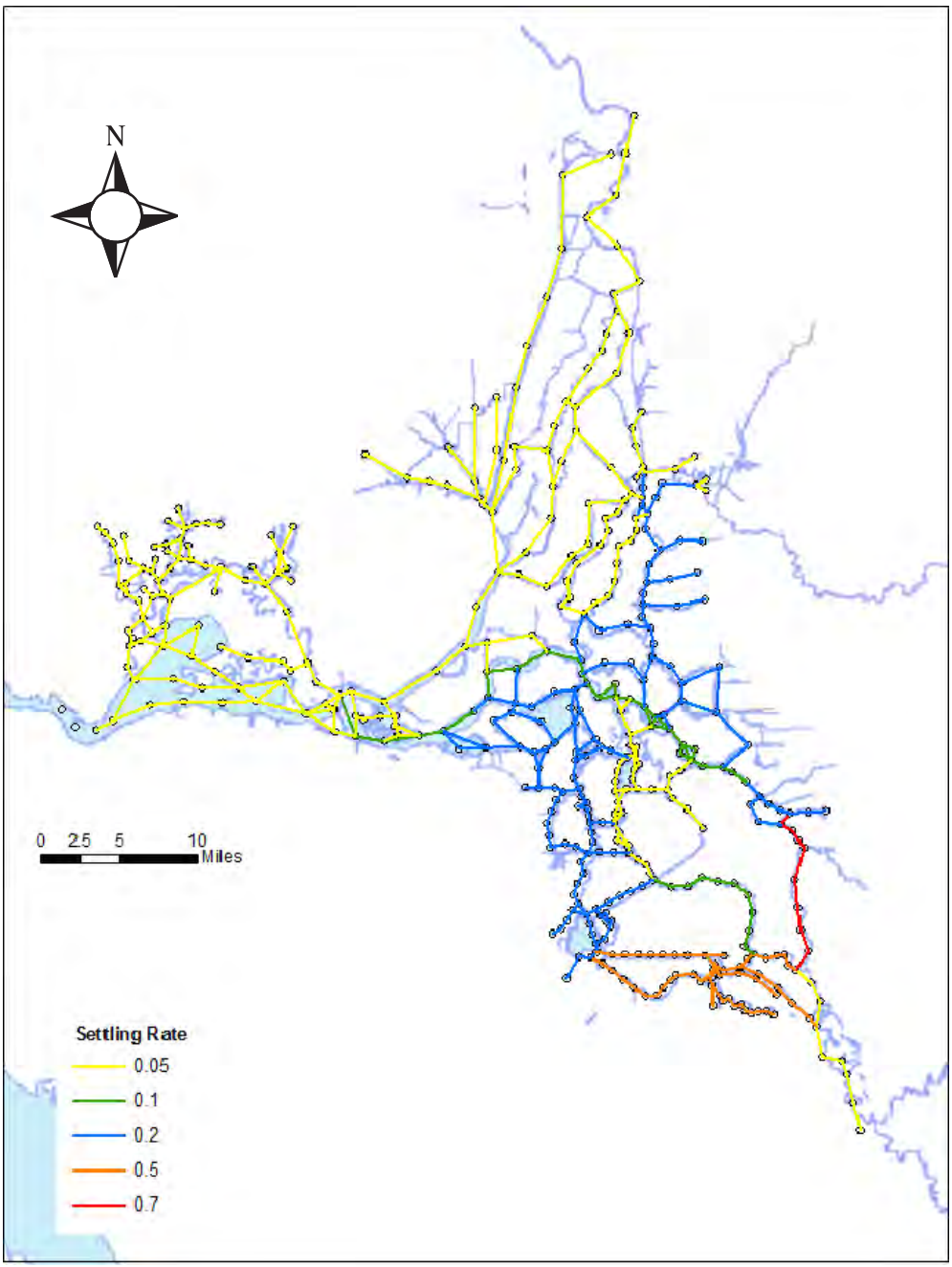

Figure 7-2 Calibrated settling rate values

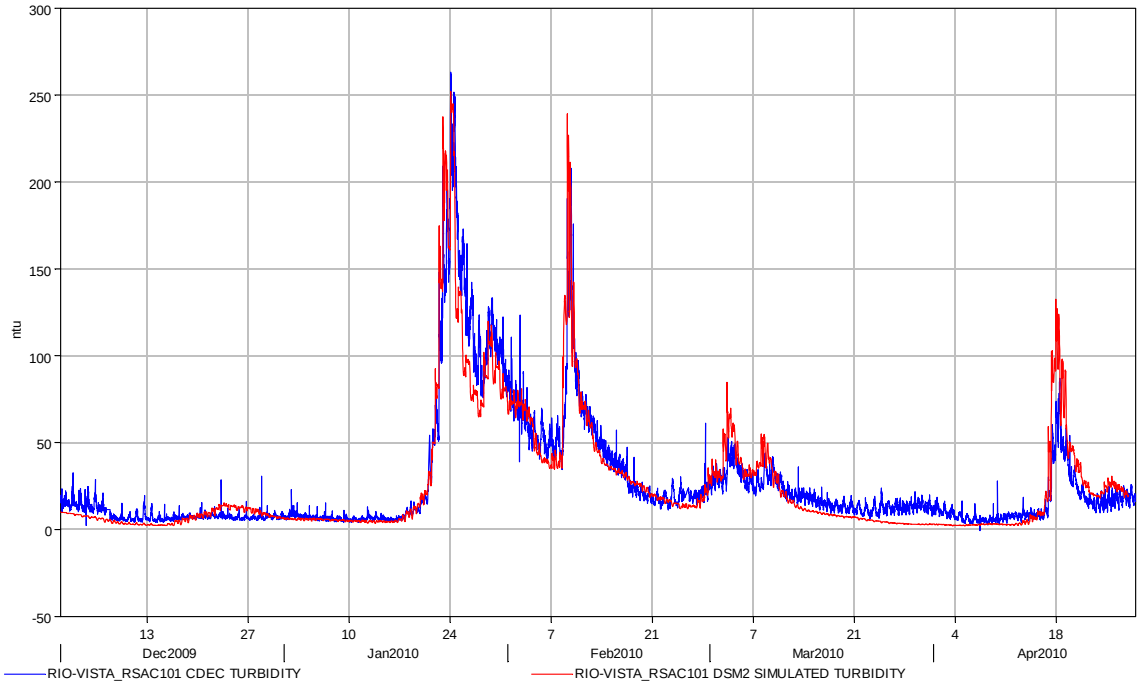

Figure 7-3 Turbidity comparison, Sacramento River at Rio Vista (15 minute interval)

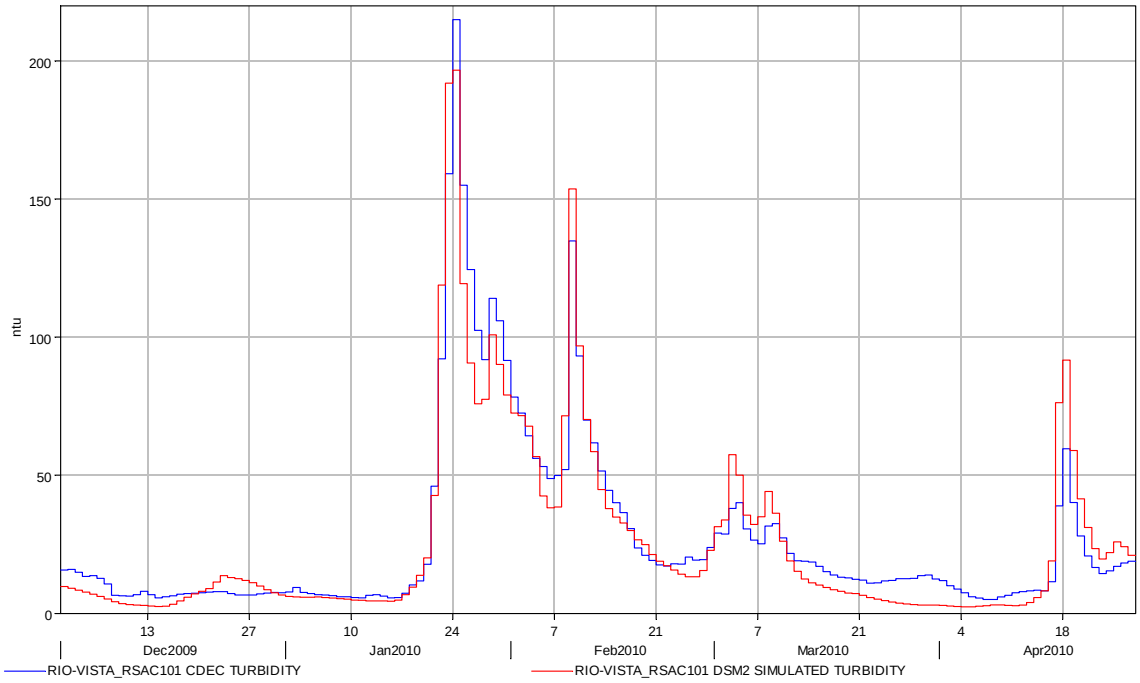

Figure 7-4 Daily-averaged turbidity comparison, Sacramento River at Rio Vista

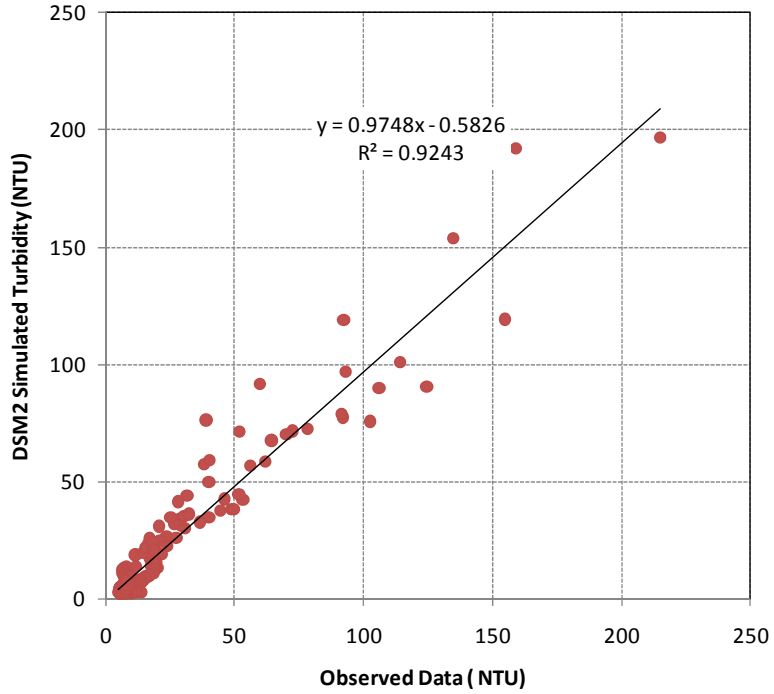

Figure 7-5 Regression analysis of daily averaged values, Sacramento River at Rio Vista

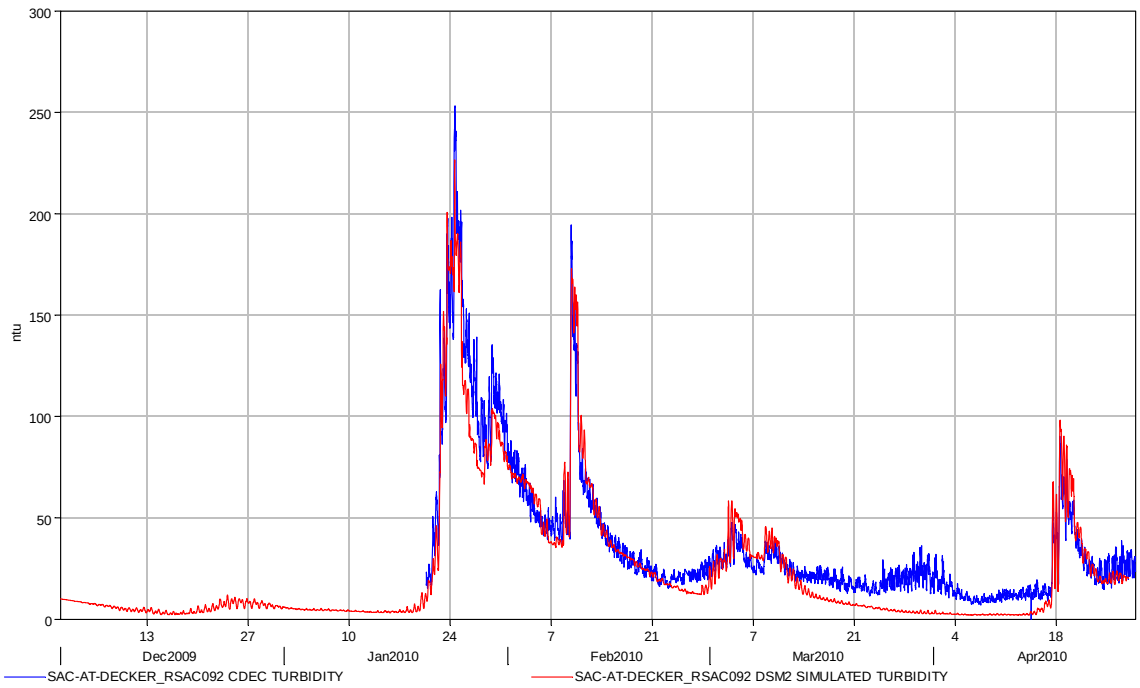

Figure 7-6 Turbidity comparison, Sacramento River at Decker Island (15 minute interval)

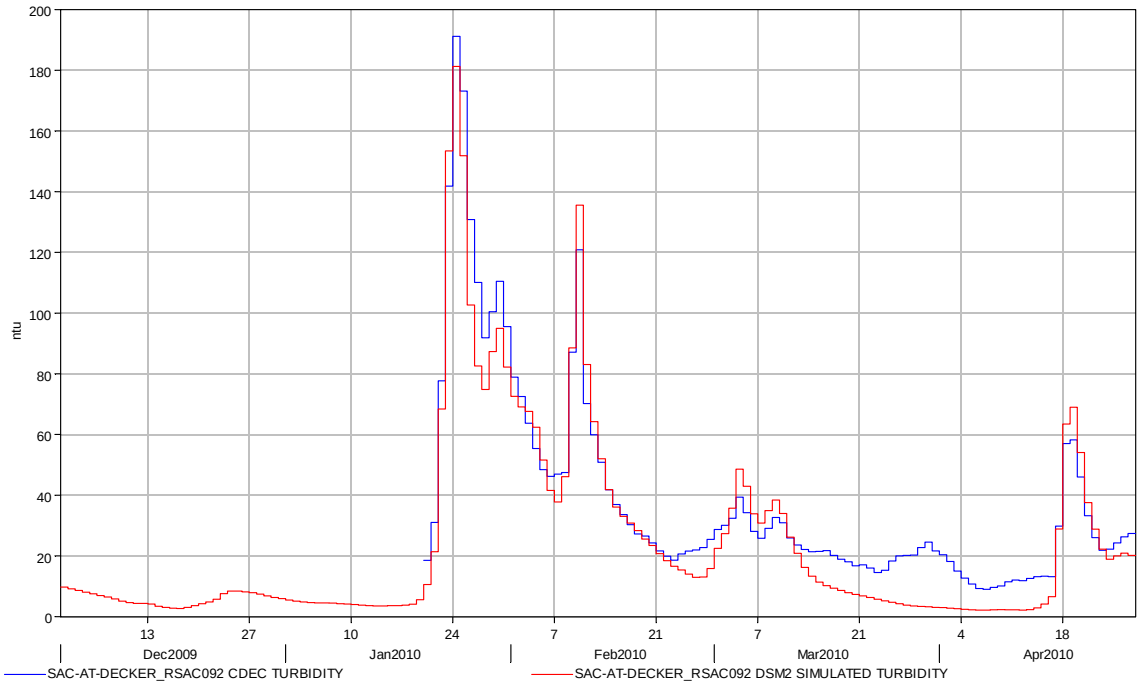

Figure 7-7 Daily-averaged turbidity comparison, Sacramento River at Decker Island

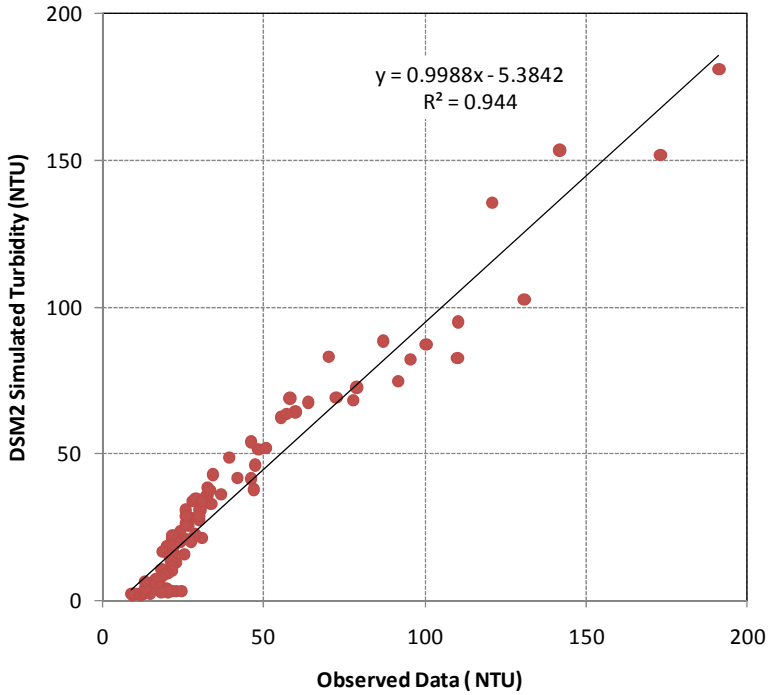

Figure 7-8 Regression analysis of modeled result and field data, Sacramento River at Decker Island

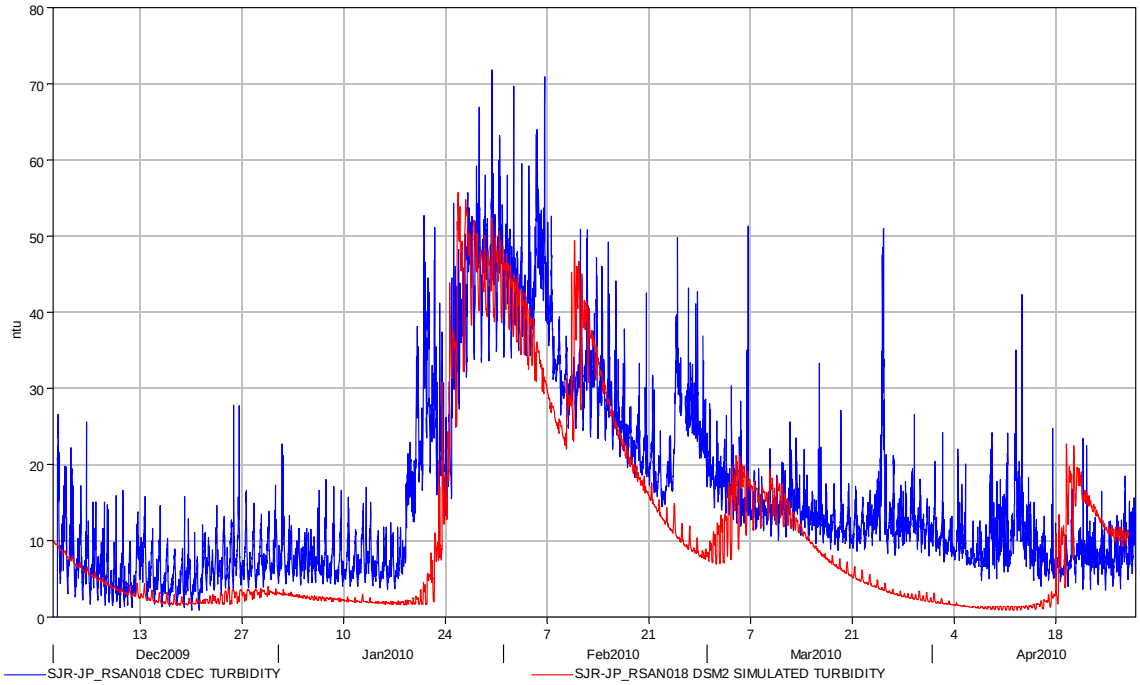

Figure 7-9 Turbidity comparison at Jersey Point

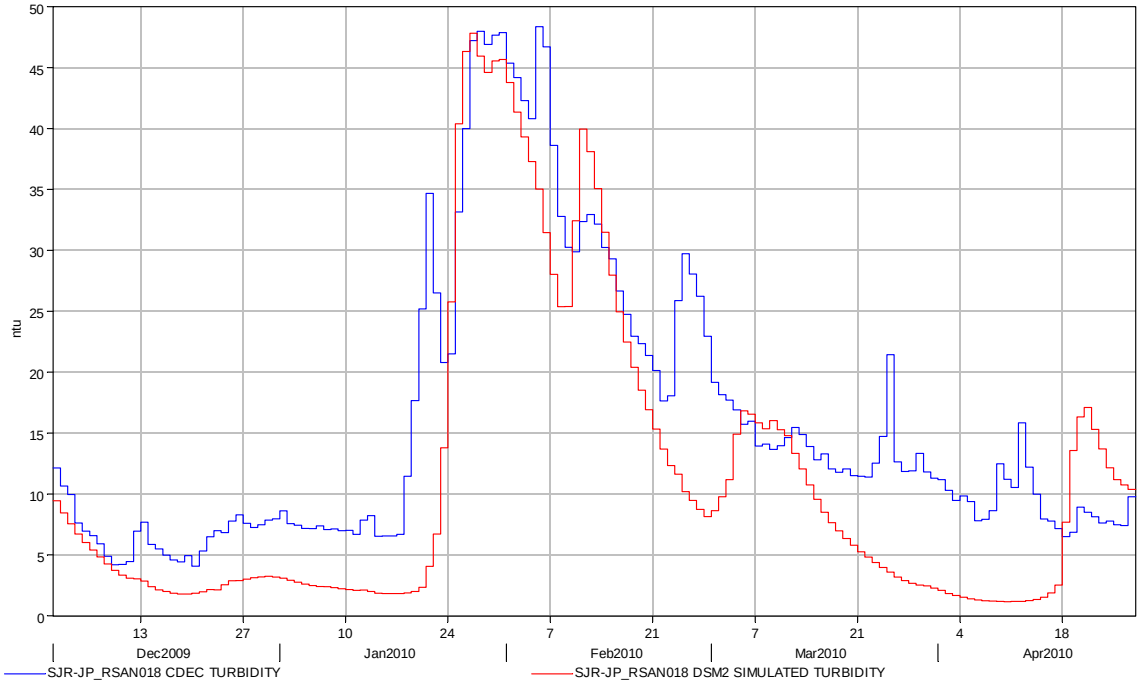

Figure 7-10 Daily-averaged turbidity comparison at Jersey Point

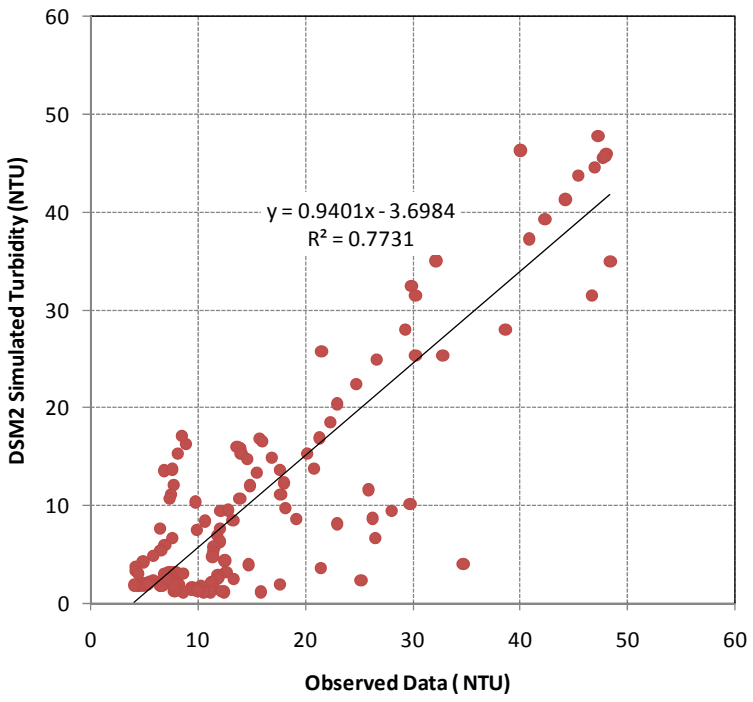

Figure 7-11 Regression analysis of modeled result and field data at Jersey Point

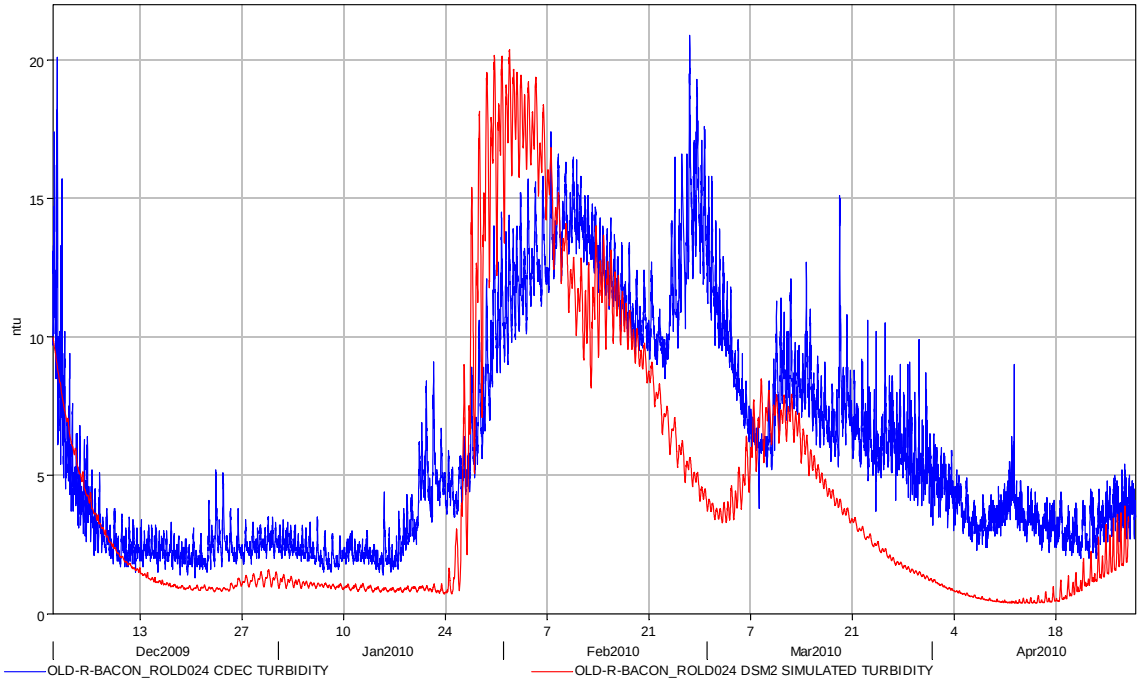

Figure 7-12 Turbidity comparison at Old River Bacon Island

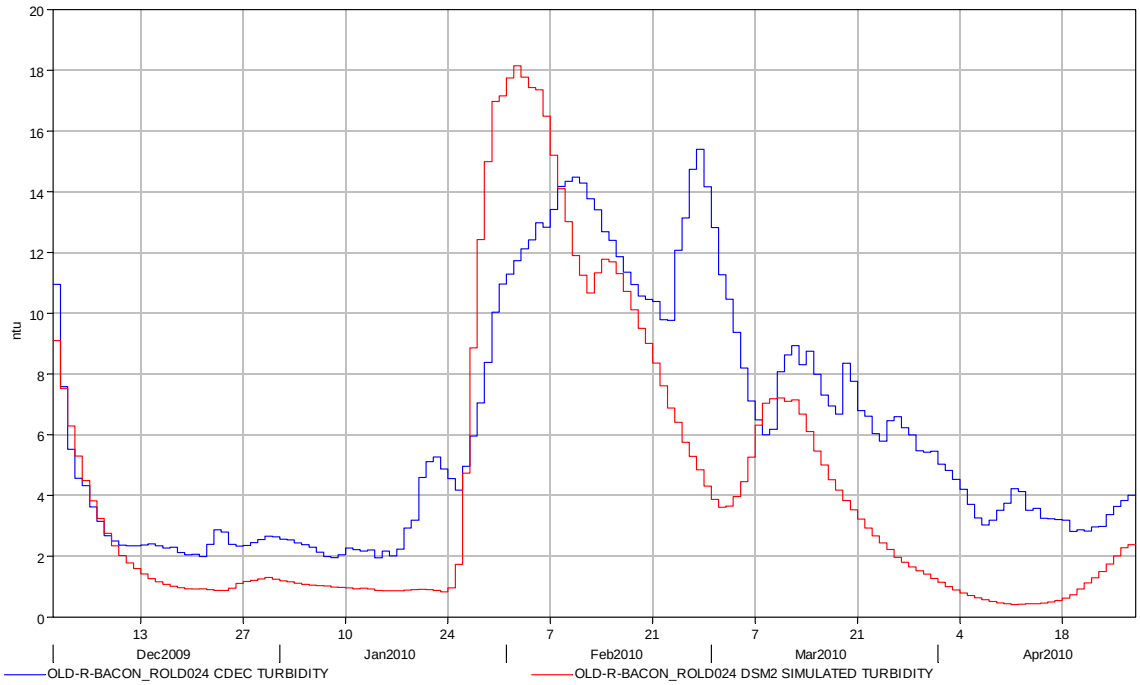

Figure 7-13 Daily-averaged turbidity comparison at Old River Bacon Island

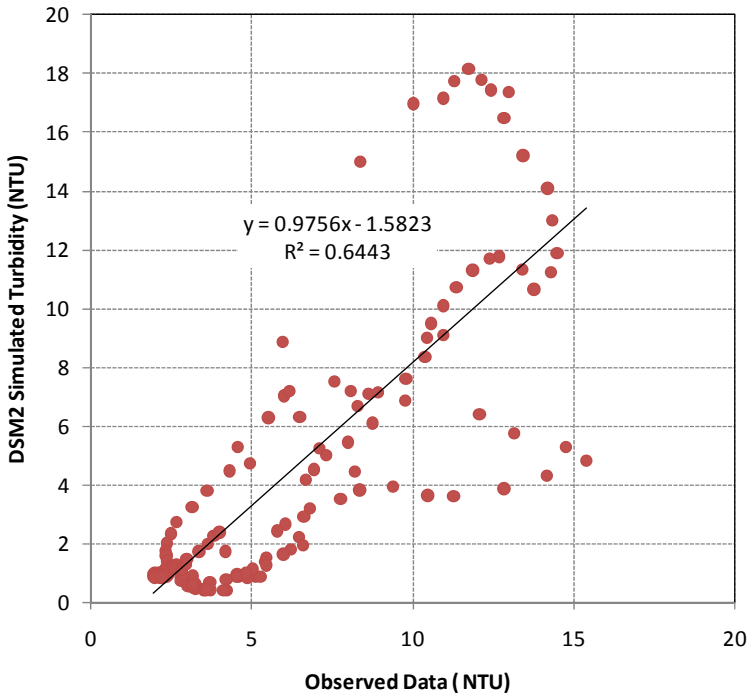

Figure 7-14 Regression analysis of modeled result and field data at Old River Bacon Island

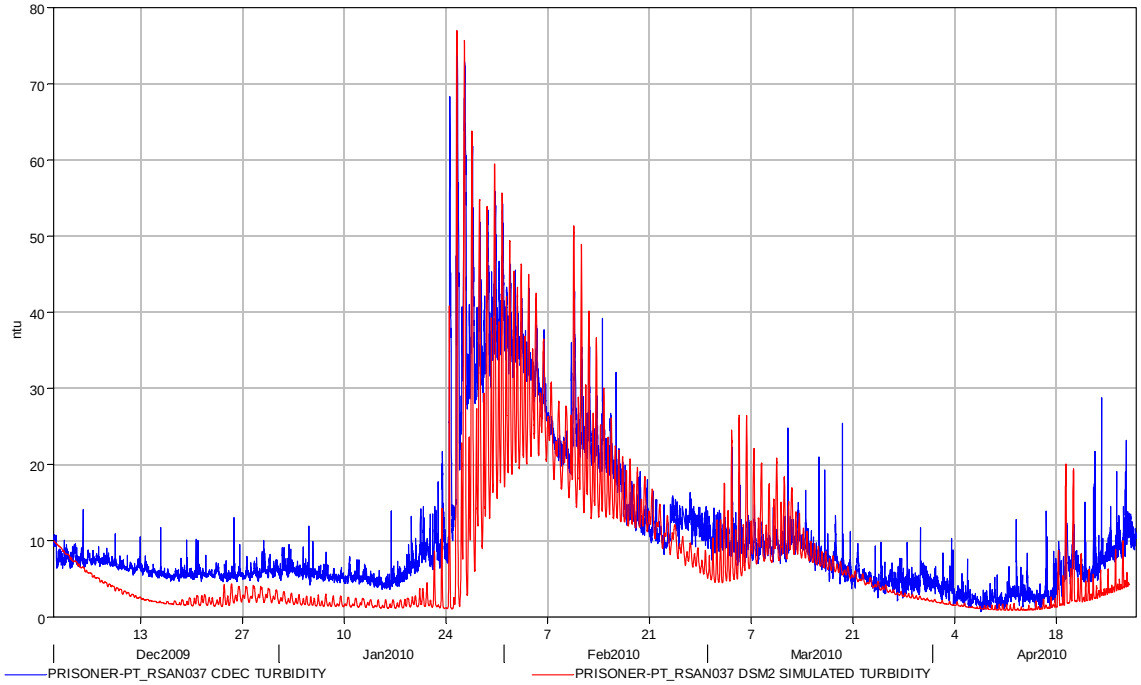

d

Figure 7-15 Turbidity comparison, Sacramento River at Prisoners Point

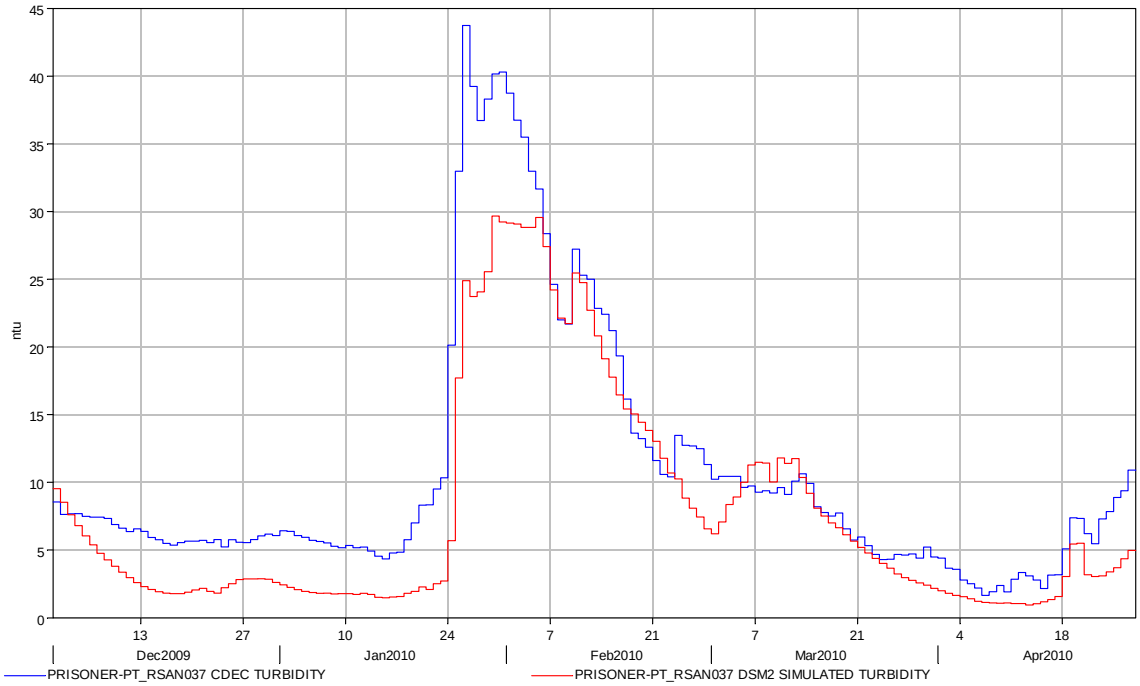

Figure 7-16 Daily-averaged turbidity comparison, Sacramento River at Prisoners Point

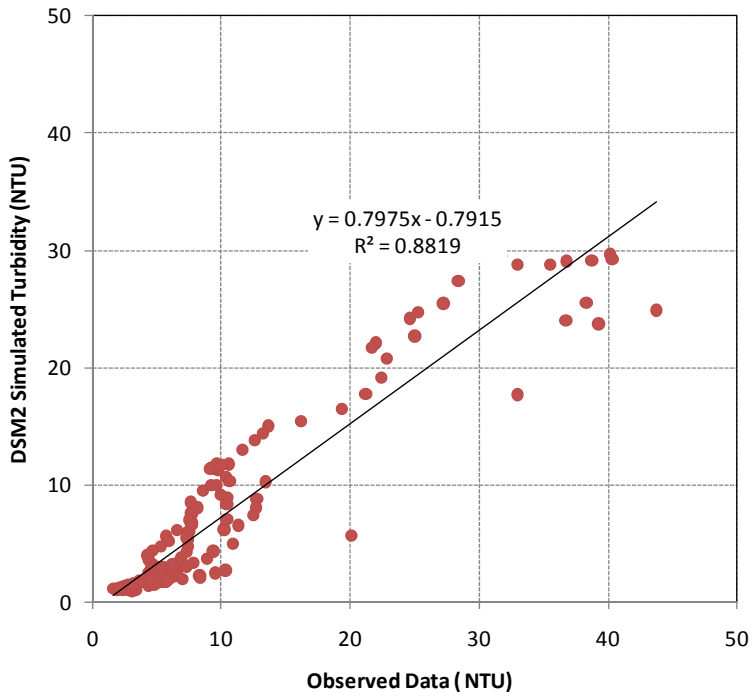

Figure 7-17 Regression analysis of modeled result and field data at Prisoners Point

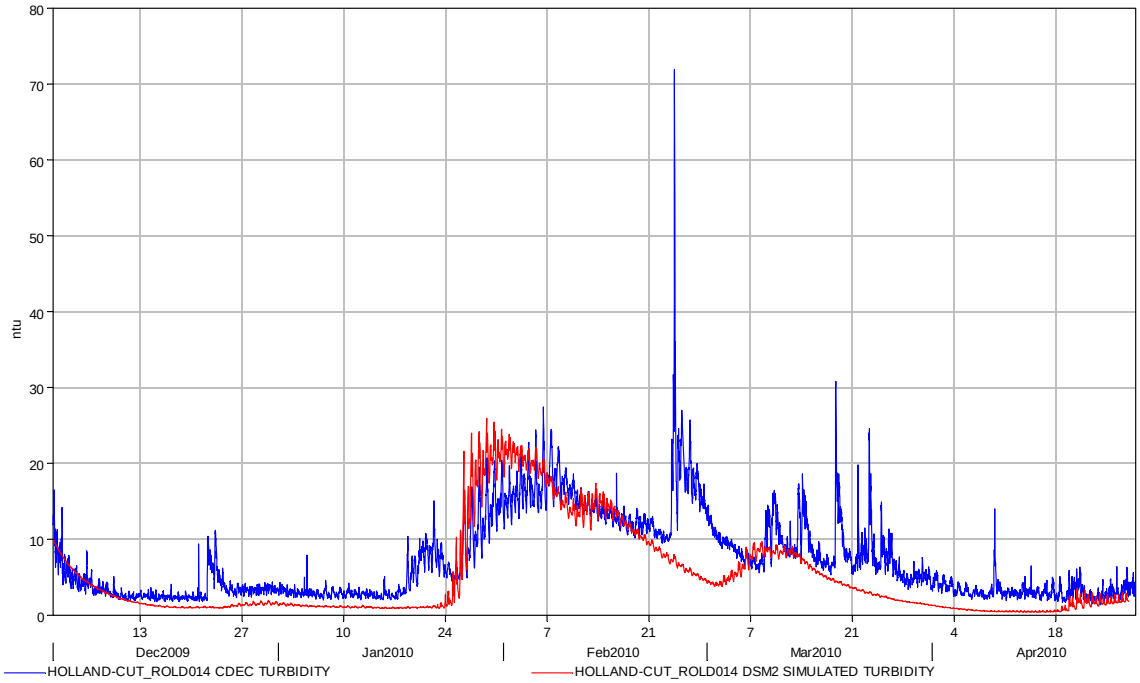

Figure 7-18 Turbidity comparison, Sacramento River at Holland Cut

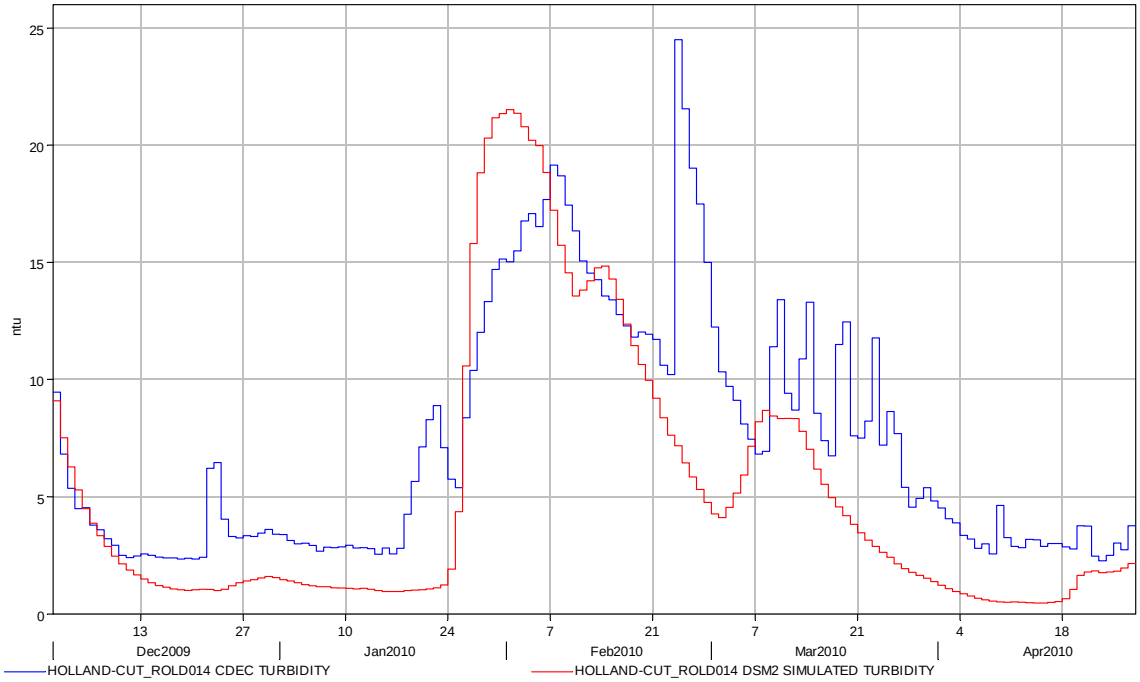

Figure 7-19 Daily-averaged turbidity comparison at Holland Cut

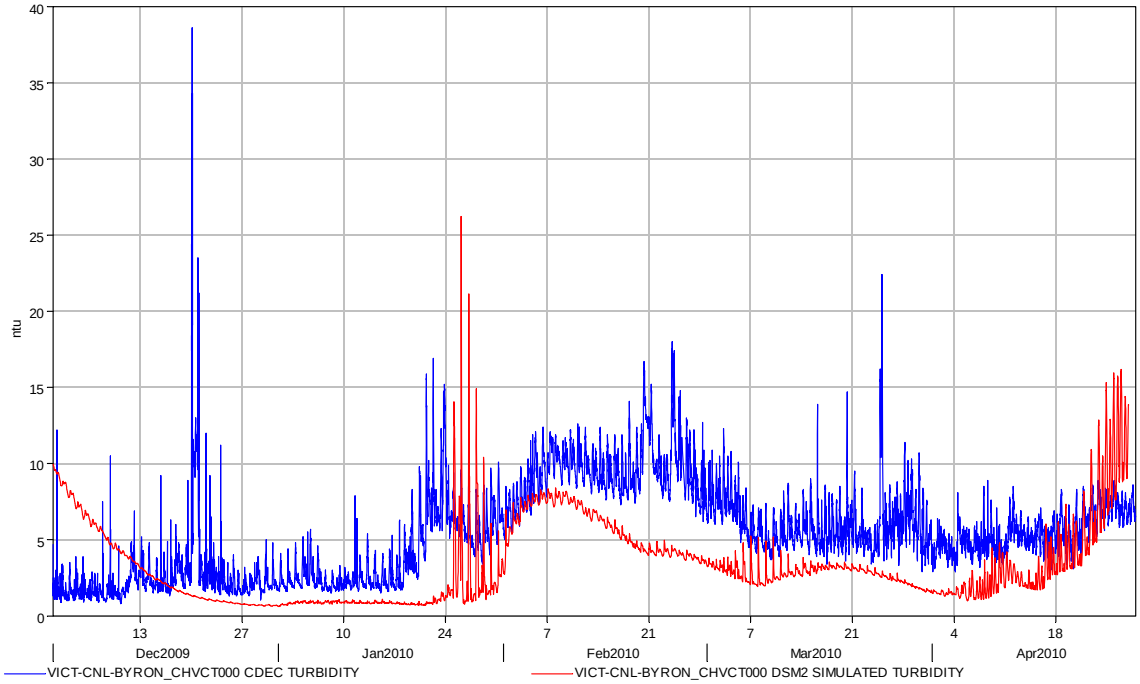

Figure 7-20 Turbidity comparison at Victoria Canal

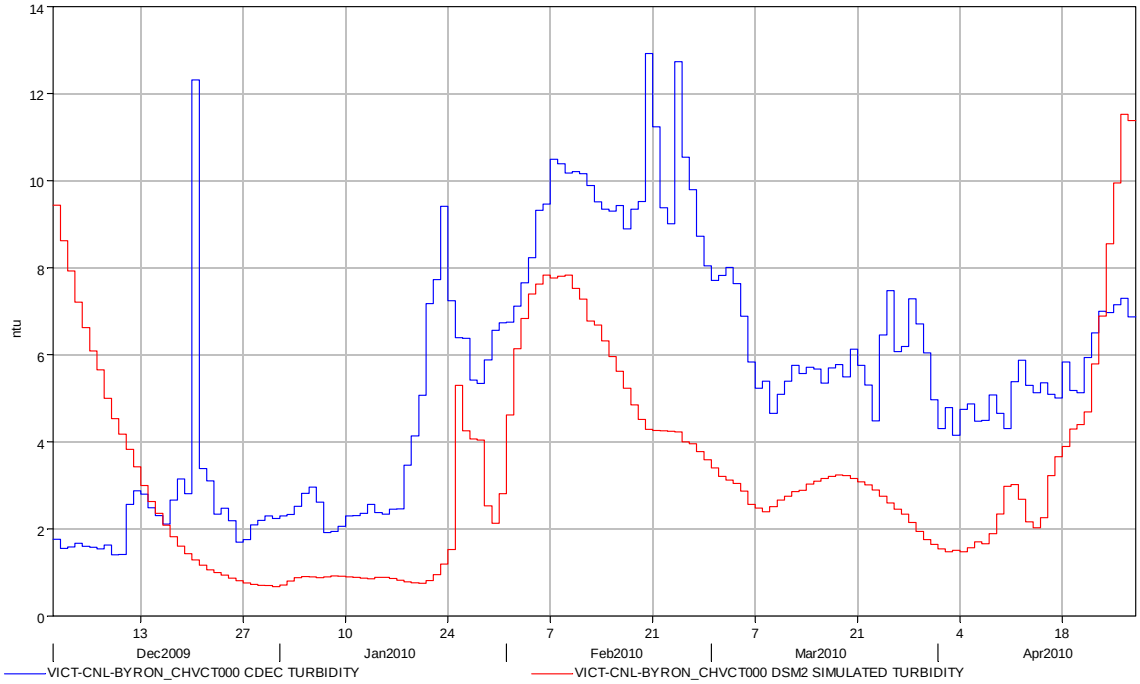

Figure 7-21 Daily-averaged turbidity comparison at Victoria Canal

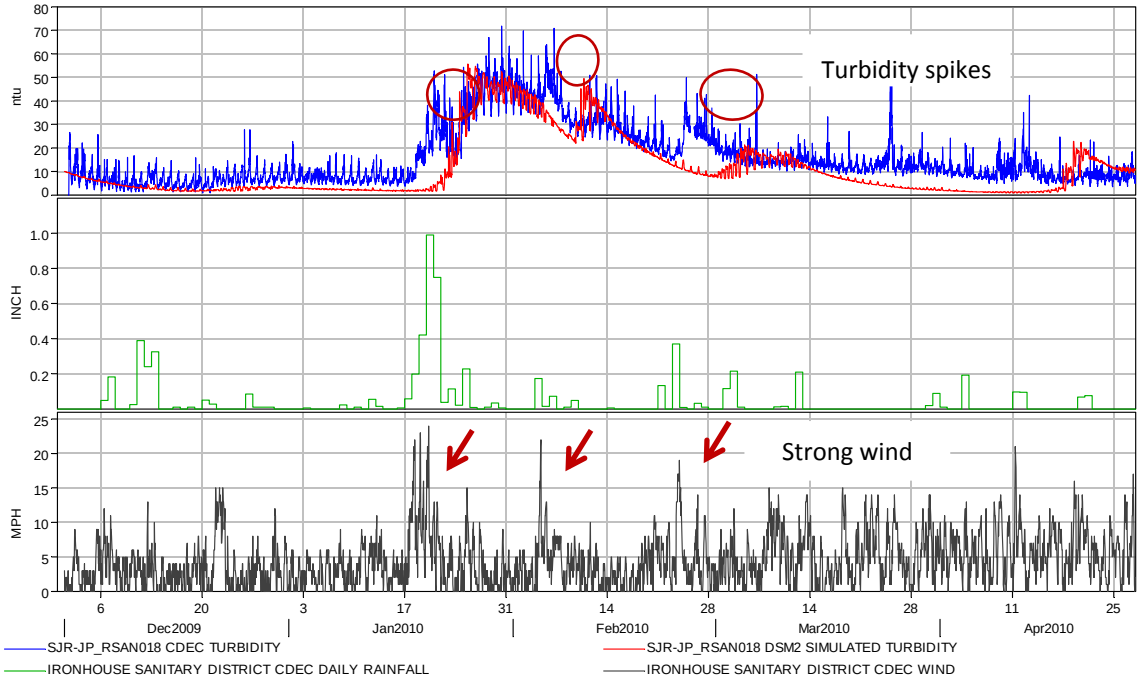

Figure 7-22 Compare turbidity spikes at Jersey Point with rainfall and wind data

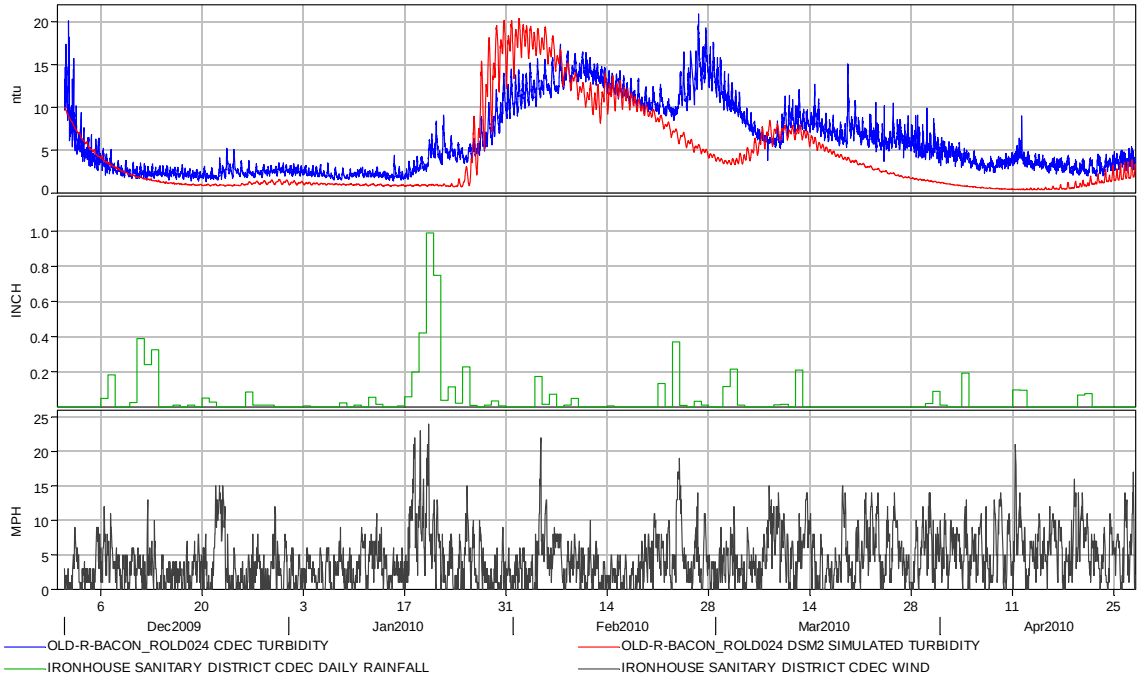

Figure 7-23 Compare turbidity spikes at Bacon Island with rainfall and wind data

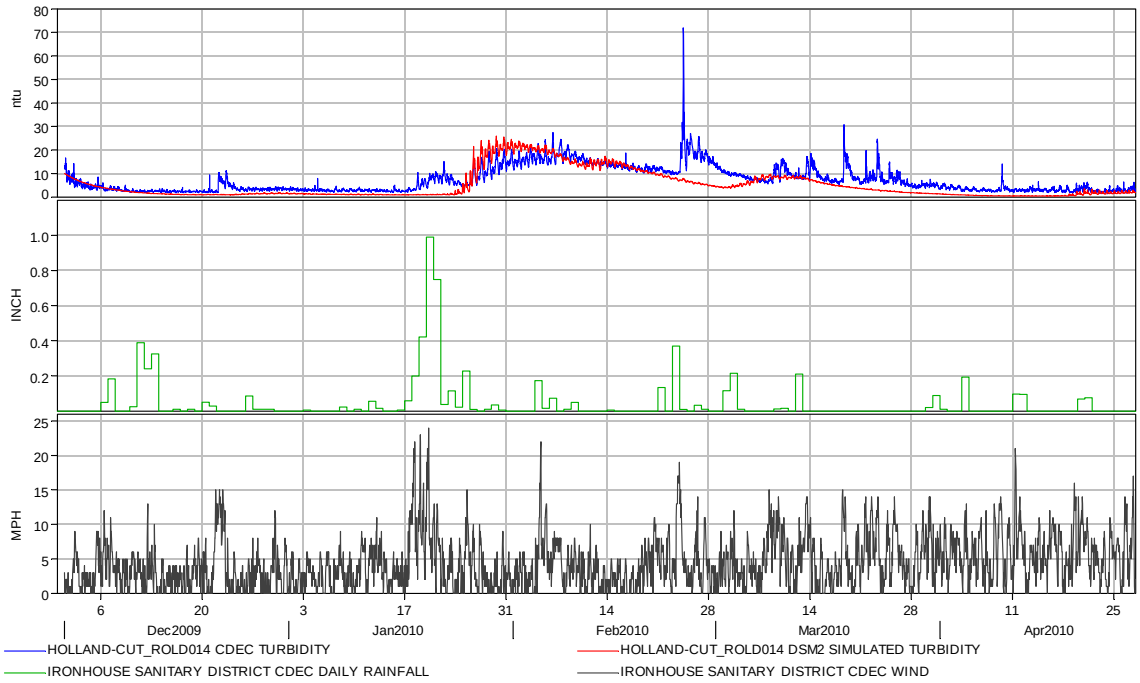

Figure 7-24 Compare turbidity spikes at Holland Cut with rainfall and wind data

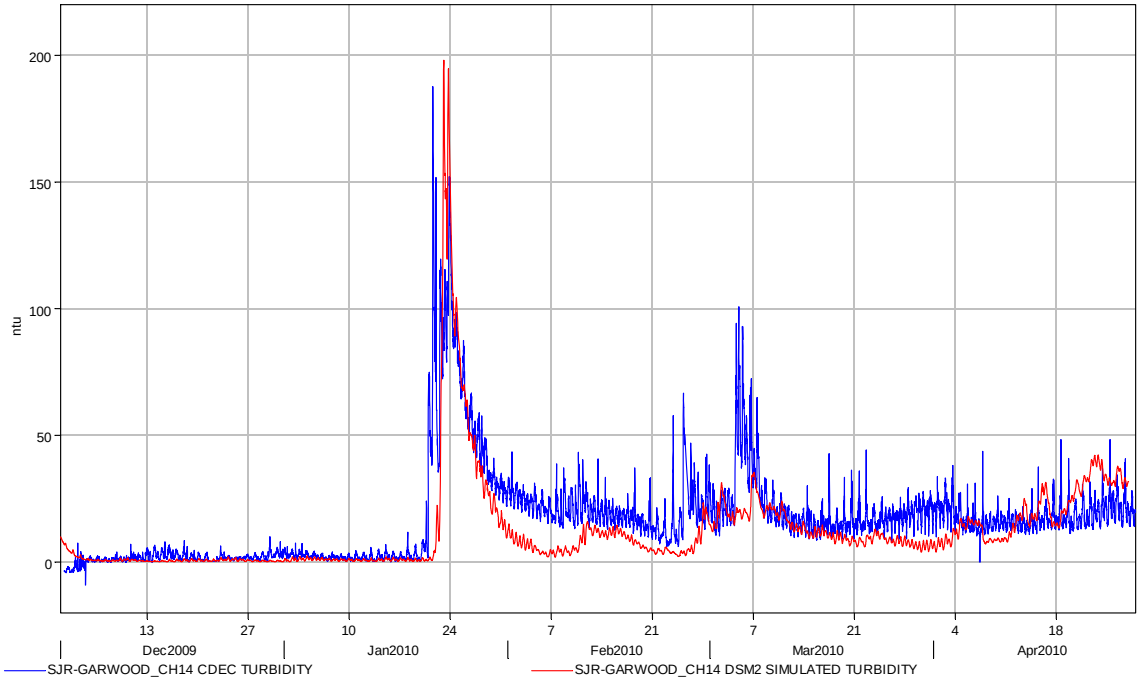

Figure 7-25 Turbidity comparison at San Joaquin River Garwood

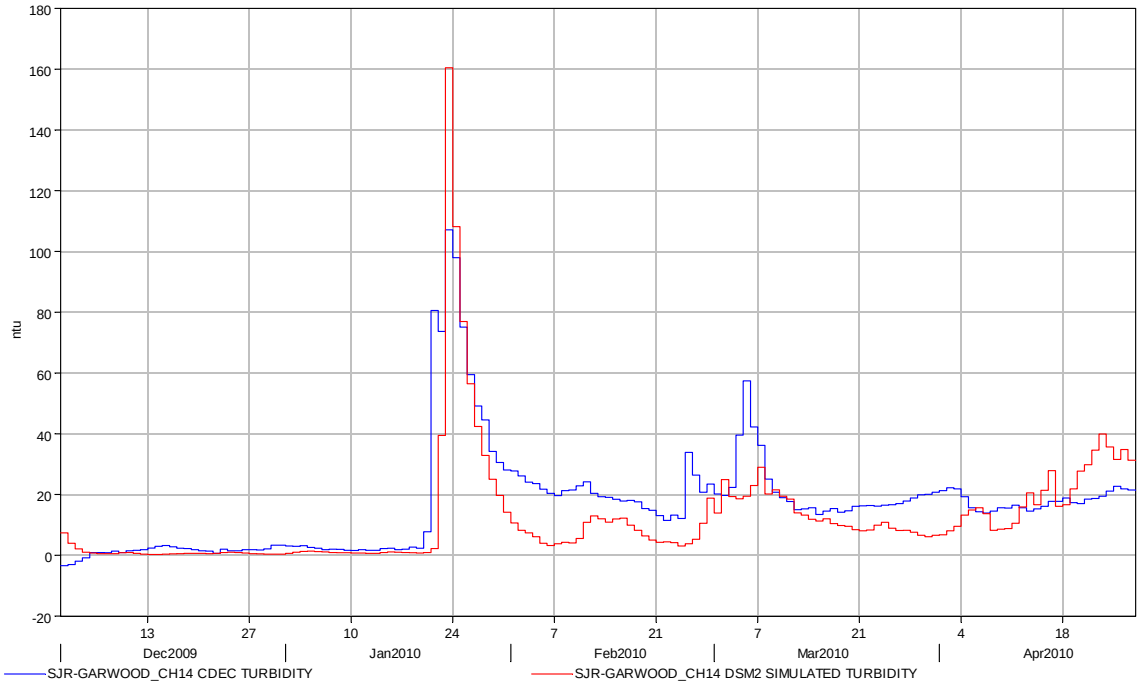

Figure 7-26 Daily-averaged turbidity comparison at San Joaquin River Garwood

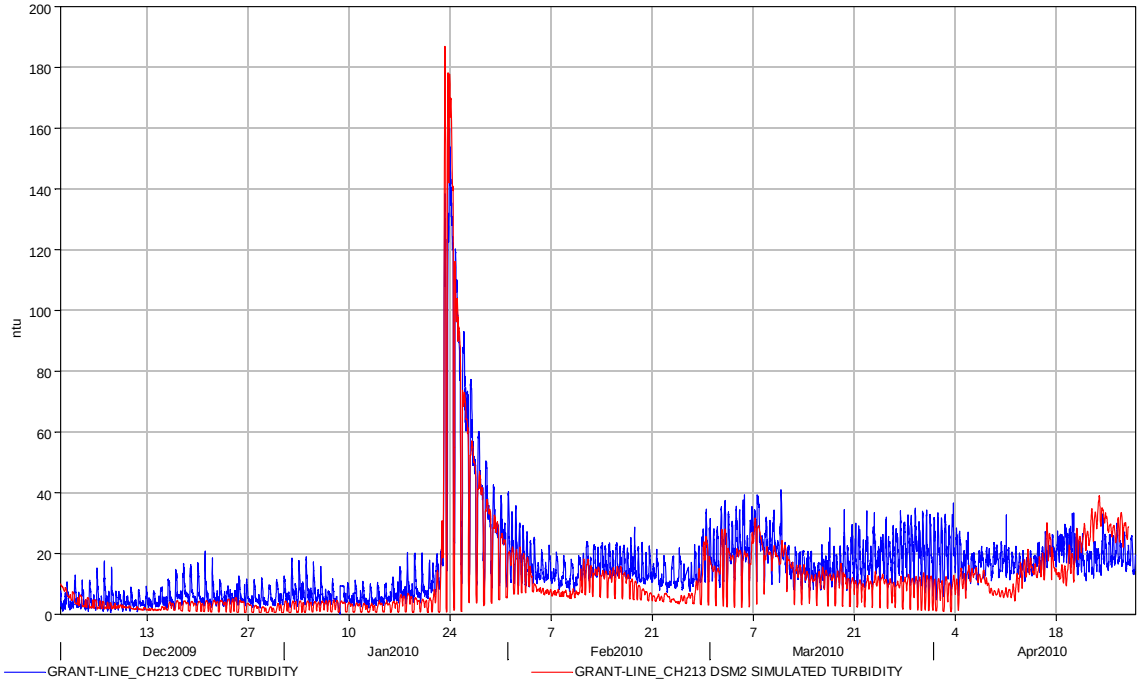

Figure 7-27 Turbidity comparison at Grant Line Canal

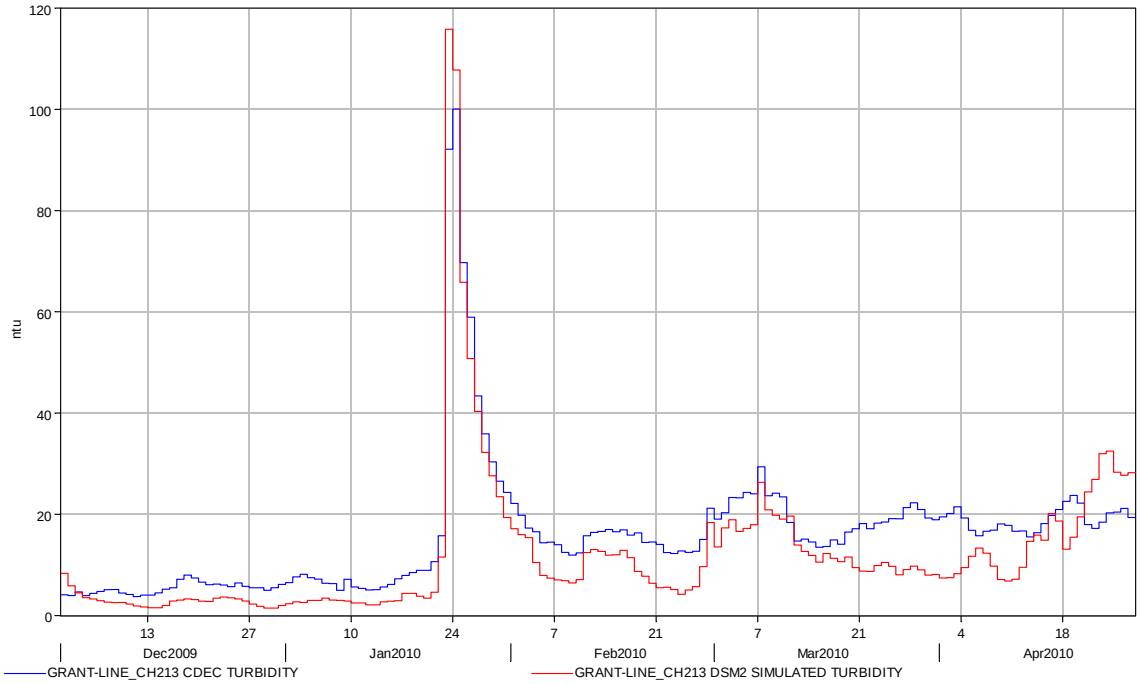

Figure 7-28 Daily-averaged turbidity comparison at Grant Line Canal

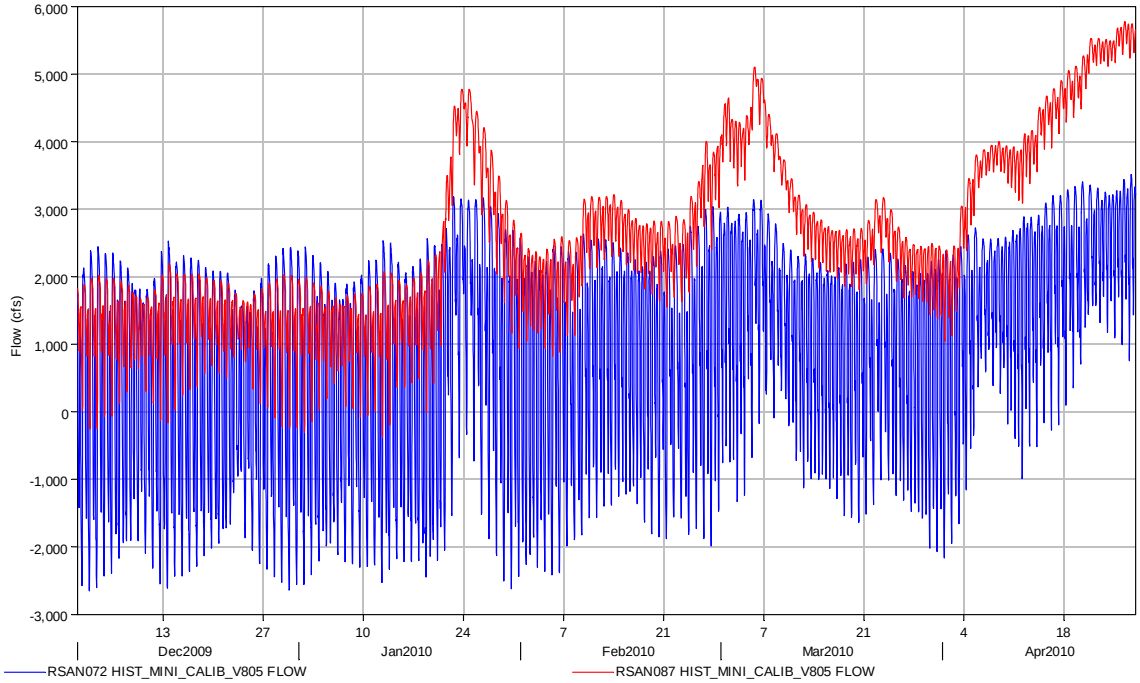

Figure 7-29 Flow at San Joaquin River Mossdale (RSAN087) and Brandt Bridge (RSAN072)

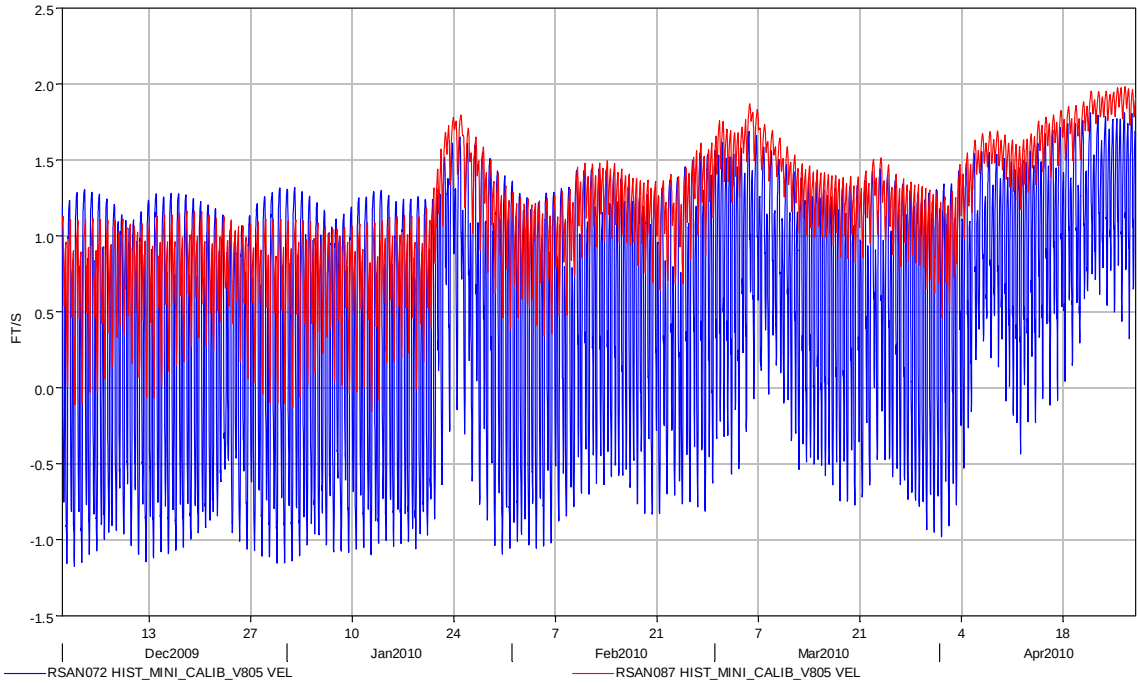

Figure 7-30 Velocity at San Joaquin River Mossdale and Brandt Bridge

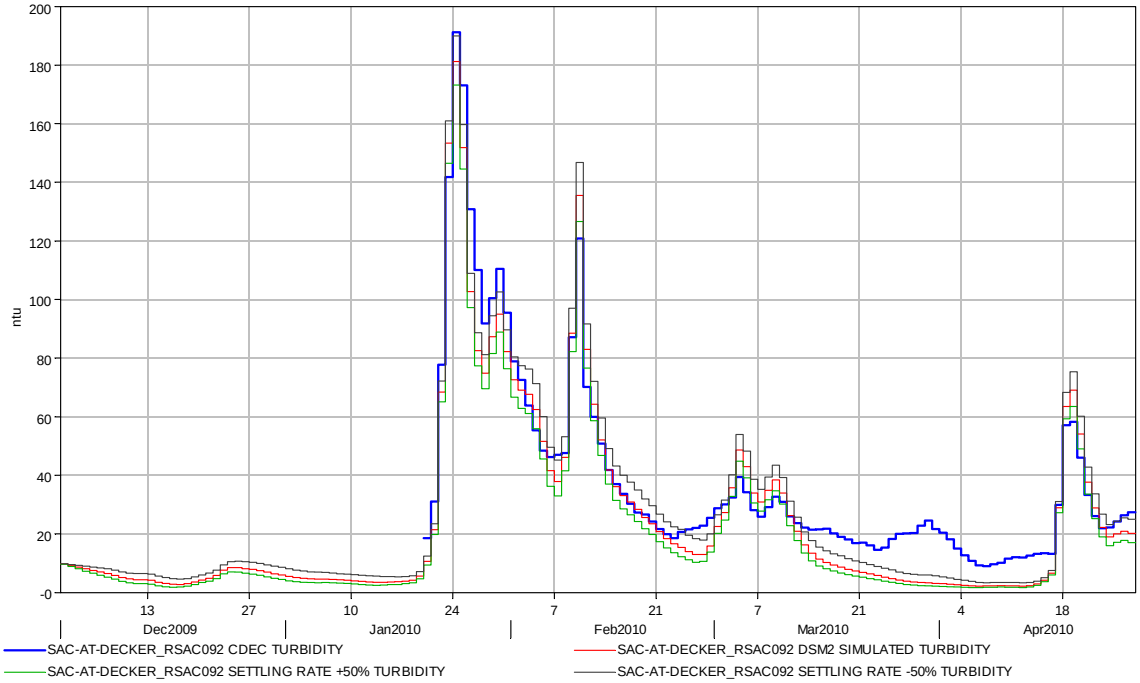

Figure 7-31 Settling rate sensitivity test result at Decker Island

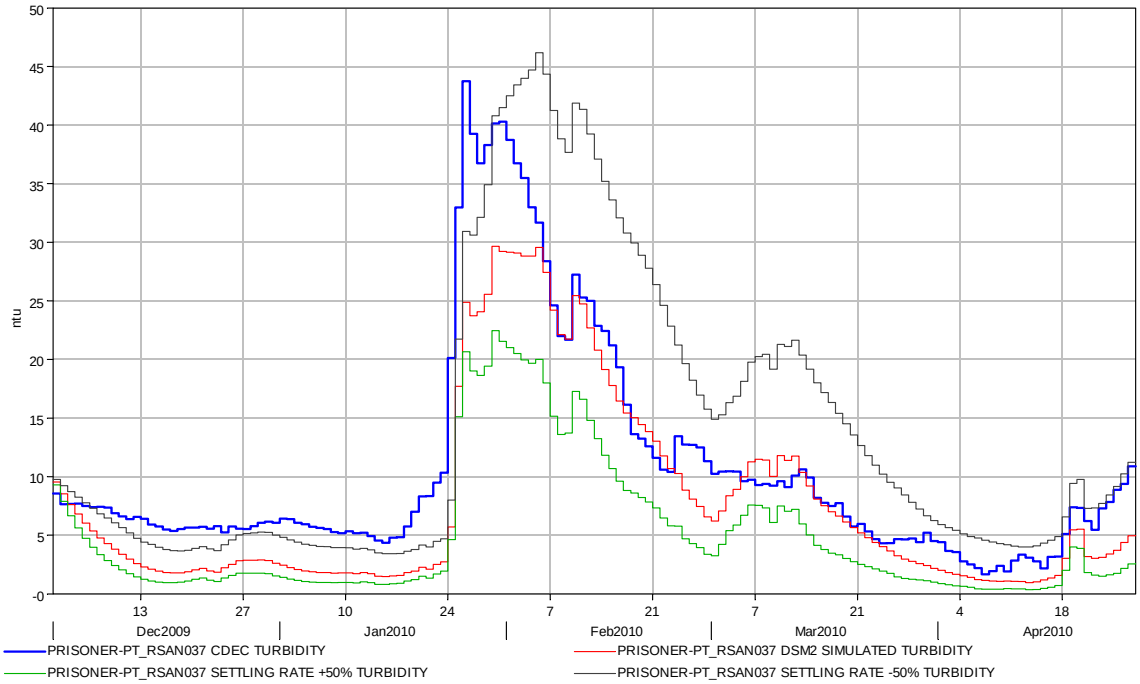

Figure 7-32 Settling rate sensitivity test result at Prisoners Point

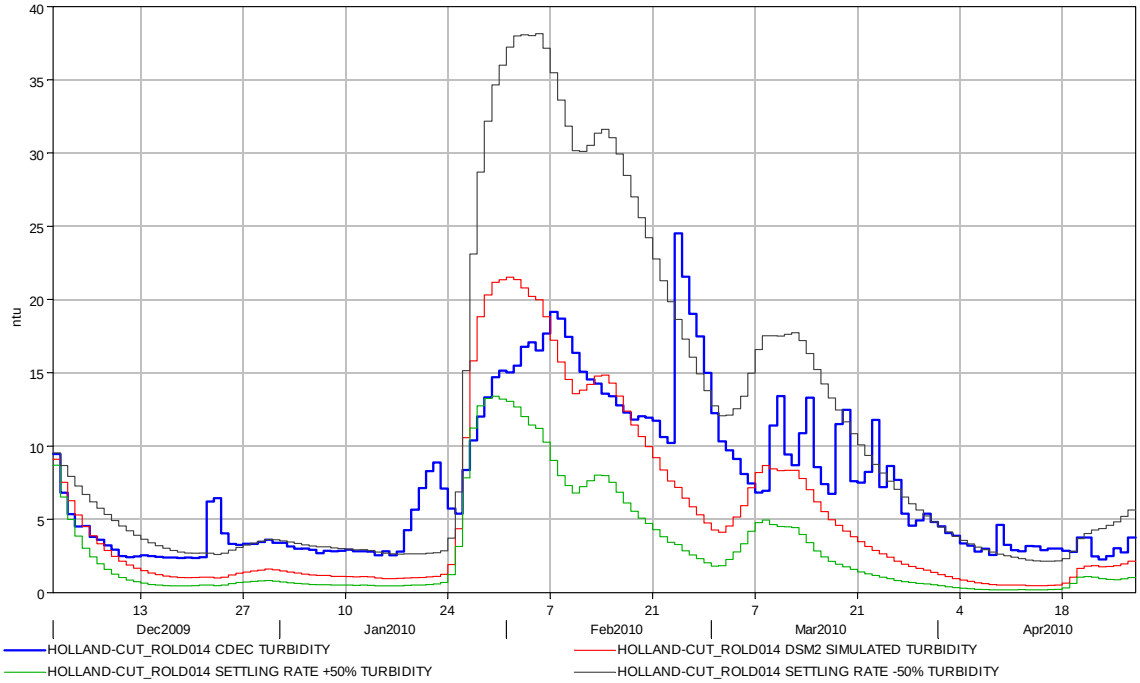

Figure 7-33 Settling rate sensitivity test result at Holland Cut

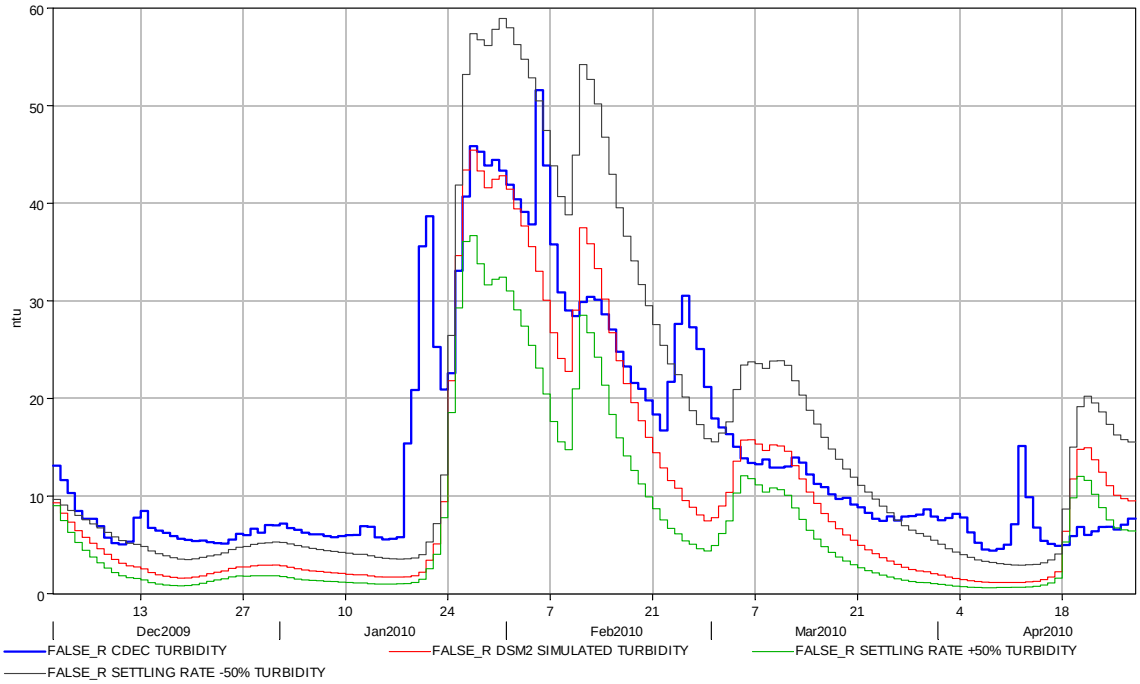

Figure 7-34 Settling rate sensitivity test result at False River

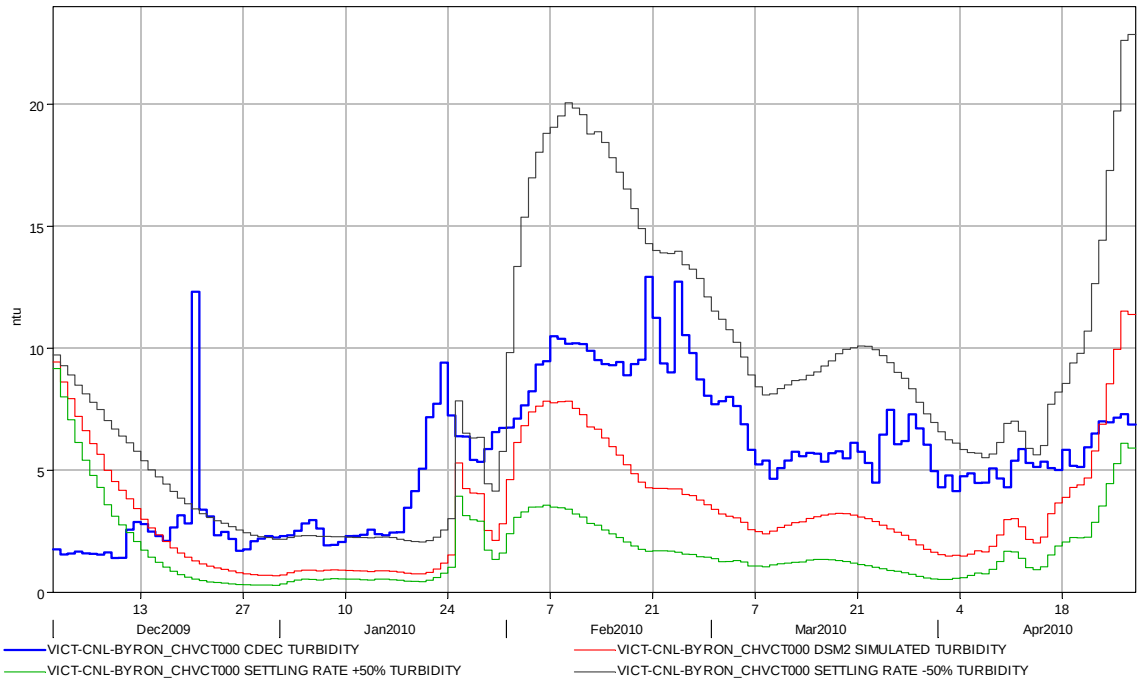

Figure 7-35 Settling rate sensitivity test result at Victoria Canal

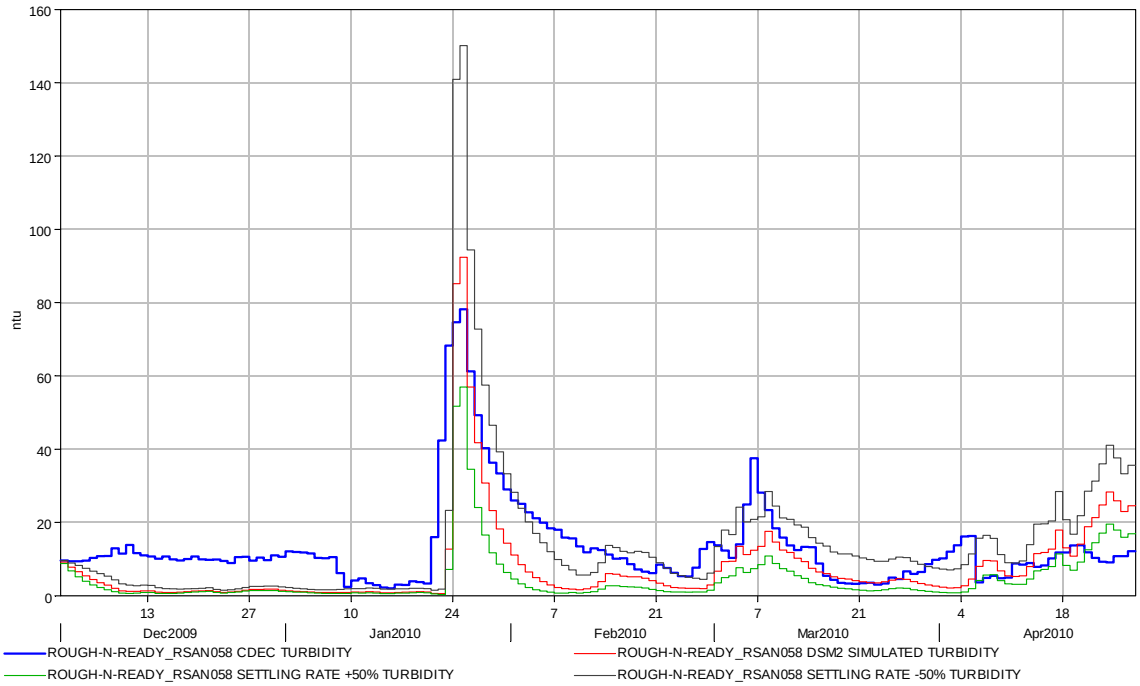

Figure 7-36 Settling rate sensitivity test result at Rough and Ready Island

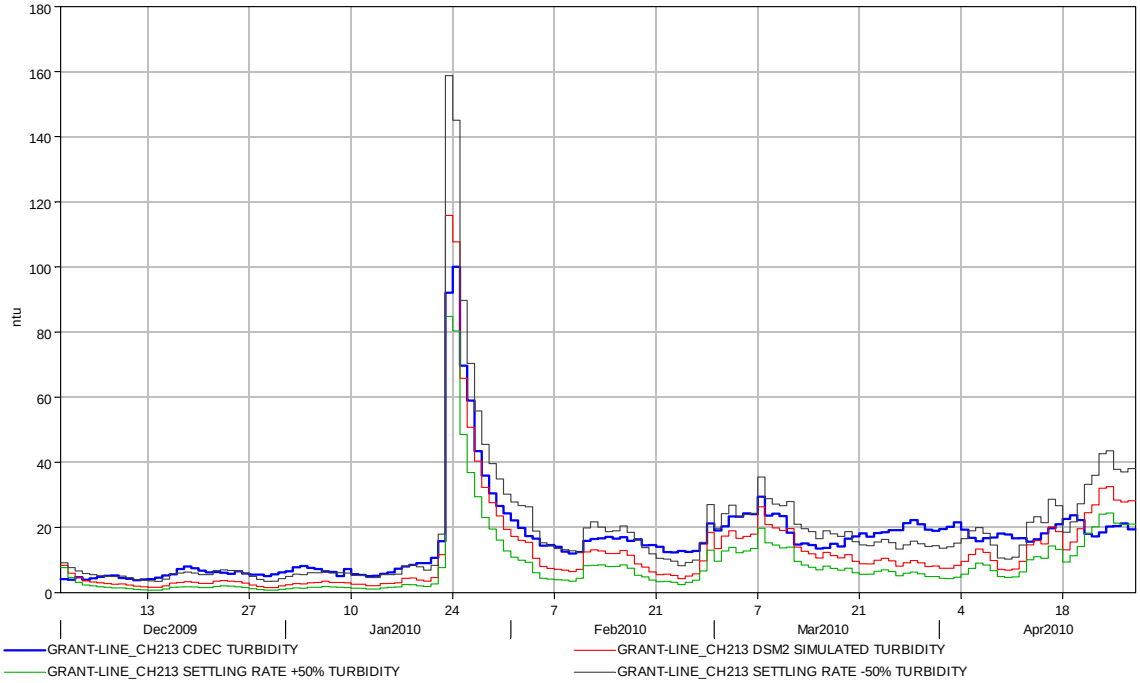

Figure 7-37 Settling rate sensitivity test result at Grant Line Canal

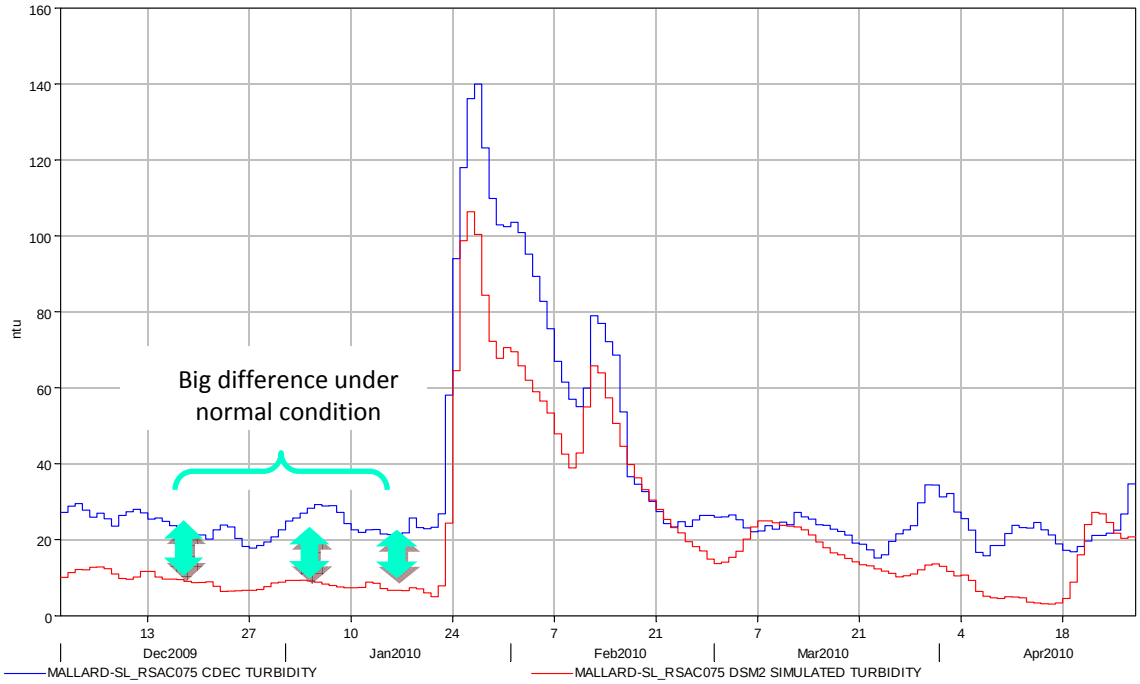

Figure 7-38 Daily-averaged turbidity comparison at Mallard

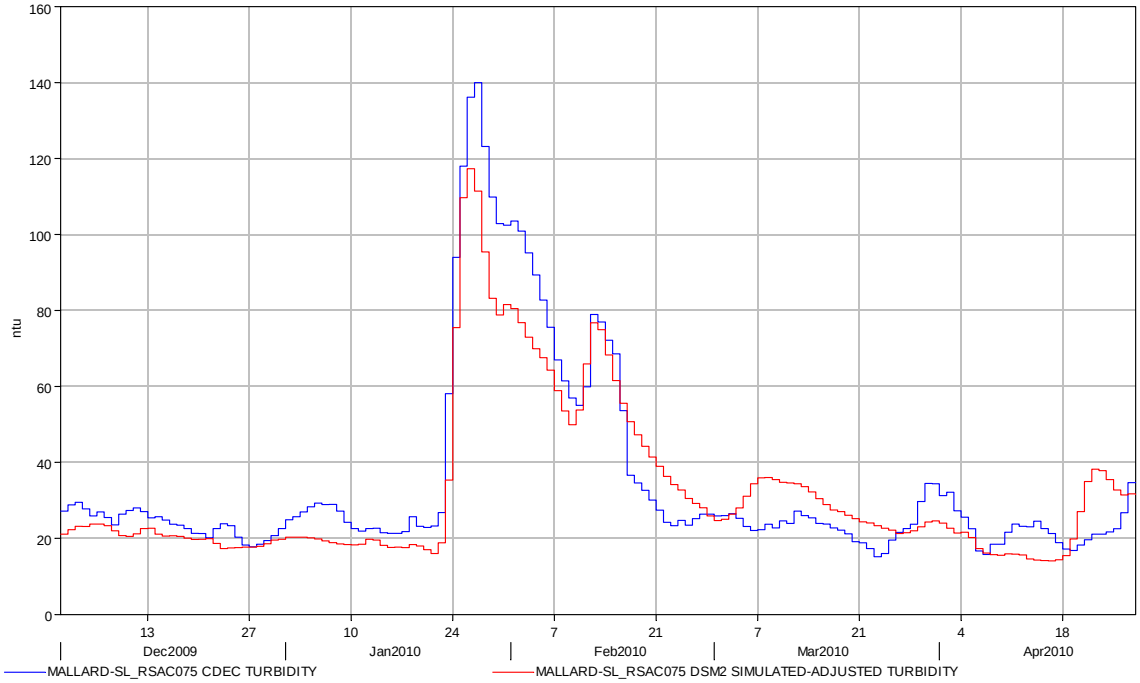

Figure 7-39 Adjusted turbidity comparison at Mallard

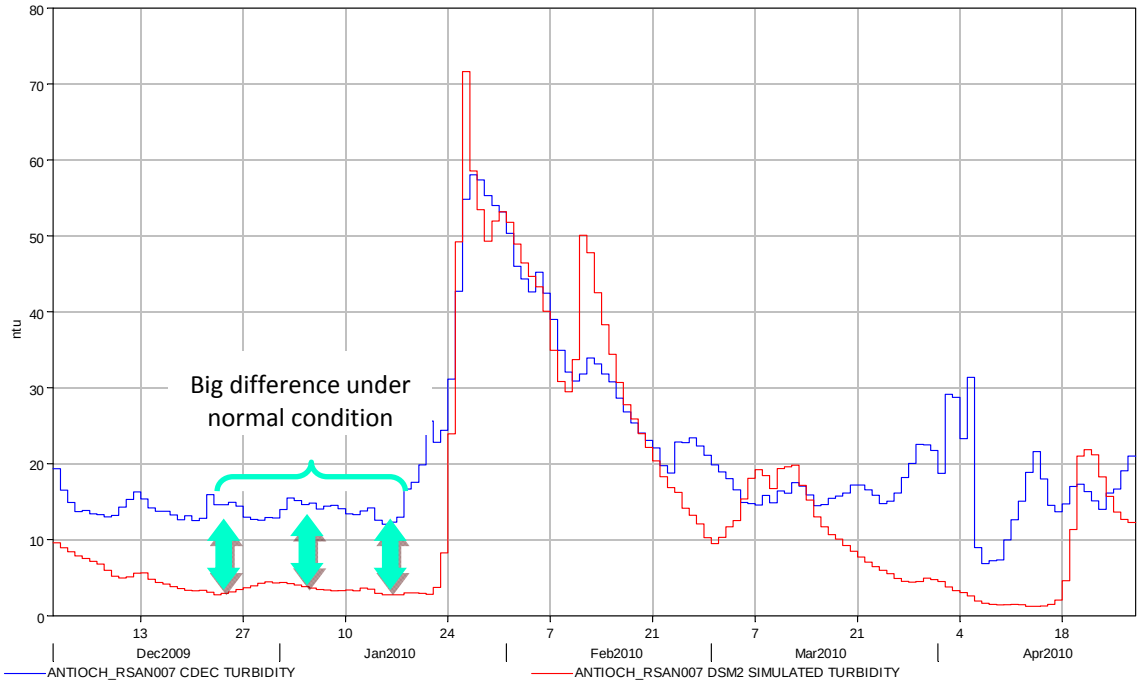

Figure 7-40 Daily-averaged turbidity comparison at Antioch

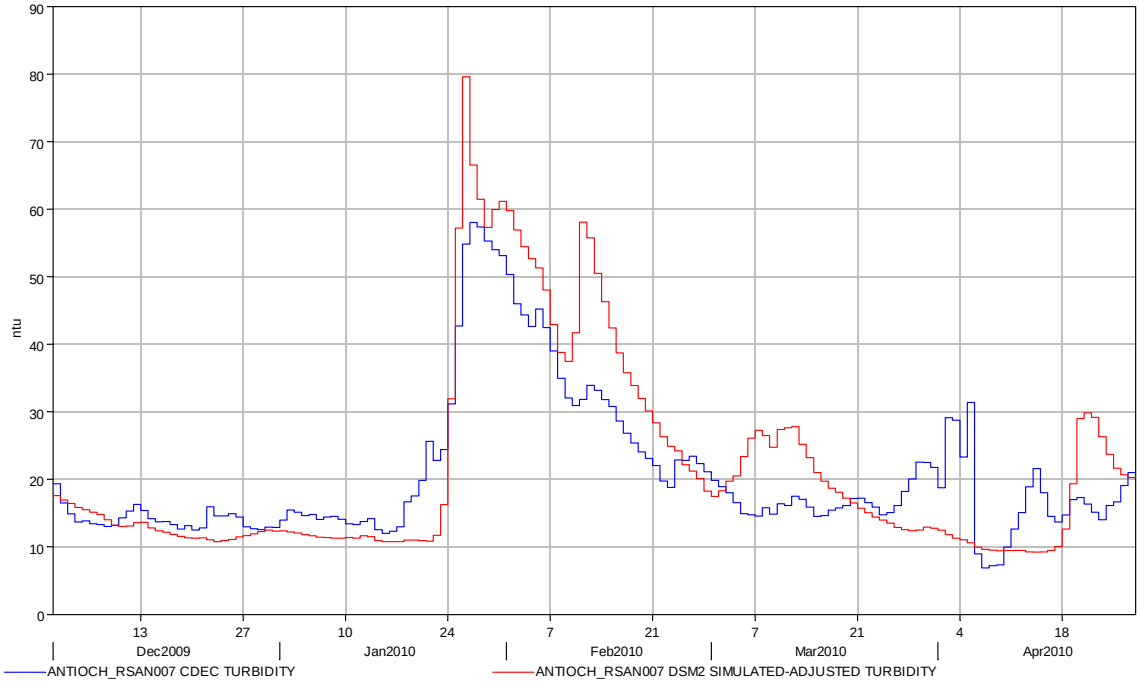

Figure 7-41 Adjusted turbidity comparison at Antioch

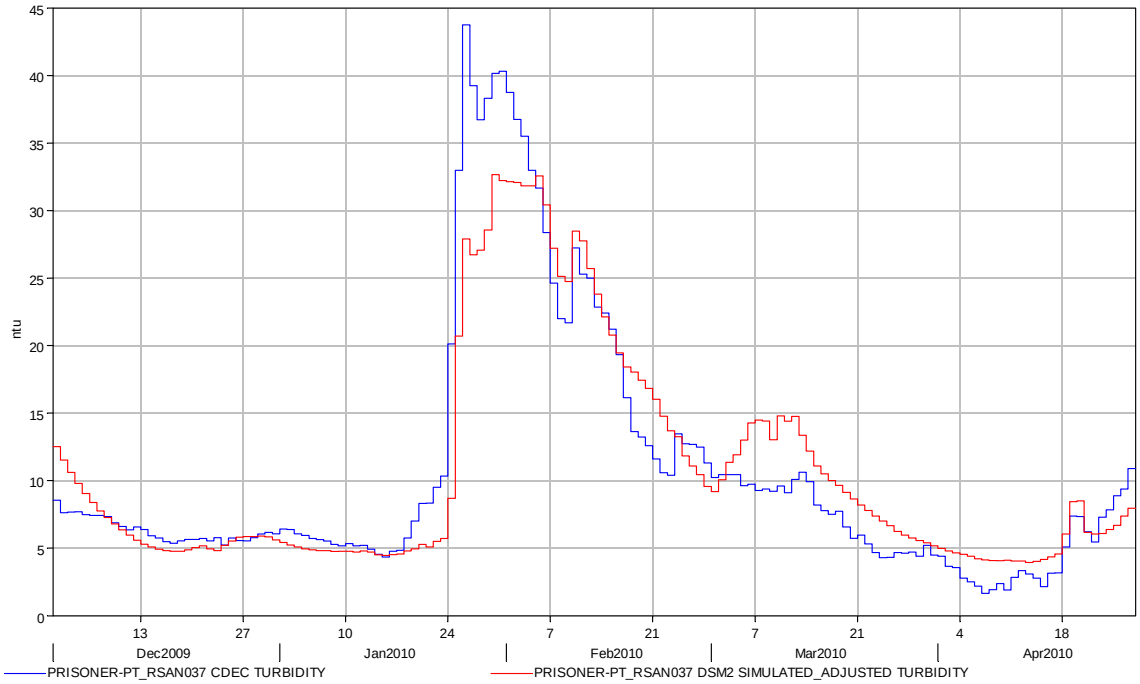

Figure 7-42 Adjusted turbidity comparison at Prisoners Point

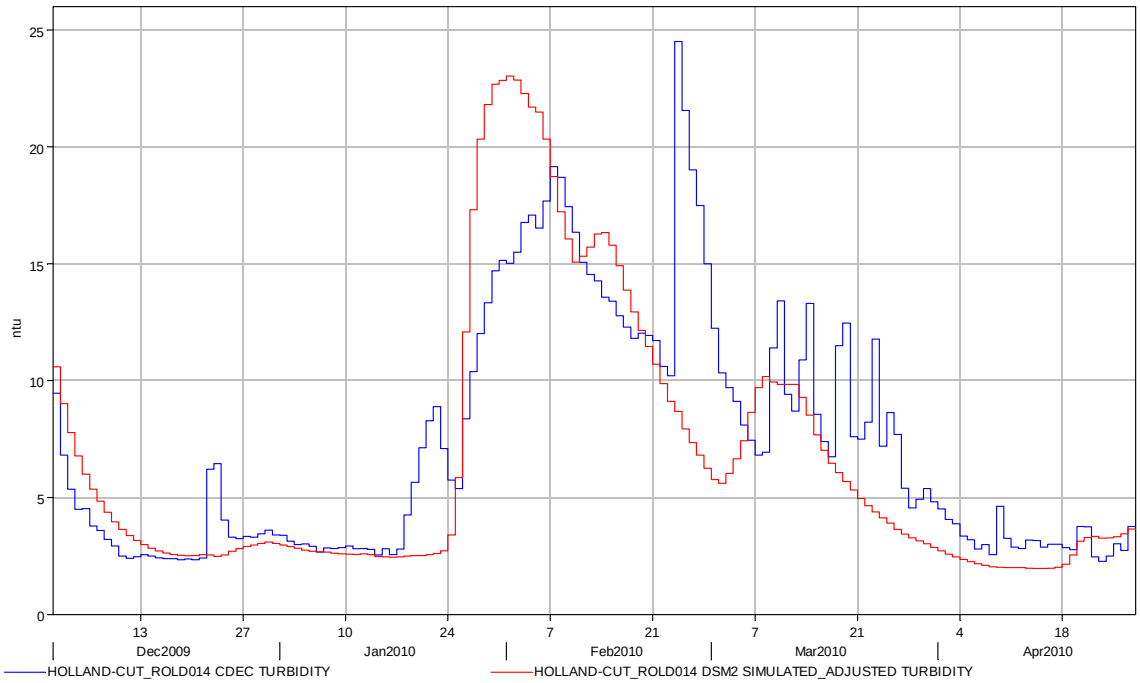

Figure 7-43 Adjusted turbidity comparison at Holland Cut

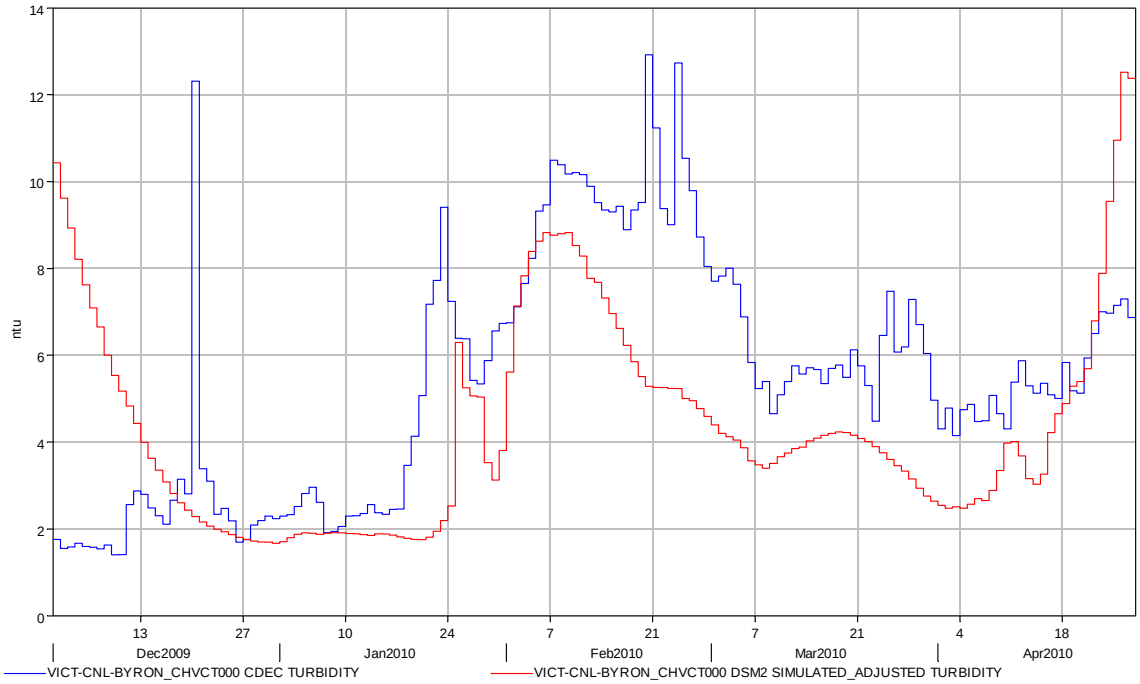

Figure 7-44 Adjusted turbidity comparison at Victoria Canal

Methodology for Flow and Salinity Estimates in the Sacramento-San Joaquin Delta and Suisun Marsh

32nd Annual Progress Report
June 2011

Chapter 8
DSM2 Grid Map Tool

Authors: Nicky Sandhu and En-Ching Hsu,
Delta Modeling Section,
Bay-Delta Office,
California Department of Water Resources

Contents

8 DSM2 Grid Map Tool 8-1
8.1 Introduction 8-1
8.2 Geographical Information 8-1
8.3 Design 8-2
8.4 Implementation Details 8-2
8.5 Storage Format 8-3
8.6 User Interface Overview 8-4
8.6.1 Login 8-4
8.6.2 Upload 8-5
8.6.3 Viewing the Grid 8-5
8.6.4 Viewing Channel Information 8-8
8.6.5 GIS Tools 8-9
8.6.6 Managing Studies 8-9
8.6.7 Editing Mode 8-10
8.6.8 Editing Nodes 8-10
8.6.9 Editing Channels 8-10
8.6.10 Editing Reservoirs 8-14
8.6.11 Editing Gates 8-14
8.7 Conclusion 8-14
8.8 References 8-15

Figures

Figure 8-1 Data flow for DSM2 grid map 8-2
Figure 8-2 Sample grid 8-4
Figure 8-3 Example log in page 8-4
Figure 8-4 Example study upload 8-5
Figure 8-5 Example grid elements: reservoirs 8-6
Figure 8-6 Example grid elements: gates 8-6
Figure 8-7 Example base maps 8-7
Figure 8-8 Example channel display 8-8
Figure 8-9 GIS tools 8-9
Figure 8-10 Example study inputs 8-9
Figure 8-11 Node editing 8-10

Figure 8-12 Flow line editing 8-11
Figure 8-13 Edit Channel Cross section 8-11
Figure 8-14 Edit Channel Cross section (detail) 8-12
Figure 8-15 Edit Channel Cross section (profile points) 8-12
Figure 8-16 Edit Channel Cross section (elevation profile) 8-13
Figure 8-17 Edit Channel Cross section (generate or clear) 8-13
Figure 8-18 Editing reservoirs 8-14

Table

Table 8-1 GIS data format 8-3

8 DSM2 Grid Map Tool

8.1 Introduction

DSM2 is a 1-dimensional hydrodynamic and water quality model that simulates flow, stage, and conservative and non-conservative constituents in the Sacramento–San Joaquin Delta. The physical geometry is represented in DSM2 by channel lengths, channel cross sections, reservoir areas, and reservoir bottom elevations. These inputs are derived from geographical data, which are now available in computer systems and referred to as Geographical Information Systems (GIS).

Since 1998, DSM2 geometry has been handled with the Cross-Section Development Program (DWR, Delta Modeling Section 1998). CSDP has worked well for many years, but it is not inherently geo-referenced and has reached the end of its useful life. The DSM2 Grid Map Tool offers all the capabilities of CSDP and several more, and may serve to replace CSDP for DSM2 bathymetry and channel development.

This tool links the information contained in GIS with the DSM2 input text files. It provides a way to view the DSM2 grid of channels, reservoirs, and gates overlaid on a map. This provides a much needed visual context for understanding how elements of the DSM2 grid map onto the physical features they represent. The map can be changed to a US topographical, elevation contour map and a Satellite view for different perspectives.

The grid map tool enables the user to search the grid for a particular element and to measure the lengths of arbitrary line segments and areas of polygons. Elevation and elevation profiles along a line are also readily accessible.

Furthermore, the grid map tool has an edit mode for editing the locations of the nodes, the flow lines of channels, and the outline of reservoir areas.

The grid map tool is built on the Google Maps API and is designed to be used within a modern Web browser. Data are hosted online for ease of accessibility for a wide audience of users and to support the large data sets required to provide the elevation functionality. The application is secured using Google accounts with ability to add other OpenID [http://openid.net/] providers in the future.

8.2 Geographical Information

The basic information used is the digitized base maps available via Google Maps services [http://code.google.com/apis/maps/documentation/javascript/v2/services.html]. Google Maps serves the DSM2 grid map at a particular zoom level using image tiles that are assembled in a Web browser to provide a seamless stitched map. These image tiles are customized in the grid map tool to provide US topographical image tiles and depth-based color-coded image tiles for depth context over a spatial area.

Length and area calculations are provided using Google Maps APIs, which use a modified Mercator projection. This is sufficiently accurate (within +/- 0.2%) in an area the size of the Delta (MTL n.d.).

Elevation information used to calculate the channel cross-sections and reservoir bottom elevations are provided from a Digital Elevation Model (DEM) raster with a 10mx10m cell size. The DEM information currently being used is derived from best bathymetry data and LIDAR data available as of November 2010 and may be revised in the future as more recent data are available.

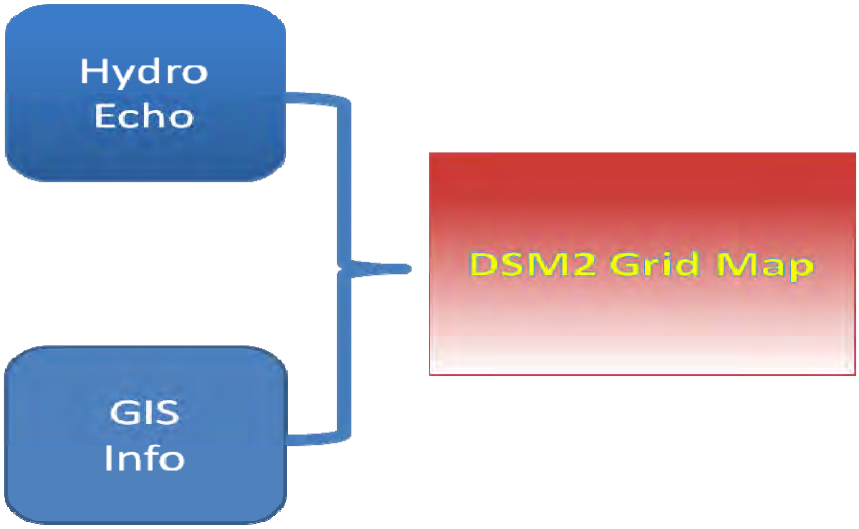

Figure 8-1 Data flow for DSM2 grid map

8.3 Design

DSM2 Hydro is a hydrodynamic model. The input to this program is provided as text files, and the time series as a US Army Corps of Engineers' Hydrologic Engineering Center Data Storage System (HEC-DSS) file. This information is copied to a file at runtime, which is referred to as the echo file. It contains all the text information from the various input files reproduced in one large file.

The structure of the text information for DSM2 Hydro consists of tables of information. Each table consists of a name, followed by a line of column names, followed by rows of data, and ending with the END keyword. This echo file serves as one of the inputs to the DSM2 Grid Map Tool.

The other file is a text file with table input similar to GIS data. A description is provided in the storage format section. The GIS data input file is required only for the DSM2 Grid Map Tool and is not directly used by the DSM2 Hydro program (Figure 8-1).

If GIS data are missing for any element, there is a fallback strategy to placing the element, the location of which can then be edited using this tool.

The grid map tool works on the information from these 2 files—hydro echo and GIS information—and can change the GIS data based on user activities. The user can always extract the latest echo and GIS data inputs from the tool. The echo file will reflect any changes made using the tool. Furthermore, the echo file can be used with minor configuration changes to run the DSM2 Hydro program with this updated information.

8.4 Implementation Details

The grid map tool is written to be an online Web application. The application is designed to be used with a modern browser such as Google Chrome 9+, Firefox 3+, Safari 4+, or IE 9+. Older browsers such as IE 8 and below are prompted to install a Google Chrome plug-in, which enables the functionality for older browsers [http://en.wikipedia.org/wiki/Web_browser#Standards_support].

For hosting and user management, Google's infrastructure is leveraged using the Google App Engine. This enables a cost effective and proven security platform and relieves DWR from having to maintain commodity infrastructure. Google Maps now require users to obtain a Google account. If needed, the authentication for the user can be moved to any OpenID [http://openid.net/] compliant account in the future.

An online application was chosen because no proprietary software other than a browser needs to be downloaded, which allows for quicker updates. Also, the large amount of elevation data needed for this application doesn't have to be packaged, distributed, and downloaded, removing yet another updating task.

Finally, the application stores its data in a text format (rather than a proprietary binary format), which allows us to move to another tool, if needed.

The application is written in Java. Parts of the Java program are translated to JavaScript using the Google Web Toolkit [http://code.google.com/webtoolkit/] because the application is designed to be an online application for use in a modern browser [http://en.wikipedia.org/wiki/Web_browser#Standards_support].

The source code is released under GPL v3 and is available from http://code.google.com/p/dsm2-grid-map/.

8.5 Storage Format

The GIS data are stored in text files using the table format similar to the DSM2 input format. A description of each element and its data and storage is detailed in Table 8-1.

The GIS data are stored in a separate file because the data are not needed as input for DSM2. However, the information in the data-linked Hydro echo file is calculated again as the GIS data changes.

Table 8-1 GIS data format

Element type	GIS data	Storage
Node or Junction	Latitude and longitude in decimal degrees	Table with each row containing node ID and a pair of latitude and longitude values
Channel length	A line represented as many pairs of latitude and longitude excluding the beginning and ending points (derived from node data)	Table with each row containing channel ID and all the pairs of latitude and longitude values separated by commas
Reservoir areas	A closed loop represented by many pairs of latitude and longitude	Table with each row containing the reservoir ID and all the pairs of latitude and longitude values separated by commas
Channel Cross sectional profile	The line on the surface represented by origin and end points. The profile is then stored as points with distance from origin along the line and the elevation at that point.	Table with each row representing the channel ID and cross section's distance from upstream node to identify cross section. The origin and end points are stored as latitude and longitude values. The profile is stored as a pair of values representing the distance along the line and the elevation at that point

Note: All latitude and longitude are stored to the 8th decimal place in decimal degrees.

Figure 8-2 Sample grid

8.6 User Interface Overview

This section describes the application and includes screen snapshots to highlight the various features. The application can be accessed at http://dsm2grid.appspot.com

Figure 8-2 is a view of a version of DSM2 Grid zoomed into the western Delta region. The blue lines are the channel connections, the green labeled circles are the nodes.

8.6.1 Login

Once setup with a login account with Google, simply follow this link [http://dsm2grid.appspot.com/] in your browser (Google Chrome is recommended). Click on the "Sign in" Button, and enter your username and password (Figure 8-3).

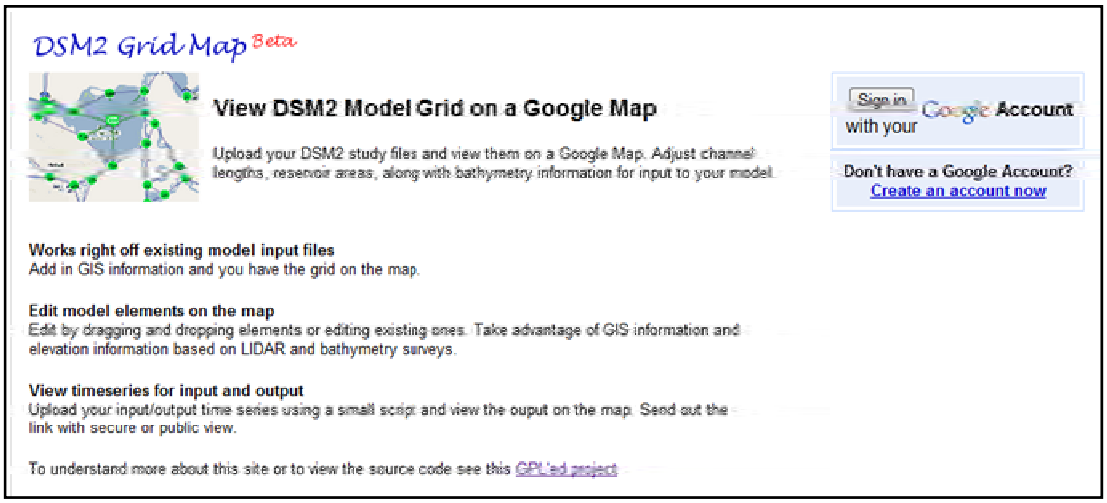

Figure 8-3 Example log in page

Figure 8-4 Example study upload

8.6.2 Upload

To get started with the application, 2 files must be uploaded. A Hydro echo file is needed. This may be generated from a DSM2 setup by running Hydro with the "-e" option, which generates this file in the output folder without running the hydrodynamics.

The second file that is needed is a GIS input file. If a file is not available, the nodes will be placed in a predefined location (south of Sacramento). However, to get started with the Sacramento-San Joaquin Delta, GIS file input file is provided here: http://dsm2-grid-map.googlecode.com/files/gis.inp . This is a preliminary version and should be taken as a draft product.

Once logged in, click on the Studies link and then on the Upload Study tab (Figure 8-4). Enter a name for the study, browse to the Hydro echo file generated from Hydro for the second input, and browse to the GIS input file. Once these fields are specified, click on the upload button.

8.6.3 Viewing the Grid

The grid is displayed as lines for channels: circular green makers for nodes, green square markers for reservoirs, and blue markers for gates (Figure 8-5 and Figure 8-6 on next page).

To navigate to different areas of the map, use either the panning and zooming controls toward the top left; or the mouse drag for panning and mouse wheel for zoom; or the arrow keys for panning and +/- for zoom in/out.

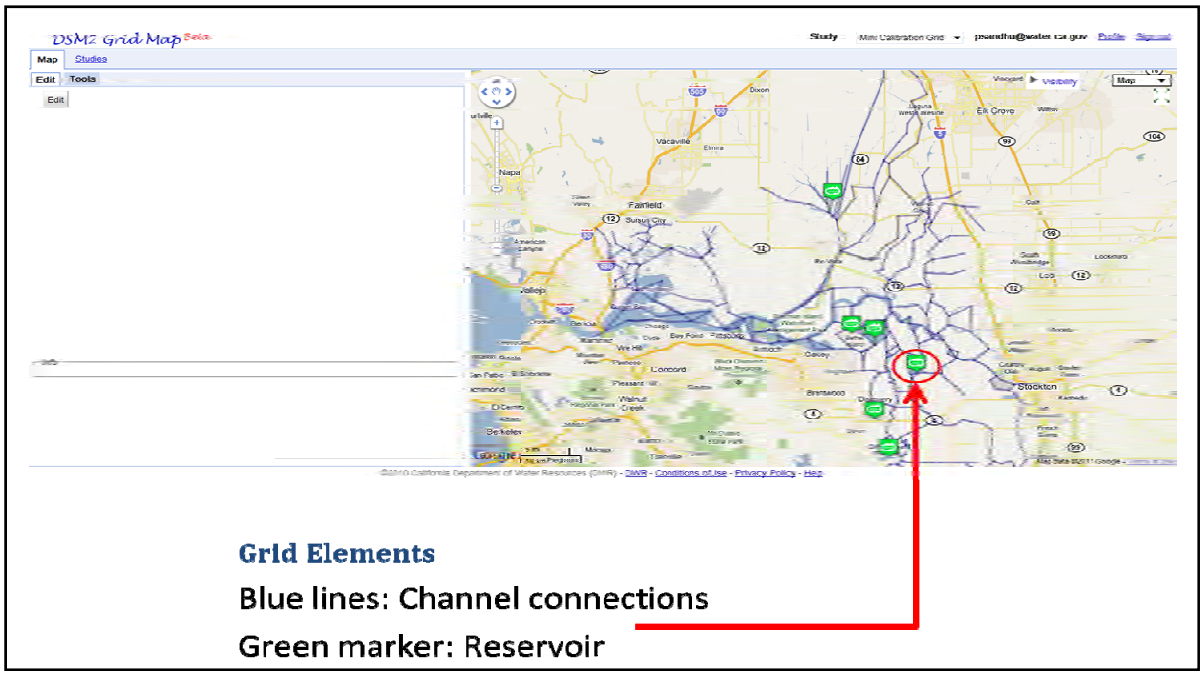

Figure 8-5 Example grid elements: reservoirs

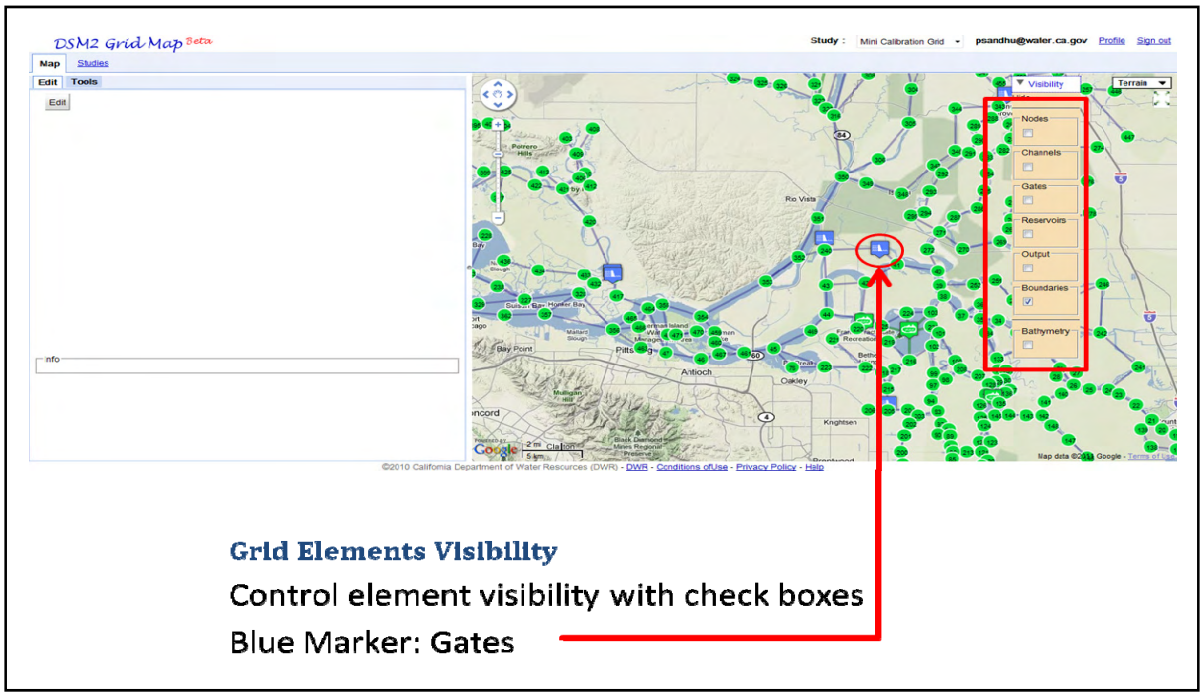

Figure 8-6 Example grid elements: gates

Base maps that form the background can be switched using the control highlighted in Figure 8-7. In addition to the base map from Google, the satellite view, terrain view, and US topographical area are available. Other custom base maps may be added if available and needed in the future.

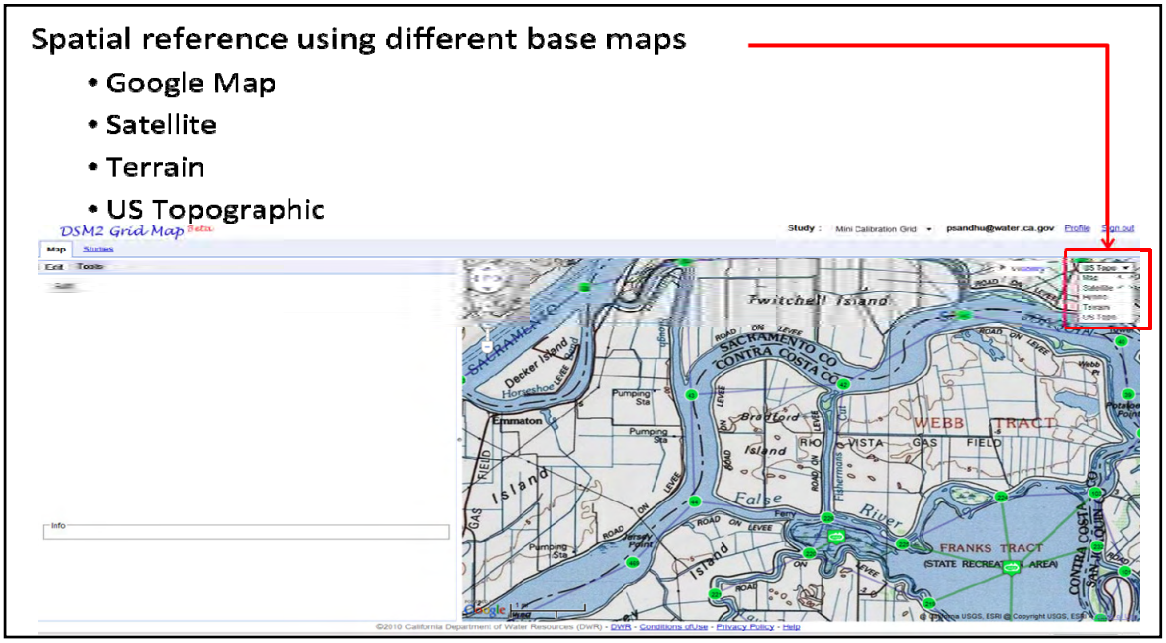

Figure 8-7 Example base maps

8.6.4 Viewing Channel Information

Channels are displayed as straight blue connection lines between nodes. By clicking on a channel connection line, the flow line and cross sections are displayed. The flow line is displayed as a red line, and its length is used to calculate the length of the channel. The cross sections are calculated from DSM2 input where they are represented as elevation vs. area, wetted perimeter, and top width relationships. The direction of the channel is represented in square brackets next to its ID as upstream node → downstream node (Figure 8-8).

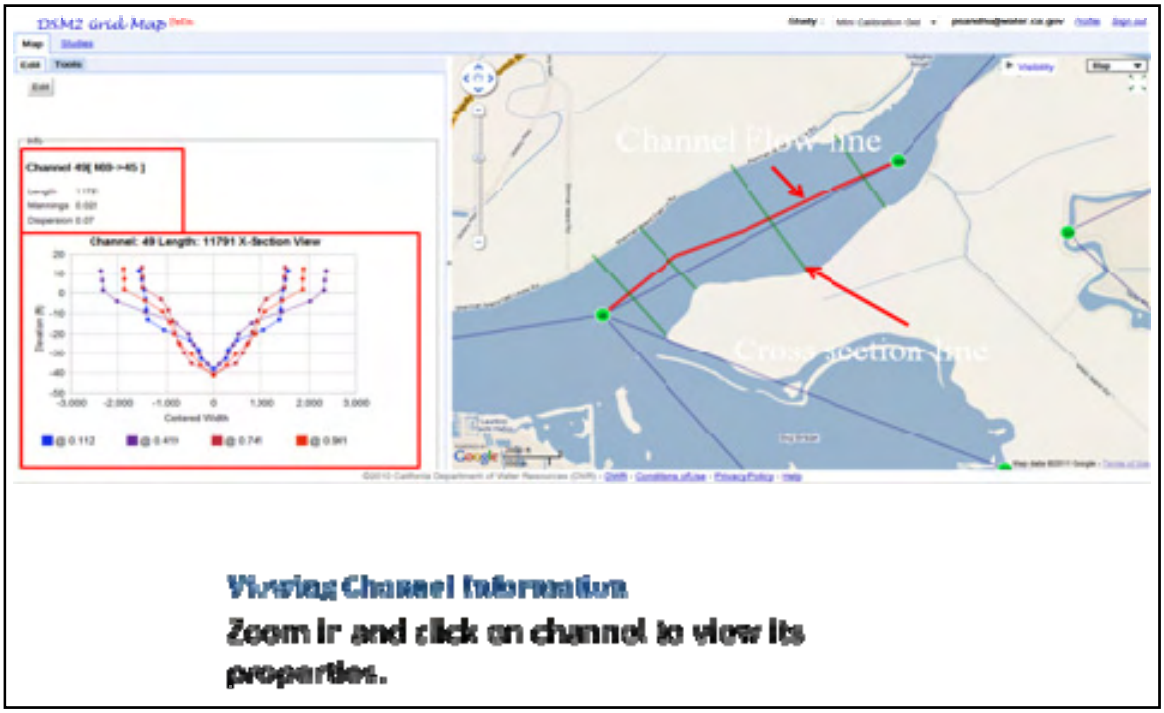

Figure 8-8 Example channel display

8.6.5 GIS Tools

Tools to measure lengths and areas are available under the Tools tab (Figure 8-9). The elevation and elevation profile along a line can also be obtained using the tools highlighted.

The flow lines for all channels can be displayed by clicking the flow line button.

A channel or node can be quickly located by typing its ID into the box and clicking "Find …" button. The map will center at the found element.

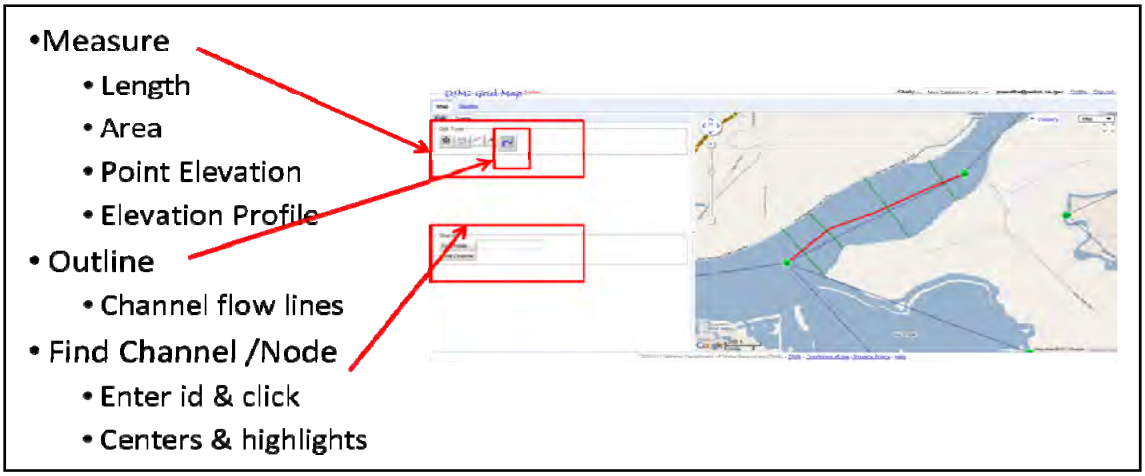

Figure 8-9 GIS tools

8.6.6 Managing Studies

A study is the combination of the Hydro input file and the GIS input file. Studies are given names during the upload process. A management screen allows a user to delete or share the selected studies (Figure 8-10).

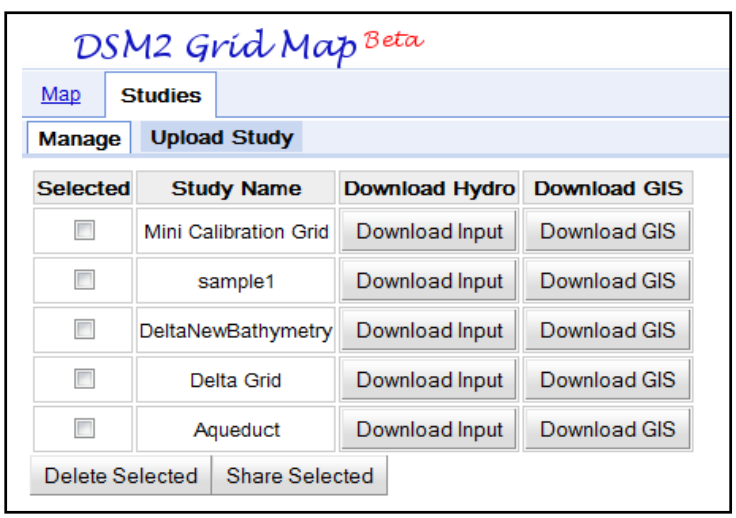

Figure 8-10 Example study inputs

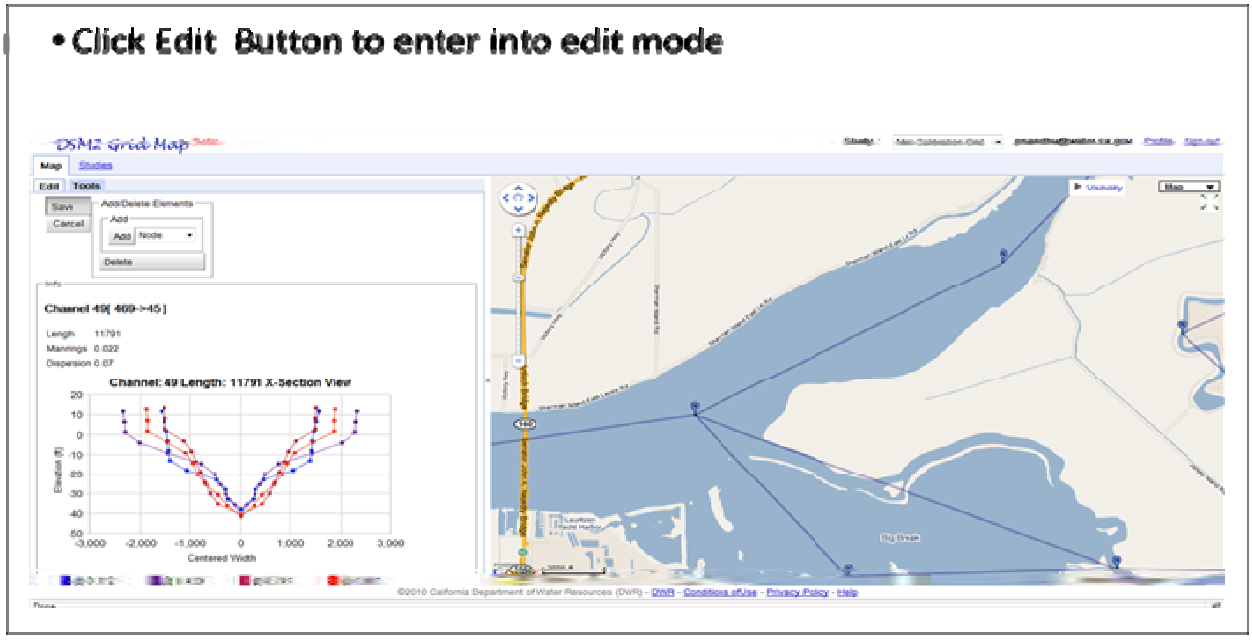

Figure 8-11 Node editing

8.6.7 Editing Mode

Clicking the edit button changes the node representation to blue balloons with an “N” symbol.

8.6.8 Editing Nodes

Hovering over a node highlights the node ID. In this mode the nodes can be dragged and placed at desired location (Figure 8-11).

8.6.9 Editing Channels

Click on channels to display the flow lines as red lines with square dots that can be dragged and placed to change the shape of the flow line (Figure 8-12). Click on the channel connection line (blue line) to display green lines perpendicular to the red flow line. These are the top view representation of channel cross sections. Click on a particular green channel cross section line to display the cross sections profile, the elevation profile from the DEM, and the bathymetry points projected onto the cross section surface from up to 400 feet upstream and downstream of that point (Figure 8-13 and Figure 8-14). Cross sections can be edited by dragging and placing existing profile points or adding new ones (Figure 8-15). These cross sections can be made to conform to the elevation profile by clicking the “Snap to elevation profile” button (Figure 8-16). The channel cross sections can be cleared en-mass and generated at reasonable distances using the “Clear XSections” and “Generate XSections” buttons (Figure 8-17).

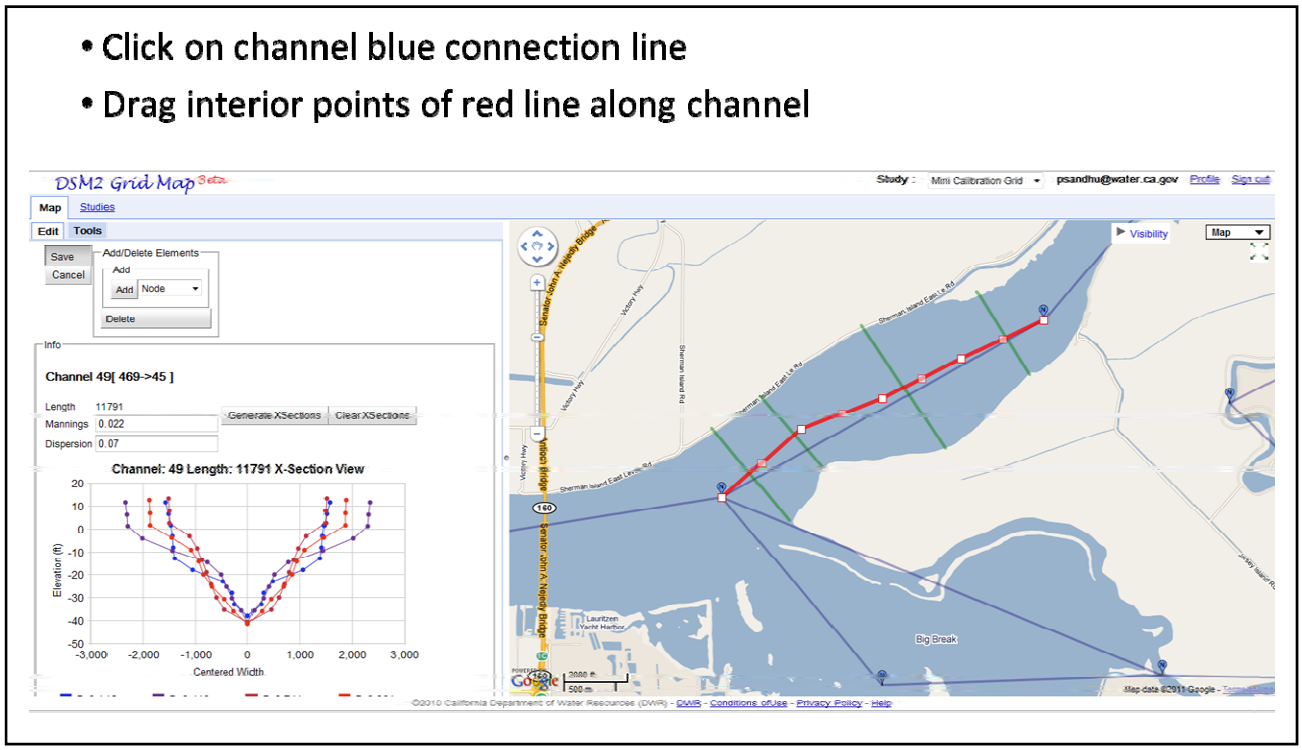

Figure 8-12 Flow line editing

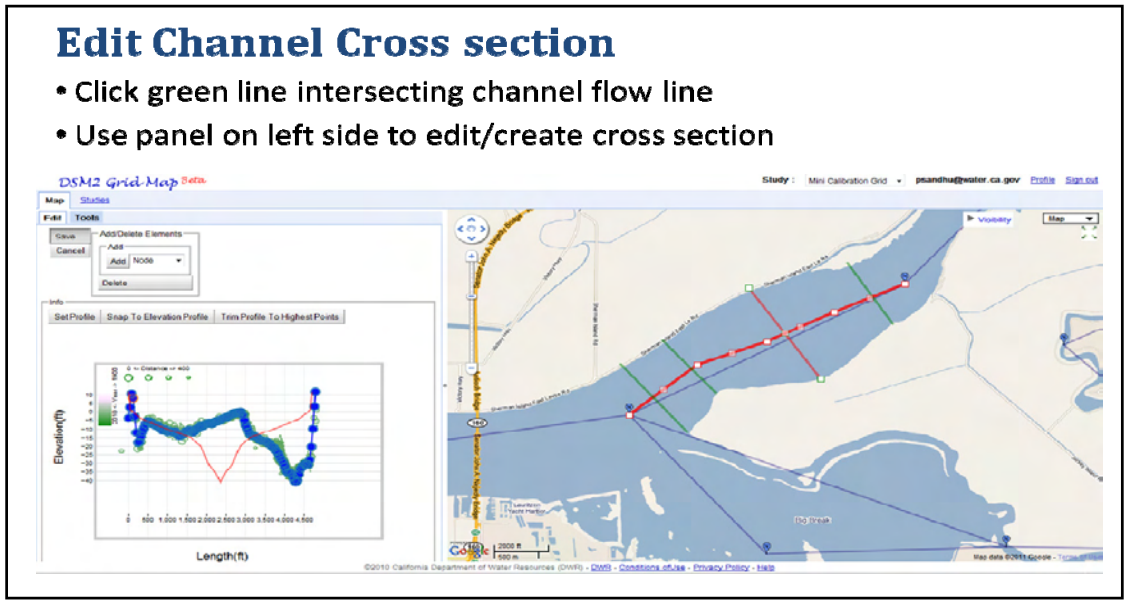

Figure 8-13 Edit Channel Cross section

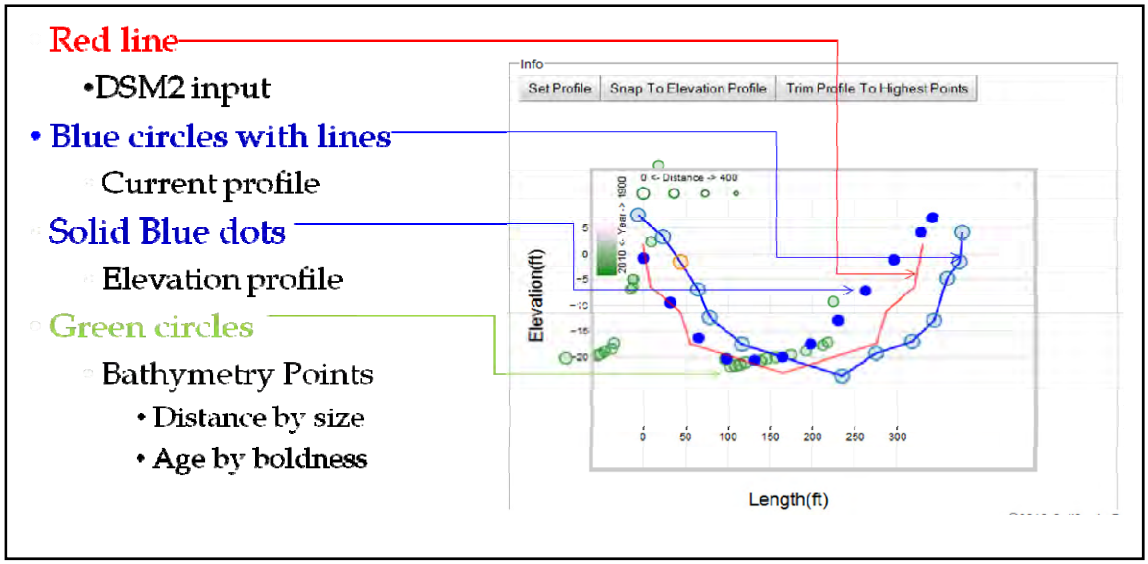

Figure 8-14 Edit Channel Cross section (detail)

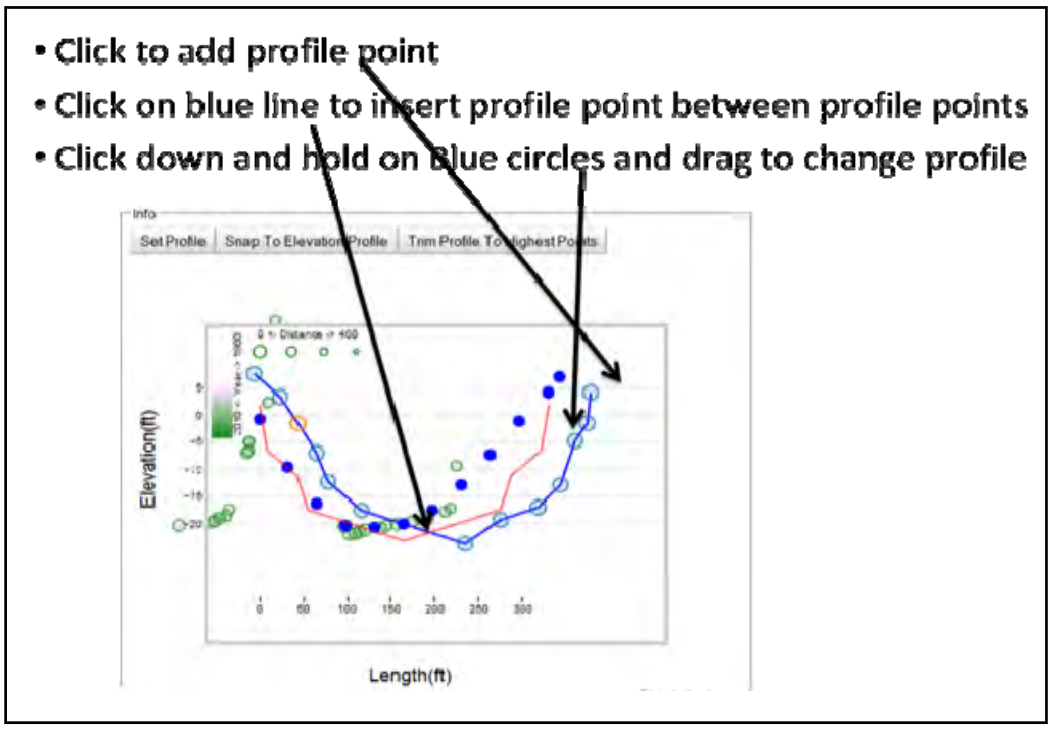

Figure 8-15 Edit Channel Cross section (profile points)

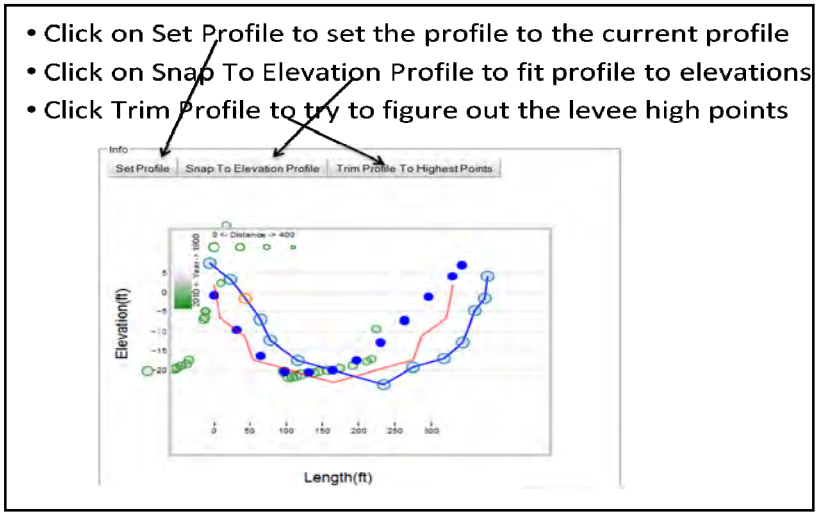

Figure 8-16 Edit Channel Cross section (elevation profile)

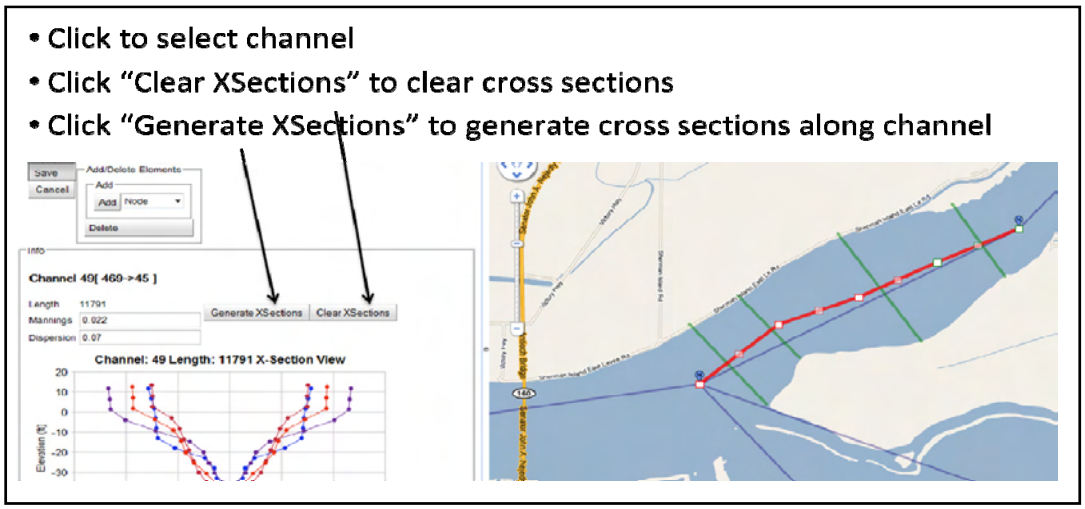

Figure 8-17 Edit Channel Cross section (generate or clear)

8.6.10 Editing Reservoirs

Reservoirs are represented as green markers. Click these in the edit mode to highlight the area as a blue-filled region. The outline of this region has square dots that can be dragged and placed to define the area (Figure 8-18). The "Recalculate Bottom Elevation" button uses the DEM data to calculate the average bottom elevation for the area defined and update the bottom elevation of that reservoir.

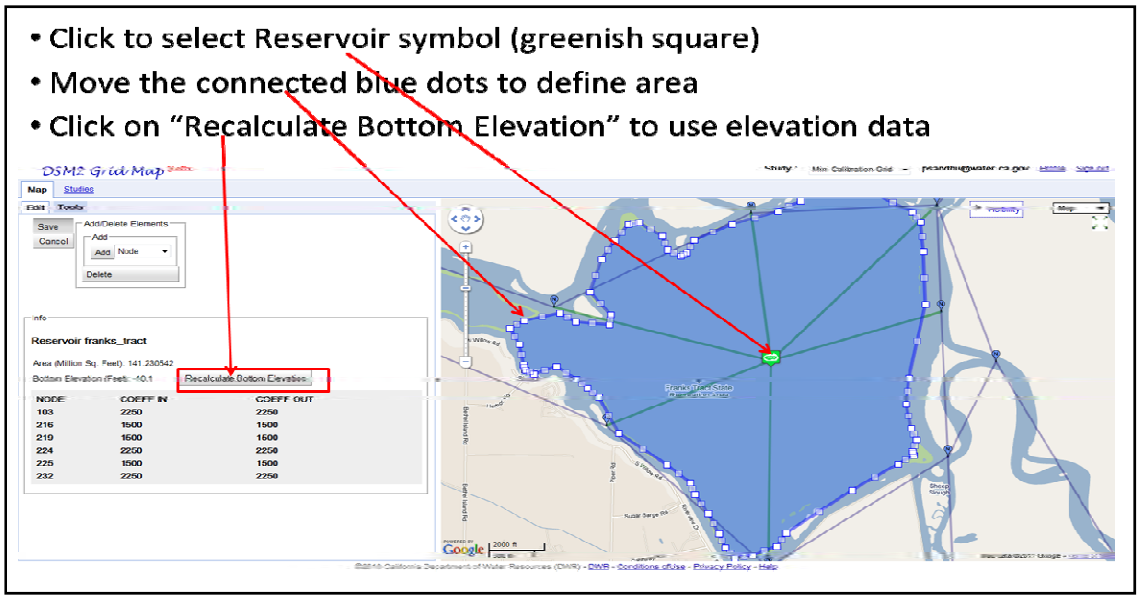

Figure 8-18 Editing reservoirs

8.6.11 Editing Gates

Gates are blue markers. Their locations can be edited by moving them to the desired location of the gate. GIS data for the gate location are not a direct input to the hydrodynamics. The gates can be defined at node locations only; the user should match as closely as possible the node at which the gate is defined.

8.7 Conclusion

GIS has evolved to a level where a direct integration is possible between derived model inputs and the original GIS data. This is a needed step in understanding how physical features are represented in the model.

This approach also highlights how far the Web browser has come and can now be used as a GIS application leveraging Google Maps. It also highlights the advantages of such an approach, e.g., support for multiple platforms, no software downloads, and doing away with bulk data downloads needed to support GIS activities. This allows easier access to information by the public and non-GIS personnel.

However, this tool is not a replacement for general purpose GIS applications such as ArcGIS. In fact, it is complementary to those applications and needs the capabilities provided in such tools.

We are currently evaluating how to integrate the features provided here with ArcGIS.

8.8 References

DWR, Delta Modeling Section. "19th Annual Progress Report to the State Water Resources Control Board, Chapter 6." *California Dept. of Water Resources.* June 1998. http://modeling.water.ca.gov/delta/reports/annrpt/1998/1998Ch6.pdf (accessed April 2011).

DWR, Delta Modeling Section. "32nd Annual Progress Report to the State Resources Control Board." Delta Modeling Section, 2011.

MTL. *Calculate distance, bearing and more between Latitude/Longitude points.* http://www.movable-type.co.uk/scripts/latlong.html#ellipsoid.

Methodology for Flow and Salinity Estimates in the Sacramento-San Joaquin Delta and Suisun Marsh

32nd Annual Progress Report
June 2011

Chapter 9
DOC Validation with DSM2

Authors: Siqing Liu and Robert Suits,
Delta Modeling Section,
Bay-Delta Office,
California Department of Water Resources,
and
Marcia Scavone-Tansey,
Division of Environmental Services,
California Department of Water Resources

Contents

9 DOC Validation with DSM2 9-1
9.1 Summary 9-1
9.2 Background 9-1
9.3 Study Methodology 9-1
9.4 Study Results 9-8
9.5 Conclusions 9-8
9.6 References 9-9

Figures

Figure 9-1 Assumed DOC for Delta inflows for simulation of historical conditions 9-3
Figure 9-2 DOC assumed for agricultural drainage by Delta region 9-5
Figure 9-3 Example of daily range and daily average DOC in DSM2-simulated conditions 9-6
Figure 9-4 Locations DSM2-simulated daily DOC compared to measured DOC 9-7
Figure 9-5 DSM2-simulated daily DOC and measured DOC, July 1990–1994 9-10
Figure 9-6 DSM2-simulated daily DOC and measured DOC, 1995–1998 9-18
Figure 9-7 DSM2-simulated daily DOC and measured DOC, 1999–2002 9-20
Figure 9-8 DSM2-simulated daily DOC and measured DOC, 2003–2006 9-22
Figure 9-9 DSM2-simulated daily DOC and measured DOC, 2007–2010 9-24
Figure 9-10 DSM2-simulated daily DOC fingerprint and measured DOC, 1991–1994 9-26

9 DOC Validation with DSM2

9.1 Summary

Using the Delta Simulation Model II (DSM2), historical Delta dissolved organic carbon (DOC) was simulated over the period 1990 through 2010 and compared to available measured data. DOC fingerprints were generated at several locations to evaluate how contributions of various sources of DOC in the Delta vary by location.

9.2 Background

DWR's Delta Modeling Section is a participant in the Real Time Data Forecasting group (RTDF), a technical subcommittee of the Municipal Water Quality Investigations Program (MWQI). One of the key goals of RTDF is to develop the capability to produce short-term forecasts of Delta DOC. Aligned with this goal is the documentation of current DSM2 capability for reproducing historically observed DOC throughout the Delta. This task was identified as a deliverable in the 2009-2010 RTDF Work Plan (California Department of Water Resources, Municipal Water Quality Investigations Program 2009). A comparison of DSM2–simulated and measured DOC for the period of 1991 through 1997 was documented earlier (Pandey 2001). Since that analysis, 13 years of measured DOC data have been collected, including periods of continual monitoring in the Sacramento River at Hood, in the San Joaquin River at Vernalis, and at Banks Pumping Plant. In addition, simulated fingerprinting of sources of water quality constituents has become a helpful way of understanding model performance. This chapter summarizes the methods and results from an expanded DSM2 simulation of historical Delta DOC.

9.3 Study Methodology

Delta hydrodynamics for the period of 1990 through 2010 were simulated using the DSM2 hydrodynamic module (DSM2-HYDRO). The source for stage and flow data was the California Data Exchange Center (CDEC). The agriculture withdrawals and drainage flows were calculated by the Delta Island Consumptive Use Model (DICU), documented previously by DWR (1995). Several gates are installed and operated each year in the Delta. The simulation of these structures followed the documentation provided by the Interagency Ecological Program DSM2 Project Work Team is available at http://www.water.ca.gov/dsm2pwt/data.

After historical Delta hydrodynamics were simulated, Delta DOC was simulated by assuming that DOC in the Delta behaved as a conservative constituent. Boundary DOC for Delta inflows and for the downstream boundary at Martinez was developed by MWQI using available grab sample and continuously monitored data. Figure 9-1 presents the DOC values for the Delta inflows; the downstream boundary at Martinez was assumed to have a constant value of 2 mg/L.

DOC concentrations in agricultural drainage were based upon a study by Marvin Jung and Associates (2000), which assigned monthly DOC according to island location with respect to 3 Delta regions. These regions and the DOC values assumed in agricultural drainage are shown in Figure 9-2.

DSM2-simulated DOC is presented at every location that had observed DOC data. While grab samples were taken at a specific time on a given day, the grab sample results were plotted along with DSM2-simulated daily average DOC. One reason for this approach is that DSM2 water quality module (DSM2-QUAL) was calibrated to daily average electrical conductivity (EC); hourly variations in simulated EC or DOC are not typically shown. A second reason is that simulated DOC in the Delta tends to have a modest

tidal variation. Figure 9-3 shows the DSM2-simulated daily range for 15-minute DOC at Clifton Court Forebay, Old River at Bacon Island, and Jersey Point for 1991-1993. The daily range in simulated DOC varies by location, but is usually small compared to the daily average DOC. Over the 1991-2010 period, the daily range in simulated DOC at Clifton Court Forebay, Old River at Bacon Island, and Jersey Point DOC is 0.1 mg/L, 0.3 mg/L, and 0.2 mg/L, respectively.

The availability of measured DOC in the Delta from grab samples is extensive for the period 1990—1994 but much less for later periods. Continuous DOC is available at Banks Pumping Plant starting December 22, 2001; in the Sacramento River at Hood, starting February 22, 2003; and for the San Joaquin River at Vernalis, starting March 28, 2005. Figure 9-4 shows the locations where DSM2-simulated daily DOC is compared to measured DOC for the 1991-1994 period. Measured data are available at fewer locations for subsequent 4-year intervals.

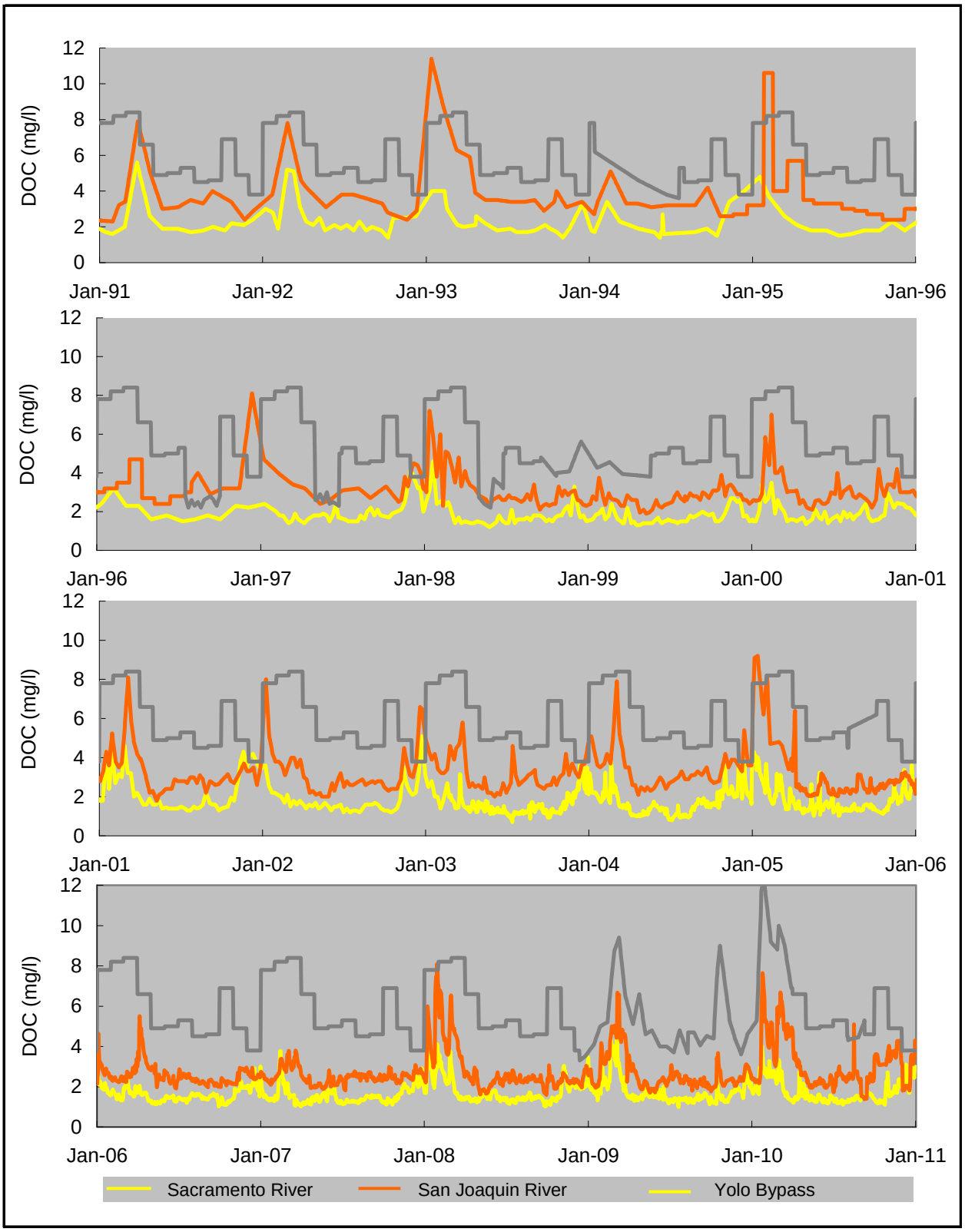

Figure 9-1 Assumed DOC for Delta inflows for simulation of historical conditions

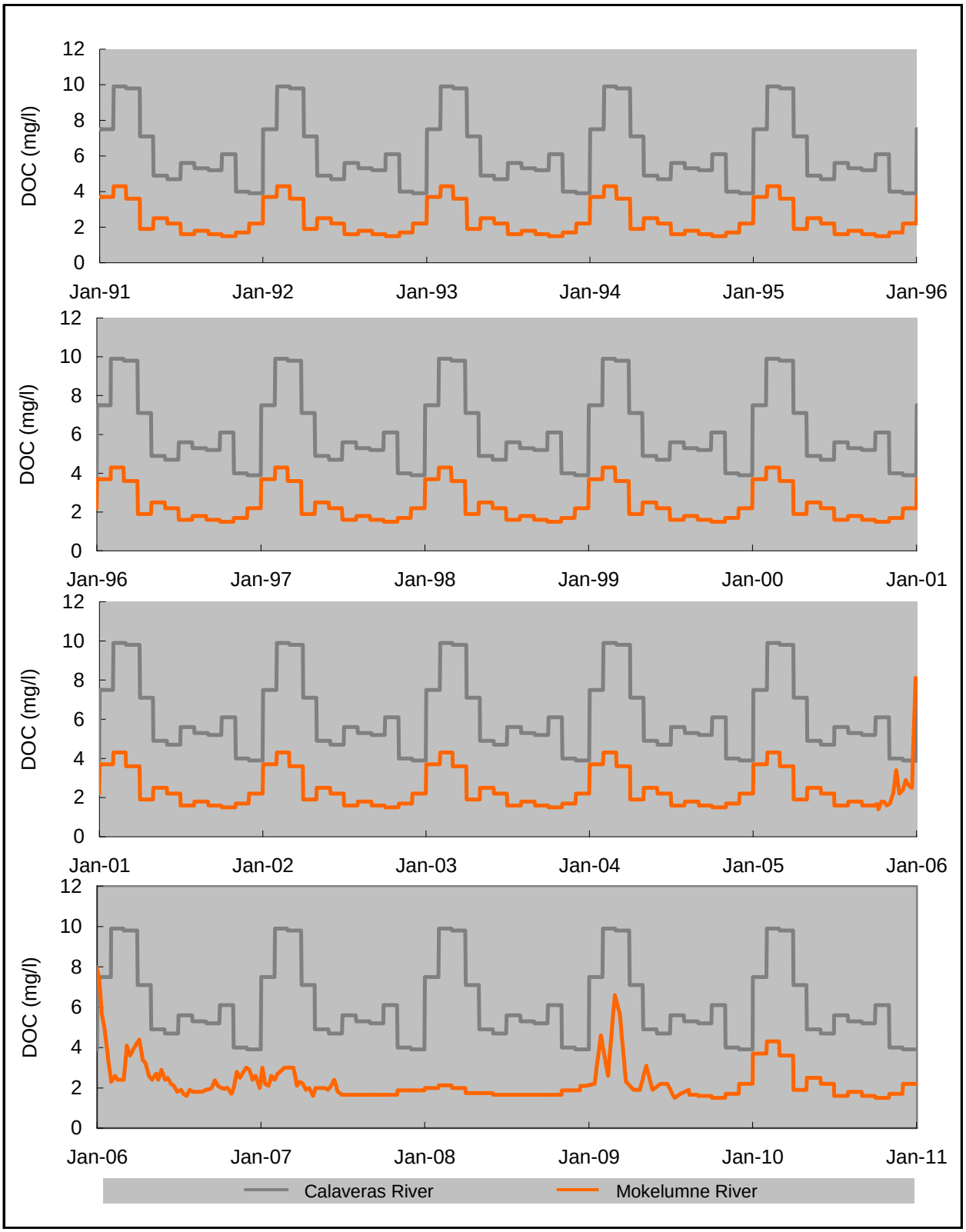

Figure 9-1 (cont.) Assumed DOC for Delta inflows for simulation of historical conditions

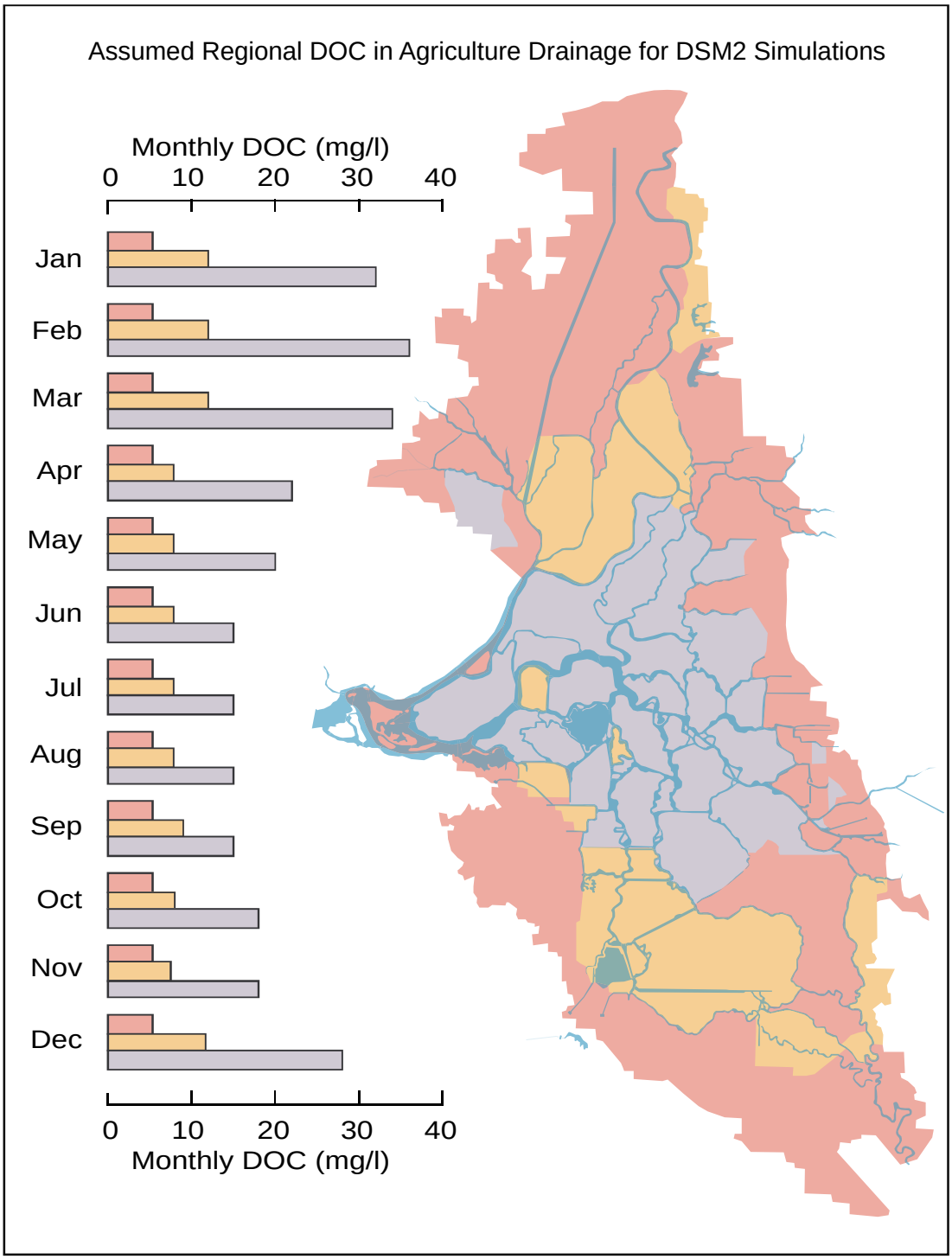

Figure 9-2 DOC assumed for agricultural drainage by Delta region

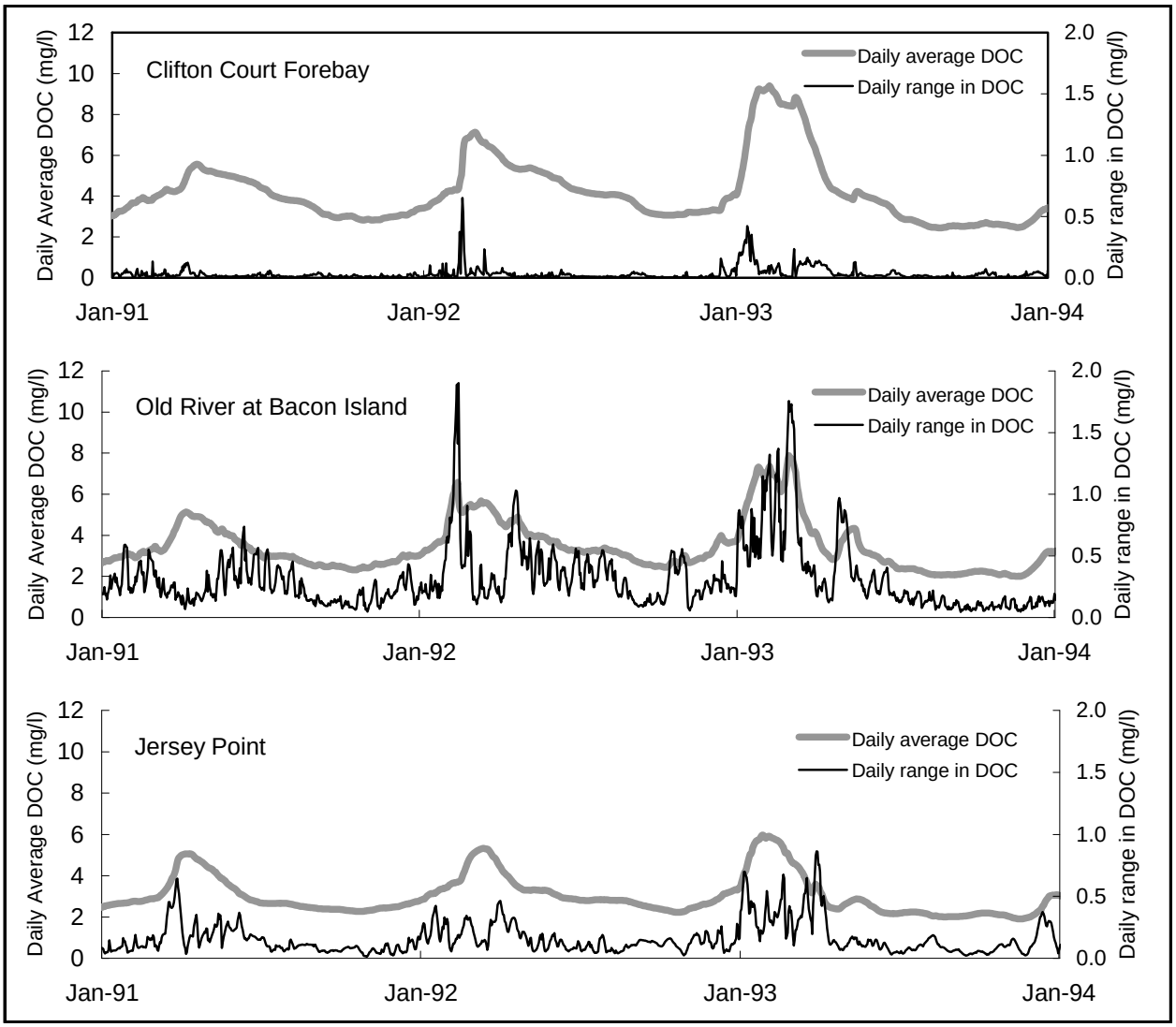

Figure 9-3 Example of daily range and daily average DOC in DSM2-simulated conditions

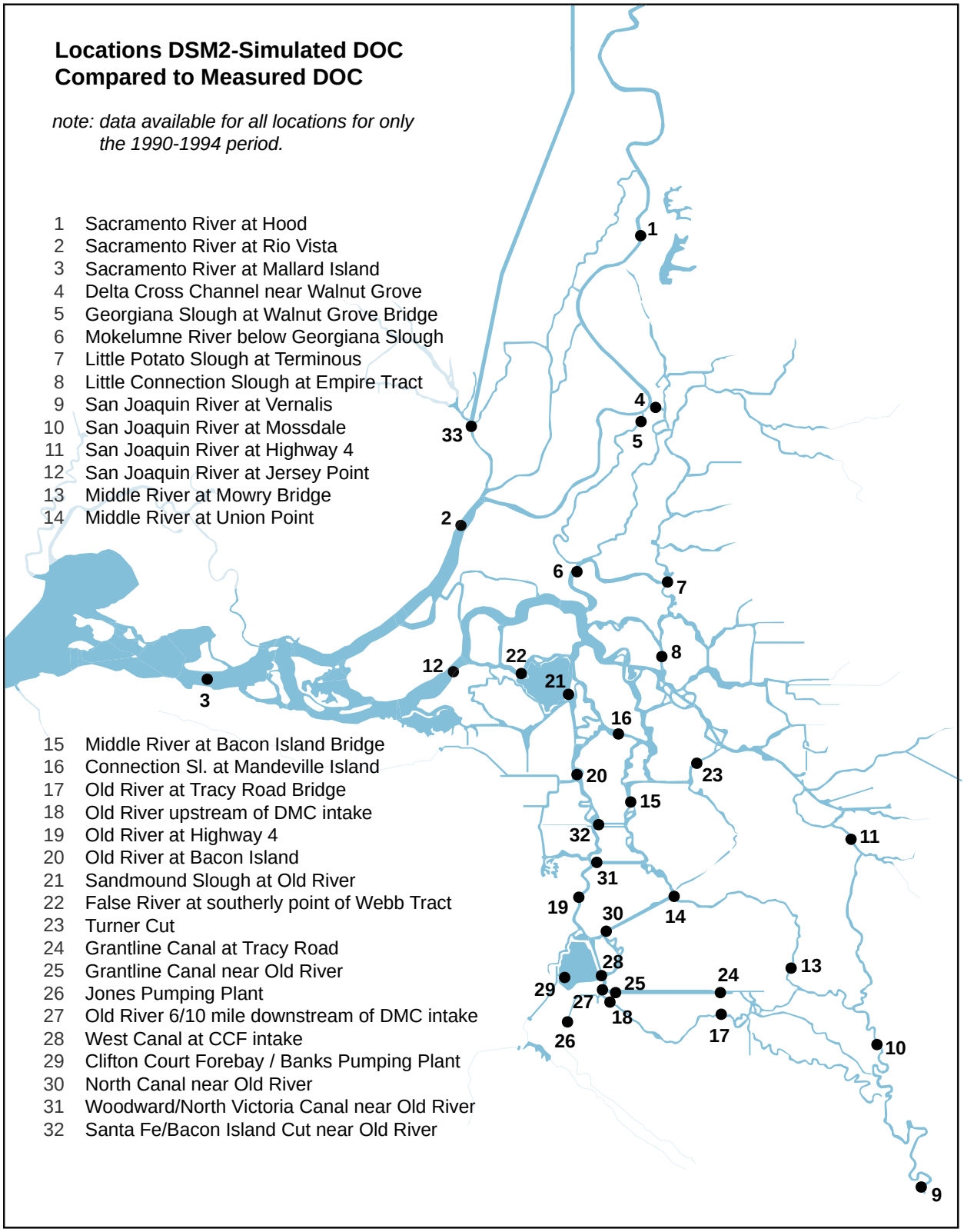

Figure 9-4 Locations DSM2-simulated daily DOC compared to measured DOC

9.4 Study Results

Comparison of simulated and measured DOC is separated into 5 time periods to facilitate analysis considering the varying availability of measured data. These periods are June 1990-1994, 1995-1998, 1999-2002, 2003-2006, and 2007-2010, with results presented in Figure 9-5 through Figure 9-9[1]. These figures also show the DSM2 input boundary DOC at Sacramento River at Hood and San Joaquin River at Vernalis along with the grab sample or continuous DOC to show how the boundary time series was developed at these 2 locations.

The DSM2 simulation of historical Delta DOC conditions reproduces measured DOC well. The timing and magnitude of yearly peak DOC in the winter was successfully reproduced by DSM2 throughout the Delta during the July 1990 through 1994 period. The continued good performance in subsequent years at the locations measured DOC was available (Banks Pumping Plant, Jones Pumping Plant, Old River at Bacon Island, Old River at Highway 4) indicates that the simulated DOC Delta wide was likely accurate as well.

In contrast to a DSM2 simulation of Delta EC, successful simulation of Delta DOC is not as sensitive to accurate modeling of sea water intrusion because the major sources of DOC in the Delta are the Sacramento and San Joaquin Rivers and in-Delta island discharges. Fingerprints of DOC can be generated to explain relative sources of DOC at any location in the Delta at a specific time. This practice is routinely performed in monthly updates of DSM2 simulations of historical conditions for the Real Time Data Forecasting group (RTDF). Past results can be accessed at MWQI's RTDF website at http://www.water.ca.gov/waterquality/drinkingwater/rtdf_rprt.cfm

In Figure 9-10, DOC fingerprint results are shown for 1991 through 1994 at 6 locations: Clifton Court Forebay, Jones Pumping Plant, Middle River at Union Point, Old River at Tracy Road, Old River at Bacon Island, and San Joaquin River at Jersey Point (see Figure 9-4 for these locations).

The DOC fingerprints show significant contribution to yearly winter peak DOC periods in the south Delta by the San Joaquin River inflow and drainage from Delta islands. Considering how well the simulated DOC tracked the measured DOC in the south Delta, Figure 9-10 indicates that the simulated island drainage is adequate for generating meaningful results. Figure 9-10 also shows that summertime island drainage is a significant contributor to DOC in Old River at Tracy Road. Moving downstream to Old River at Bacon Island and at San Joaquin River at Jersey Point, Figure 9-10 as expected shows in-Delta drainage contributing less to the overall DOC. At Old River at Bacon Island and Jersey Point, both the Sacramento River inflow and the San Joaquin River inflow are important for producing the annual peak DOC values.

9.5 Conclusions

The simulation of historical Delta DOC conditions with DSM2 provides meaningful results. Significant errors at times observed in DSM2 simulation of historical Delta EC conditions do not translate into significant DOC errors. The annual pattern of rising DOC in the winter time is reproduced in the DSM2 simulation. The DOC simulation indicates that the significant sources of DOC for the yearly peak period depend upon the location in the Delta: Delta island drainage and San Joaquin River inflow in the south Delta; and Sacramento River and San Joaquin River inflow in the central and west Delta.

---

[1] Figures 9-5 through 9-10 are placed in the final pages of this chapter.

9.6 References

California Department of Water Resources, Division of Planning. "Estimation of Delta Island Diversions and Return Flows." Division Report, State of California, Department of Water Resources, Sacramento, CA., 1995.

California Department of Water Resources, Municipal Water Quality Investigations Program. *Municipal Water Quality Investigations Program 2009-2010 Workplan.* 2009. http://www.water.ca.gov/waterquality/drinkingwater/workplans.cfm (accessed March 2011).

Jung, Marvin. "Revision of Representative Delta Island Return Flow Quality for DSM2 and DICU Model Runs." Prepared under DWR contract by Marvin Jung and Associates, Inc., CALFED Ad-Hoc Workgroup to Simulate Historical Water Quality Conditions in the Delta, 2000.

Pandey, G. "Chapter 3: Simulation of Historical DOC and UVA Conditions in the Delta." *Methodology for Flow and Salinity Estimates in the Sacramento-San Joaquin Delta and Suisun Marsh. 22nd Annual Progress Report from the California Department of Water Resources to the State Water Resources Control Board*, 2001.

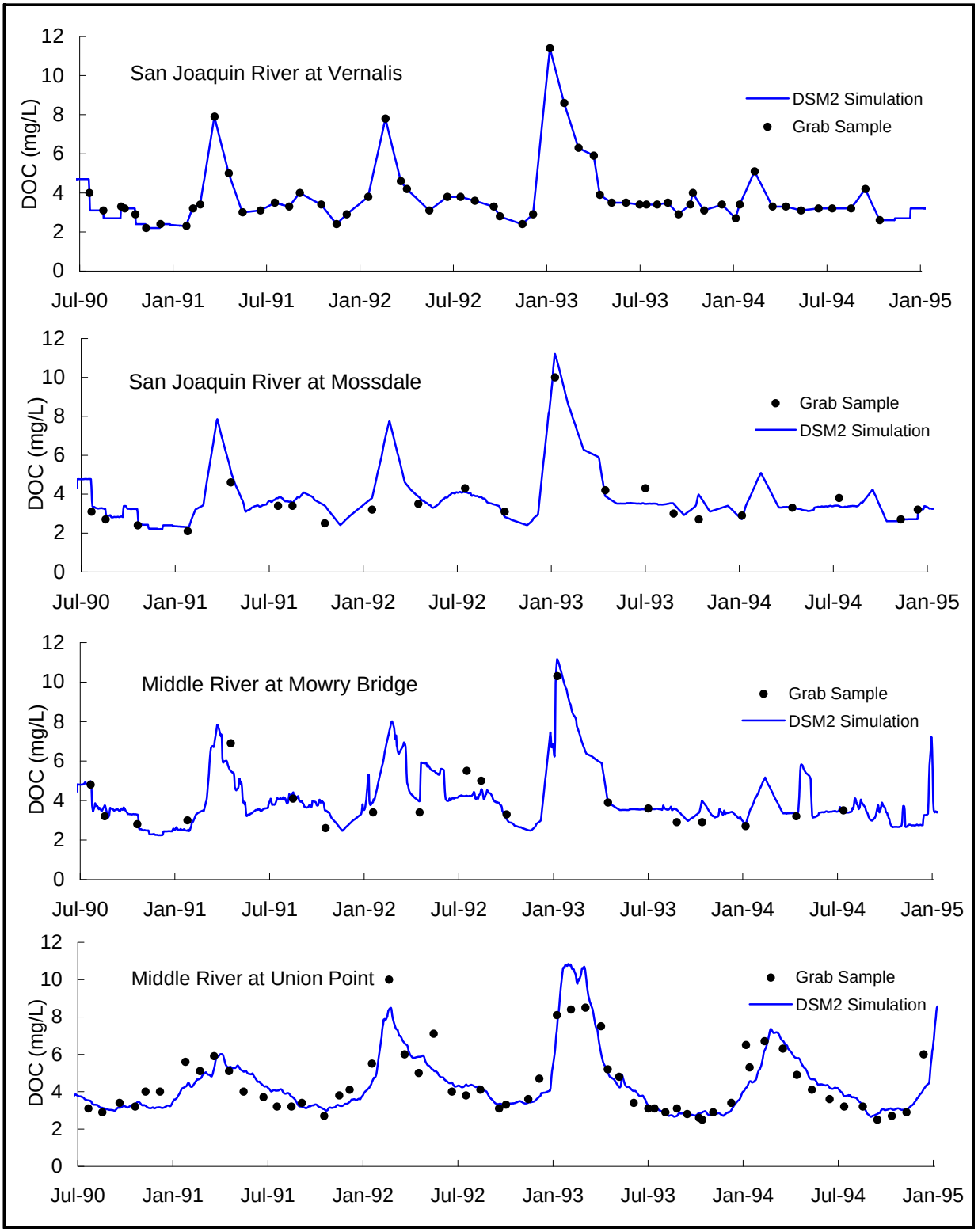

Figure 9-5 DSM2-simulated daily DOC and measured DOC, July 1990–1994

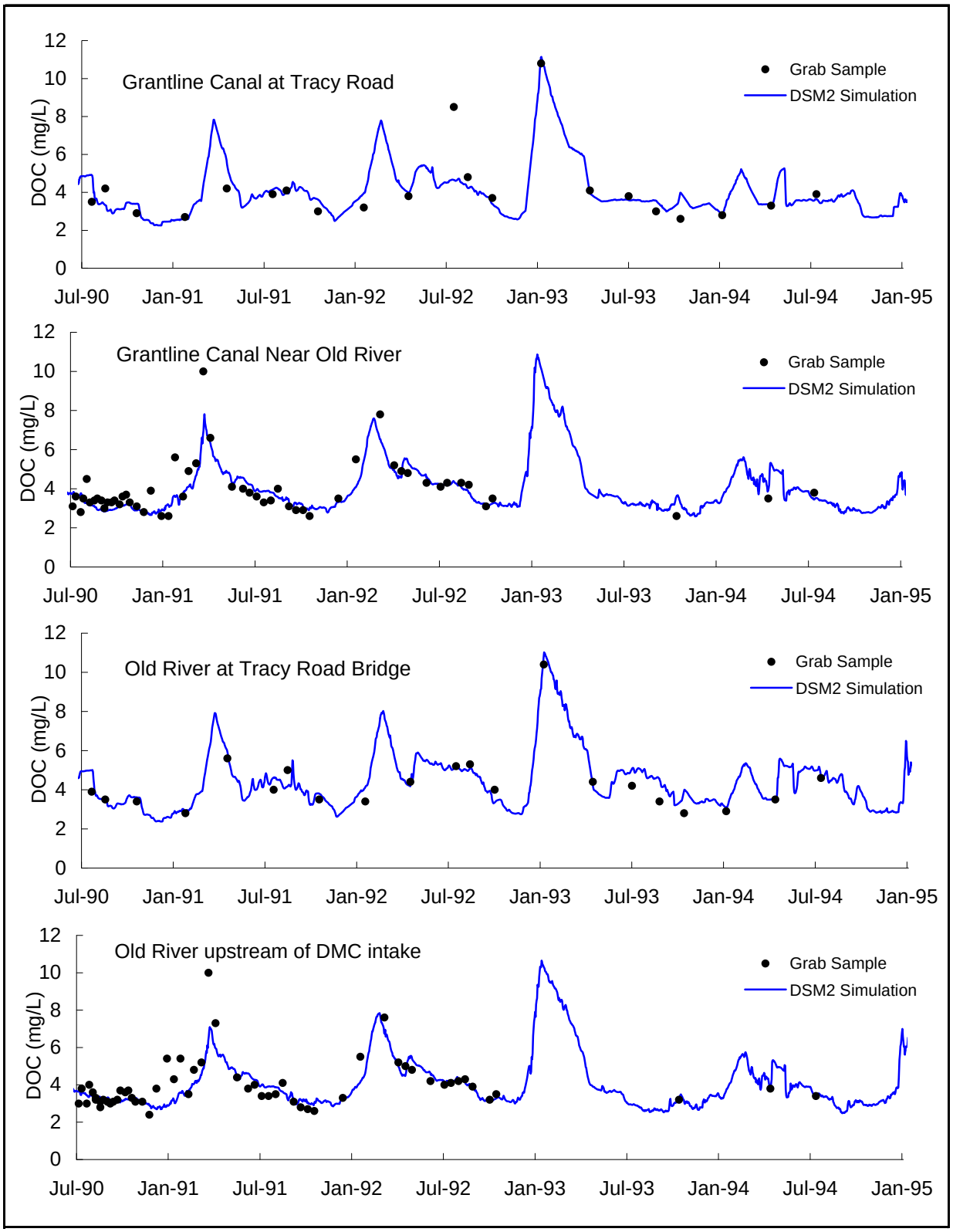

Figure 9-5 (cont.) DSM2-simulated daily DOC and measured DOC, July 1990–1994

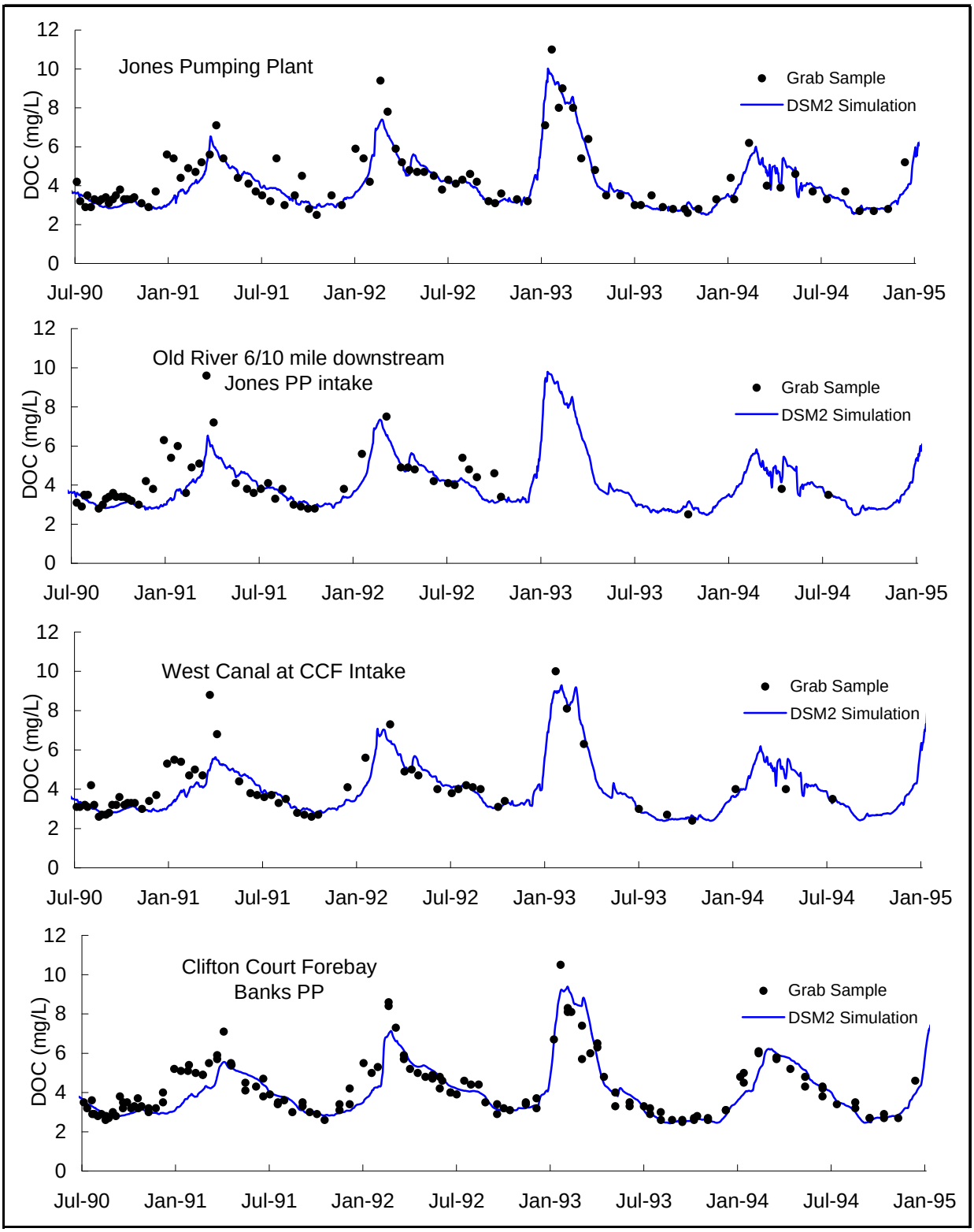

Figure 9-5 (cont.) DSM2-simulated daily DOC and measured DOC, July 1990–1994

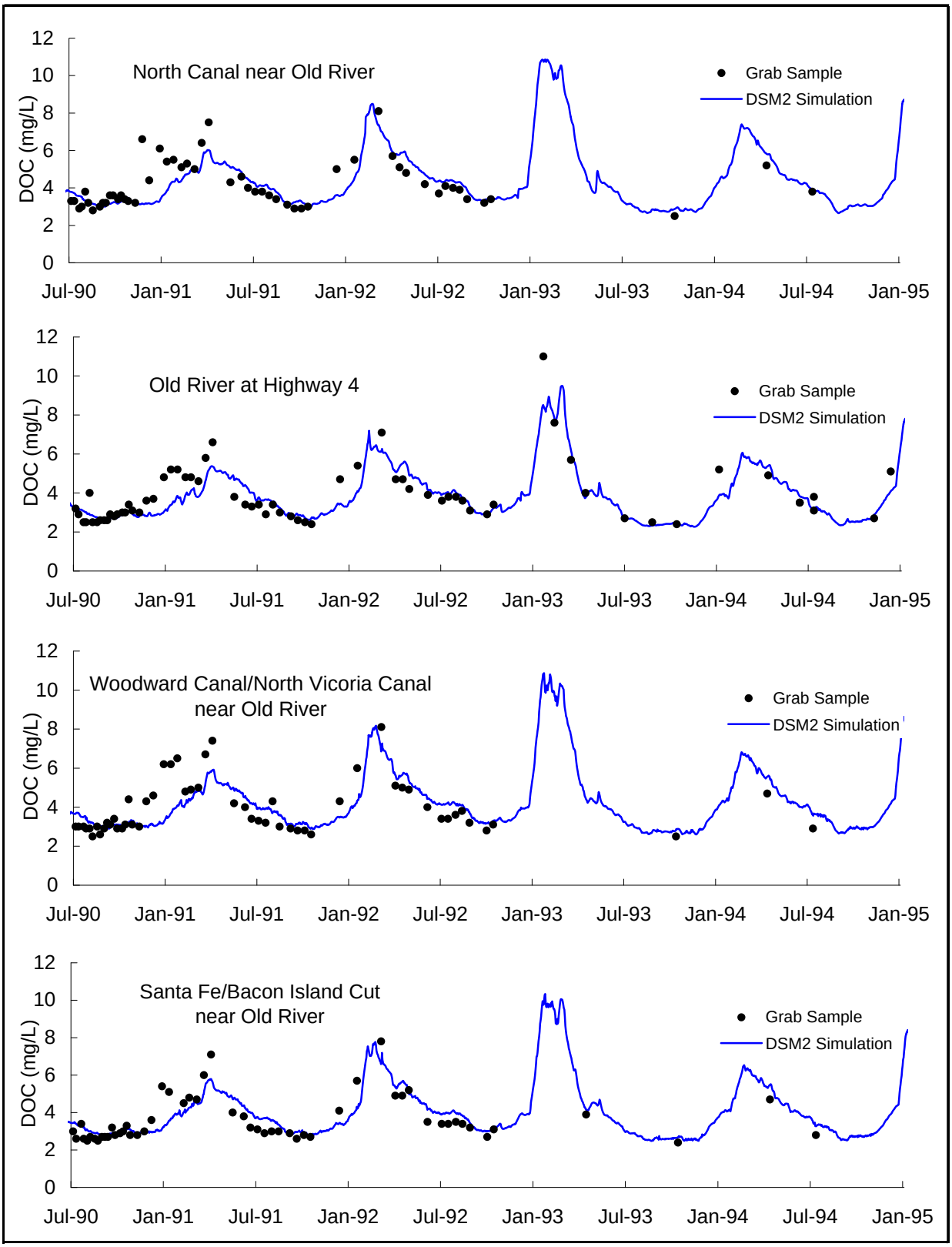

Figure 9-5 (cont.) DSM2-simulated daily DOC and measured DOC, July 1990–1994

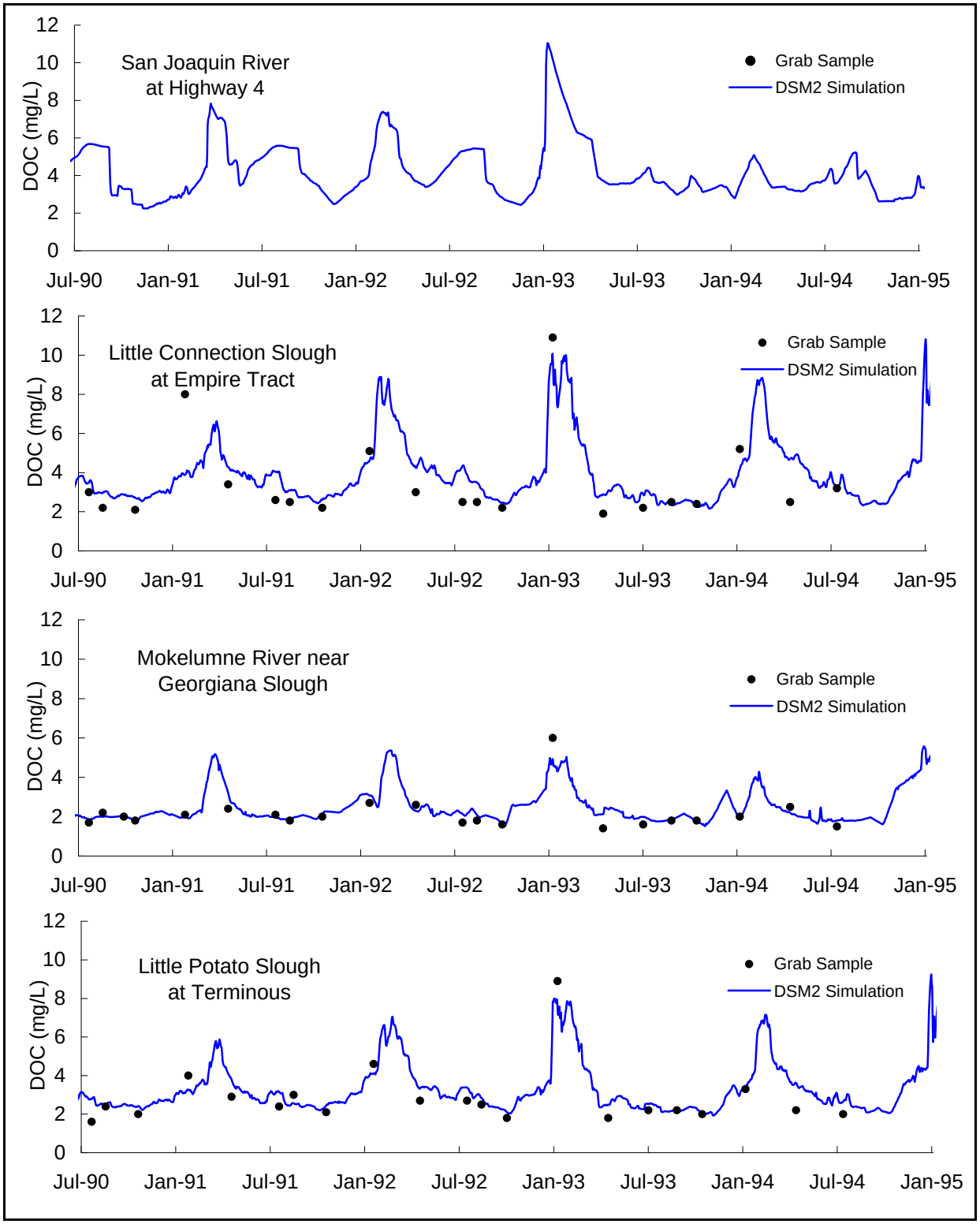

Figure 9-5 (cont.) DSM2-simulated daily DOC and measured DOC, July 1990–1994

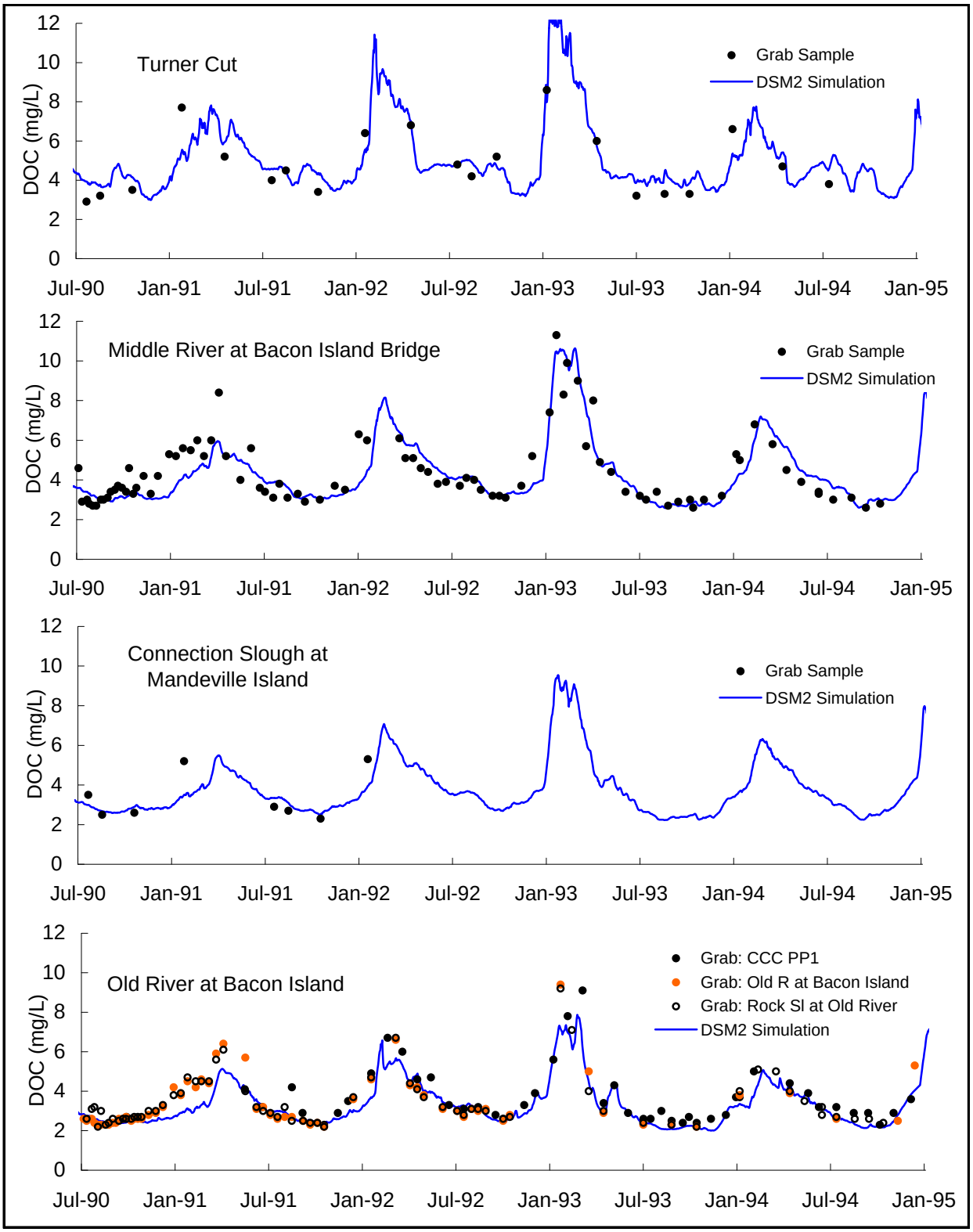

Figure 9-5 (cont.) DSM2-simulated daily DOC and measured DOC, July 1990–1994

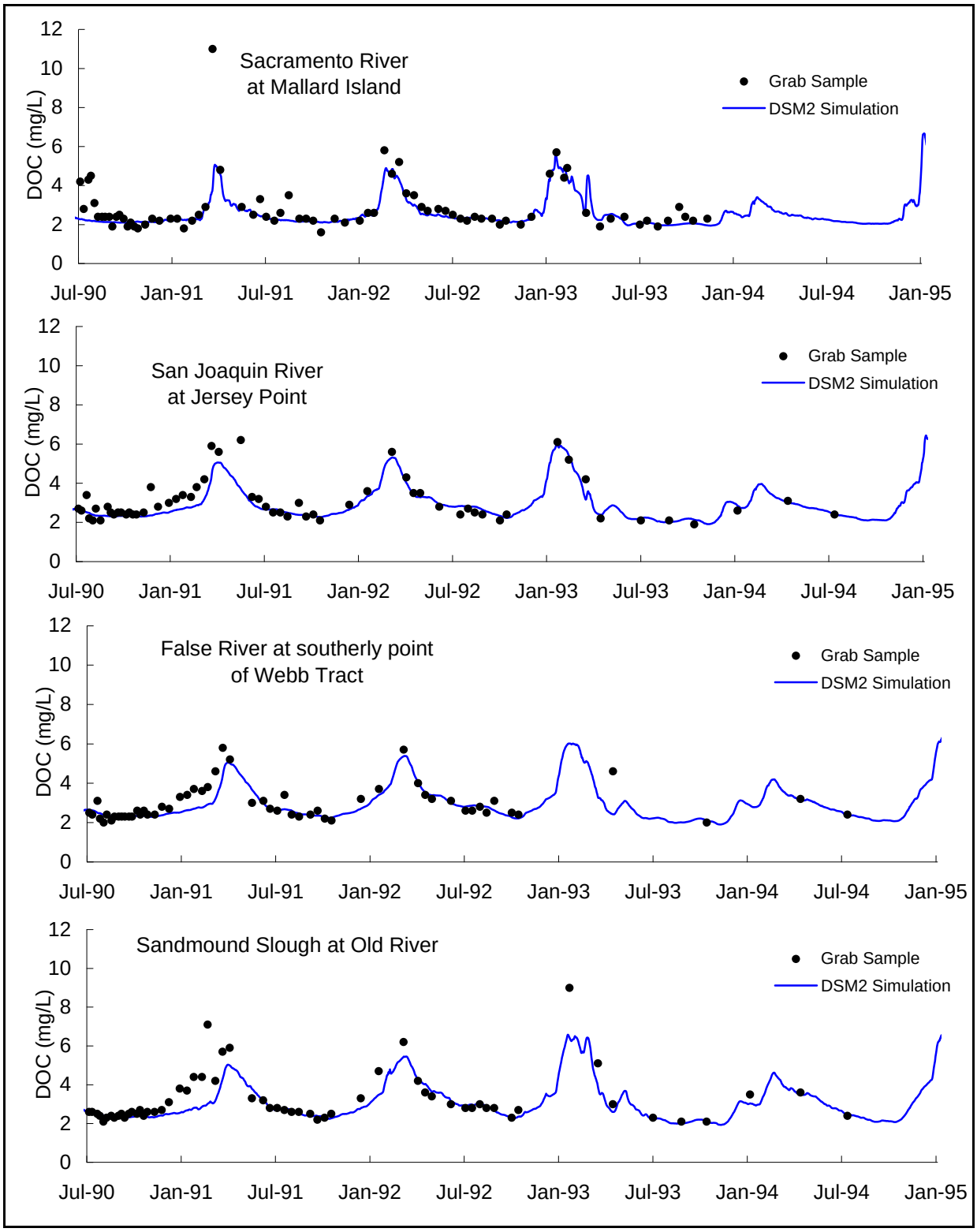

Figure 9-5 (cont.) DSM2-simulated daily DOC and measured DOC, July 1990–1994

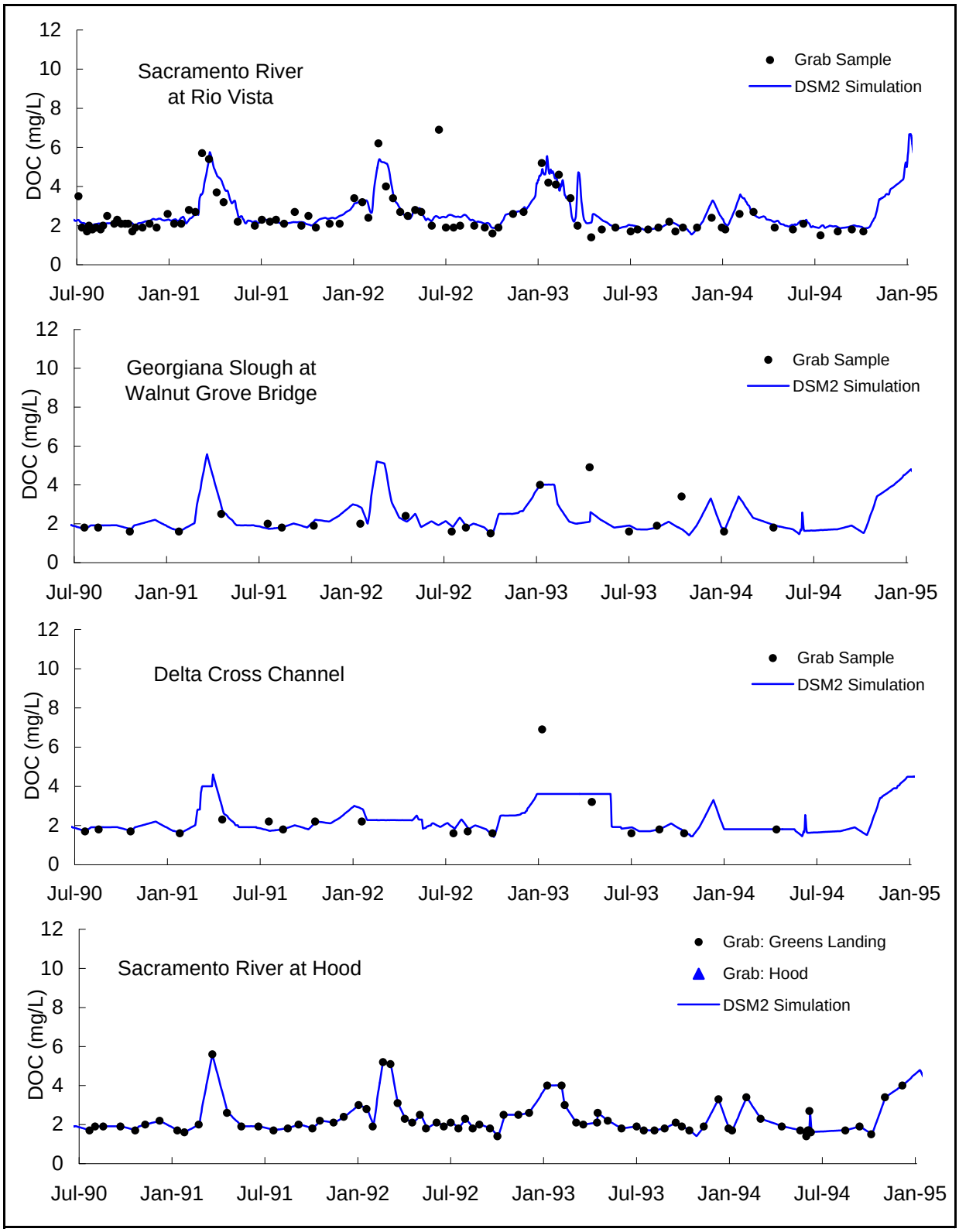

Figure 9-5 (cont.) DSM2-simulated daily DOC and measured DOC, July 1990–1994

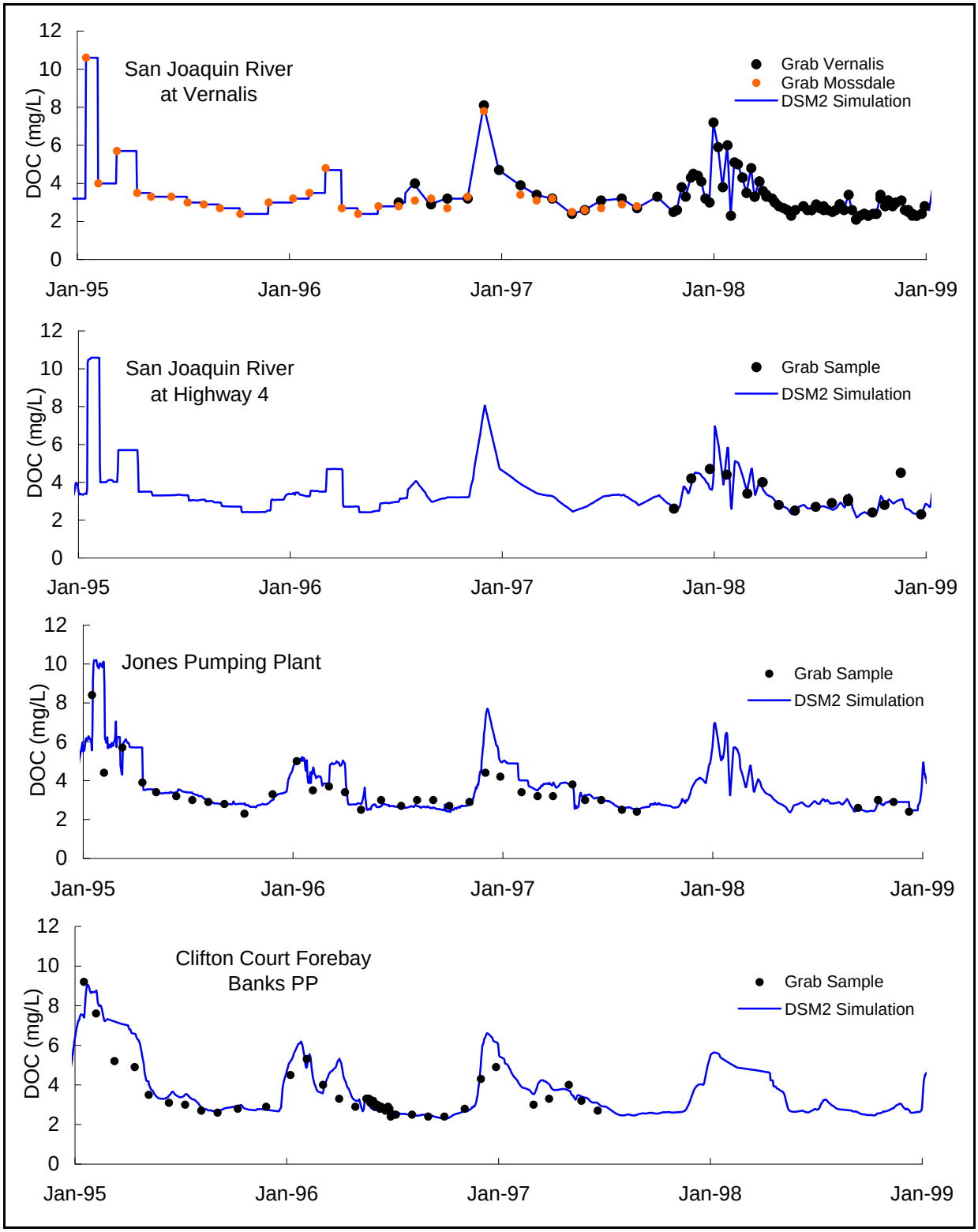

Figure 9-6 DSM2-simulated daily DOC and measured DOC, 1995–1998

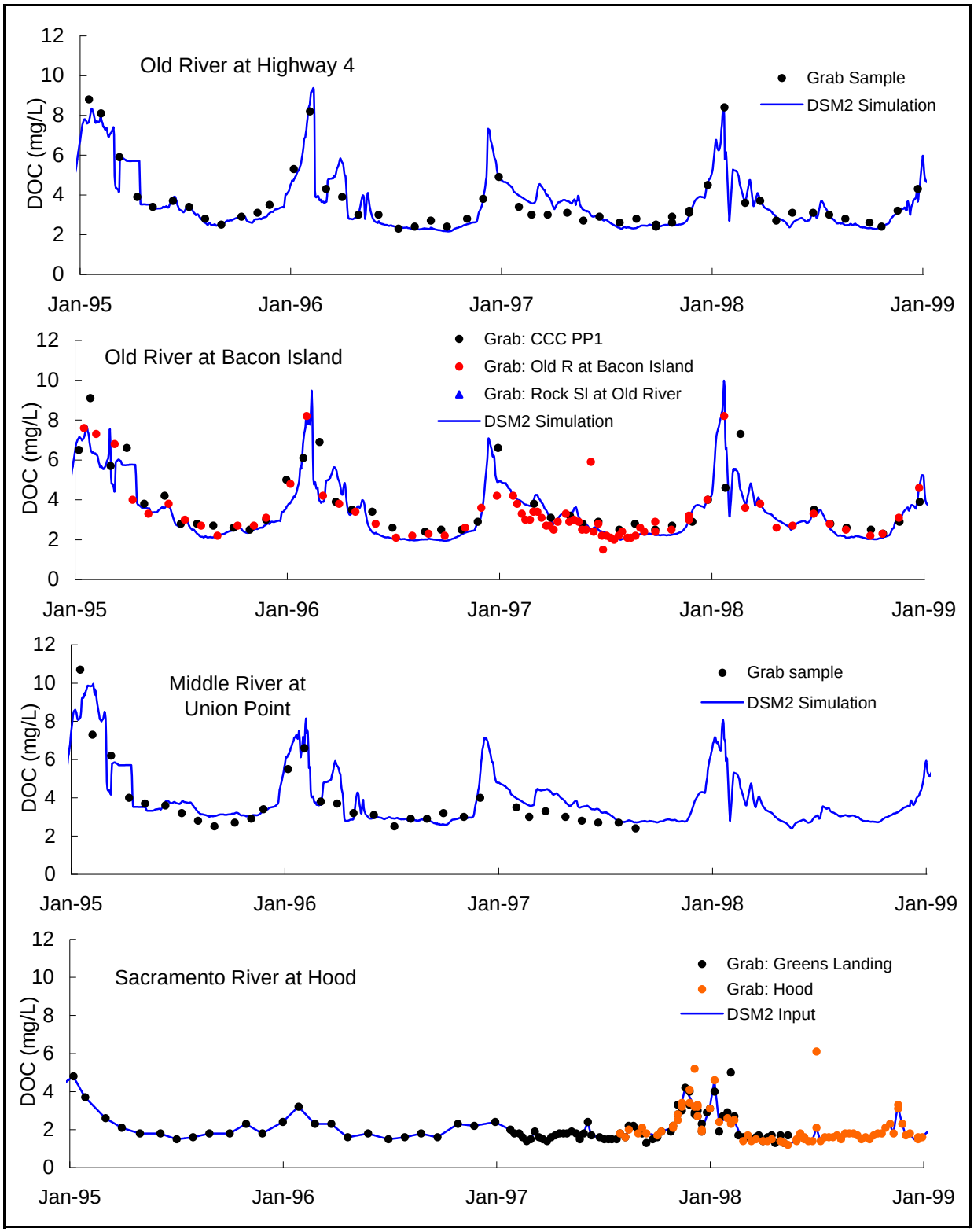

Figure 9-6 (cont.) DSM2-simulated daily DOC and measured DOC, 1995–1998

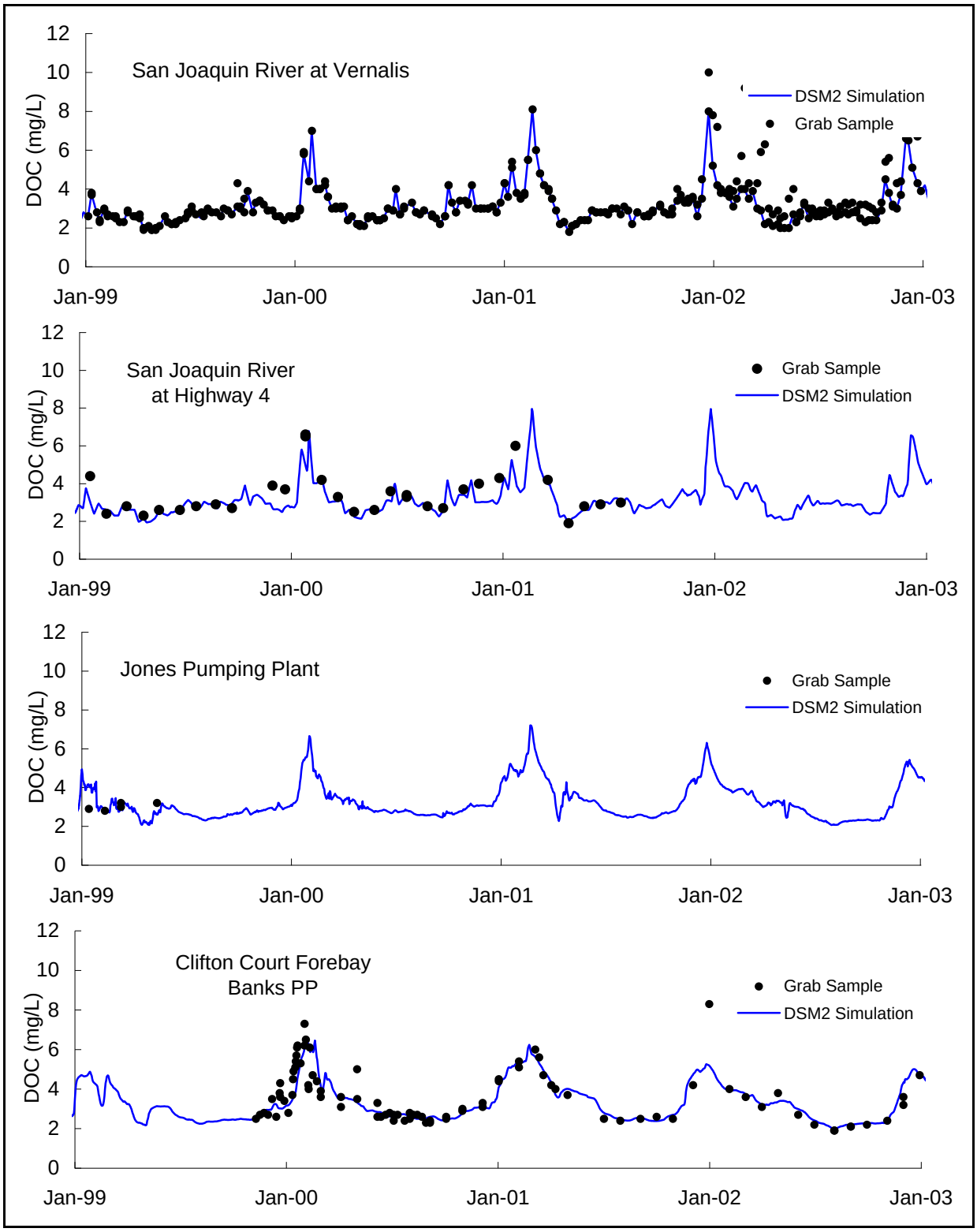

Figure 9-7 DSM2-simulated daily DOC and measured DOC, 1999–2002

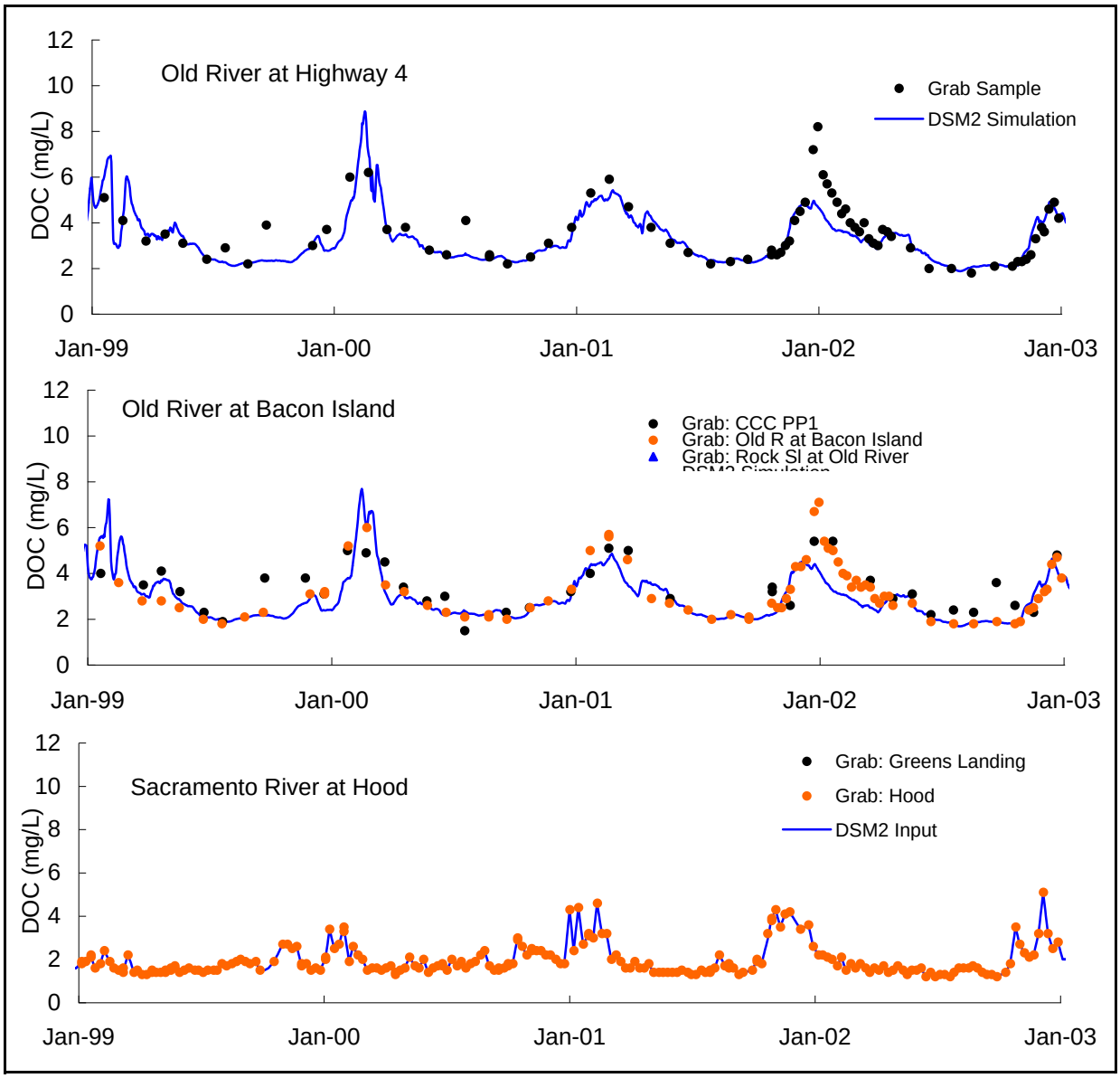

Figure 9-7 (cont.) DSM2-simulated daily DOC and measured DOC, 1999–2002

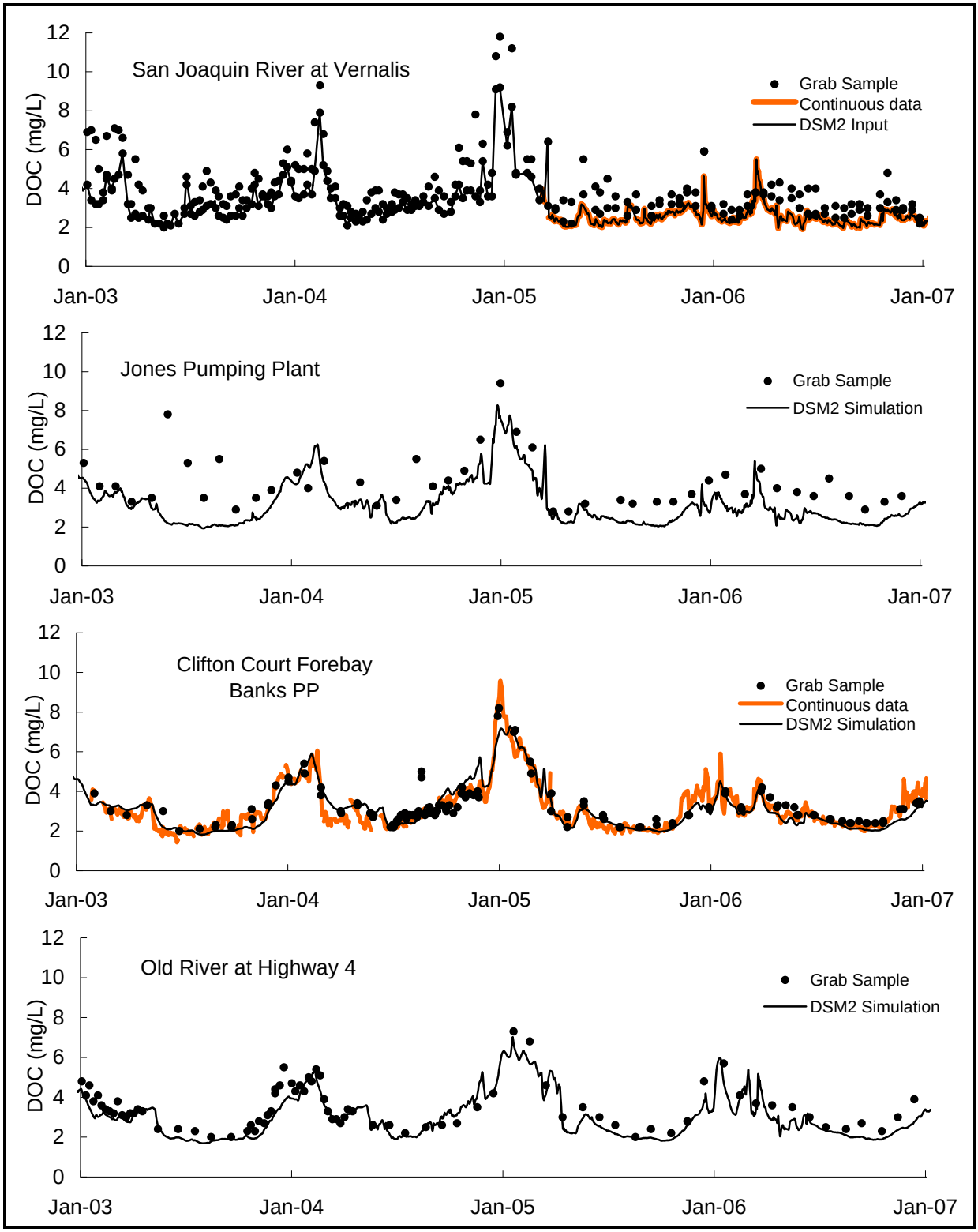

Figure 9-8 DSM2-simulated daily DOC and measured DOC, 2003–2006

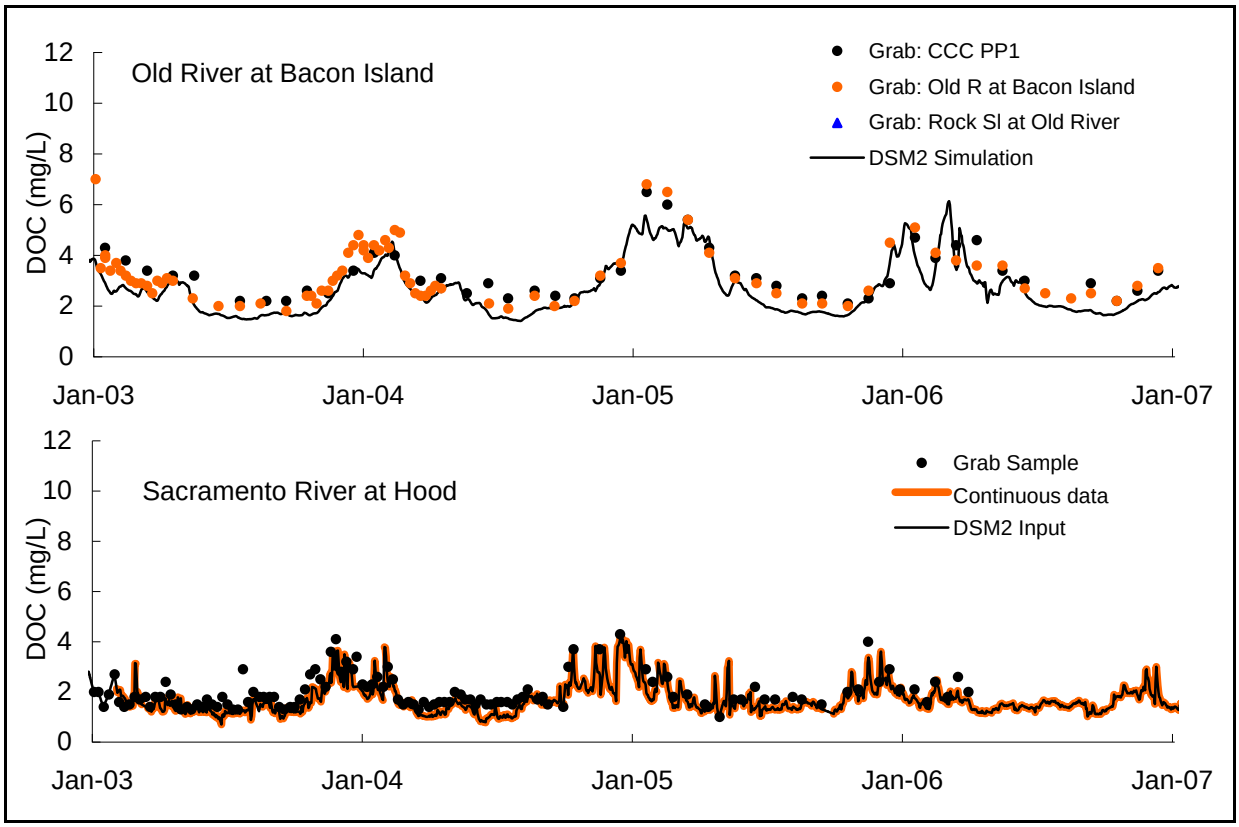

Figure 9-8 (cont.) DSM2-simulated daily DOC and measured DOC, 2003–2006

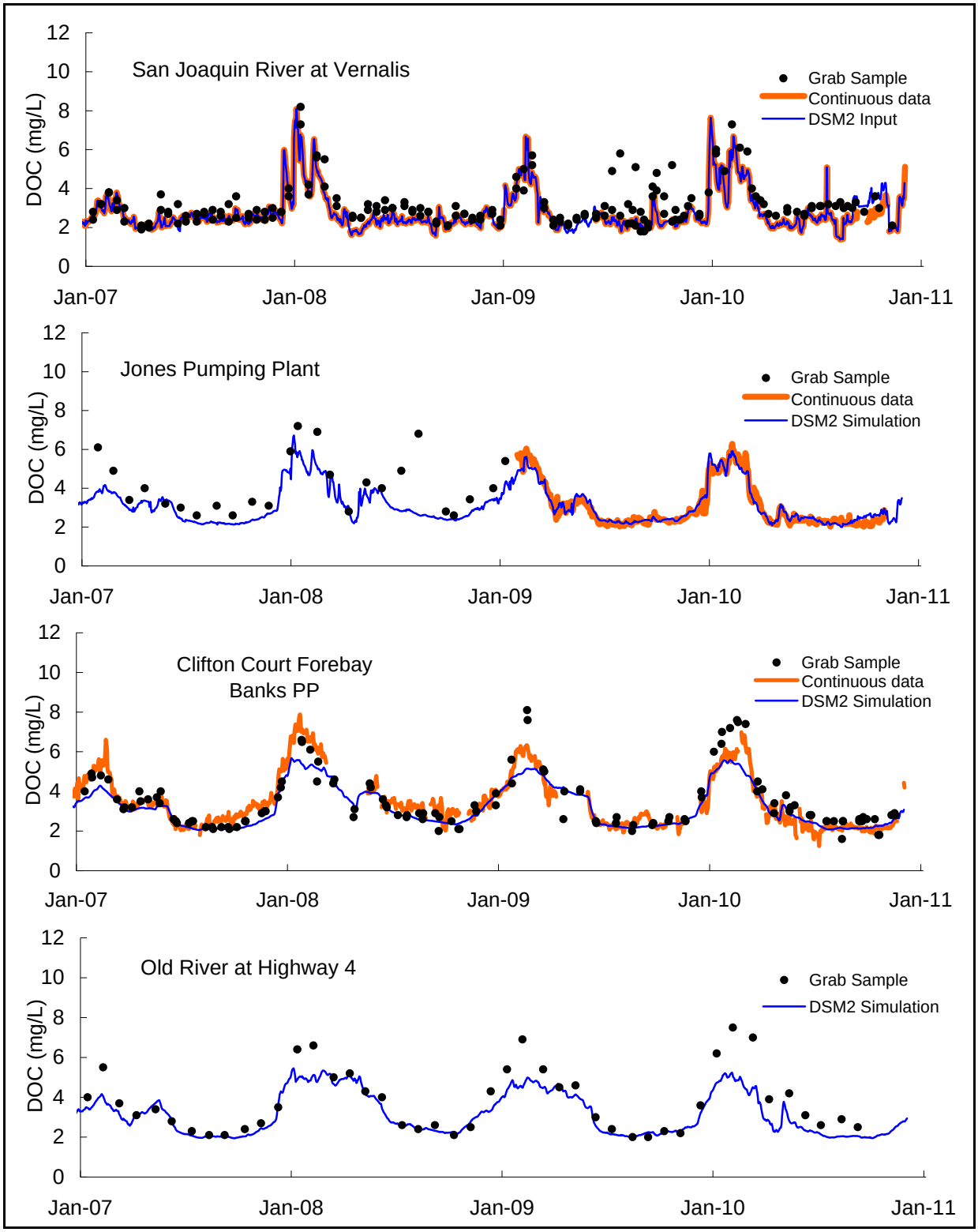

Figure 9-9 DSM2-simulated daily DOC and measured DOC, 2007–2010

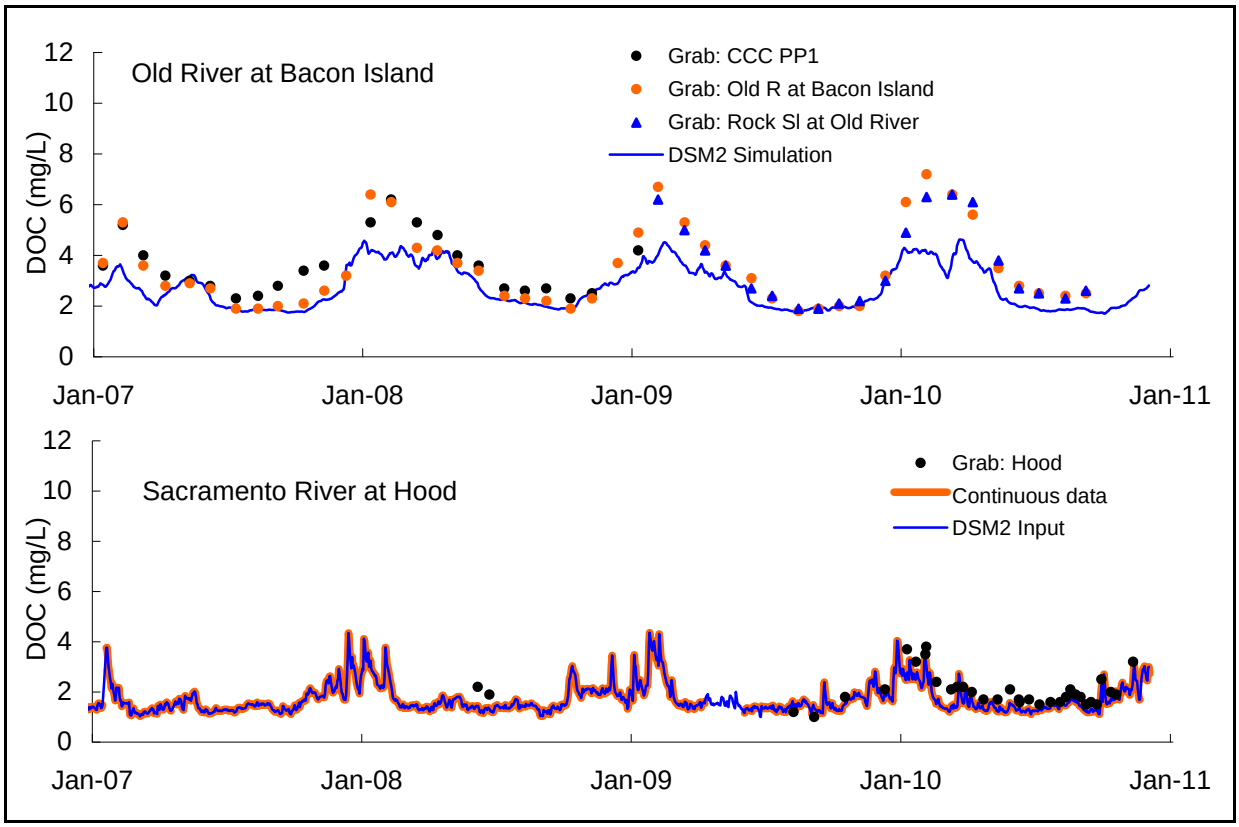

Figure 9-9 (cont.) DSM2-simulated daily DOC and measured DOC, 2007–2010

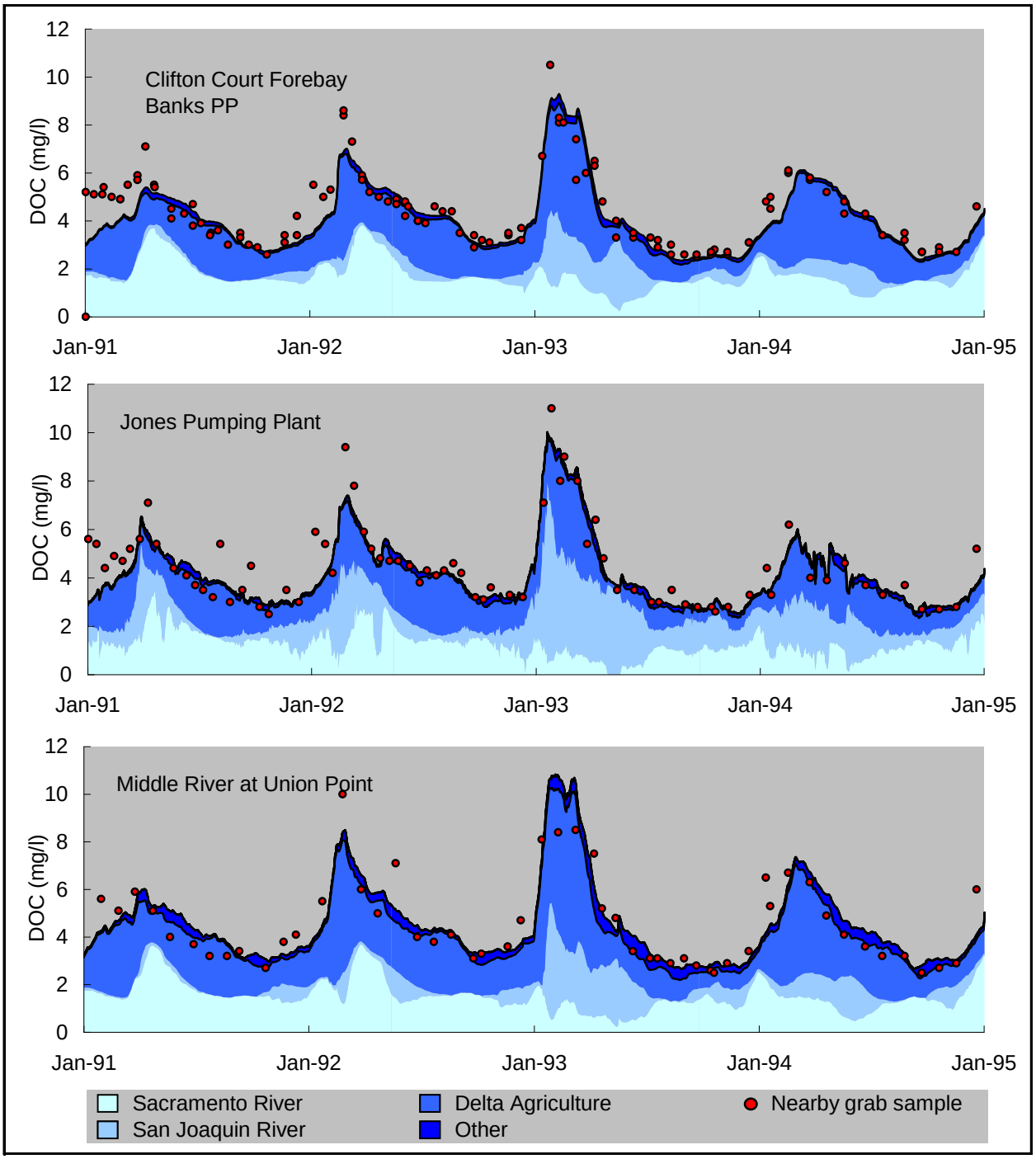

Figure 9-10 DSM2-simulated daily DOC fingerprint and measured DOC, 1991–1994

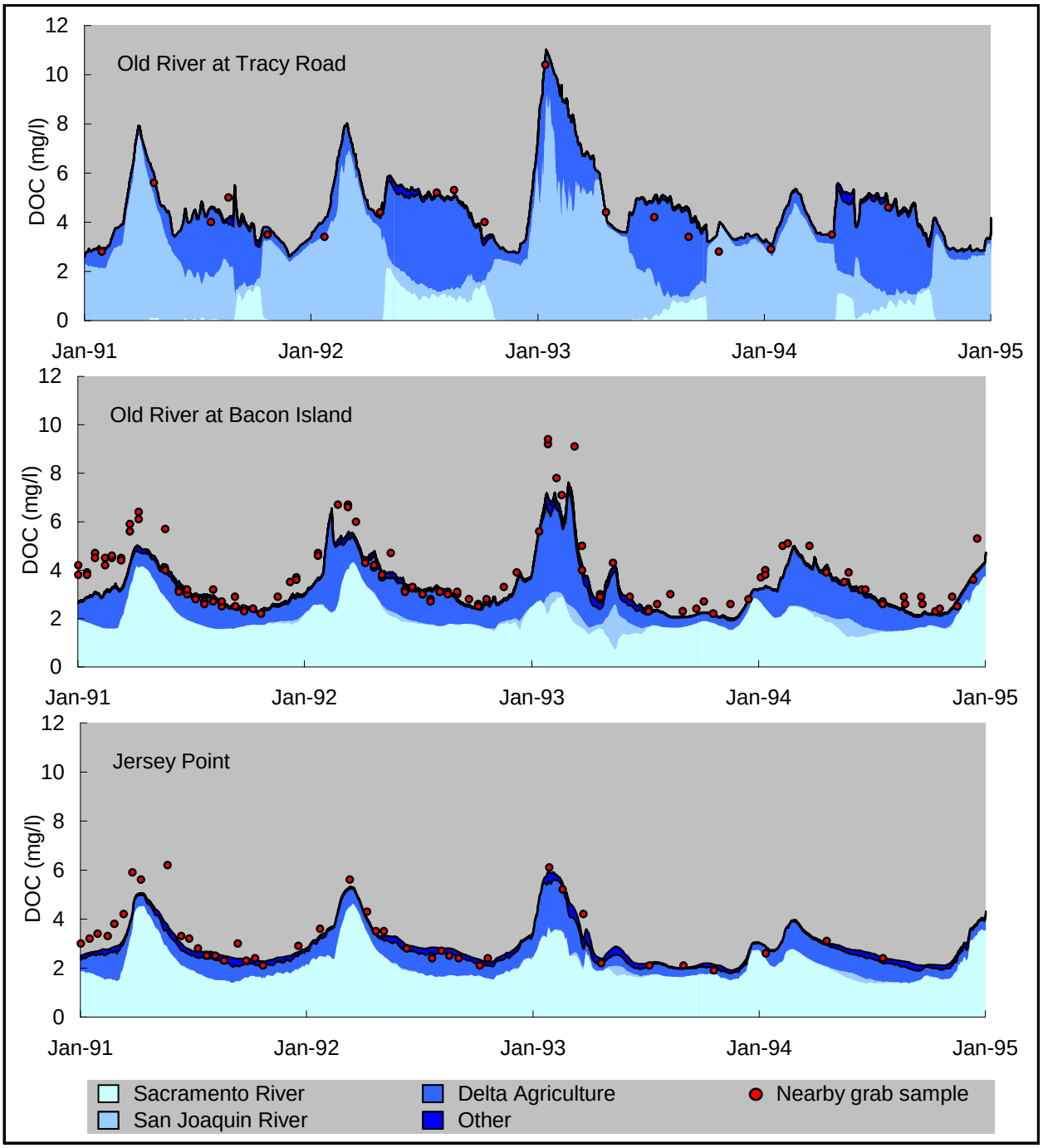

Figure 9-10 (cont.) DSM2-simulated daily DOC fingerprint and measured DOC, 1991–1994

Methodology for Flow and Salinity Estimates in the Sacramento-San Joaquin Delta and Suisun Marsh

32nd Annual Progress Report
June 2011

Chapter 10
DSM2 Comparison Report Tool

Authors: En-Ching Hsu,
Delta Modeling Section,
Bay-Delta Office,
California Department of Water Resources

Contents

10 DSM2 Comparison Report Tool 10-1
10.1 Introduction 10-1
10.2 Development Framework 10-1
10.3 Tool Demonstration: Input Comparison Tool 10-2
10.4 Tool Demonstration: DSS Comparison Tool 10-4
10.4.1 Configuration File Preparation 10-5
10.4.2 DSM2 Planning Study 10-9
10.4.3 DSM2 Model Calibration 10-11
10.5 Conclusions 10-13
10.6 References 10-13

Figures

Figure 10-1 Working diagrams for input comparison report tool and output comparison report tool 10-2
Figure 10-2 Input comparison report tool GUI 10-2
Figure 10-3 Input comparison report 10-3
Figure 10-4 Highlighted differences from reservoir in example input comparison report 10-3
Figure 10-5 Extended reservoir table in example input comparison report 10-4
Figure 10-6 Input comparison example for non-unique lookup names 10-4
Figure 10-7 Example to execute output comparison tool 10-4
Figure 10-8 Sample configuration file for output comparison tool 10-7
Figure 10-9 Time series plot example for 5 comparison modes 10-8
Figure 10-10 DSM2 output comparison report for planning studies 10-10
Figure 10-11 A demonstration for displaying percentage root mean square differences on Google Map 10-10
Figure 10-12 Time series plot (1) daily average time series (2) monthly average time series (3) difference for daily time series (4) overlaid water year type on daily average time series 10-11
Figure 10-13 Percentage root mean square error for turbidity comparison (COMPARE_MODE 5) 10-12
Figure 10-14 Time series plot example for turbidity comparison (COMPARE_MODE 5) 10-12

Table

Table 10-1 Files required for each comparison mode 10-8

10 DSM2 Comparison Report Tool

10.1 Introduction

While running the Delta Simulation Model II (DSM2) for different scenarios, it is essential for model investigation to know the changes that have been made to input files and subsequent changes to DSM2 outputs. Analyzing DSM2 model input and output changes with existing tools involves manual steps that are cumbersome and inefficient. The objective for this tool development is to automate the comparison process. The goal is to reduce duplicate effort and human errors, and provide a systematic way for study comparison.

DSM2 input files are located in different places based on input categories and properties. DSM2 gathers all the input files and summarizes them into a single echo file. Hence, input comparisons can be easily done using text difference tools, since DSM2 the echo file is in text format. These tools usually precisely point out where the differences are. However, they tend to return irrelevant or redundant differences that come from extra space, tabs, and lines. The `DSM2Modifier` variable, in particular, causes the most redundancies because it is a variable globally replaced and differs from one scenario to another. Also, text comparison tools point out only which lines have been changed, but not tables such as channel, reservoir, or cross section. The input comparison tool developed here reads DSM2 input files and prints out a summary table that shows the number of additional records in either study as well as the number of modified records. The details are presented and grouped by table properties. The tool filters out changes from `DSM2 Modifier` and shows the actual changes between 2 files.

DSM2 results are stored in HEC-DSS files, a time series data storage system developed by the US Corps of Engineers' Hydrologic Engineering Center. The most common practice for output comparison is opening DSS files by VISTA, HEC-DSSVue, or VTOOL and manually going through each time series. The effort to select corresponding time series, select time window, and calculate difference can get very tedious when there are many scenarios and output locations involved. The manual process cannot be saved, and the same effort needs to be repeated—not to mention human operation errors and eyeballing accuracy. There is a great need for a tool to automate the comparison process, and that is the reason to develop this output comparison report tool. This tool reads DSM2 DSS output files and generates an HTML report based on instructions in a configuration file. It is designed to cover about 80% of what people usually want to review. The report is useful in viewing observed and modeled time series, model output comparison, and calibration plots. The interactive time series plot gives users options to adjust time windows, overlay water year type, and view the differences. The report can be viewed anytime once it is produced. The HTML format enhances the capability to post the study online and allows users to interact with the interface.

10.2 Development Framework

The capability to retrieve HEC-DSS file is required for this development. HEC-DSSVue and VISTA are commonly used to visualize and analyze DSS files. There are reasons to select VISTA (Sandhu 1998) as the library for this tool development. First, VISTA is part of the DSM2 delivery package; therefore, there is no need for additional installation if users keep their DSM2 and VISTA packages up-to-date. VISTA has a `/script` folder to locate all add-on applications. The scripts are written in VSCRIPT, which is a Jython-based language. HTML syntax and JavaScript are printed as strings in the script. SVG technology (Wikipedia contributors 2011) is used for time series plots because of its fast display speed and no need

to generate image files ahead of time. Most browsers, such as Google Chrome, Mozilla Firefox, and IE9+, support SVG format. Google Chrome is recommended for best performance.

Error! Reference source not found. shows how the tool works. To compare inputs, open the Input Comparison Tool and specify two echo files (Hydro echo, Qual, echo or *.inp files). The report will be generated in a user-designated folder.

The Output Comparison Tool accepts up to 3 DSS files. Usually, the observed data goes to FILE0 since it will be presented as dots while FILE1 and FILE2 are solid lines. The configuration file contains all specifications for global output setups, file locations, scenario names, output locations, and time windows of interest.

Both Input and Output Tools are launched through a command prompt. For the Input Tool, type "`compare_inp`" to open the GUI. For the Output Tool, type "`compare_dss your_configuration_file.inp`" to run the program. More details will be given in the next 2 sections.

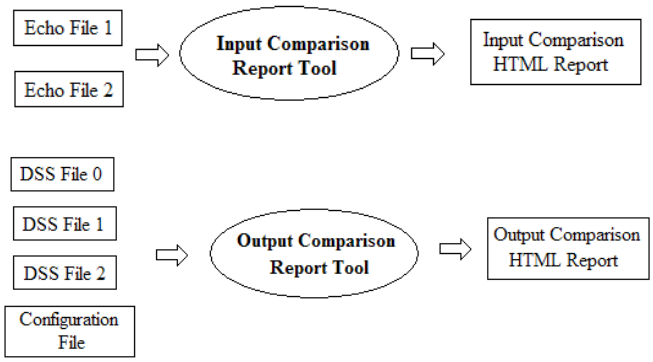

Figure 10-1 Working diagrams for input comparison report tool and output comparison report tool

10.3 Tool Demonstration: Input Comparison Tool

The Input Comparison Tool is launched by typing "`compare_inp`" in a command prompt window. A GUI will appear as shown in Figure 10-2. Four inputs are required to generate the report: echo file 1 and file 2, the HTML page output directory, and filename. Once they are all assigned, click on "Create HTML Report" and the report will be generated and pop up. The report also can be opened anytime from the designated directory. In addition, it is fine to store multiple comparisons in the same directory as long as different HTML filenames are assigned.

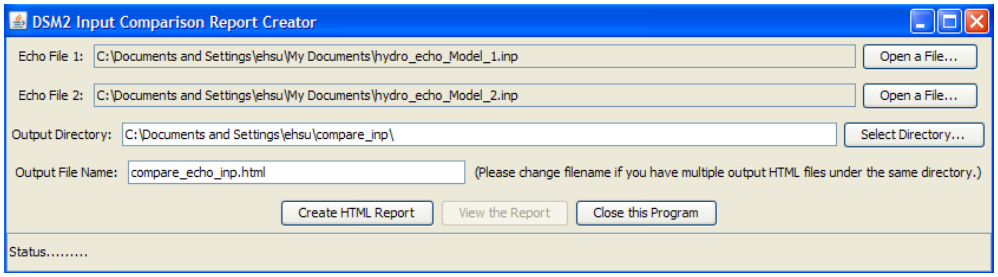

Figure 10-2 Input comparison report tool GUI

A sample input comparison report is shown in Figure 10-3. On top of the page, a summary table shows how many extra records were added to echo files 1 and 2 and how many modifications there are between the two echo files by each category. Using reservoir for example, there is 1 extra record in echo file 1, 1 extra record in echo file 2 and 4 modifications made. The details as shown in Figure 10-4 can be seen by clicking on the "RESERVOIR" hyperlink in the summary table or scrolling down the page. The reservoir table can be expanded to Figure 10-5 by clicking ⊞ at the upper left corner. The table can be collapsed by clicking ⊟.

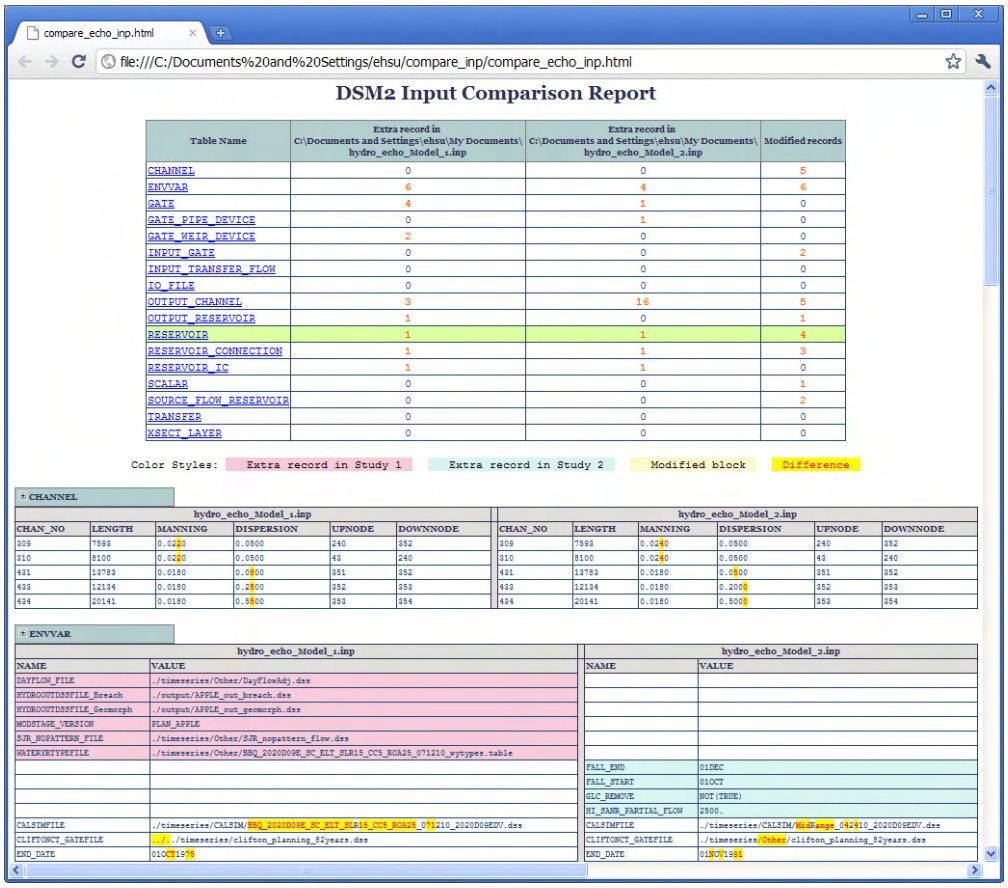

Table Name	Extra record in C:\Documents and Settings\ehsu\My Documents\hydro_echo_Model_1.inp	Extra record in C:\Documents and Settings\ehsu\My Documents\hydro_echo_Model_2.inp	Modified records
CHANNEL	0	0	5
ENVVAR	6	4	6
GATE	4	1	0
GATE_PIPE_DEVICE	0	1	0
GATE_WEIR_DEVICE	2	0	0
INPUT_GATE	0	0	2
INPUT_TRANSFER_FLOW	0	0	0
IO_FILE	0	0	0
OUTPUT_CHANNEL	3	16	5
OUTPUT_RESERVOIR	1	0	1
RESERVOIR	1	1	4
RESERVOIR_CONNECTION	1	1	3
RESERVOIR_IC	1	1	0
SCALAR	0	0	1
SOURCE_FLOW_RESERVOIR	0	0	2
TRANSFER	0	0	0
XSECT_LAYER	0	0	0

hydro_echo_Model_1.inp						hydro_echo_Model_2.inp					
CHAN_NO	LENGTH	MANNING	DISPERSION	UPNODE	DOWNNODE	CHAN_NO	LENGTH	MANNING	DISPERSION	UPNODE	DOWNNODE
309	7593	0.0220	0.0500	240	352	309	7593	0.0240	0.0500	240	352
310	8100	0.0220	0.0500	43	240	310	8100	0.0240	0.0500	43	240
431	13783	0.0180	0.0800	351	352	431	13783	0.0180	0.0800	351	352
433	12134	0.0180	0.2000	352	353	433	12134	0.0180	0.2000	352	353
434	20141	0.0180	0.5000	353	354	434	20141	0.0180	0.5000	353	354

hydro_echo_Model_1.inp		hydro_echo_Model_2.inp	
NAME	VALUE	NAME	VALUE
DAYFLOW_FILE	./timeseries/Other/DayFlowAdj.dss		
HYDROOUTDSSFILE_Breach	./output/APPLE_out_breach.dss		
HYDROOUTDSSFILE_Geomorph	./output/APPLE_out_geomorph.dss		
MODSTAGE_VERSION	PLAN_APPLE		
SJR_NOPATTERN_FILE	./timeseries/Other/SJR_nopattern_flow.dss		
WATERVRTYPEFILE	./timeseries/Other/BEQ_2020D09E_SC_ELT_SLR15_CC5_ROA25_071210_wytypes.table		
		FALL_END	01DEC
		FALL_START	01OCT
		GLC_REMOVE	NOT(TRUE)
		HI_SANK_PARTIAL_FLOW	2500.
CALSIMFILE	./timeseries/CALSIM/BEQ_2020D09E_SC_ELT_SLR15_CC5_ROA25_071210_2020D09EDV.dss	CALSIMFILE	./timeseries/CALSIM/MidRange_042410_2020D09EDV.dss
CLIFTONCT_GATEFILE	../../timeseries/clifton_planning_82years.dss	CLIFTONCT_GATEFILE	./timeseries/Other/clifton_planning_82years.dss
END_DATE	01OCT1978	END_DATE	01NOV1981

Figure 10-3 Input comparison report

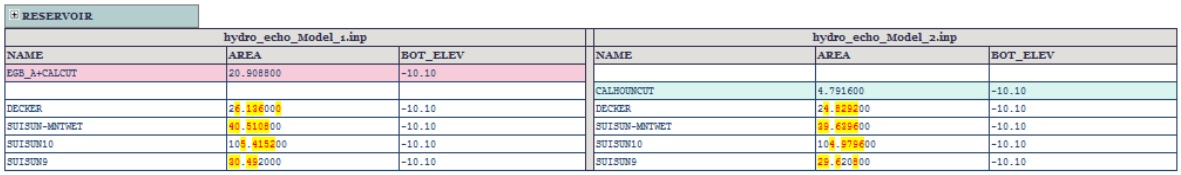

hydro_echo_Model_1.inp			hydro_echo_Model_2.inp		
NAME	AREA	BOT_ELEV	NAME	AREA	BOT_ELEV
EGB_A+CALCUT	20.908800	-10.10			
			CALHOUNCUT	4.791600	-10.10
DECKER	26.136000	-10.10	DECKER	24.829200	-10.10
SUISUN-MNTWET	40.510800	-10.10	SUISUN-MNTWET	39.639600	-10.10
SUISUN10	105.415200	-10.10	SUISUN10	104.875600	-10.10
SUISUN9	30.492000	-10.10	SUISUN9	29.620800	-10.10

Figure 10-4 Highlighted differences from reservoir in example input comparison report

RESERVOIR

NAME	AREA	BOT_ELEV	NAME	AREA	BOT_ELEV
DECKER	26.136000	-10.10	DECKER	24.829200	-10.10
			CALHOUNCUT	4.791600	-10.10
EGB_A+CALCUT	20.908800	-10.10			
LTL_HOLLAND	0.304920	-10.10	LTL_HOLLAND	0.304920	-10.10
MCCORWIL	51.400800	-10.10	MCCORWIL	51.400800	-10.10
PROSPECT	51.400800	-10.10	PROSPECT	51.400800	-10.10
SUISUN-MNTWET	40.510800	-10.10	SUISUN-MNTWET	38.639600	-10.10
SUISUN10	105.415200	-10.10	SUISUN10	104.979600	-10.10
SUISUN12	63.597600	-10.10	SUISUN12	63.597600	-10.10
SUISUN3	33.105600	-10.10	SUISUN3	33.105600	-10.10
SUISUN9	30.492000	-10.10	SUISUN9	28.620800	-10.10
bethel	15.503100	-8.10	bethel	15.503100	-8.10
clifton_court	91.868000	-10.10	clifton_court	91.868000	-10.10
discovery_bay	19.632000	-16.00	discovery_bay	19.632000	-16.00
franks_tract	141.786400	-10.10	franks_tract	141.786400	-10.10

Figure 10-5 Extended reservoir table in example input comparison report

In the reservoir example in Figure 10-5, “NAME” is unique for all the entries, and it is easy to see additions, deletions, and changes. However, while looking reservoir connections (Figure 10-6), there are repeating entries in the first column, RES_NAME; for some other cases, repeating entries are shown in the first and second columns. It is thus better to highlight them as blocks than to try getting a precise list of changes.

RESERVOIR_CONNECTION

hydro_echo_Model_1.inp				hydro_echo_Model_2.inp			
RES_NAME	NODE	COEF_IN	COEF_OUT	RES_NAME	NODE	COEF_IN	COEF_OUT
				CALHOUNCUT	324	1100.000	1100.000
DECKER	352	400.000	400.000	DECKER	352	350.000	700.000
DECKER	353	130.000	90.000				
EGB_A+CALCUT	324	800.000	500.000				
LTL_HOLLAND	318	1000.000	500.000	LTL_HOLLAND	318	2000.000	500.000
LTL_HOLLAND	319	250.000	550.000	LTL_HOLLAND	319	250.000	550.000
clifton_court	900	1200.000	0.000	clifton_court	900	1000.000	0.000

Figure 10-6 Input comparison example for non-unique lookup names

10.4 Tool Demonstration: DSS Comparison Tool

In order to run the Output Comparison Tool, a configuration file needs to be prepared and placed in an empty folder. Because the Output Tool stores the calculated statistics and parsed information in JavaScript files, the best practice is to create a new empty folder for each comparison configuration file and then in the command prompt window, make this folder as the working directory. The Output Comparison Tool can be launched by typing “`compare_dss your_configuration_filename`” (Figure 10-7). The computation time depends on DSS file sizes and output locations selected. More than 80% of the computation time goes to the root mean square difference calculation. Therefore, if the DSS file size is relatively large, it is recommended to turn on the global variable “`CALCULATE_SPECIFIED_RMSE_ONLY`” so that unselected locations will not be included in the root mean square difference calculation. The following subsections illustrate configure file preparation and give examples of a planning study and model calibration.

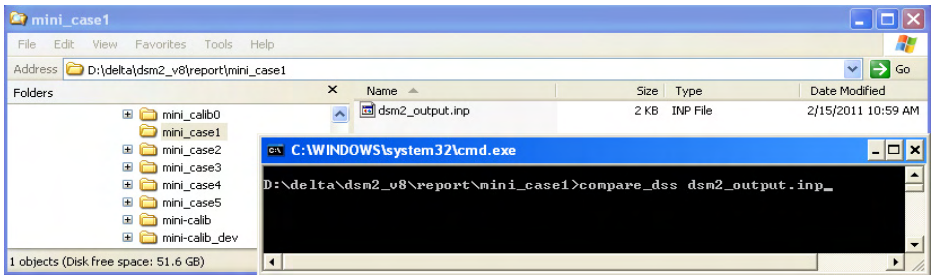

Figure 10-7 Example to execute output comparison tool

10.4.1 Configuration File Preparation

A sample configuration file is shown in Figure 10-8. There are several blocks that need to be completed. In Table 10-1, a summary table shows files required for each comparison mode. The sample output time series plots are shown in Figure 10-9. The table and figures follow the explanation of blocks.

The “GLOBAL_CONTROL” block is used to control global output by giving MODE for each CONTROLLER. The default value for the ON/OFF switch is OFF. (1) For web browser, there is limit for loading certain megabytes of data in a single page. Therefore, this tool converts each time series into daily average, daily maximum, daily minimum, and monthly average for plotting so that it does not take too much storage and loading memory.

“PLOT_ORIGINAL_TIME_INTERVAL” is used when we want to see the plot for the original time interval whose time interval is less than one day, e.g., 15 minutes data. However, it is not recommended to turn this on when the length of data is more than a year. (2) Most of the computation time goes to root mean square difference calculation. Therefore, if there is no interest to investigate root mean square difference other than the specified output locations, turning this mode on will save time. (3) The output time series plots are presented based on OUTPUT/NAME alphabetically by default. There are cases in which users want to view their time series plots based on the order that is given. For example, order from upstream to downstream or from inland toward ocean. In those cases, turn “DONT_SORT_STATION_NAME” on. (4) “DEFAULT_TIME_INTERVAL” is used as a filter for E part in DSS file. This is to avoid non-unique matches for outputs with identical B part and C part but different E part. (5) “COMPARE_MODE” is used to specify report type, and it is assigned by mode numbers. There are 5 options available: plotting observed data only (MODE=1), plotting modeled data only (MODE=2), comparing 2 modeled outputs (MODE=3), comparing a model output with observed data (MODE=4), and comparing 2 model outputs with observed data (MODE=5).

SCALAR” is utilized to control the setups for input DSS files and output HTML file. The details for each item are listed as below.

FILE0:	file name and path for observed data. This will be presented as dot plot by default.
FILE1:	file name and path for primary modeled data. This will be presented as solid green line plot.
FILE2:	file name and path for secondary modeled data. This will be presented as dash blue line plot.
NAME0:	name to present FILE0 data. This is the name used in report and time series plot.
NAME1:	name to present FILE1 data. This is the name used in report and time series plot.
NAME2:	name to present FILE2 data. This is the name used in report and time series plot.
OUTDIR:	report output directory
OUTFILE:	report output HTML name
NOTE:	notes for this report
ASSUMPTIONS:	assumptions made for the report
MODELER:	modeler’s name

The VARIABLE block is used to specifically define output paths. Four columns are in this block. NAME is the given name for this setup, and it provides the connection for the name used in the OUTPUT block. REF0 is the reference used for observed data, which is presented as a dotted line. REF1 is the reference used as primary (base case) model output, which is presented as a solid green line plot. REF2 is the reference used as secondary (alternative study) model output, which is presented as a dashed blue line plot. The format to specify each reference is seen in Figure 10-8. This gives users the flexibility to assign the particular time series they want to compare with. For example, they may all come from one file or customized file combinations, different part B (station name), different part C (data type) or part E (time interval).

OUTPUT is used to specify the locations of interest for plotting time series. By default, putting Part B + "_" + Part C, e.g. ROLD024_FLOW, is equal to "FILE0::/ROLD024/FLOW//15MIN// FILE1::/ROLD024/FLOW//15MIN// FILE2::/ROLD024/FLOW//15MIN//". Part E is taken from the `DEFAULT_TIME_INTERVAL` variable from the GLOBAL_CONTROL block.

This tool also accepts simple wild-card rules. For example, *_EC will output all the EC stations and ROLD024_* will print out all data types associated with ROLD024. For the customizations defined in the VARIABLE block, giving the exact path names will plot those time series in a single figure.

TIME_PERIODS is used to specify periods of interest. Those time windows will turn to a list as a dropdown menu in HTML report so that users can switch each time window by simple selection. The first column in this block is name for a time window which has the format of "DDMMMYYYY hhmm – DDMMMYYYY hhmm", for example, 01OCT1976 2400 – 30SEP1991 2400.

```
# A template file to compare 2 DSM2 outputs
GLOBAL_CONTROL
CONTROLLER                        MODE
PLOT_ORIGINAL_TIME_INTERVAL       OFF
CALCULATE_SPECIFIED_RMSE_ONLY     OFF
DONOT_SORT_STATION_NAME           ON
DEFAULT_TIME_INTERVAL             15MIN
COMPARE_MODE                      5
END

SCALAR
NAME         VALUE
FILE0        D:/delta/dsm2_v8/report/dssfiles/Model_2.dss        # input file 0
NAME0        "Observation"
FILE1        D:/delta/dsm2_v8/report/dssfiles/Model_1.dss        # input file 1
NAME1        "Model 1"
FILE2        D:/delta/dsm2_v8/report/dssfiles/Model_2.dss        # input file 2
NAME2        "Model 2"
OUTDIR       D:/delta/dsm2_v8/report/case5
OUTFILE      DSM2_compare.html
NOTE         "A long funny note"
ASSUMPTIONS  "I am assuming this is defined"
MODELER      BDO
END

VARIABLE
NAME          REF0                                REF1                              REF2
TEST1   FILE2:://ROLD024/FLOW//15MIN//   FILE1:://ROLD024/FLOW//15MIN//    FILE2:://ROLD024/FLOW//15MIN//
TEST2   FILE1:://ROLD024/FLOW//15MIN//   FILE1:://ROLD034/FLOW//15MIN//    FILE2:://ROLD059/FLOW//15MIN//
TEST3   FILE1:://ROLD024/FLOW//15MIN//   FILE2:://ROLD034/FLOW//15MIN//    FILE2:://ROLD024/EC//15MIN//
END
```

Figure 10-8 Sample configuration file for output comparison tool

Table 10-1 Files required for each comparison mode

MODE	1 Observed data only	2 Modeled data only	3 Two models comparison	4 One model output with observed data	5 Two model outputs with observed data
FILE0	✔			✔	✔
FILE1		✔	✔	✔	✔
FILE2			✔		✔

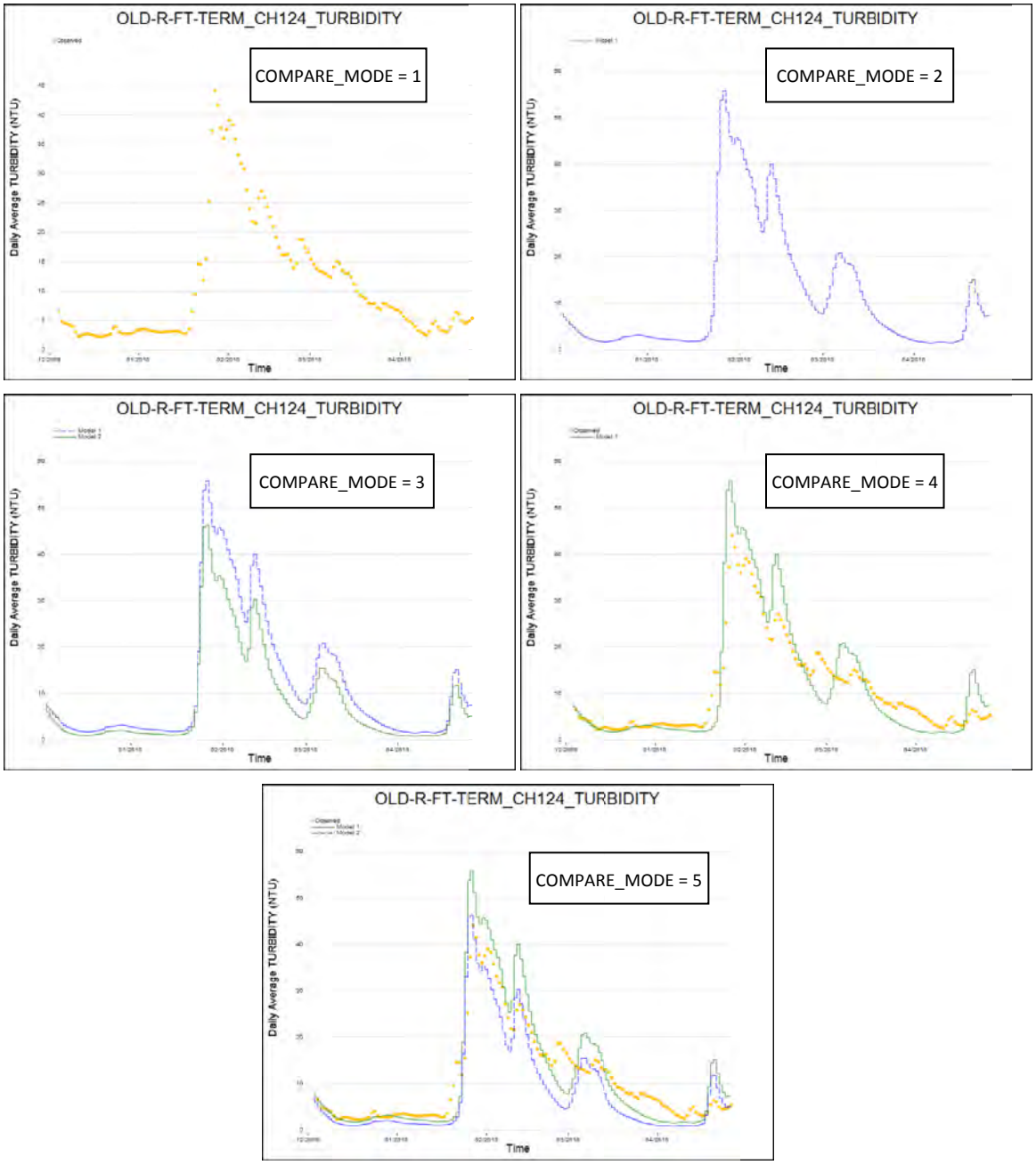

Figure 10-9 Time series plot example for 5 comparison modes

10.4.2 DSM2 Planning Study

An output report for DSM2 planning study (COMPARE_MODE=3) is used as an example (Figure 10-10). On top of the report, there is a title for this report which includes the names specified in NAME0, NAME1, and NAME2. Note and assumptions are the strings/sentences from the configuration file. Following them are functionalities available to control time series plot. “Data Conversion for Plot” by default provides 4 data conversion options: daily average, daily maximum, daily minimum, and monthly average. If GLOBAL/PLOT_ORIGINAL_TIME_INTERVAL is ON, an extra option will be added to the list. “User Defined Time Window” contains the time windows specified in configuration file. When the option is changed, the corresponding time window is also shown in the line beneath it. “Customize Time Window” allows users to change the time window of the time series plot by giving starting and ending dates. “Show Differences on plot” by clicking the checkbox will append differences on each time series plot. “Show water year type on plot” by clicking the checkbox will display the water year as background in each plot. “Threshold value to highlight percentage differences” is used to highlight percentage root mean square difference values that are higher than the criterion set in the input box. “Table Statistics” is used to switch between root mean square difference and percentage root mean square difference.

After the functionality division, there is the tabbed division that categorizes outputs by data types (part B in DSS file). The output can be easily browsed by clicking through the tabs, e.g., flow, EC, stage, velocity, etc. Clicking on “Show time series plots” will draw time series plots for locations specified in the OUTPUT block. Besides the time series plots, the root mean square statistic is calculated for specified output locations. If the switch for CALCULATE_SPECIFIED_RMSE_ONLY is OFF, the statistic will be calculated for all stations in the DSS file and can be viewed by clicking “open all stations” to expand the entire table. The statistic is calculated for the pre-defined time windows and 5 water year types. Percentage root mean square difference is normalized from root mean square difference with the maximum amplitude of the data set. Next to each statistics’ value, there are green or red arrows that provide users a quick overview of the comparison result. Green means that the model 2 (secondary study) value is higher than model 1 (primary study), while red means model 2 is lower than model 1. The report tool also allows users to view the percentage root mean square differences on Google map which provides spatial variation and a big picture of the differences (clicking on “View Map”). A demo for the Google Map output is shown in Figure 10-11. Each location point is clickable for a popup info box.

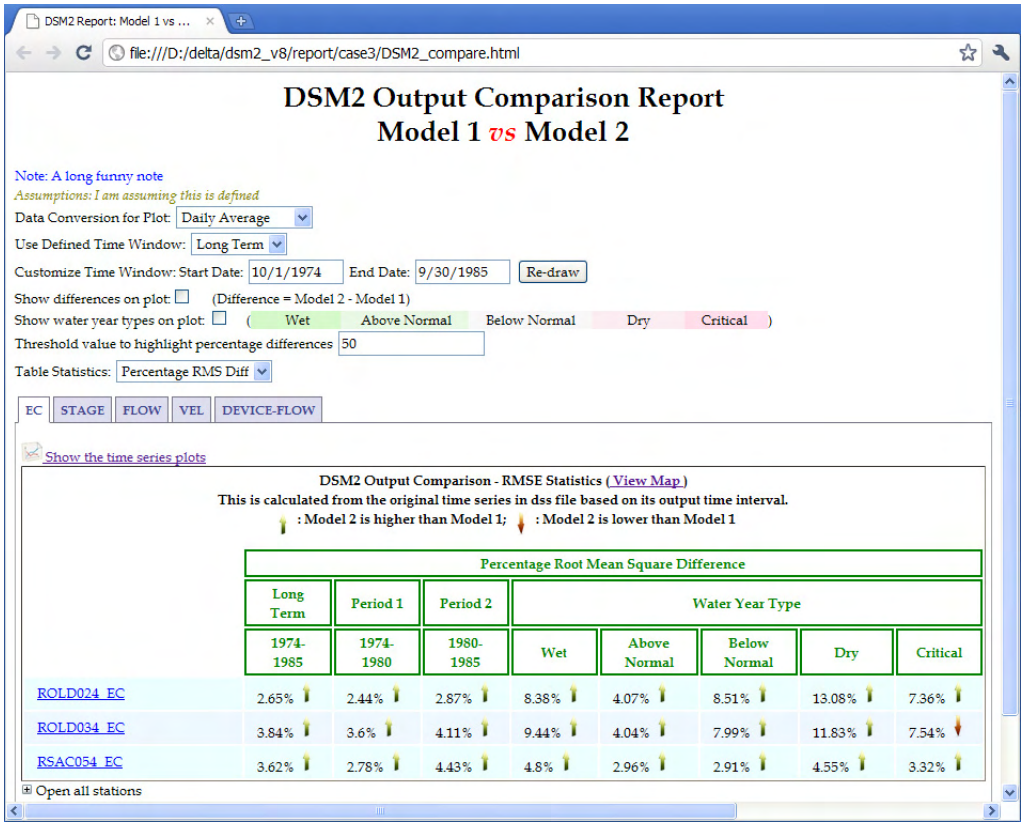

	Percentage Root Mean Square Difference							
	Long Term	Period 1	Period 2	Water Year Type				
	1974-1985	1974-1980	1980-1985	Wet	Above Normal	Below Normal	Dry	Critical
ROLD024_EC	2.65%	2.44%	2.87%	8.38%	4.07%	8.51%	13.08%	7.36%
ROLD034_EC	3.84%	3.6%	4.11%	9.44%	4.04%	7.99%	11.83%	7.54%
RSAC054_EC	3.62%	2.78%	4.43%	4.8%	2.96%	2.91%	4.55%	3.32%

Figure 10-10 DSM2 output comparison report for planning studies

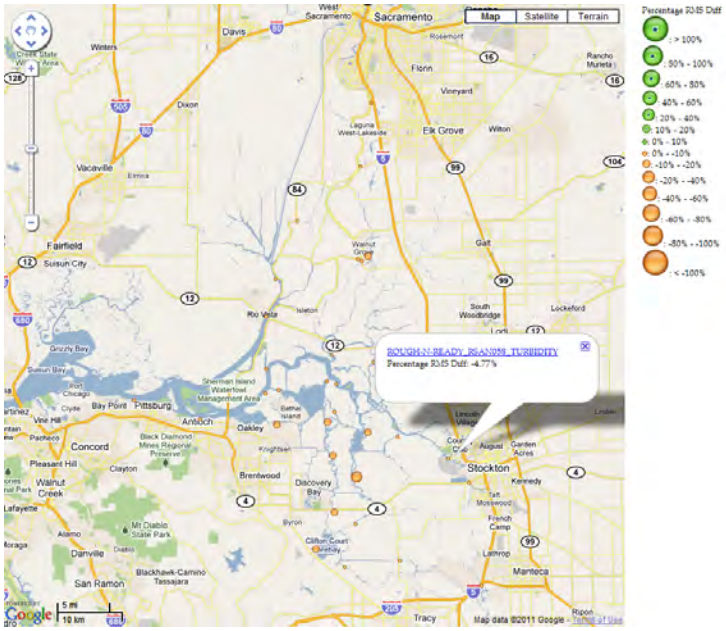

Figure 10-11 A demonstration for displaying percentage root mean square differences on Google Map

Figure 10-12 is an example time series plot. Daily average values are the default time series plot (Figure 10-12 [1]). Any changes made for the selection in “Data Conversion for plot” will re-draw the time series to selected display time interval, e.g., monthly average as shown in Figure 10-12 [2]. When clicking “Show difference on plot,” the difference is calculated by subtracting Model 2 from Model 1 and is shown under those 2 time series (Figure 10-12 [3]). To investigate the correlation with water year type is of great interest; therefore, this tool enables users to overlay water year types as background color to help users observe the associated patterns (Figure 10-12 [4]). These tools help to visually investigate the differences between the 2 models.

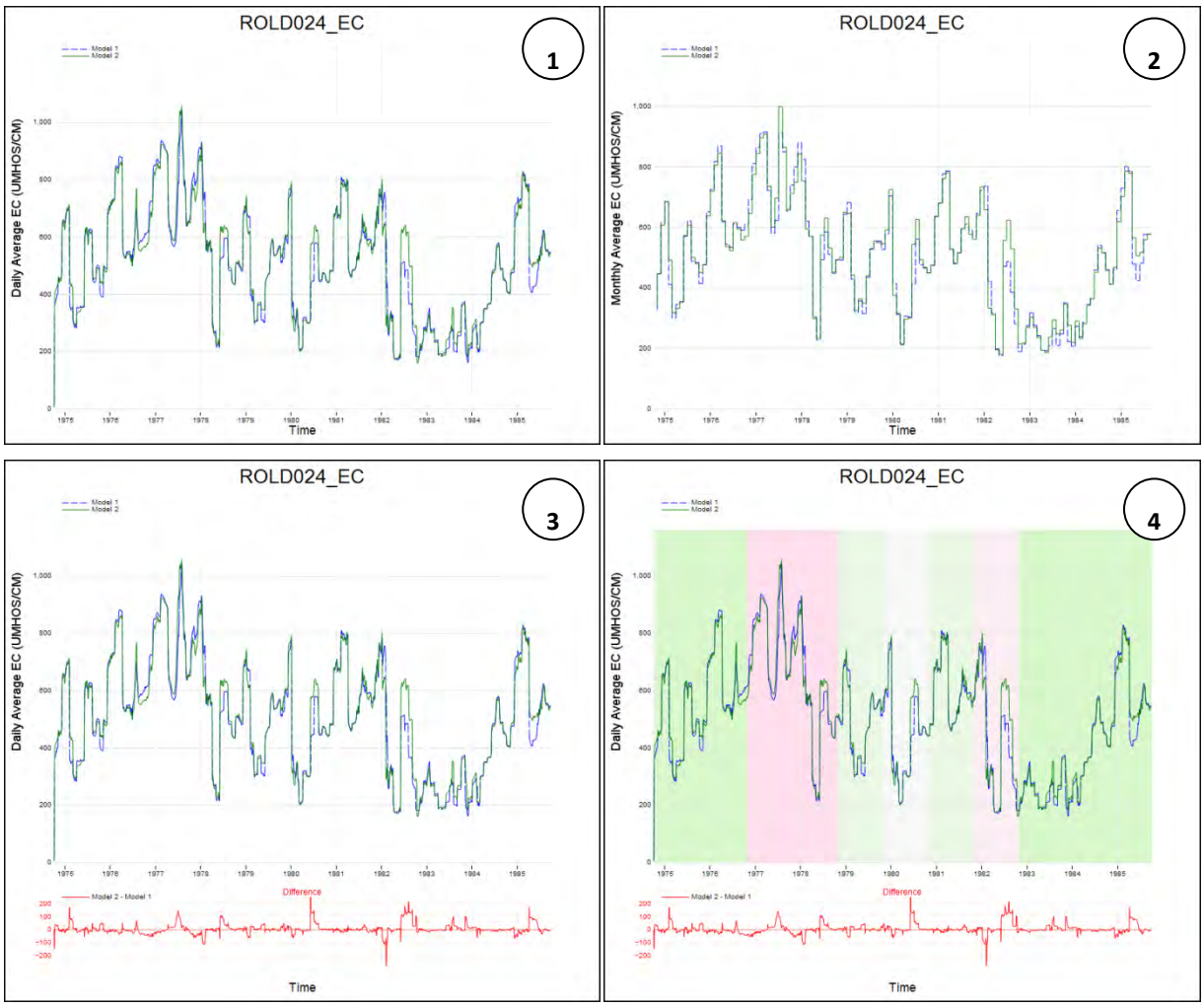

Figure 10-12 Time series plot (1) daily average time series (2) monthly average time series (3) difference for daily time series (4) overlaid water year type on daily average time series

10.4.3 DSM2 Model Calibration

Model calibration consists of changing values of model input parameters in an attempt to match field data within some acceptable criteria. Comparison among scenarios is an essential but time-consuming task to investigate the sensitivities for the adjustment to each parameter. An example of comparing scenarios from the mini calibration (CH2MHill 2009) and the corresponding observed data are used as an example (COMPARE_MODE=5). The time window extracted from Nov 30, 2009, to Apr 30, 2010, is

within a dry water year. Percentage root mean square error (RMSE) is calculated for each model and summarized (

Figure 10-13). The table also can be extended to all locations in DSS file by clicking “Open all stations.” For the example in

Figure 10-13, Model 1 has a smaller RMSE than model 2 at most locations; that implies the parameter setup in model 1 yields a better representation for observed data. This is the basic information that modelers always want to capture so that they may know the sensitivity of the parameter and come out with a better number for the next parameter adjustment. Figure 10-14 shows the capability of this tool to plot all the time series and the difference on a single figure. It helps modelers visually observe the variations over time, especially the responses at peaks and troughs. This information may be smoothed out in overall statistic calculation.

TURBIDITY

Show the time series plots

DSM2 Output Comparison - RMSE Statistics (View Map)

This is calculated from the original time series in dss file based on its output time interval.

: Model 1/Model 2 is higher than Observed; : Model 1/Model 2 is lower than Observed

	Percentage Root Mean Square Difference													
	FULL		2010		Water Year Type									
	2009-2010		2010-2010		Wet		Above Normal		Below Normal		Dry		Critical	
	M1	M2	M1	M2	M1	M2	M1	M2	M1	M2	M1	M2	M1	M2
ANTIOCH_RSAN007_TURBIDITY	10.92%	12.18%	11.36%	12.66%	0%	0%	0%	0%	0%	0%	9.91%	11.05%	0%	0%
FREEPORT_RSAC155_TURBIDITY	3.4%	3.45%	3.77%	3.83%	0%	0%	0%	0%	0%	0%	3.37%	3.42%	0%	0%
GEORGIANA-SL_TURBIDITY	3.73%	3.9%	4.16%	4.35%	0%	0%	0%	0%	0%	0%	3.69%	3.86%	0%	0%
OLD-R-FT-TERM_CH124_TURBIDITY	10.49%	9.65%	11.71%	10.74%	0%	0%	0%	0%	0%	0%	10.38%	9.55%	0%	0%
SJR-JP_RSAN018_TURBIDITY	11.92%	14.6%	13.03%	16%	0%	0%	0%	0%	0%	0%	11.8%	14.45%	0%	0%

Open all stations

Figure 10-13 Percentage root mean square error for turbidity comparison (COMPARE_MODE 5)

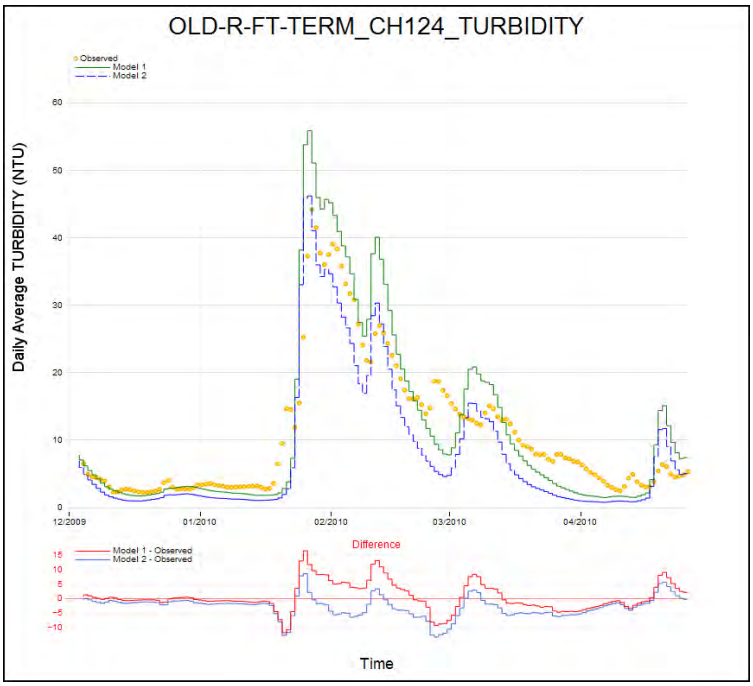

Figure 10-14 Time series plot example for turbidity comparison (COMPARE_MODE 5)

10.5 Conclusions

The latest VISTA package can be downloaded from http://code.google.com/p/dsm2-vista/downloads/list. Once you have downloaded the zip file, extract it and replace the existing VISTA folder in your local machine. That should be the folder that your environmental variable `VISTA_HOME` points to. The time series plot is generated by taking advantage of SVG technology (scalable vector graphics), a non-proprietary format supported for most browsers in their latest releases (Google Chrome provides best performance as this report is written). VISTA is an active project and under GNU general public license agreement. It is now maintained by Bay Delta Office at DWR and under Subversion control. Users can check out the latest product and know what the ongoing developments are. Those developments are enhancement for VISTA GUI and its functionalities, improvement or bug fix for VScript, capabilities to take incorporate different data types, and many useful add-ons tool and handy scripts. Therefore, it is recommended to check out the updates from the code hosting page from time to time. Also, posting feedback and comments are encouraged. The goal is to have more users utilize this tool to make their comparison process more efficient and share their results easier and to have a better communication among DSM2 modelers and people from different communities.

10.6 References

CH2MHill. " DSM2 Recalibration." 2009.

Sandhu, Nicky. "Chapter 8: VISTA (Visualization Tool and Analyzer)." *Methodology for Flow and Salinity Estimates in the Sacramento-San Joaquin Delta and Suisun Marsh. 19th Annual Progress Report from the California Department of Water Resources to the State Water Resources Control Board*, 1998.

Wikipedia contributors. *"Scalable Vector Graphics," Wikipedia, The Free Encyclopedia.* April 15, 2011. http://en.wikipedia.org/wiki/Scalable_Vector_Graphics (accessed April 2011).